Water Technology and Sciences

Included in Thomson Reuters Science Citation Index® (ISI) • Expanded Thomson Reuters Research Alert® (ISI) • EBSCO • ProQuest • Elsevier • Redalyc

Vol. VI, No. 4, July-August, 2015

Water Technology and Sciences

Edit Board

Editorial coordination and careful editing: Helena Rivas- López • **Editorial assistance and editorial layout**: Luisa Guadalupe Ramírez-Martínez • **Figures design**: Luisa Guadalupe Ramírez-Martínez and Rosario Castro-Rivera • **Coordination arbitration**: Elizabeth Peña and Bibiana Bahena • **Proofreading English**: Ellen Weiss • **Logo design and cover**: Oscar Alonso-Barrón • **Design format**: Gema Alín Martínez-Ocampo • **Marketing**: Marco Antonio Bonilla-Rincón.

Editorial Committee

©***Water Technology and Sciences.*** Vol. VI, No. 4, July-August, 2015, is a bimonthly publication edited by the Instituto Mexicano de Tecnología del Agua, Paseo Cuauhnáhuac 8532, Colonia Progreso, Jiutepec, Morelos, C.P. 62550, telephone +52 (777) 3 29 36 00, extension 474, www.imta.gob.mx/tyca, fsalinas@tlaloc.imta.mx. Responsible editor, Nahún Hamed García Villanueva; Copyright No. 04-2013-121014514100-203, granted by the Instituto Nacional de Derechos de Autor. ISSN pending. Responsible for the latest update of this issue: Sub-Department of Dissemination and Circulation, Francisco José Salinas Estrada, Paseo Cuauhnáhuac 8532, Colonia Progreso, Jiutepec, Morelos, C.P. 62550.

Water Technology and Sciences is the traslation of *Tecnología y Ciencias del Agua*, which is the continuation of the following journals: *Irrigación en México* (1930-1946); *Ingeniería hidráulica en México* (1947-1971); *Recursos hidráulicos* (1972-1978), and *Ingeniería hidráulica en México*, second period (1985-2009).

Coordination for editorial comments, click here give

For subscriptions, click here

Water Technology and Sciences

Vol. VI, No. 4, July-August, 2015

Cover: Motozintla de Mendoza and Mazapa de Madero, Chiapas, Mexico. Views from the Guatamela border. Comparison between the dry and rainy seasons, the Bacanton and Xelaju river basins and tributaries of the Grijalva River.

Studies performed in the middle and lower basins of the Grijalva River confirm the presence of heavy metals in water and sediments in the rivers and lakes that compose the basin, as well as at the mouth of this river in the Gulf of Mexico. Nevertheless, few investigations exist about the presence of metals in the upper basin, which is relevant to understanding the origin of these pollutants and their dynamics throughout the entire basin. See article "Metal Concentrations in Water and Sediments in the Upper Grijalva River Basin, Mexico-Guatemala Border" by Laino-Guanes *et al*. (pp. 61-74).

Photo: Karim Musálem Castillejos.

La Purisima Oasis, located in the northern portion of the municipality of Comondu, Baja California Sur, Mexico. The oasis gives life to a wide range of palm and fruit trees, from which the El Pilon mountain can be seen, a natural monument measuring 400 meters high. The oasis gets its name "La Purisima" from the Jesuit priests who saw an abstract image of the Virgin Mary in the 18th century.

Photo: Javier A. Arce Meza.

Contents

Technical articles

Contenido

Artículos técnicos

Streamflow Forecasting for the Turbio River using the Discrete Kalman Filter

• Fernando González-Leiva • Laura Alicia Ibáñez-Castillo* •
Universidad Autónoma Chapingo, México
*Corresponding Author

• Juan B. Valdés •
The University of Arizona at Tucson, USA

• Mario Alberto Vázquez-Peña • Agustín Ruiz-García •
Universidad Autónoma Chapingo, México

Abstract

González-Leiva, F., Ibáñez-Castillo, L. A., Valdés, J. B., Vázquez-Peña, M. A., & Ruiz-García, A. (July-August, 2015). Streamflow Forecasting for the Turbio River using the Discrete Kalman Filter. *Water Technology and Sciences* (in Spanish), 6(4), 5-24.

This paper proposes the use of the discreet Kalman filter (DKF) along with an autoregressive model with exogenous inputs (ARX) for short-term streamflow forecasting with lead times of 24, 48, 72 and 96 hours. This model was applied to the Turbio River basin, located in the state of Guanajuato and a portion of the state of Jalisco, Mexico. This area is vulnerable to flooding during rainy periods which normally occur in the region. The forecasting was based on available precipitation and streamflow data from the years 2003 and 2004. The results indicate that the forecasts performed with one-step ahead, that is with a 24-hour lead time, present better fits than 48, 72 and 96-hour lead times in terms of Nash-Sutcliffe, MSE and RMSE.

Keywords: Kalman filter, autoregressive models, short-term streamflow forecasting.

Resumen

González-Leiva, F., Ibáñez-Castillo, L. A., Valdés, J. B., Vázquez-Peña, M. A., & Ruiz-García, A. (julio-agosto, 2015). Pronóstico de caudales con Filtro de Kalman Discreto en el río Turbio. Tecnología y Ciencias del Agua, *6(4), 5-24.*

Se propuso la implementación del algoritmo del Filtro de Kalman Discreto (DKF) junto con un modelo autorregresivo con entrada exógena (ARX) para realizar el pronóstico de caudales a corto plazo con 24, 48, 72 y 96 horas de anticipación en la cuenca del río Turbio, localizada en el estado de Guanajuato y parte del estado de Jalisco, México, vulnerable a inundaciones durante los periodos de lluvias que se presentan normalmente en la zona. La información de precipitación y caudal disponible con las que se realizaron los pronósticos corresponde a las series de los años 2003 y 2004. Los resultados obtenidos indican que los pronósticos realizados un paso hacia adelante, es decir, con un tiempo de 24 horas de anticipación, presentaron los mejores ajustes en términos de Nash-Sutcliffe, MSE y RMSE, que los pronósticos realizados a 48, 72 y 96 horas de anticipación.

Palabras clave: *Filtro de Kalman, modelos autorregresivos, pronósticos de caudales a corto plazo.*

Received: 10/09/2014
Aceepted: 29/04/2015

Introduction

Due to climate change (IPCC, 2007; Mendoza *et al*., 2009; Montero- Martínez, Ojeda-Bustamante, Santana-Sepúlveda, Prieto-González, & Lobato-Sánchez, 2013) and its foreseeable influence on the severity, frequency and impact of floods and droughts, forecasted estimates of future hydrological phenomena have become increasingly important over recent years. These predictions are essential to the efficient functioning of hydric infrastructure and to mitigate natural disasters caused by environmental conditions (WMO, 2009).

According to Valdés, Mejía-Velázquez, & Rodríguez-Iturbe (1980), when predicting streamflows a causal relationship can be presumed among precipitation at several points in a basin, different moments in time and the mean streamflow at a point in the outlet on a particular day. This causal relationship, called the response function, can be represented by a black box model. Since the beginning of the1960s, autoregressive models have been widely used in hydrology and water resources for annual and periodic hydrological time-series modeling.

The application of these models in hydrology has been attractive, particularly since the autoregressive form is dependent on time and is easy to use (Salas, Delleur, Yevjevich, & Lane, 1980; Box, Jenkins, & Reinsel, 2013). The Kalman Filter algorithm has been proposed in recent years to forecast streamflows in hydrological systems, jointly with mathematical rainfall-runoff models of hydrographic basins (Moradkhani, Sorooshian, Gupta, & Houser, 2005; Xie & Zhang, 2010; Lü *et al*., 2013; Morales-Velázquez, Aparicio, & Valdés, 2014; Abaza Anctil, Fortin, & Turcotte, 2014), and an emphasis on the optimal estimation of state parameters with models using the technique known as data assimilation (Moradkhani, DeChant, & Sorooshian, 2012; Liu *et al*., 2012; Shi, Davis, Zhang, Duffy, & Yu, 2014; Samuel, Coulibaly, Dumedah, & Moradkhani, 2014, Liu, *et al*., 2015; Yucel, Onen, Yilmaz, & Gochis, 2015; Li, Ryu, Western, & Wang, 2015). Nevertheless, continuous and complete streamflow series are needed to use these models, which may not be available in developing countries such as Mexico. According to Perevochtchikova (2013), the CLICOM climatology and *BANDAS* surface water databases for Mexico has recurring problems with poor accessibility, notable differences among sectors and gaps in the time series. This makes them difficult to use for the comparison and analysis of spatial and temporal evolutions, systematization of data and construction of indicators and local models.

The discrete Kalman filter (DKF) was proposed by Kalman (1960) with the least squares method as a recursive solution for the linear filtering of discrete data. It is a mathematical procedure that operates using prediction and correction mechanisms. This algorithm forecasts the new state based on the previous estimation, adding a correction term proportional to the prediction error in order to statistically minimize that error. Thus, the state of a dynamic system can be estimated if information is known about the dynamic system, the statistics of the noisy system, the measuring errors and initial conditions (Gelb, 1974; Simon, 2001; Welch & Bishop, 2006).

Streamflow forecasting for hydrographic basins is one of the procedures used in specific hydrological fields to enable making decisions based on risk planning in order to mitigate the negative impact of floods— such as the regulation of reservoirs and the issuance of early flood warnings in populated areas. In Mexico, Morales-Velázquez, Aparicio and Valdés (2014) evaluated the usefulness of the discrete Kalman filter (DKF) algorithm to forecast floods in order to regulate flows in the Angel Corbino Corzo dam, or *Peñitas*, belonging to the Grijalva hydroelectric system.

The present work proposes the use of the discrete Kalman filter (DKF) algorithm along with an ARX autoregressive model with exogenous inputs to forecast short-term streamflows with lead times of 24, 48, 72 and 96 hours in the Turbio River basin, located in the state of Guanajuato and portions of the state of Jalisco, Mexico. This area is vulnerable to floods during the rainy periods registered in the region.

Materials and Methods

Description of the Basin

Figure 1 shows the location and representation of the Turbio River basin, which is located in the Lerma-Santiago Hydrological

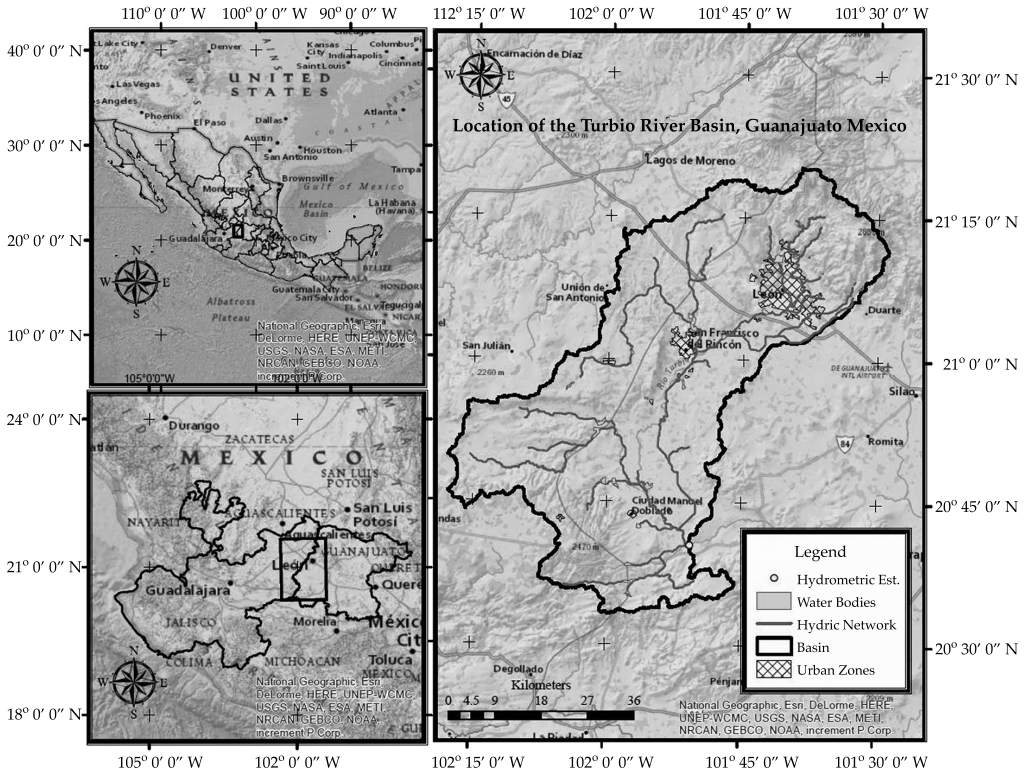

Figure 1. Location of the Turbio River basin.

Region 12, in the states of Guanajuato and Jalisco, between 20° 32′ 42″ and 21° 21′ 18″ latitude north and 101° 27′ 82″ and 102° 17′ 57″ longitude west. The main towns in the basin are Ciudad de León, San Francisco del Rincón,Purísima de Bustos and Manuel Doblado. The total area of the basin is 3 322 km^2 up to Las Adjuntas hydrometric station, located at 20° 40′ 32″ latitude north and 101° 50′ 40″ longitude west, 58.8% of which is in the state of Guanajuato and 41.2% in the state of Jalisco. The highest altitude in the basin's watershed is 2 670 masl and the outlet at the hydrometric station is at 1 723 masl. The mean slope of the basin is 11%. The main channel has a level difference of 323 m and the concentration time of the basin is 21 hours. The annual mean precipitation is 659 mm, according to the climate normals for the period 1981 – 2010 (SMN, 2014), with a rainfall regime that begins in June and ends in October, during which 89% of the total annual precipitation falls, which are intense and of short duration.

The largest dams in the region are El Palote and El Barrial. The former is in the Ciudad de León and provides potable water and flood control. It has a maximum capacity of 17 Mm^3. El Barrial is located in San Francisco del Rincón and was designed to control floods and as a source of water for irrigation. It has a capacity of 55.26 Mm^3. Other notable dams include Santa Efigenia, with a capacity of 42.75 Mm^3; Jalpa Vieja, with 14.38 Mm^3; Ciénaga de Galvanes, with 11 Mm^3, and Potrerillos, with 15 Mm^3. All of these serve the dual purpose of irrigation and flood control (Conagua, 2014b).

Climatological Information

The precipitation information used as input for the forecasting model was obtained from the *CLICOM* database (SMN, 2014), using daily series for the years 2003 and 2004, the periods with the largest amount of complete records for the basin. Table 1 shows a total of 11 weather stations distributed throughout the area of the Turbio River basin.

Hydrometric Information

Daily mean streamflows were obtained from the *BANDAS* database (Banco Nacional de Aguas Superficiales (NationalSurface Water Bank)) (Conagua, 2014a) for data series from the years 2003 and 2004. Table 2 summarizes the quantiles for maximum streamflows registered in Las Adjuntas hydrometric stations according to the National Water Commission and reports by the Guanajuato Civil Protection (2012).

Methodology

Since the beginning of the 1960s, autoregressive models have been widely used in hydrology and water resources for annual and periodic hydrological time-series modeling. The application of these models to hydrology has been attractive primarily because the autoregressive approach depends on time and they are easy to implement (Salas *et al.*, 1980; Box *et al.*, 2013).

The creation of an *ARX* autoregressive model with exogenous inputs was proposed to predict mean streamflows based on historical series for Las Adjuntas hydrometric station, obtained from the *BANDAS* database (Conagua, 2014a). The *ARX* model relates the inputs and outputs of the system through a

Table 2. Return periods for maximum flows in Las Adjuntas hydrometric station..

Return period (years)	Flow (m^3/s)
2	44.35
5	84.60
10	111.24
20	136.8
50	169.88
100	194.67
500	251.96
1 000	276.59

Source: Guanajuato Civil Protection (2012).

Table 1. Weather stations in the Turbio River Basin.

Station Code	Name	Municipality	State	Agency
11020	El Palote	León	Guanajuato	SMN
11025	Hacienda de Arriba	León	Guanajuato	SMN/CEAG
11035	La Sandía	León	Guanajuato	SMN
11036	Adjuntas	Manuel Doblado	Guanajuato	SMN/CEAG
11045	Media Luna	León	Guanajuato	SMN
11153	La Laborcita	León	Guanajuato	SMN
11157	San Francisco del Rincón	Peñuelas	Guanajuato	SMN
11159	San Francisco del Rincón	El Barrial Dam	Guanajuato	SMN
14123	San Diego Alejandría	San Diego Alejandría	Jalisco	SMN
14157	Unión de San Antonio	Unión de San Antonio	Jalisco	SMN
14369	La Vaquera	Arandas	Jalisco	SMN

Source: SMN (2014).

linear difference equation with constant coefficients (Hsu, Moradkhani, & Sorooshian, 2009):

$$y_{t+1} = \sum_{i=0}^{na} \alpha_i y_{t-i} + \sum_{j=0}^{nb} \beta_j r_{t-j} + e_{t+1} \quad (1)$$

where y_t and r_t are the observed streamflow and rainfall for time t, which represents one day; e_{t+1} is the error term in the streamflow estimate; α_i and β_j are parameters. The indices *na* and *nb* specify the number of previous streamflow and rainfall observations, which is what an *ARX* autoregressive model would be (*na, nb*).

Once the overall structure of the *ARX* is known, the state-space formulations are useful for any type of Kalman Filter. Equation (1) can be represented in the spatial form of the states as:

$$x_{k+1} = Ax_k + Bu_k + w_k \quad (2)$$

$$z_k = Hx_k + v_k$$

where x_{k+1} is the present streamflow (not observed) of size (n x 1); A is the matrix of α_i parameters, of size (n x n); x_k is the streamflow over time k of size (n x 1); B is the matrix of exogenous parameters β_j of size (n x m); u_k represents the vector that contains the mean precipitation registered in the basin for time k of size (m x 1); z_k is the measured streamflow over time k of size (m x 1); H is the transformation matrix that maps the vector of states in the measuring domain with dimensions (m x n); w_k and v_k are vectors that represent the Gaussian noise in the process and the noise in the measurement for each observation, with sizes (m x 1), such that:

$$w_k \sim N(0, Q) \quad (3)$$

$$v_k \sim N(0, R)$$

For the specific case of the disturbance covariance matrix R, this was defined according to that reported by Moralez-Velázquez *et al.*, 2014. The matrix was represented as $\alpha^* q_{(k-1)}$, where α is a proportionality constant which represents a constant error equal to a fraction of the streamflow over the previous time (k – 1). The value of α in all cases was 5% with respect to the immediately preceding streamflow. That 5% is the error believed to be committed by the person who measures the streamflows. According to equation (2), the dynamics of a system makes a simpler representation possible, providing statistical descriptions of the behavior of the system (Gelb, 1974).

State-space models are basically a convenient notation with which to manage a wide range of time series models. This methodology is based on stochastic models to estimate and control problems, with the supposition of the erroneous nature of the measurements (Ramírez,2003).

Lastly, the system represented by equation (2) consists of a deterministic component and a stochastic component which reflect uncertainty in the model (Lee & Singh, 1998).

In equation (3), Q and R can change over time, but they are generally considered constants for simplicity purposes (Simon, 2001) and their expected values can be represented as:

$$Q = E\left[w_k w_k^T\right]$$

$$R = E\left[v_k v_k^T\right] \quad (4)$$

Thus, the *ARX* model is a state-space representation facilitates the application of the Kalman Filter to obtain the streamflow forecast over time (k + 1) based on the streamflow series registered for time k. It includes the daily mean precipitation in the basin as the exogenous input component of the model and follows the algorithm scheme for state estimators shown in Figure 2 (Kim, 2011).

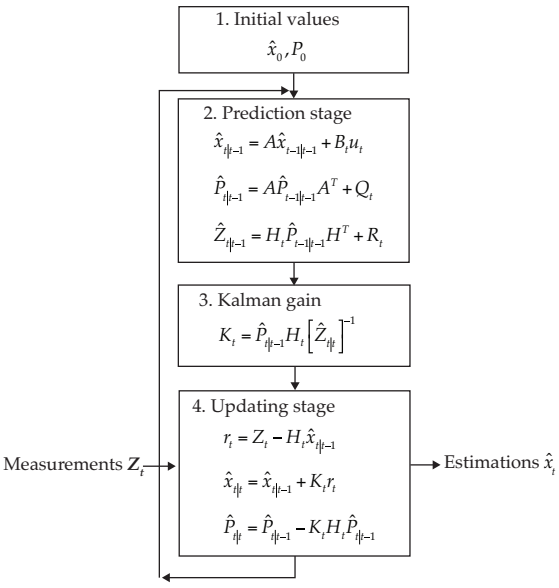

Figure 2. Algorithm for the Discrete Kalman Filter. Source: Kim (2011).

To create the *ARX* model, a routine was programmed in Matlab® using the toolbox systems identification to obtain the order of the autoregressive process according to the number of terms represented in equation (1).

Given that the parameters estimated by the *ARX* model can vary for periods with more precipitation and/or for abrupt changes in streamflows, a warm-up period (P) was established to estimate the parameters and begin the forecasting of streamflows over time ($t_0 + P$).

Once the length of the period is defined, forecasts were obtained from time ($t_0 + P$) up to time ($t_0 + 2P$), the parameters of the *ARX* model for the period ($2P$) were recalculated, and forecasting was reinitiated, this time from ($t_0 + 2P$) to ($t_0 + 3P$). This was continued successively, as described in Figure 3. The implementation of the *ARX + DKF* was thereby done dynamically and with state matrices which were varied for each particular period, decreasing the noise generated in the process, represented in equation (2) by w_k.

In order to identify differences among the forecasts for L steps ahead, that is, with lead times of 24, 48, 72 and 96 hours, a routine in Matlab® was executed which used information from the state over time (k) to advance without updating L steps in the timeline. After reaching the desired L position, the first forecasted state was updated, as described in Figure 4. The cycle was performed taking into account the calibration periods for the *ARX* model described in Figure 3.

To evaluate the fit of the forecasts to the measured data, the main statistics were calculated according to Gupta, Kling, Yilmanz and Martínez (2009) for the methodology described previously. The mean squared error (MSE) (Mood, Graybill, & Boes, 1974) and its corresponding normalization, and the Nash-Sutcliffe efficiency (Nash & Sutcliffe,1970) were the two criteria employed since they are the most widely used to calibrate and evaluate hydrological models with observed data.

In addition, a prediction interval was determined at a 95% probability for each forecast series, according to Chatfield (2004). In order to test the suppositions of the general Kalman filter theory, probability distribution functions were fit for errors $e_k = x_k - \hat{x}_k$ in the series evaluated.

Results and Discussion

The second-order autoregressive ($na = 2$) was the *ARX* model that presented the best fit for streamflows for the years 2003 and 2004 and the first-order ($nb = 1$) had the best fit for precipitation. These are shown in Tables 3 and 4, respectively. Both tables show that the models mentioned represent the best fit based on the Nash-Sutcliffe coefficients, especially for the 24-hour forecast which, as will be seen below, is the one with the best fit for the discrete Kalman filter. In addition, it is always desirable for the model to not only present the best fit but also have the lowest number of terms possible, which makes it easier to manage.

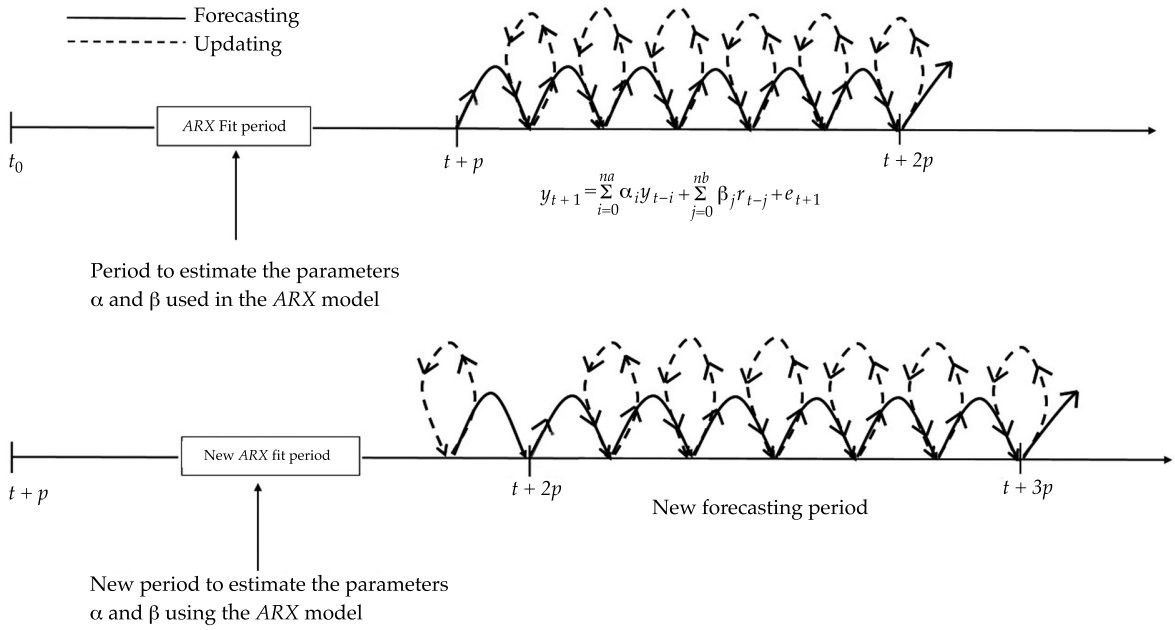

Figure 3. Description of the flow forecasting process according to periods for estimating the parameters for the model *ARK + DKF*.

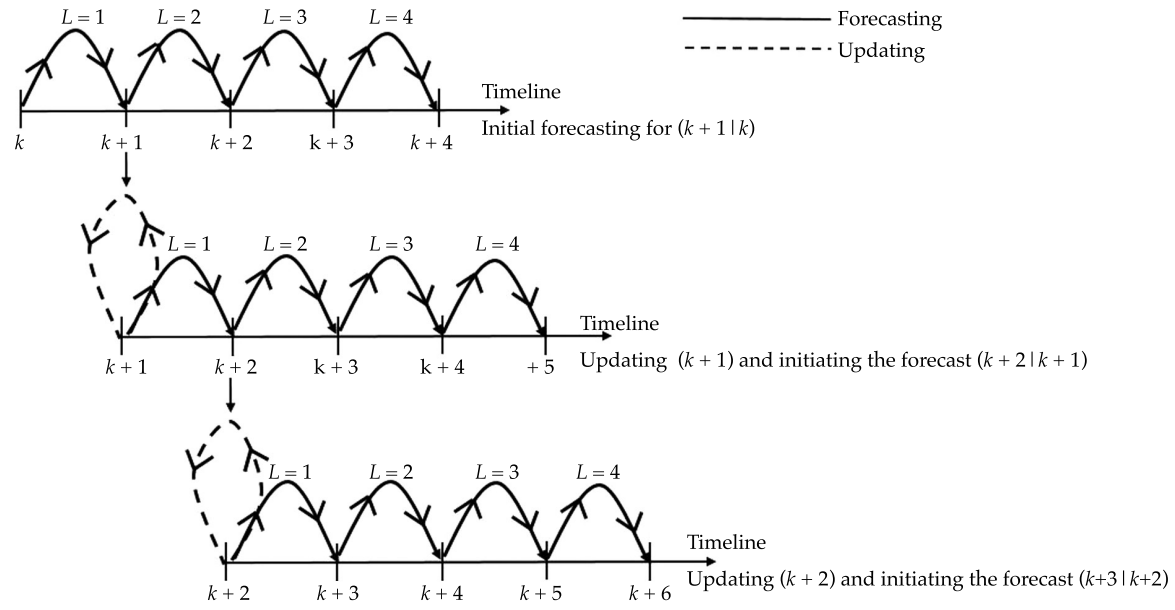

Figure 4. Description of flow forecasting with *L* steps ahead, after the calibration period.

The streamflow forecasting results obtained with the ARK+DKF model based on information from the year 2003 for the Turbio River basin are presented next. The model used a 20-year period for prior calibration and subsequent forecasting for the year 2003. The

Table 3. Comparison of fits in statistical terms for different *ARX* model orders (*na*, *nb*) for short-term flow forecasting, year 2003 series.

ARX (*na*,*nb*)[1]		MSE[2]				RMSE[3]				Nash-Sutcliffe			
na	***nb***	**24 h**	**48 h**	**72 h**	**96 h**	**24 h**	**48 h**	**72 h**	**96 h**	**24 h**	**48 h**	**72 h**	**96 h**
1	2	49.88	116.76	194.74	282.17	7.06	10.81	13.95	16.8	0.94	0.85	0.75	0.64
2	1	41.37	103.63	188.29	291.01	6.43	10.18	13.72	17.06	0.95	0.87	0.76	0.63
2	2	60.48	125.92	212.3	312.48	7.78	11.22	14.57	17.68	0.92	0.84	0.73	0.60
2	3	62.63	131.93	216.52	312.58	7.91	11.49	14.71	17.68	0.92	0.83	0.72	0.60
3	1	65.34	154.05	252.88	403.66	8.08	12.41	15.90	20.09	0.92	0.80	0.68	0.48
3	2	91.08	177.80	273.81	430.19	9.54	13.33	16.55	20.74	0.88	0.77	0.65	0.45
3	3	117.26	201.31	275.28	409.97	10.83	14.19	16.59	20.25	0.85	0.74	0.65	0.48

[1]*na* = autoregressive order for flows; *nb* = autoregressive order for precipitation.
[2]MSE = *Mean Squared Error*.
[3]RMSE = *Root Mean Squared Error*.

Table 3. Comparison of fits in statistical terms for different *ARX* model orders (*na*, *nb*) for short-term flow forecasting, year 2004 series.

ARX (*na*, *nb*)		MSE				RMSE				Nash-Sutcliffe			
na	***nb***	**24 h**	**48 h**	**72 h**	**96 h**	**24 h**	**48 h**	**72 h**	**96 h**	**24 h**	**48 h**	**72 h**	**96 h**
1	2	16.96	39.15	61.52	82.04	4.12	6.26	7.84	9.06	0.92	0.82	0.72	0.63
2	1	16.32	39.13	62.16	83.13	4.04	6.26	7.88	9.12	0.93	0.82	0.72	0.62
2	2	16.83	39.42	62.32	83.33	4.10	6.28	7.89	9.13	0.92	0.82	0.72	0.62
2	3	26.54	57.70	87.39	113.28	5.15	7.60	9.35	10.64	0.88	0.74	0.60	0.48
3	1	15.56	36.99	59.76	80.79	3.95	6.08	7.73	8.99	0.93	0.83	0.73	0.63
3	2	16.22	37.73	60.78	82.02	4.03	6.14	7.80	9.06	0.93	0.83	0.72	0.63
3	3	30.20	63.53	87.29	108.77	5.50	7.97	9.34	10.43	0.86	0.71	0.60	0.50

calibration period chosen was the one with the best statistical results with the ARK+DKF. These statistics will be shown later.

Figure 5 presents the streamflow forecasting obtained for $L = 1$ or with a 24-h lead time. A difference in the time scale can be seen between maximum precipitation and peak streamflow, especially for the maximum event in September 2003. This may be due to the presence of various dams in the Turbio River basin. Nevertheless, the peak streamflow for the maximum event in July 2003 was lower than that for September even though precipitation was higher in July. This may be due to antecedent moisture conditions in the soils in the basin between July and September. A similar situation is observed later in Figure 10, which corresponds to the forecast for 2004. Future investigations can consider a Kalman filter with antecedent moisture as an additional external variable, measured as rainfall 5-days prior, as is used by the runoff curve number technique to calculate runoff (McCuen, 2005).

Likewise, forecasts were performed for different steps ahead— $L = 2$ or 48-h, $L = 3$ or 72-h, and $L = 4$ or 96-h lead time, in order to quantify the prediction errors, taking into account the scheme described in Figure 4.

Table 5 summarizes the statistics for the different forecasts over time using the data from the 2003 series.

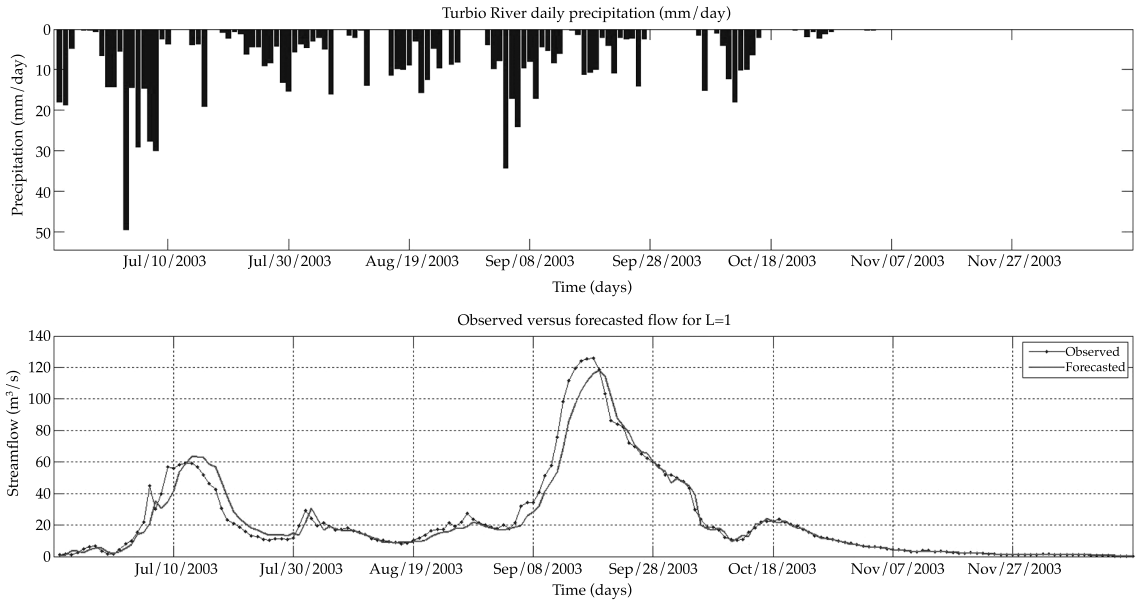

Figure 5. Streamflow forecasts for $L = 1$ or 24-h lead time with *ARX + DKF* in the Turbio River basin for the 2003 series..

Better results were obtained with streamflow forecasts performed one-step head, that is, with a 24-h lead time, than with 48, 72 and 96 hours lead time.

According to the statistical summary in Table 5, the mean for the forecasted streamflows tends to remain the same as the observed streamflows. The Nash-Sutcliffe efficiency coefficient decreases when the RMSE increases as the forecasting advances L steps ahead, decreasing the reliability of the forecasts performed. The results regarding the percentage bias (PB) for all the forecasts over time indicate that the model tends to underestimate streamflows. The results present a behavior characteristic of low, medium and high streamflows according to the dispersion along the 45 degree line in Figure 6. Therefore, the data were grouped into three classes: $Q < 20$ m^3/s, 20 m^3/s $\leq Q \leq$ 60 m^3/s and $Q >$ 60 m^3/s (see Figure 7),according to the dispersion pattern in Figure 6.

The scatter plots in Figure 7 are presented in the following order: graphs of $L = 1$ (a,b,c), graphs of $L = 2$ (d,e,f), graphs of $L = 3$ (g,h,i), graphs of $L = 4$ (j,k,l). For the series corresponding to the year 2003 (Table 6), the *ARX + DKF* presenting the best forecasts for streamflow were obtained with $L = 1$ and $L = 2$ for ranges under 20 m^3/s, in terms of the RMSE and the Nash-Sutcliffe (see graphs a and d).

Meanwhile, forecasts with $L = 3$ and $L = 4$ for the same range did not present the best results according to the statistics evaluated. With the streamflow forecast for the range 20-60 m^3/s (see graphs b,e,h,k in Figure 7), the *ARX+DKF* tended to underestimate the forecasted streamflows, and this index was higher for forecasted streamflows over 60 m^3/s (graphs c, f, I, l in Figure 7).

As described previously, the theory assumes that the forecasting errors $e = (x - \hat{x})$ come from a normal distribution. In this sense, the supposition was verified for errors obtained in the forecasted series with 24, 48, 72 and 96 hours lead time.

Table 5. Statistical summary for different forecasts using *ARX + DKF* in the Turbio River basin for the 2003 series..

Statistics	Mean	MSE	RMSE	R^2	Nash-Sutcliffe	PB
Streamflow forecasts $L = 1$	22.6	41.37	6.43	0.97	0.95	-3.82
Streamflow forecasts $L = 2$	22.0	103.63	10.18	0.93	0.87	-6.14
Streamflow forecasts $L = 3$	21.6	188.29	13.72	0.87	0.76	-7.87
Streamflow forecasts $L = 4$	21.2	291.01	17.06	0.80	0.63	-9.35
Observed Flows	20.1	-	-	-	-	-

PB = percent bias.

Figure 8 presents the fits obtained for the forecasting errors taking into account the different time steps. In general terms, all the errors fit a scaled student-*t* distribution.

According to Chatfield (2001), in practice the errors do not always fit a normal distribution because of the asymmetry that may be present, the presence of atypical data which generates distributions with heavy tails and the errors associated with data that contaminate the distribution of the errors in the forecasting. Accordingly, it is suggested that the value to obtain a given probability be selected based on the distribution of the data

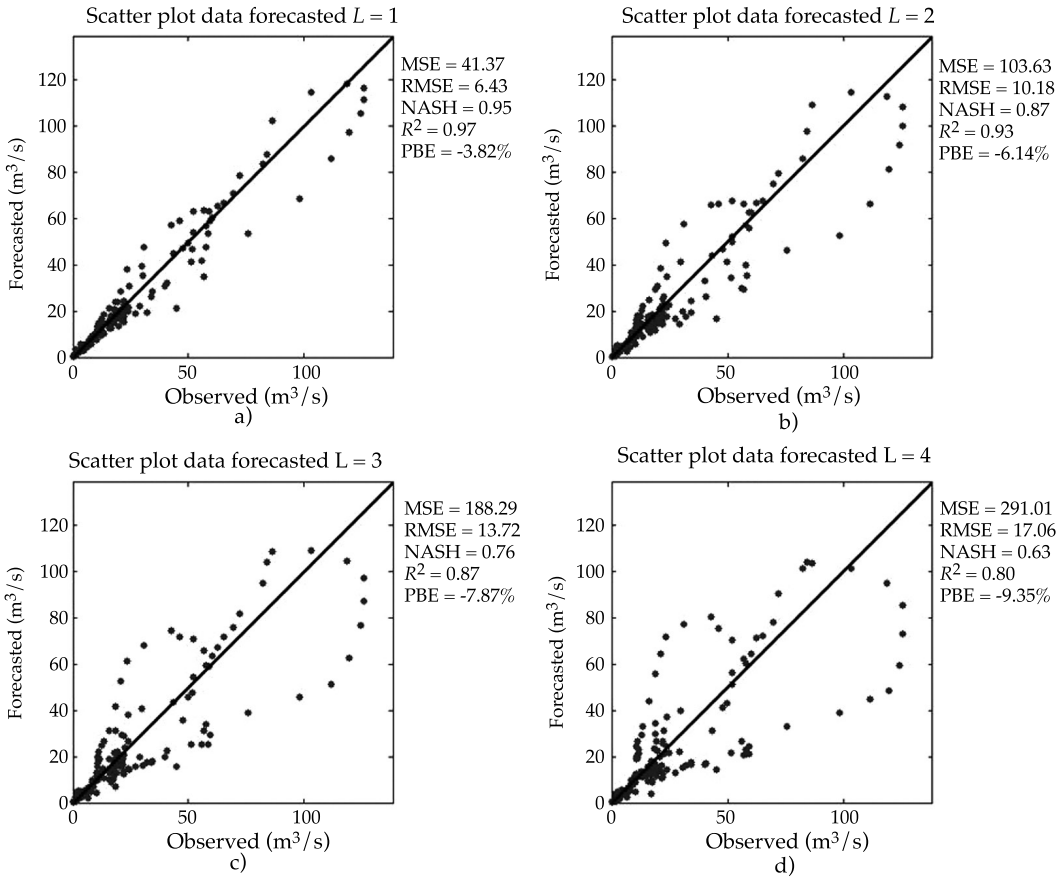

Figure 6. Comparative scatter plots for forecasts with 24 (a), 48 (b), 72 (c) and 96-hr (c) lead times in the Turbio River basin for the 2003 series.

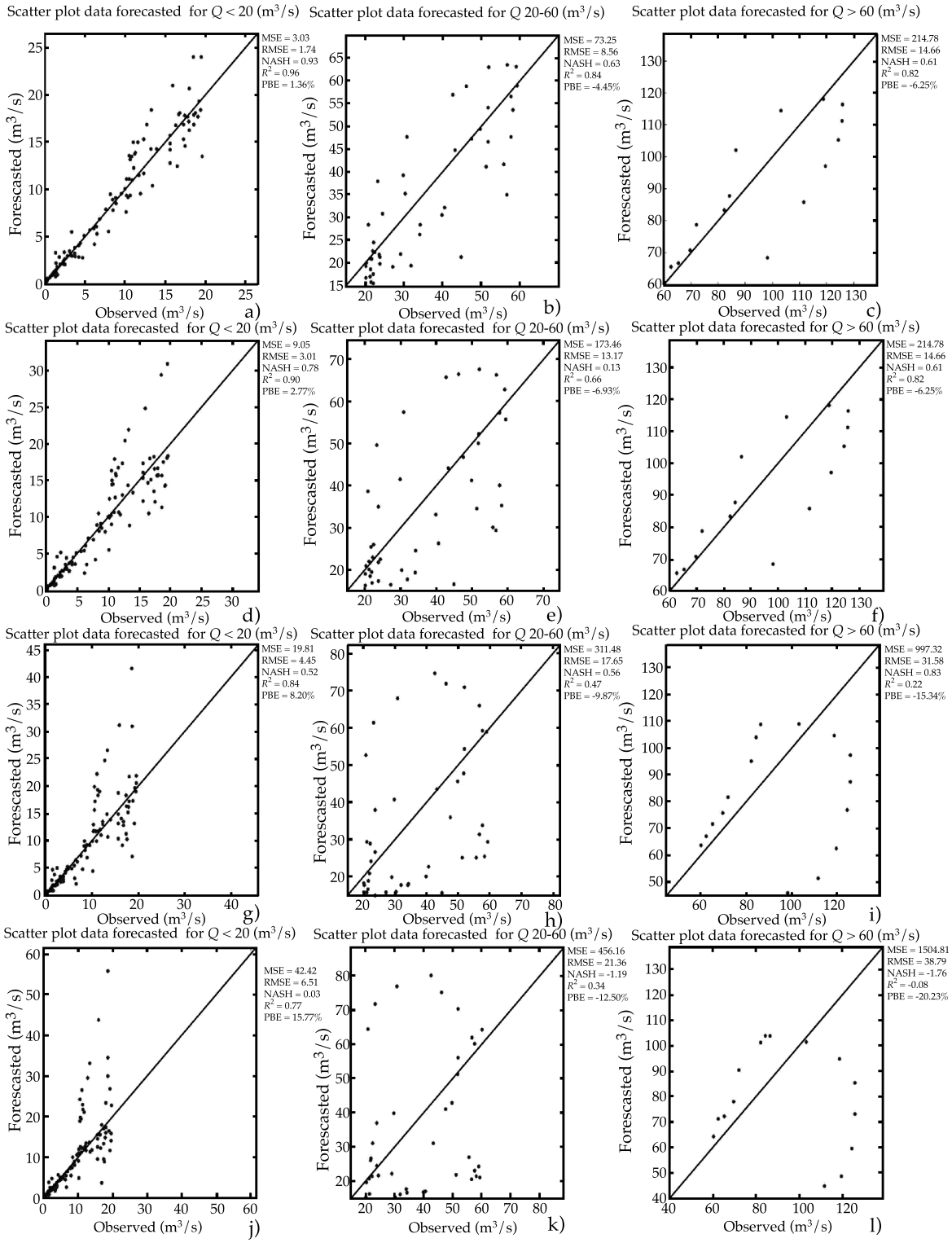

Figure 7. Scatter plots of forecasts grouped into different time steps using data from the year 2003.

Table 6. Statistical summary of the forecasts grouped into different time steps using data from the year 2003.

Forecasts	Range	MSE	RMSE	R^2	Nash-Sutcliffe	PB
$L = 1$ 24 h	$Q < 20$ m³/s	3.03	1.74	0.96	0.93	1.36
	$20 \leq Q \leq 60$ m³/s	73.25	8.56	0.84	0.63	-4.45
	$Q > 60$ m³/s	214.78	14.66	0.82	0.61	-6.25
$L = 2$ 48 h	$Q < 20$ m³/s	9.05	3.01	0.9	0.78	2.77
	$20 \leq Q \leq 60$ m³/s	173.46	13.17	0.66	0.13	-6.93
	$Q > 60$ m³/s	214.78	14.66	0.82	0.61	-6.25
$L = 3$ 72 h	$Q < 20$ m³/s	19.81	4.45	0.84	0.52	8.20
	$20 \leq Q \leq 60$ m³/s	311.48	17.65	0.47	0.10	-9.87
	$Q > 60$ m³/s	997.32	31.58	0.22	-0.83	-15.34
$L = 4$ 96 h	$Q < 20$ m³/s	42.42	6.51	0.77	-0.03	15.77
	$20 \leq Q \leq 60$ m³/s	456.16	21.36	0.34	-1.19	-12.50
	$Q > 60$ m³/s	1 504.81	38.79	0.08	-1.76	-20.23

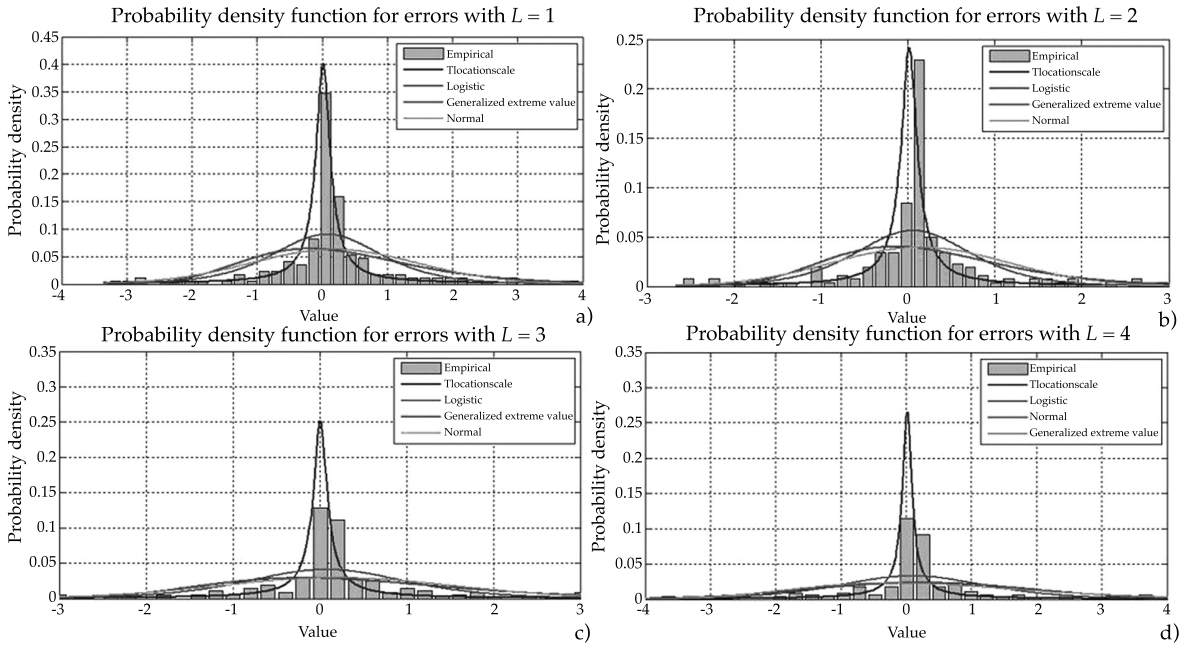

Figure 8. Probability Distribution Functions for Forecasting Errors obtained with 24 (a), 48 (b), 72 (c) and 96 hours (d) lead time in the Turbio River basin for the series 2003.

when it has been fitted with its parameters.

In order to establish the degree of uncertainty related to forecasting with different time steps, prediction intervals were determined for each point value according to criteria established by Chatfield (2004).

Figure 9 presents the prediction interval at a 95% probability for the forecast with a 24-h lead time using the 2003 series. This forecast is acceptable since most of the observed streamflows are within the range of the intervals calculated for the series, unlike the

intervals obtained for the event on Sept 08, 2003 and Sept 15, 2003 in which the observed streamflows fell outside the calculated range, and were correlated with the data grouped in Figure 7 for the class $Q > 60$ m3/s with $L = 1$.

Figure 10 presents the streamflow forecast for the 2004 series using the *ARX+DKF* with a 24-h lead time.

In this forecasting series, the 36-day period had the best fit, considering a second-order autoregression for streamflows and a first-order for number of days with precipitation, as shown previously in Table 4. The statistics for the forecasting with the 2004 series are shown in Table 7.

The best results were obtained from the streamflows forecasted with L= 1, or with 24-h lead time, according to the statistics reported in Table 7.

The mean of the forecasting of the series with $L = 1$ tends to depart from the observed data series and the forecasting with $L = 2$, $L = 3$, $L = 4$.

In general terms, as time progresses the forecasts tend to lose the efficiency reflected in the Nash-Sutcliffe, MSE and RMSE values, tending to underestimate the data according to the values reported by the PB.

The streamflows forecasted for the 2004 series were grouped with the same structure as that used for the forecasts performed with data from the 2003 series. In this case, the ranges were $Q < 20$ m^3/s and $Q \geq 20$ m^3/s, according to the dispersion of the data obtained in Figure 11.

Figure 12 presents the results from the graphs of $L = 1$ (a,b), $L = 2$ (c,d), $L = 3$ (e,f) and $L = 4$ (g,h). The best fits were obtained for streamflows under 20 m^3/s, as observed in the series for the year 2003 (see graphs a, c, e, g).

Graphs b,d,f and h in Figure 12 show that the forecasts for $Q \geq 20$ m^3/s tend to lose reliability for all time steps in function of the degree of dispersion from the observed values. This is reflected by the increase in the RMSE

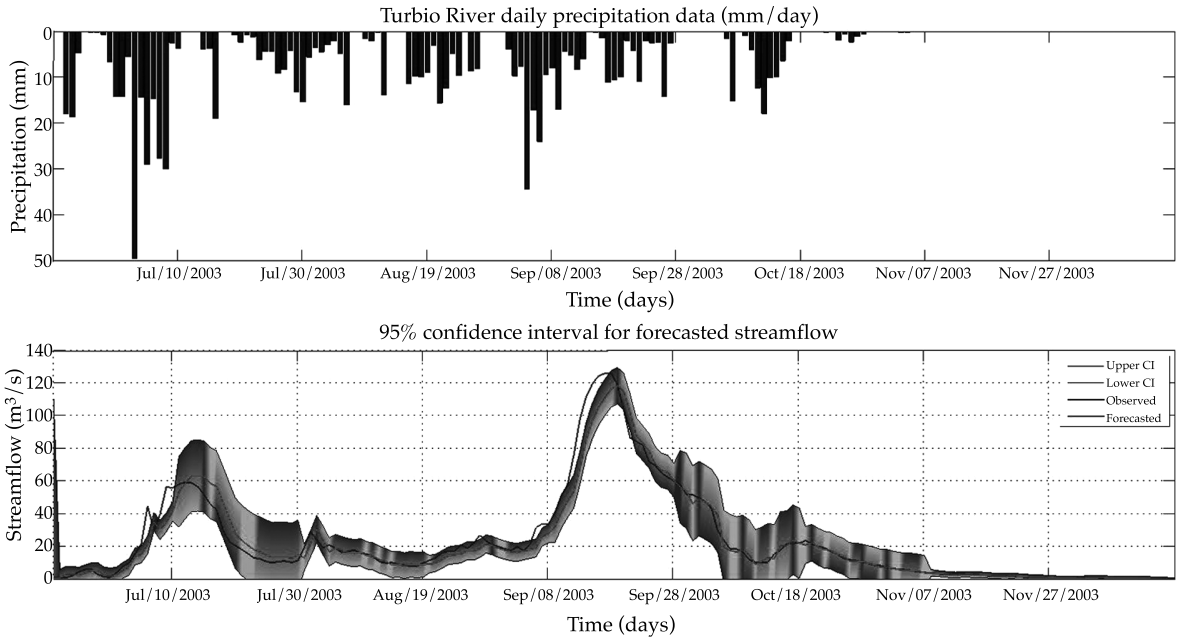

Figure 9. Forecast interval of 95% probability for $L = 1$, or 24-h lead time in the Turbio River basin for the 2003 series.

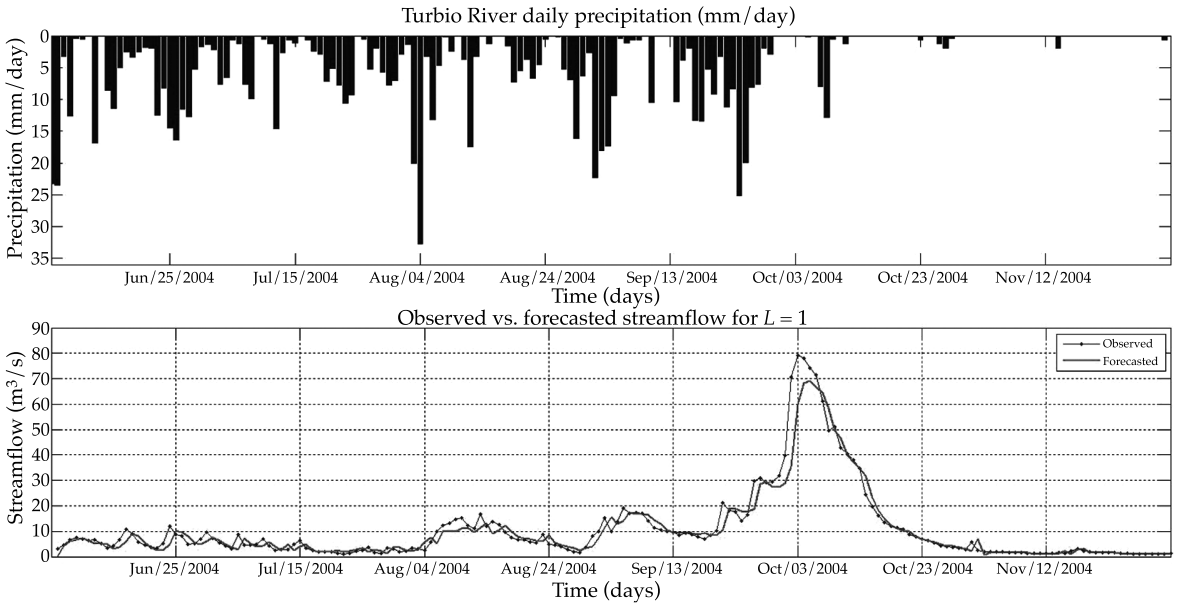

Figure 10. Forecasted streamflows for $L = 1$ or 24 hours lead time with *ARX + DKF* in the Turbio River basin for the 2004 series.

Table 7. Statistical summary for forecasts with different steps using the *ARX + DKF* in the Turbio River basin for the 2004 series.

Statistics	Mean	MSE	RMSE	R^2	Nash-Sutcliffe	PB
Streamflow forecasts $L = 1$	10.12	16.32	4.04	0.96	0.93	-5.64
Streamflow forecasts $L = 2$	9.64	39.13	6.26	0.91	0.82	-10.02
Streamflow forecasts $L = 3$	9.18	62.16	7.88	0.86	0.72	-14.14
Streamflow forecasts $L = 4$	8.76	83.13	9.12	0.80	0.62	-17.84
Observed Flows	8.16	-	-	-	-	-

and decrease in the Nash-Sutcliffe coefficient as the forecast is performed with longer lead times, as shown by the statistics in Table 8.

As in the case of the results obtained from the 2003 series, the forecasting errors were fitted to a scaled student-t distribution for the different time steps, as discussed previously.

According to the fit of the errors shown in Figure 13, the prediction interval was calculated at a 95% probability with data corresponding to $L = 1$, or a 24-h lead time. Satisfactory fit values were obtained with respect to the observed values (Figure 14) in most of the intervals calculated, unlike the forecasts between October 1, 2004 and Oct 4, 2004, whose intervals did not include observed values from the same time period, more closely resembling the data grouped in the range $Q \geq 20$ m^3/s with a 24-h lead time, as reported in Figure 12.

Kim, Tachikawa and Takara (2004) implemented the Kalman filter using the CDRMV3 model for streamflow forecasts and found better results with forecasts performed 1 hour later compared to 12 hours later, evaluated in terms of the RMSE.

Meanwhile, in terms of the Nash-Sutcliffe, Hirpa *et al.* (2013) found better results for

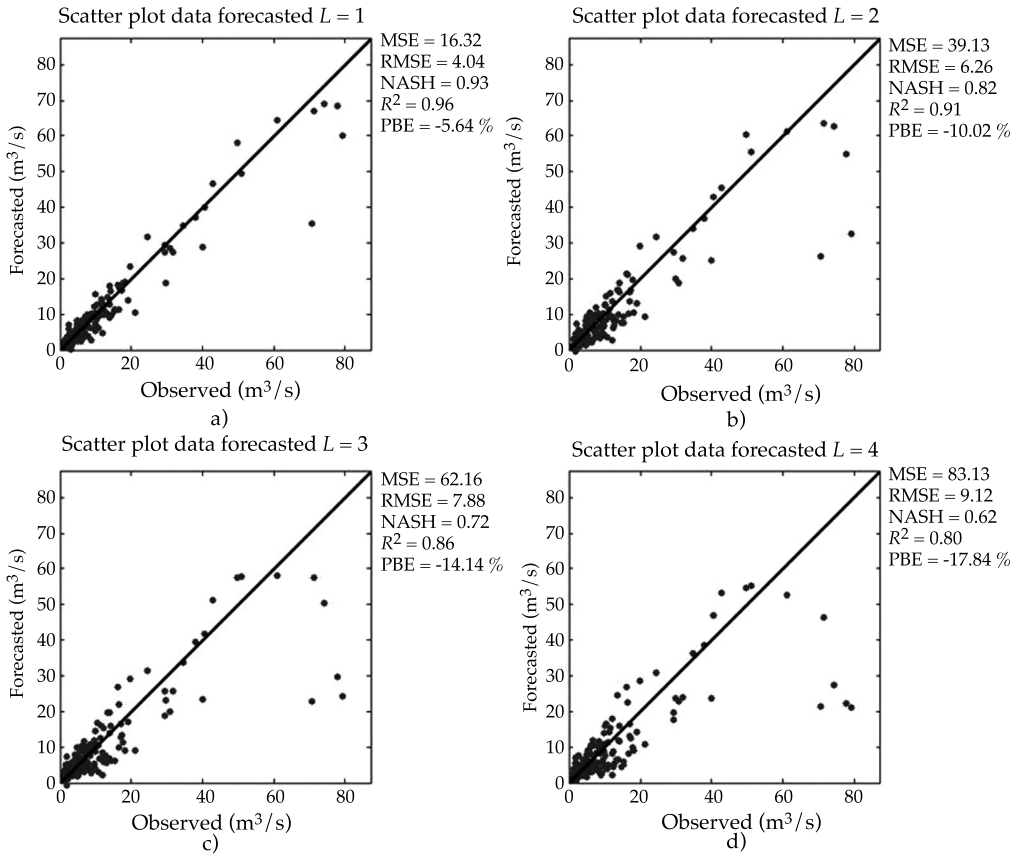

Figure 11. Comparative scatter plots for forecasts with 24 (a), 48 (b), 72 (c) and 96-hour (c) lead times in the Turbio River basin for the 2004 series.

streamflow forecasts performed with a 1-day lead time than with a 15-day lead time in the Ganges and Brahamaputra rivers in Asia.

The present work forecasted streamflows for the years 2003 and 2004 since the *BANDAS* database for those years had the most complete and best quality data for input into the Kalman filter model. Later works may be able to test the Kalman filter in basins with more complete flow data, possibly attempting to access the Federal Electric Commission's flow database. Although access to this database is not free, unlike the National Water Commission's *BANDAS* database.

Conclusions

The streamflow forecast with the ARX + DKF was satisfactorily implemented for the Turbio River basin for the years 2003 and 2004. The results obtained demonstrated that the forecasts performed with one-step ahead (L = 1), or a 24-hour lead time, had a better fit than those with 2, 3 and 4 time steps (48, 72 and 96-hour lead time) in terms of the Nash Sutcliffe, MSE and RMSE.

The periods prior to the calibration are important to the ARX+DKF model's methodology, to improve its forecast over time,

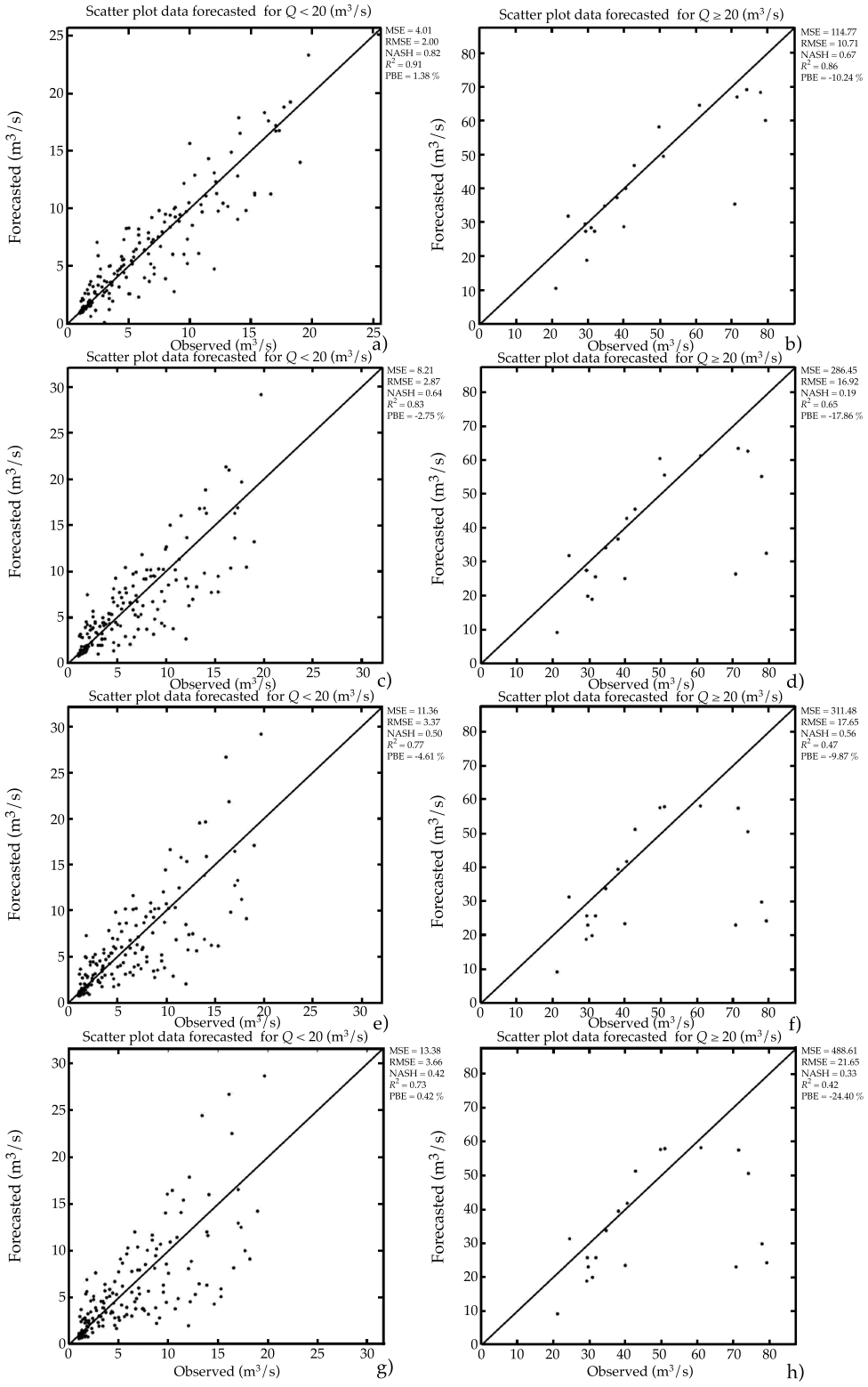

Figure 12. Scatter plots grouped for forecasts with different time steps using using data from the year 2004.

Table 8. Statistical summary for forecasts grouped by different time steps using data from the year 2004.

Forecasts	Range	MSE	RMSE	R^2	Nash-Sutcliffe	PB
$L = 1$ 24 h	$Q < 20$ m³/s	4.01	2.00	0.91	0.82	-1.38
	$Q \geq 20$ m³/s	114.77	10.71	0.86	0.67	-10.24
$L = 2$ 48 h	$Q < 20$ m³/s	8.21	2.87	0.83	0.64	-2.75
	$Q \geq 20$ m³/s	286.45	16.92	0.65	0.19	-17.86
$L = 3$ 72 h	$Q < 20$ m³/s	11.36	3.37	0.77	0.50	-4.61
	$Q \geq 20$ m³/s	468.61	21.65	0.42	-0.33	-24.40
$L = 4$ 96 h	$Q < 20$ m³/s	13.38	3.66	0.73	0.42	-6.41
	$Q \geq 20$ m³/s	468.61	21.65	0.42	-0.33	-24.40

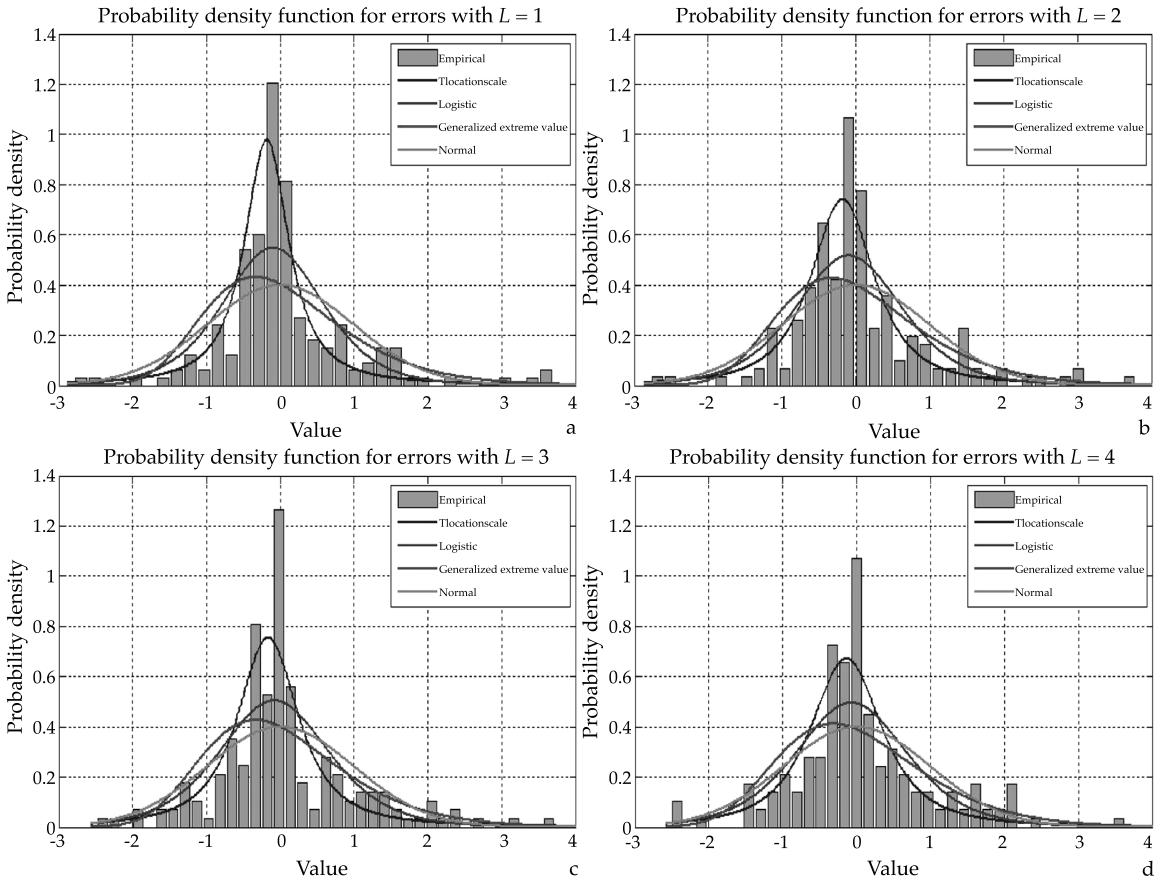

Figure 13. Probability distribution functions for forecasting errors obtained with 24, 48, 72 and 96-hour lead times in the Turbio River basin for the series from the year 2004.

given that the response function in the basin can vary based on the periods of the hydrological cycle or the presence of considerable meteorological events.

The forecasting errors related to the two series evaluated did not fit a normal distribution, which theoretically would be present, but rather the presence of atypical data

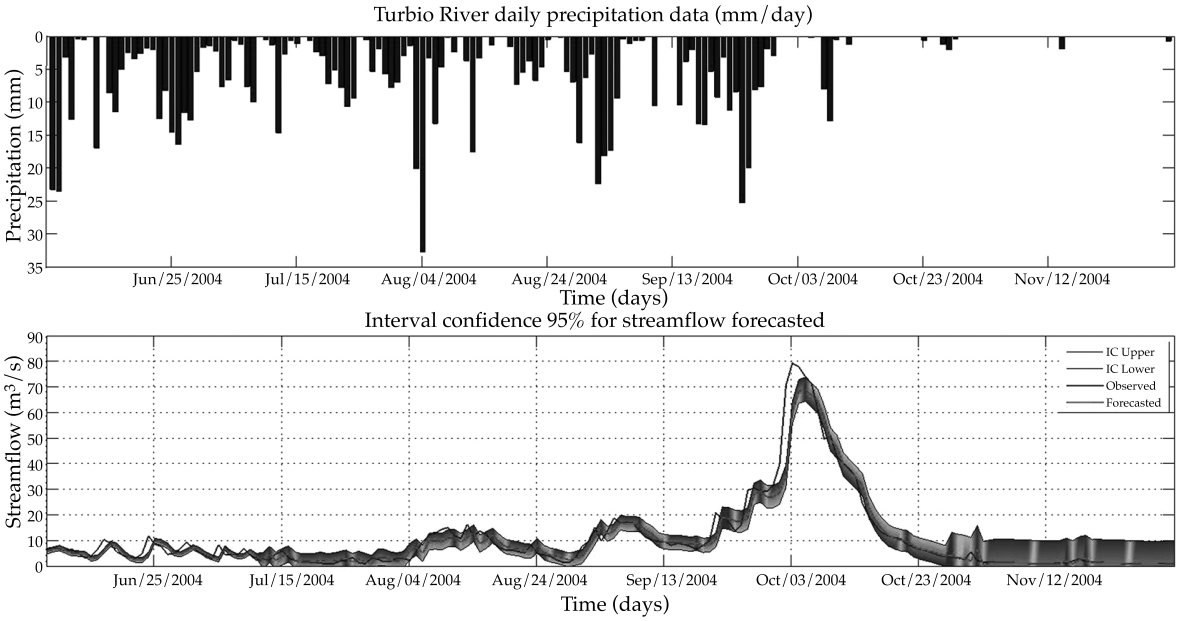

Figure 14. Prediction interval at a 95% probability for $L = 1$ or 24-hour lead time in the Turbio River basin for the 2004 series..

attributed to the quality of the information generated distributions with heavy weights, corresponding to the student-*t* distribution.

It can be difficult to implement techniques such as the Kalman filter for streamflow forecasting in basins with very poor or deficient instrumentation if the measurement of flow is not continuous or does not exist, or the quality of the registries are poor or short-term. In fact, this is why this work in the Turbio River basin implemented the Kalman filter based on the years 2003 and 2004.

Future works could (a) include antecedent moisture as an exogenous variable for the Kalman filter and (b) apply the Kalman filter in basins containing instruments belonging to the Federal Electric Commission, where the continuity and quality of the registries may be more complete than those from the *BANDAS* database.

References

Abaza, M., Anctil, F., Fortin, V., & Turcotte, R. (2014). Sequential Streamflow Assimilation for Short-Term Hydrological Ensemble Forecasting. *Journal of Hydrology, 519*, 2692-2706.

Box, G. E., Jenkins, G. M., & Reinsel, G. C. (2013). *Time Series Analysis: Forecasting and Control* (746 pp) (4th edition). New Jersey: John Wiley & Sons.

Chatfield, C. (2001). Prediction Intervals for Time-Series Forecasting (475-494 pp). In *Principles of Forecasting*. Philadelphia, USA: Springer US.

Chatfield, C. (2004). *The Analysis of Time Series: An Introduction* (313 pp) (6th edition). Florida: Chapman & Hall/CRC Press.

Conagua (2014a). *Banco Nacional de Aguas Superficiales, BANDAS*. México, DF: Comisión Nacional del Agua. Recuperado de ftp://ftp.conagua.gob.mx/bandas/bases_datos_bandas.

Conagua (2014b). *Sistema de Seguridad de Presas*. México, DF: Comisión Nacional del Agua Recuperado de: http://www.conagua.gob.mx/atlas/.

Gelb, A. (1974). *Applied Optimal Estimation*. Massachusetts: MIT Press. (374 pp).

Gupta, H. V., Kling, H., Yilmaz, K., & Martinez, G. F. (2009). Decomposition of the Mean Squared Error and NSE Performance Criteria: Implications for Improving Hydrological Modelling. *Journal of Hydrology*, *377*, 80-91.

Hsu, K. L., Moradkhani, H., & Sorooshian, S. (2009). A Sequential Bayesian Approach for Hydrologic Model Selection and Prediction. *Water Resources Research*, *45*(12)., 1-15. W00B12, doi:10.1029/2008WR006824.

Hirpa, F. A., Hopson, T. M., De Groeve, T., Brakenridge, G. R., Gebremichael, M., & Restrepo, P. J. (2013). Upstream Satellite Remote Sensing for River Discharge Forecasting: Application to Major Rivers in South Asia. *Remote Sensing of Environment*, *131*, 140-151.

IPCC (2007). *Cambio climático 2007: Informe de síntesis* (104 pp.). R. K. Pachauri & A. Reisinger (directores de la publicación). Contribución de los Grupos de Trabajo I, II y III al Cuarto Informe de Evaluación del Grupo Intergubernamental de Expertos sobre el Cambio Climático. Ginebra: IPCC.

Kalman, R. E. (1960). A New Approach to Linear Filtering and Prediction Problems. *Journal of Fluids Engineering*, *82*(1), 35-45.

Kim, P. (2011). *Kalman Filter for Beginners: with Matlab Examples* (232 pp.). Seoul, Korea: CreateSpace.

Kim, S., Tachikawa, Y., & Takara, K. (2004). *Embedding Kalman Filter into a Distributed Hydrological Model* (pp. 21-25). IHP Conference (with WSUD), Adelaide, Australia, November, 21-26.

Lee, Y. H., & Singh, V. (1998). Application of the Kalman Filter to the Nash Model. *Hydrological Processes*, *12*(5), 755-767.

Li, Y., Ryu, D., Western, A. W., & Wang, Q. J. (2015). Assimilation of Stream Discharge for Flood Forecasting: Updating a Semidistributed Model with an Integrated Data Assimilation Scheme. *Water Resources Research*, *51*(5), 3238-3258. doi: 10.1002/2014WR016667.

Liu, J., Wang, J., Pan, S., Tang, K., Li, C., & Han, D. (2015). A Real-Time Flood Forecasting System with Dual Updating of the NWP Rainfall and the River Flow. *Natural Hazards*, *77*(2), 1161-1182.

Liu, Y., Weerts, A. H., Clark, M., Hendricks-Franssen, H. J., Kumar, S., Moradkhani, H., & Restrepo, P. (2012). Advancing Data Assimilation in Operational Hydrologic Forecasting: Progresses, Challenges, and Emerging Opportunities. *Hydrology and Earth System Sciences*, *16*(10), 105-119.

Lü, H., Hou, T., Horton, R., Zhu, Y., Chen, X., Jia, Y., Wang, W. & Fu, X. (2013). The Streamflow Estimation Using the Xinanjiang Rainfall Runoff Model and Dual State-Parameter Estimation Method. *Journal of Hydrology*, *480*, 102-114.

Matlab® R2013b. MathWorks, Inc.

McCuen, R. H. (2005). *Hydrologic Analysis and Design* (859 pp) (3rd edition). Upper Saddle, USA: Prentice Hall PTR.

Mendoza, V. M., Villanueva, E. E., Garduño, R., Nava, Y., Santisteban, G., Mendoza, A. S., Oda B., & Adem, J. (2009). Thermo-Hydrological Modelling of the Climate Change Effect on Water Availability in Two Hydrologic Regions of Mexico. *International Journal of Climatology*, *29*, 1131-1153.

Montero-Martínez, M. J., Ojeda-Bustamante, W., Santana-Sepúlveda, J. S., Prieto-González, R., & Lobato-Sánchez, R. (abril-junio, 2013). Sistema de consulta de proyecciones regionalizadas de cambio climático para México. *Tecnología y Ciencias del Agua, 4(2),* 113-128.

Moradkhani, H., DeChant, C. M., & Sorooshian, S. (2012). Evolution of Ensemble Data Assimilation for Uncertainty Quantification Using the Particle Filter-Markov Chain Monte Carlo Method. *Water Resources Research*, *48*(12), 1-13. 41:W05012, doi: 10.1029/2004WR003604.

Moradkhani, H., Sorooshian, S., Gupta, H. V., & Houser, P. R. (2005). Dual State-Parameter Estimation of Hydrological Models Using Ensemble Kalman Filter. *Advances in Water Resources*, *28*(2), 135-147.

Mood, A., Graybill, F., & Boes, D. (1974). *Introduction to the Theory of Statistics* (229 pp) (3rd edition). Singapore: McGraw-Hill.

Morales-Velázquez, M. I., Aparicio, J., & Valdés, J. B. (2014). Pronóstico de avenidas utilizando el Filtro de Kalman Discreto. *Tecnología y Ciencias del Agua, 5*(2), 85-110.

Nash, J. E., & Sutcliffe, J. V. (1970). River Flow Forecasting through Conceptual Models Part I. A Discussion of Principles. *Journal of Hydrology*, *10*, 282-290.

Perevochtchikova, M. (2013). Retos de la información del agua en México para una mejor gestión. Realidad, Datos y Espacio. *Revista Internacional de Estadística y Geografía*, *4*(1), 42-57.

Protección Civil Guanajuato (2012). Recuperado de: http://proteccioncivil.guanajuato.gob.mx/atlas/hidrometeorologico/hidro_cuenca_turbio.php.

Ramírez, Á. S. (2003). *El Filtro de Kalman*. Nota técnica. Banco Central de Costa Rica, División Económica, Departamento de Investigaciones Económicas.

Salas, J. D., Delleur, J. W., Yevjevich, V., & Lane, W. L. (1980). *Applied Modeling of Hydrologic Time Series* (484 pp). Colorado, USA: Highlands, Co., Water Resources Publications.

Samuel, J., Coulibaly, P., Dumedah, G., & Moradkhani, H. (2014). Assessing Model State and Forecasts Variation in Hydrologic Data Assimilation. *Journal of Hydrology*, *513*, 127-141.

SMN (2014). *Sistema de Información Climática Computarizada CLICOM*. México, DF: Servicio Meteorológico Nacional.

Simon, D. (2001). Kalman filtering. *Embedded Systems Programming*, *14*(6), 72-79.

Shi, Y., Davis, K. J., Zhang, F., Duffy, C. J., & Yu, X. (2014). Parameter Estimation of a Physically Based Land Surface Hydrologic Model Using the Ensemble Kalman Filter: A Synthetic Experiment. *Water Resources Research*, *50*(1), 706-724.

Valdés, J. B., Mejía-Velázquez, J. M., & Rodríguez-Iturbe, I. (1980). *Filtros de Kalman en la hidrología: predicción de descargas fluviales para la operación óptima de embalses*. Informe Técnico No. 80-2. Caracas: Universidad Simón Bolívar, Decanato de Estudios de Posgrado, Posgrado en Planificación e Ingeniería de Recursos Hídricos.

Welch, G., & Bishop, G. (2006). *An Introduction to the Kalman Filter*. Chapel Hill: University of North Carolina at Chapel Hill.

WMO (2009). *WMO Report No 168. Guide to hydrological practices volume II: Management of water resources and application of hydrological practices*. Geneva: World Meteorological Organization.

Xie, X., & Zhang, D. (2010). Data Assimilation for Distributed Hydrological Catchment Modeling Via Ensemble Kalman Filter. *Advances in Water Resources*, *33*(6), 678-690.

Yucel, I., Onen, A., Yilmaz, K. K., & Gochis, D. J. (2015). Calibration and Evaluation of a Flood Forecasting System: Utility of Numerical Weather Prediction Model, Data Assimilation and Satellite-Based Rainfall. *Journal of Hydrology*, *523*, 49-66.

Institutional Address of the Authors

M.I. Fernando González Leiva
Dra. Laura Alicia Ibáñez Castillo
Dr. Mario Alberto Vázquez Peña
Dr. Agustín Ruiz García

Posgrado en Ingeniería Agrícola y Uso Integral del Agua
Universidad Autónoma Chapingo
Km. 38.5 carretera México-Texcoco
56230 Chapingo, Estado de México, México
Teléfono: +52 (595) 9521 551
fernando.gleiva@gmail.com
libacas@gmail.com
mvazquezp@correo.chapingo.mx
agustinruizg@gmail.com

Dr. Juan B. Valdés

The University of Arizona at Tucson
Hydrology and Water Resources
United States of America
1133 James E. Rogers
Harshbarger Bldg. Room 318E
Tucson AZ 85721, USA
jvaldes@email.arizona.edu

Hydraulic Similitude among the High Andean Hydrological Systems and Transfer of Hydrometeorological Information

• Oswaldo Ortiz-Vera* •
Universidad Nacional Agraria La Molina, Perú
*Corresponding Author

Abstract

Ortiz-Vera, O. (July-August, 2015). Hydraulic Similitude among the High Andean Hydrological Systems and Transfer of Hydrometeorological Information. *Water Technology and Sciences* (in Spanish), 6(4), 25-44.

The objective of this work was to determine the laws governing hydraulic similitude among the high Andean hydrological systems. To this end, dimensionless hydrological parameters and physical hydraulic models play an important role. The study finds that the Gravelius index, the convergence ratio and the orographic coefficient are necessary and sufficient conditions to determine hydraulic similitude. The parameters obtained from the dimensionless analysis along with conditions of similarity enable exchanging information among similar hydrological systems. Given the dimensionless morphometry on which this methodology is based, its application can be generalized to hydrological systems in other regions, among regions within countries as well as internationally.

Keywords: Andean hydrological systems, hydraulic similarity, transfer, hydrometeorological information.

Resumen

Ortiz-Vera, O. (julio-agosto, 2015). Similitud hidráulica de sistemas hidrológicos altoandinos y transferencia de información hidrometeorológica. Tecnología y Ciencias del Agua, *6(4), 25-44.*

El objeto de este estudio fue determinar las leyes que rigen la similitud hidráulica entre sistemas hidrológicos altoandinos. Para ello, los parámetros adimensionales en hidrología, al igual que en hidráulica de modelos físicos, jugaron papel preponderante. Se encontró que los parámetros índice Gravelius, relación de confluencias y coeficiente orográfico, son condiciones necesarias y suficientes para una aproximación de similitud hidráulica. Los parámetros obtenidos mediante análisis dimensional, unidos a las condiciones de semejanza, permite intercambiar información entre sistemas hidrológicos similares. La morfometría adimensional en la que se sustenta esta metodología permite generalizar su aplicación a sistemas hidrológicos de otra región o interregiones subnacionales e internacionales.

***Palabras clave**: sistemas hidrológicos altoandinos, similitud hidráulica, transferencia, información hidrometeorológica.*

Received: 26/09/2014
Accepted: 14/04/2015

Introduction

Hydrometeorological information is generally scarce, and particularly runoff information which serves as the basis of every hydraulic project. The greatest difficulties are obviously experienced by developing countries (Jimenez & Farías, 2005). The lack or scarcity of hydrometric and sedimentological information in basins prevents conducting consistent regional analyses, creating problems for planning, designing and operating hydraulic projects (Jimenez & Farías, 2005; ICOLD, 2008). This situation requires a continued search for simple methodologies that enable generating enough local information with good enough quality for practical purposes. This is achieved using approximation criteria for hydraulic similitude among systems.

The study of similitude between a model and a prototype, with sufficient operations of the scale model, has made it possible to

build large engineering works that have contributed to the development of humanity (Sotelo-Ávila, 1977; Rodríguez Díaz, 2001). Nevertheless, man is the author of all this, and has not been able to obtain an exact similitude between model and prototype. Even so, transferring the results from the model to the prototype has been sufficient to solve a large number of problems encountered in actual situations (Streeter & Wilie, 2000; Vergara, 1993; Sotelo-Ávila, 1977; Rodríguez Díaz, 2001). This inspired the development of the present work which consists of identifying natural hydrological systems with hydraulic similitude, whose conditions can be used to transfer information from one system to another similar system (Streeter & Wilie, 2000; Vergara, 1993; Sotelo-Ávila, 1977; Rodríguez Díaz, 2001). In the marvelous setting of nature, over millions of years, something similar to what man typically does artificially has occurred in terms of similitude. Through the natural dynamic actions of recurring causes and effects in intrinsically similar natural systems, hydrological systems that are similar to each other have been created.

The objective of the present work is to develop a methodological basis that enables identifying similar hydrological systems using dimensionless parameters as indications of geometric, kinematic and dynamic similitude. Based on the principle of hydraulic similitude, these similitude parameters, and others that can be dimensionally deduced from physical phenomena occurring in a basin, are converted into functions to transfer information among similar hydrological systems in the high Andes region (Streeter & Wilie, 2000; Vergara, 1993; SoteloÁvila, 1977; Rodríguez Díaz, 2001).

The application of the methodology is limited to the high Andes region where the area receiving precipitation coincides with the collector area and where precipitation is the most important and only input variable in the system. The fact that the basins in the high Andes are the hydrological units which are territorially farthest from the hydrographic system also makes this area most affected by the availability of information (Jimenez & Farías, 2005; Rocha, 2006).

The results from this investigation will certainly be used by the Peru Ministry of the Environment, through research centers in sectors pertaining to the National Water Authority and National Weather and Hydrology Service, as well as national and international institutions involved in research about global climate change.

Methodology

Study Area

The study area consists of a sample of 70 micro-basins in the high Andes, all located in the Department of Cajamarca, in northern Peru, where the Andes mountain range creates a very steep and irregular topography with sheer cliffs and narrow inter-Andean valleys. The result is a large variety of ecological floors with an impressive amount of biodiversity corresponding to each microclimate. All the hydrological units are located between 1 500 and 4 200 masl, where the annual mean temperatures range from 9° C (highest zones) to 25° C (lowest zones), and annual mean precipitation ranges from 400 to 1 200 mm/year. Many of these micro-basins, which are regulated by small dams, served as the basis of the development of agriculture in the inter-Andean valleys, having supported large pre-Incan populations.

Dimensional Analysis of the Hydrological Systems

The most significant physical phenomenon in the high Andes basins is precipitation-runoff, which are cause and effect variables, respectively, where precipitation depends on the climatic characteristics and runoff on the nature of each micro-basin (Chow, 1993). In simple terms, if real evapotranspiration is dis-

regarded, the simplified phenomenon can be represented by the variables shown in Table 1.

The variables are grouped by dimensionless parameters by applying the Pi theorem by Vaschy-Buckingham (Streeter & Wilie, 2000; Sotelo-Ávila, 1977; Rodríguez Díaz, 2001). As a result of this analysis, physical laws that govern the high Andes hydrological systems were obtained, represented by the dimensionless parameters shown in equations (1), (2), (3), (4) and (5):

$$\pi_1 = \frac{Q}{AP} \quad (1)$$

$$\pi_2 = \frac{H}{\sqrt{A}} \quad (2)$$

$$\pi_3 = \frac{I * t}{H} \quad (3)$$

$$\pi_4 = \frac{Q}{I * A} \quad (4)$$

$$\pi_5 = \frac{p}{\sqrt{A}} \quad (5)$$

where:

π = dimensionless parameter.
Q = runoff flow.
A = projection of the receptor-collector area on the horizontal plane.
P = pluviometric precipitation.
H = mean height above sea level.
I = intensity of precipitation.
t = duration of intense precipitation.
p = perimeter of the basin.

Disregarding real evapotranspiration in this analysis can be justified because the duration of storms are relatively short. For longer periods, the hydrological balances should include this component or include it as decreases in the runoff coefficients (Chow, 1993; Aparicio, 1997).

Dimensionless Geometric Similitude Parameter

This is given by the dimensionless parameter shown in equation (5), where multiplying both sides by 0.28 results in the Gravelius index ($Kc = 0.28^* \pi_5$) presented in equation (6). This dimensionless parameter is obtained by the relation of the perimeter of a basin to the perimeter of an imaginary circle with the same area as the basin (Askoa-Ibizate, 2004; Docampo, De Vikeña, Rico, & Rallo, 2009; Gravelius, 1914).

$$K_c = 0.28\frac{p}{\sqrt{A}} \quad (6)$$

The Gravelius index influences the configuration of the surface drainage network and the geometry of the direct runoff hydrograph,

Table 1. Variables and dimensions of precipitation-runoff.

Main variables of precipitation-runoff	
Variable	**Dimension**
1. Pluvial precipitation: *P*	LT^{-1}
2. Intensity of pluvial precipitation: *I*	LT^{-1}
3. Duration of rainfall: *t*	T
4. Projection of the receptor-collector area: *A*	L^2
5. Height above sea level: *H*	L
6. Runoff flow: *Q*	L^3T^{-1}
7. Perimeter of the basin: *p*	L

and thus influences the magnitude of peak flows (Senciales, 2005; Askoa-Ibizate, 2004; Docampo, De Vikeña, Rico, & Rallo, 2009; Antigüedad, 1980; Gaspari *et al*., 2012). In addition, the ranges of this parameter have been very useful to classify basins according to their geometry, such as those shown in Table 2 (Henaos, 1988). Because this parameter most efficiently describes the shape of a basin, it is a good reference for the geometric similitude among hydrological systems.

As an analogy, from the hydraulics from physical models it can be inferred that two or more hydrological systems are geometrically equal if they have the same Gravelius index. It is worth mentioning that the term "equal" does not have a mathematical connotation but simply refers to "hydrological equality" which for practical purposes, as in statistics, is accepted based on a particular level of valid approximation.

Oval micro-basins more quickly concentrate surface flows, generating sudden and violent peaks and rapid recessions resulting from extreme storms. Unlike the behavior of elongated basins, these characteristics favor direct runoff and hydric erosion to the determinant of aquifer recharge (Ibáñez, Moreno, & Gisberbert, 2005; Docampo, De Vikeña, Rico, & Rallo, 2009; Antigüedad, 1980; Gaspari *et al*., 2012; Gaspari, 2002; Martínez, 1986).

Dimensionless Instantaneous Runoff Parameter

This is given by the dimensionless parameter in equation (4), where by substituting the left side with the direct runoff coefficient ($\pi_4 = C$) it is converted into the equation representing the old Rational method (7). This methodology is simple but still valid for estimating peak discharges (hydrograph peaks) based on precipitation data (Chow, 1993; Aparicio, 1997):

$$Q_{max} = CIA \qquad (7)$$

where:

Q_{max} = peak direct runoff flow.
C = runoff coefficient.
I = maximum precipitation intensity inherent in the concentration time of the basin.
A = receptor-collector area projected on the horizontal plane.

Dimensionless Sustained Runoff Parameter

This is given by equation (1), which is converted into equation (8) when substituting the left side with an average coefficient ($K = \pi_1$). This expression can be used to determine average multi-annual runoff flows which involves direct runoff and underground components (Chow, 1993; Universidad Nacional de Colombia-Sede Medellín, s.f.; Aparicio, 1997):

$$Q = K A P \qquad (8)$$

where:

Q = average flow during the study period.
A = area of the precipitation receptor-collector basin.
P = "Effective precipitation" during the study period.

Table 2. Standard shapes of basins based on the Gravelius index.

Shapes of hydrological systems based on the Gravelius coefficient		
Geometric Class	**Class Range**	**Shape of Basin**
K_{c1}	$1 < K_C \leq 1.25$	Round oval
K_{c2}	$1.25 < K_C \leq 1.50$	Oblong oval
K_{c3}	$1.50 < K_C \leq 1.75$	Elongated oblong

K = Runoff coefficient.

In terms of "effective precipitation," since this deals with longer periods it obviously includes losses from real evapotranspiration and storage in the soil.

Dimensionless Orographic Parameter and Dynamic Similitude

This is represented by equation (2), where squaring both sides results in the dimensionless parameter shown in equation (9), known as the orographic coefficient, C_O ($\pi^2_2 = C_O$), a parameter associated with the gravitational forces of surface flows and, therefore, with potential hydric erosion and the generation of hydraulic energy (Henaos, 1988):

$$C_o = \frac{H^2}{A} \qquad (9)$$

The high Andes systems with their steep topography and high altitudes have very high orographic coefficients, which is indicative of a large erosive capacity and sediment transport (Henaos, 1988). Therefore, this parameter is considered to serve as a good reference for dynamic similitude.

As an analogy, from the hydraulics of physical models it can be inferred that two or more hydrological systems in the high Andes have dynamic similitude if they have equal orographic coefficients, where "equal" has the same meaning as for geometric similitude.

Parameter for the Average Convergence Ratio and Kinematic Similitude

This dimensionless parameter, also influenced by the Gravelius index, describes the spatial or geometric configuration of the drainage network and expresses the degree of ramifications in the network (Askoa-Ibizate, 2004; Docampo, De Vikeña, Rico, & Rallo, 2009; Antigüedad, 1980; Cruz-Santillán, & Tamés, 1983; Horton, 1945; Gaspari, 2002). It is quantified by applying equations (10) and (11), prior to which the surface drainage network needs to be categorized. The Horton methodology is preferred for this purpose (Antigüedad, 1980; Cruz-Santillán, & Tamés, 1983; Gaspari *et al*., 2012; Gravelius, 1914; Gaspari, 2002; Martínez, 1986).

Because of the influence of the spatial configuration of the drainage network, the average convergence ratio is considered to be a good reference for the kinematic similitude among the hydrological systems:

$$r_c = \frac{n_i}{n_{i+1}} \qquad (10)$$

$$R_C = \frac{1}{n}\sum_{1}^{n} r_{ci} \qquad (11)$$

Where:

r_c = partial convergence ratio.
n_i = number of natural courses of order i.
n_{i+1} = number of courses of order immediately higher than i (i = 1, 2, 3,...., N-1).
N = order number of the basin.
r_{ci} = each of the partial "n" values.
R_C = average convergence ratio.

As an analogy, from the model and the prototype it can be inferred that two hydrological systems have kinetic similitude if their average convergence ratio is equal, where "equal" has the same meaning as for the previous two cases.

Dimensionless Rainfall Parameter

This parameter is given by equation (3) and describes the characteristics of the pluviometric precipitation in the basin as a variable with a spatial and temporal distribution. The most

intense periods are observed during short time periods and at higher altitudes above sea level, and vice versa (Chow, 1993; Aparicio, 1997). This is very important to the generation of maximum runoff (peak flows) based on precipitation data, and it also explains why precipitation in the high Andean basins is dependent on the height above sea level.

Hydraulic Similitude of Hydrological Systems

As an analogy, from the hydraulics of physical scale models, two or more high Andes hydrological systems are similar if they simultaneously meet the conditions for geometric, kinematic and dynamic similitude, with the particular level of approximation adopted previously.

Dimensionless Transfer Parameters

After the hydraulic similitude of the systems has been determined, all the dimensionless parameters that control the laws of the phenomenon studied (equations (1), (2), (3), (4) and (5)) are converted into transfer functions, based on the parameter in which the variable of interest is located (Streeter & Wilie, 2000; Sotelo-Ávila, 1977; Rodríguez Díaz, 2001).

Sometimes, in order to improve the quality of the transfer, parameters can be combined to obtain another dimensionless parameter (or parameters) with a larger number of variables. For example, the dimensionless parameter shown in equation (12) is the result of combining equations (1) and (2), which is very important for runoff transfer (Streeter & Wilie, 2000; Sotelo-Ávila, 1977; Rodríguez Díaz, 2001).

$$\pi_{12} = \frac{QH}{A^{3/2}P} \tag{12}$$

Appling the similitude principle for a pair of origin and destination basins, the dimensionless parameter shown in equation (12) is as shown in equation (13), or its equivalent (15), as a function of scales (Streeter & Wilie, 2000; Sotelo-Ávila, 1977; Rodríguez Díaz, 2001):

$$\frac{Q_o H_o}{A_o^{3/2} P_o} = \frac{Q_d H_d}{A_d^{3/2} P_d} \tag{13}$$

The sub-indices of the variables in the left and right sides of this equation correspond to origin and destination systems, respectively:

$$Q_d = \left(\frac{H_o}{H_d}\right)\left(\frac{P_d}{P_o}\right)\left(\frac{A_d}{A_o}\right)^{3/2} Q_o \tag{14}$$

$$Q_d = H_e^{-1} P_e A_e^{3/2} Q_o \tag{15}$$

Where:

H_e = height scale.
P_e = precipitation scale.
A_e = area scale.
Q_o = total flow in the basin of origin.
Q_d = total flow transferred to the destination basin.

Another variable that is scarce is the intensity of maximum storms, whose transfer function is obtained from equation (3), which using the similitude principle is converted into equation (16) or its equivalent (17), as a function of scales:

$$\frac{I_o t_o}{H_o} = \frac{I_d t_d}{H_d} \tag{16}$$

$$I_d = \left(\frac{H_d}{H_o}\right)\left(\frac{t_o}{t_d}\right) I_o = H_e t_e^{-1} I_o \tag{17}$$

Where:

I_d = intensity of precipitation in the destination basin.
I_o = intensity of precipitation in the basin of origin.
t_e = scale of durations.

H_e = scale of heights.

Sample of Micro-basins in the Cajamarca High Andes Region

Seventy micro-basins in the Cajamarca-Peru region of the high Andes were selected (Table 3). They were located at the head of the Pacific and Atlantic watersheds at over 1 500 masl. In order to control errors and the costs of the present study, the following protocol was established.

- Use of cartographic maps at the same scale, 1/100 000.
- Cartographic maps developed by the same institution (IGN, Peru) to ensure that the same criteria were used to generate them.
- Processing of cartographic information using the same methodology for each case (boundary of the basin, area, perimeter, altitude, hierarchy of the drainage network, etc.). The use of 3D digital altitude models and GIS procedures are preferred.
- The variables involved in the dimensionless similitude parameters were estimated using the same methodology for each case. The Varignon statistical method of moments was used to determine the mean altitude above sea level, given by equation (18) (Chow, 1993; Aparicio, 1997):

$$\bar{H} = \frac{1}{A}\sum_{A}\Delta A_i \bar{h}_i \qquad (18)$$

Where:

$\bar{H}$ = mean height above sea level.
A = area of the basin.
ΔA_i = partial area between consecutive level curves.
$\bar{h}_i$ = average of the heights of the two level curves that bound each partial area.

The partial areas between the level curves corresponding to the study basin were divided according to the topography, generally between master curves (Chow, 1993).

Table 3. Similarity parameters among hydrological units in the high Andes region of Cajamarca, Peru.

Dimensionless hydraulic similarity parameters for micro-basins in the high Andes Cajamarca-Peru region (Scale 1/100 000)						
Micro-basin	***A*** **(km²)**	***N***	K_c	R_c	C_o (%)	**Watershed**
1. Grande1 River	72.50	3	1.27	2.70	8.22	Atlantic
2. Tallal Qda.	14.00	2	1.23	2.68	44.6	Pacific
3. Quismache River	183.80	4	1.24	2.74	2.90	Atlantic
4. Grande2 River	456.50	4	1.27	2.75	2.68	Pacific
5. Cospán River	196.50	4	1.28	2.56	4.40	Pacific
6. Porcón River	81.60	3	1.16	1.88	11.03	Atlantic
7. La Leche River	116.50	3	1.16	1.90	12.04	Atlantic
8. Huagayoc River	12.50	2	1.15	1.85	72.02	Atlantic
9. Ronquillo River	36.80	3	1.12	1.93	22.85	Atlantic
10. Mashcón River	276.10	4	1.31	3.45	1.88	Atlantic
11. Chonta River	352.80	4	1.32	3.73	1.55	Atlantic
12. Huertas Qda.	105.50	3	1.34	2.98	3.87	Pacific
13. Chausis Qda.	207.30	4	1.38	2.67	3.80	Pacific
14. Llaucán River	595.00	4	1.41	2.55	0.89	Atlantic

Table 3 (continuation). Similarity parameters among hydrological units in the high Andes region of Cajamarca, Peru. (Scale 1/100 000).

Micro-basin	A (km²)	N	$K_{c1,5258}$	R_c	C_o (%)	Watershed
15. Cascasén River	114.20	4	1.42	3.12	6.88	Atlantic
16. Azufre River	45.00	2	1.45	3.13	7.22	Atlantic
17. Poclush River	882.50	5	1.56	3.20	4.82	Pacific
18. Rejo River*	201.40	4	1.58	3.16	4.93	Pacific
19. San Juan-1 River	271.20	4	1.60	3.89	5.55	Pacific
20. Onda Qda.	130.00	3	1.60	3.52	4.81	Atlantic
21. Magdalena River	807.20	4	1.70	4.60	3.98	Pacific
22. Naranjo River	51.40	2	1.70	1.50	23.00	Pacific
23. San Miguel River	1 047.20	5	1.53	5.89	0.90	Pacific
24. San Pablo River	182.43	3	1.29	4.20	3.26	Pacific
25. Chetillano River	180.10	4	1.42	4.10	4.40	Pacific
26. San Juan-2 River	638.43	4	1.21	4.35	1.16	Pacific
27. Qda. Chantilla	94.49	3	1.31	3.25	6.51	Pacific
28. Pallac River	235.28	4	1.34	3.23	2.38	Pacific
29. Contumazá River	198.40	4	1.72	4.20	3.90	Pacific
30. La Bamba Qda.	52.21	2	1.73	4.00	4.03	Pacific
31. Chiminote Qda.	200.76	4	1.36	2.83	1.90	Pacific
32. Nazario Qda.	30.90	2	1.19	2.00	8.32	Pacific
33. La Ramada	19.14	2	1.18	1.00	8.64	Pacific
34. Del Chorro Qda.	19.63	2	1.68	1.00	19.11	Pacific
35. Cajón Qda.	22.15	2	1.17	1.00	4.06	Pacific
36. La Ramada Qda.	34.67	2	1.33	3.00	3.00	Pacific
37. LLapa River	210.32	4	1.57	3.13	5.43	Pacific
38. Honda Qda.	110.20	3	1.76	3.90	11.21	Pacific
39. Tumbadén River	309.30	4	1.37	3.56	3.71	Pacific
40. El Cardo Qda.	29.92	3	1.26	1.76	17.63	Pacific
41. Yamulán Qda.	59.85	3	1.23	2.25	12.27	Pacific
42. Chorro Blanco Qda.	36.83	3	1.46	1.75	27.13	Pacific
43. El Carrizo River	111.64	4	1.39	2.72	9.50	Pacific
44. Qda. Amillas	31.18	2	1.41	1.00	23.76	Pacific
45. Qda. Del Qilengo	30.75	2	1.43	2.00	23.51	Pacific
46. San Juan-3 River	204.35	4	1.72	3.89	4.07	Pacific
47. Asunción River	76.47	3	1.24	2.34	10.10	Pacific
48. Pinche River	21.03	2	1.34	1.00	32.35	Pacific
49. Qda Quinuas	65.38	2	1.49	7.00	11.94	Pacific
50. Yaucán River	49.91	2	1.37	3.00	15.97	Pacific
51. Qda. Tallal	19.50	2	1.43	1.00	36.88	Pacific
52. Namora River	475.70	4	1.43	4.42	2.50	Atlantic
53. Huacraruco River	136.90	4	1.29	3.83	8.51	Pacific
54. Muyoc River	319.26	4	1.41	3.38	3.28	Atlantic
55. Llantén River	401.70	4	1.26	2.57	2.49	Atlantic
56. Sanagorán River	608.10	4	1.42	4.35	2.03	Atlantic

Table 3 (continuation). Similarity parameters among hydrological units in the high Andes region of Cajamarca, Peru. (Scale 1/100 000).

Micro-basin	A (km^2)	N	$K_{c1,5258}$	R_c	C_o (%)	Watershed
57. Cañad River	249.20	4	1.40	3.22	2.70	Pacific
58. Pencayoc Qda.	243.4	4	1.49	4.50	4.65	Pacific
59. Puerto Blanco River	247.50	4	1.43	3.79	2.32	Atlantic
60. Chanta River	97.20	3	1.40	3.73	4.40	Pacific
61. Callayuc River	346.74	4	1.42	3.92	2.96	Atlántico
62. Llantén River	298.78	4	1.32	3.49	3.73	Pacific
63. El Sauce River	170.00	3	1.44	4.17	3.43	Atlantic
64. Chilca River	84.87	3	1.46	4.17	13.00	Atlantic
65. Chancayano River	598.04	4	1.48	6.63	1.55	Pacific
66. San Juan-4 River	118.91	3	1.42	3.25	8.93	Atlantic
67. Llaucano River	121.73	3	1.70	2.20	9.90	Atlantic
68. Gansul River	100.37	3	1.32	3.58	8.30	Atlantic
69. San Juan Pampa River	122.42	3	1.36	2.75	8.50	Pacific
70. Jadibamba River	243.45	4	1.49	4.50	4.65	Atlantic
Mean	**1.40**	**3.13**	**9.42**			
Standard Deviation	**0.1587**	**1.2242**	**11.6612**			
Variation coefficient	**0.1133**	**0.3911**	**1.2379**			

N = order of the basin.
*Management model for the pilot basin, Granja Porcon afforestation.

Identification of Micro-Basins with Hydraulic Similitude

The protocol established to identify and recognize the hydrological systems in the high Andes that have hydraulic similitude is summarized by the following activities:

a) Estimation of morphometric hydraulic similitude parameters: Gravelius index, convergence ratio, orographic coefficient.
b) Grouping of micro-basins by geometry using the range criteria from the Graveluis index shown in Table 2. Obviously all the hydrological units in the same range are considered geometrically similar.
c) The hydrological units in each geometric group having the largest discrepancy are excluded, such that the variation coefficient from the Gravelius index, the convergence ratio and the orographic coefficient do not exceed 0.05, 0.20 and 0.30, respectively. This level of approximation, which is accepted in practice, is justified by the level of errors committed when estimating the variables and the effects of scale.
d) The hydrological units that remain after the preceding step represent the micro-basins with hydraulic similitude.

Transfer of Hydrometeorological Information

Hydrological System with Maximum Storm Information

To illustrate the application of the transfer of information using this methodology, the Mashcon River micro-basin was used as the system of origin (Table 9). The National Meteorology and Hydrology Service's Weberbauer rain gauge station is located in the lower part of this basin (07° 10´ S, 78° 30´ W; altitude: 2 536 masl), in the area of the National University of Cajamarca campus. Until recently

this station was the only one of its type in the region with rain gauge registries.

By analyzing the frequency of annual maximum storms based on 50 years of registries and fitting the data to a Gumbel model of extreme variables, the annual maximum storm intensities could be modeled and simulated. Some of the results from these are presented in Table 10 (Chow, 1993; Aparicio, 1997). The procedure for this analysis is not included herein since it is not the objective of the present study, but rather, simply the transfer of information.

Hydrological System without Maximum Storm Information

The Jadibamba River micro-basin (mean altitude 3 218 masl) was selected a priori, but any of the micro-basins with hydraulic similitude and from the same geometric group as the basin of origin could have been selected (see Table 9). This basin, as well as others in the study region, lacks information about maximum storms, which is very important to any surface drainage project and catchment work (drainage of roads, urban rain sewers, protection of coasts, water control dams, irrigation canals, hydroelectric plants, rainwater catchment, flood prevention, etc.)

While the data can be transferred to any point of interest in the hydrological destination system, the point at the mean altitude of the destination basin (3 218 masl) was chosen for illustrative purposes, since there was no particular preference.

Results

Morphometric Dimensionless Hydraulic Similitude Parameters

The results from dimensionless morphometry studies indicate that the sample is quite heterogeneous, where variability can be seen in the variation coefficients of each one of the dimensionless hydraulic similitude parameters shown in Table 3. Here, the Gravelius index shows the least discrepancies, followed by the convergence ratio and the orographic coefficient, which clarifies the order of influence of the geometry of the basin.

The statistics from the Gravelius index — 1.40, 0.1587 and 0.1133 for arithmetic mean, standard deviation and variation coefficient, respectively — are indicators of low variability in the geometric shape and a high predominance of the oblong oval shape (mean $Kc = 1.40$) over the other two geometric shapes (Figure 1).

Meanwhile, the statistics from the sample for the convergence ratio show more variability ($C_v = 39.11\%$) in the configuration of the drainage network, while always coinciding in that the oblong oval shape of the average basin has the most bifurcations.

The extreme case corresponds to the orographic coefficient, whose variability is very high (123.79%), very sensitive to the location of the systems with respect to sea level.

Morphometric Characterization of the Micro-basins

The hydrological units in the sample were classified according to the range criteria in the Gravelius index, shown in Table 2. This resulted in the groups below:

Round Oval Micro-Basins

This group (Table 4) is made up of 12 hydrological units (17.1%), and is characterized by relatively short concentration times, generating leptokurtic outlet hydrographs in which the rise in flow is very sudden and violent, with a high risk of flooding from extreme storms.

Oblong Oval Micro-basins

This geometric group (Table 5), made up of 44 micro-basins (62.9%), has hydrological characteristics very similar to the round oval group, but with slightly less intense responses to extreme storms. This basin geometry is the most common in the study region (Figure 1).

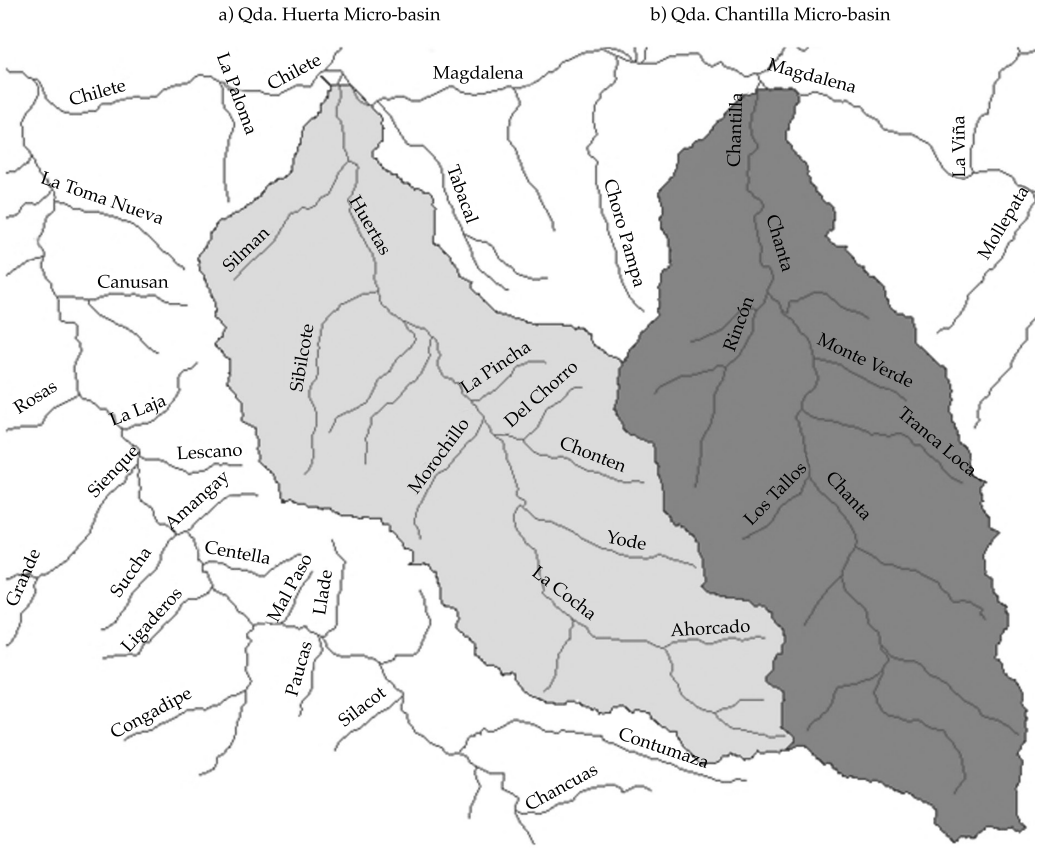

Figure 1. Hydraulic similarity of hydrological systems with an oblong oval shape.

Table 4. Group of micro-basins with a round-oval shape.

Micro-basin	Gravelius Coefficient $1 < K_c \leq 1.25$	Shape of basin
1. Tallal-1 Qda.	1.23	Round oval
2. Quismache River	1.24	Round oval
3. Porcón River	1.16	Round oval
4. La Leche River	1.16	Round oval
5. Hualgayoc River	1.15	Round oval
6. Ronquillo River	1.12	Round oval
7. San Juan-2 River	1.21	Round oval
8. Nazario Qda.	1.19	Round oval
9. La Ramada-1 Qda.	1.18	Round oval
10. Cajón Qda.	1.17	Round oval
11. Yamulán Qda.	1.23	Round oval
12. Asunción River	1.24	Round oval
Mean **Standard Deviation** **Variation Coefficient**	**1.18** **0.0411** **0.0348**	

Table 5. Group of micro-basins with an oblong oval shape.

Micro-basin	Gravelius Coefficient $1.25 < K_c \leq 1.50$	Shape of basin
1. Grande 1 River	1.27	Oblong oval
2. Grande 2 River	1.27	Oblong oval
3. Cospán River	1.28	Oblong oval
4. Mashcón River	1.31	Oblong oval
5. Chonta River	1.32	Oblong oval
6. Huertas Qda.	1.34	Oblong oval
7. Chausís Qda.	1.38	Oblong oval
8. Llaucán River	1.41	Oblong oval
9. Cascasén River	1.42	Oblong oval
10. Azufre River	1.45	Oblong oval
11. San Pablo River	1.29	Oblong oval
12. Chetillano River	1.42	Oblong oval
13. Chantilla Qda.	1.31	Oblong oval
14. Pallac River	1.34	Oblong oval
15. Chiminote Qda.	1.36	Oblong oval
16. La Ramada-2 Qda.	1.33	Oblong oval
17. Tumbadén River	1.37	Oblong oval
18. El Cardo Qda.	1.26	Oblong oval
19. Chorro Blanco Qda.	1.46	Oblong oval
20. El Carrizo River	1.39	Oblong oval
21. Amillas Qda.	1.41	Oblong oval
22. Del Qilengo Qda.	1.43	Oblong oval
23. Pinche River	1.34	Oblong oval
24. Quinuas Qda.	1.49	Oblong oval
25. Yaucán River	1.37	Oblong oval
26. Quebrada Tallal-2	1.43	Oblong oval
27. Namora River	1.43	Oblong oval
28. Huacrarucro River	1.29	Oblong oval
29. Muyoc River	1.41	Oblong oval
30. Llantén River	1.26	Oblong oval
31. Sanagorán River	1.42	Oblong oval
32. Cañad River	1.40	Oblong oval
33. Pencayoc Qda.	1.49	Oblong oval
34. Puerto Blanco River	1.43	Oblong oval
35. Chanta River	1.40	Oblong oval
36. Callayuc River	1.42	Oblong oval
37. Llantén River	1.32	Oblong oval
38. El Sauce River	1.44	Oblong oval
39. Chilca River	1.46	Oblong oval
40. Chancayano River	1.48	Oblong oval
41. San Juan-4 River	1.42	Oblong oval
42. Ganzul River	1.32	Oblong oval
43. San Juan Pampa River	1.36	Oblong oval
44. Jadibamba River	1.49	Oblong oval
Mean **Standard Deviation** **Variation Coefficient**	**1.38** **0.0677** **0.0491**	

Elongated Oblong Micro-basins

This group (Table 6) is made up of 14 hydrological units (20%), characterized by relatively longer concentration times than the two previous shapes, generating platykurtic hydrographs of the peak discharge, with more sustained flow and longer recessions. Unlike the previous two geometries, in this case the conditions for the recharge of aquifers are more favorable and loss from direct runoff is less (Figure 2).

In the three groups of classifications, the variation coefficient fell markedly, under 5% of the sample's value (11.3%), which confirms the strength of the criteria used for this classification.

Hydraulic Similitude of Hydrological Systems

In each geometric classification table presented above, the systems with hydraulic similitude have been identified by the process of elimination, taking into account the error limit established for each of the hydraulic similitude parameters.

Hydraulic Similitude of Round Oval Hydrological Systems

Four micro-basins with hydraulic similitude were identified in the group with this shape (Table 7), which represents 33.3% of the entire group and only 5.7% of the sample total.

Hydraulic Similitude of Hydrological Systems with an Elongated Oblong Shape

Seven micro-basins in this geometric class were identified as having hydraulic similitude (Table 8), equal to 50% of the entire group and only 10% of the sample total.

Hydraulic Similitude of Hydrological Systems with an Elongated Oval Shape

Twenty-three hydraulically similar hydrological units with this type of geometry were

Table 6. Group of micro-basins with an elongated oblong shape.

Micro-basin	Gravelius Coefficient $1.50 < K_c \leq 1.75$	Shape of basin
1. Poclush River	1.56	Elongated oblong
2. Rejo* River	1.58	Elongated oblong
3. San Juan-1 River	1.60	Elongated oblong
4. Qda. Onda	1.60	Elongated oblong
5. Magdalena River	1.70	Elongated oblong
6. Naranjo River	1.70	Elongated oblong
7. San Miguel River	1.53	Elongated oblong
8. Contumazá River	1.72	Elongated oblong
9. Qda. Bamba	1.73	Elongated oblong
10. Qda. Del Chorro	1.68	Elongated oblong
11. Llapa River	1.57	Elongated oblong
12. Qda. Honda	1.76	Elongated oblong
13. San Juan-3 River	1.75	Elongated oblong
14. Llaucano River	1.70	Elongated oblong
Mean **Standard Deviation** **Variation Coefficient**	**1.65** **0.0761** **0.0461**	

*Management model for the pilot basin, Granja Porcon afforestation.

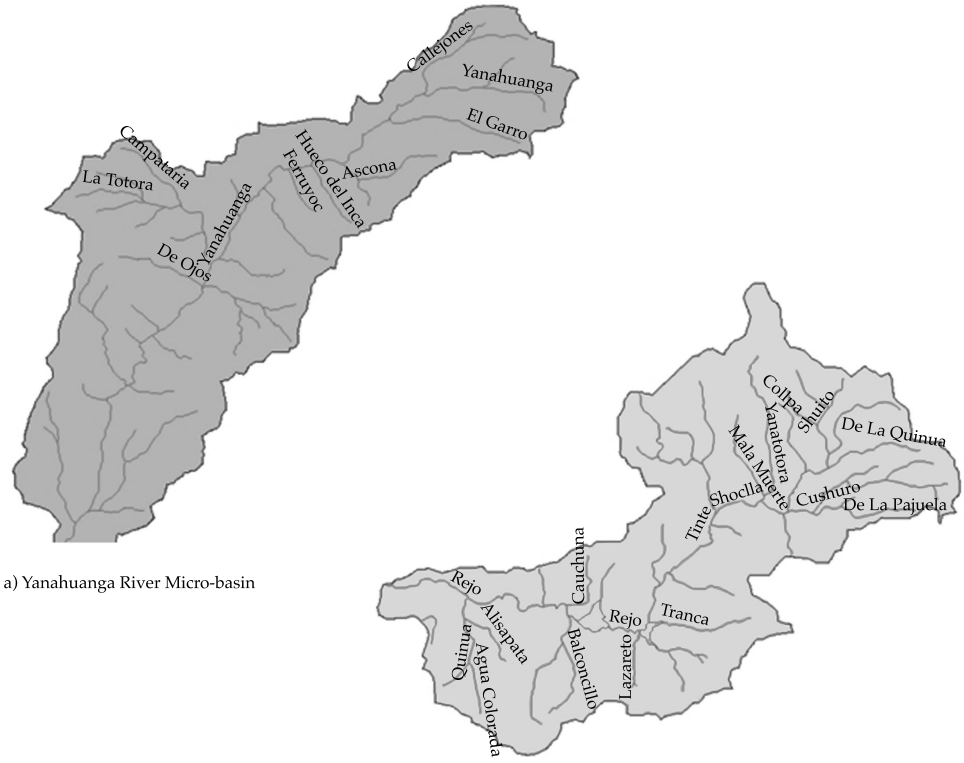

Figure 2. Hydraulic similarity of hydrological systems with an elongated oblong shape.

Table 7. Micro-basins in the high Andes with a round oval shape and hydraulic similarity.

Micro-basin	Gravelius Coefficient $1.00 < K_C \leq 1.25$	Relation of confluences (R_C)	Orographic Coefficient (%) (C_O)	Shape of Micro-basin	Watershed
1. Porcon River	1.16	1.88	11.83	Round oval	Pacific
2. La Leche River	1.16	1.90	12.04	Round oval	Atlantic
3. Yamulan Qda.	1.23	2.25	12.27	Round oval	Pacific
4. Asunción River	1.24	2.34	10.90	Round oval	Pacific
Mean	**1.20**	**2.10**	**11.76**		
Standard Dev.	**0.0435**	**0.2368**	**0.1941**		
Variation Coef.	**0.0363**	**0.1128**	**0.0165**		

identified (Table 9), equal to 52.3% of the entire group and 32.9% of the sample total. The absolute predominance of hydraulic similitude among micro-basins with this geometry is clearly shown. This statistic not only reflects the significant presence of hydrological units with this geometry but also the high tendency for hydraulic similitude in the same class or group.

It is important to highlight that for the three geometric groups, the percentage of hydrological units in the same group that tend to have hydraulic similitude is always over 33%, a very significant percentage if extended to the rest of the study region.

Table 8. Micro-basins in the high Andes with an elongated oblong shape and hydraulic similarity.

Micro-basin	Gravelius Coefficient $1.50 < K_C \leq 1.75$	Relation of confluences (R_C)	Orographic Coefficient (%) (C_O)	Shape of Micro-basin	Watershed
1. Poclush River	1.56	3.20	4.82	Elongated oblong	Pacific
2. Rejo River	1.58	3.16	4.93	Elongated oblong	Pacific
3. Onda Qda.	1.60	3.52	4.91	Elongated oblong	Atlantic
4. Magdalena River	1.70	4.60	3.98	Elongated oblong	Pacific
5. Contumazá River	1.72	4.20	3.90	Elongated oblong	Pacific
6. Bamba Qda.	1.73	4.00	4.03	Elongated oblong	Pacific
7. San Juan-3 River	1.7	3.29	4.07	Elongated oblong	Pacific
Mean	**1.66**	**3.71**	**4.38**		
Standard Dev.	**0.0797**	**0.5614**	**0.4806**		
Variation Coef.	**0.0479**	**0.1513**	**0.1098**		

Transfer of Hydrometeorological Information

Hydrological System of Origin with Maximum Storm Information

The simulation of the probabilistic Gumbel model, calibrated using statistical techniques for the best fit, resulted in information with the most diverse range of probabilities of occurrence. Some of these results are presented in Table 10, information which corresponds to the location of the Weberbauer rain gauge station in the lower basin of the Mashcon River hydrological unit (2 536 masl).

Hydrological Destination System without Maximum Storm Information

The data transferred from Table 11 were obtained according to the data in Table 10, the location of the Weberbauer station (2 536 masl) in the lower basin of the Mashcon River and the mean altitude of the Jadibamba River destination micro-basin (3 218), with the application of the transfer function shown in equation (17), considering the same standard duration of the intensities (time scale, $t_e = 1$) and an altitude scale of $H_e = 1.27$.

Discussion

Dimensionless Morphometric Characteristics of the Sample

The sample is characterized by different degrees of variability in the hydraulic similitude parameters, denoted by variation coefficients of 11.3, 39.1 and 123.8%, corresponding to the Gravelius index, convergence ratio and orographic coefficient, respectively. This behavior indicates the degree of influence of the shape of the basin on the configuration of the drainage network and the topographical factors in the same order.

Closer values of the Gravelius variation coefficients (11.3%) and the convergence ratio (39.1) indicate that the shape of the basin has more influence on the configuration of the drainage network.

The micro-basins that are most vulnerable to hydraulic erosion (higher orographic coefficient values) and with a high capacity for surface drainage (drainage networks with more bifurcations) are mostly found at the head of the Pacific watershed.

Influence of the Geometry of the Basin

The classification of the basins by geometric shape resulted in 12 round oval (17%), 44

Table 9. Micro-basins in the high Andes with an oblong oval shape and hydraulic similarity.

Micro-basin	Gravelius Coefficient $1.25 < K_C \leq 1.50$	Relation of confluences (R_C)	Orographic Coefficient (%) (C_O)	Shape of Micro-basin	Watershed
1. Grande 2 River	1.27	2.75	2.68	Oblong oval	Pacific
2. Cospán River	1.28	2.56	4.40	Oblong oval	Pacific
3. Mashcón River	1.31	3.45	1.88	Oblong oval	Atlantic
4. Chonta River	1.32	3.73	1.55	Oblong oval	Atlantic
5. Huertas Qda.	1.34	2.98	3.87	Oblong oval	Pacific
6. Chausís Qda.	1.38	2.67	3.80	Oblong oval	Pacific
7. Pallac River	1.34	3.23	2.38	Oblong oval	Pacific
8. Chiminote Qda.	1.36	2.83	1.90	Oblong oval	Pacific
9. La Ramada 2 Qda.	1.33	3.00	3.00	Oblong oval	Pacific
10. Tumbadén River	1.37	3.56	3.71	Oblong oval	Pacific
11. Llantén 1 River	1.26	2.57	2.49	Oblong oval	Atlantic
12. Cañada River	1.40	3.22	2.70	Oblong oval	Pacific
13. Puerto Blanco River	1.43	3.79	2.32	Oblong oval	Atlantic
14. Chanta River	1.40	3.73	4.40	Oblong oval	Pacific
15. Callalluc River	1.42	3.92	2.96	Oblong oval	Atlantic
16. Llantén 2 River	1.32	3.49	3.73	Oblong oval	Atlantic
17. Muyoc River	1.41	3.38	3.28	Oblong oval	Pacific
18. El Sauce River	1.44	4.17	3.43	Oblong oval	Atlantic
19. Namora River	1.43	4.42	2.50	Oblong oval	Atlantic
20. Sanagorán River	1.42	4.35	2.03	Oblong oval	Atlantic
21. San Pablo River	1.29	4.20	3.26	Oblong oval	Pacific
22. Chetillano River	1.42	4.10	4.40	Oblong oval	Pacific
23. Jadibamba River	1.49	4.50	4.65	Oblong oval	Atlantic
Average **Standard Dev.** **Variation Coef.**	**1.37** **0.062** **0.0457**	**3.50** **0.617** **0.1761**	**3.10** **0.909** **0.2932**		

oblong oval (63%) and 14 elongated oblong (20%). The predominance of the oval form (80%) in the regional sample indicates the predominance of systems that are highly vulnerable to hydraulic erosion and excessive loss from surface runoff, and have very high erosion capacities and sediment transport.

In each classification group, the Gravelius variation coefficient was under 5%, which indicates the strength of the classification criteria using Gravelius index ranges.

The marked fall in the variation coefficient of the Gravelius index in each classification group (under 5%) with respect to the sample value (11.3%) again corroborates the large influence of the geometry of the basin on the hydraulic similitude.

Hydraulic Similitude of Hydrological Systems

The frequencies of the hydraulic similitude in each geometric group, based on the limits established, were 52, 50 and 33%, corresponding to the oblong oval, elongated oval and round oval shapes, respectively. This shows a significant trend towards hydraulic similitude within each group. Nevertheless, these percentages were lower with respect to the

Table 10. Maximum precipitation intensities, Weberbauer station (altitude 2 536), Mashcon River micro-basin.

N	*J* (%)	*Tr* (years)	Maximum intensities (mm/h)				
			5 min	10 min	30 min	60 min	120 min
	00	∞	-	-	-	-	-
5	1	498.0	156.9	109.6	58.9	36.3	23.8
	2	248.0	147.0	103.2	55.4	34.1	22.2
	5	98.0	133.7	94.7	50.8	31.1	20.0
	10	48.0	123.4	88.2	47.2	28.7	18.4
	15	31.3	117.2	84.2	45.0	27.4	17.3
	20	22.9	112.7	81.3	43.4	26.3	16.6
	25	17.9	109.1	79.0	42.2	25.5	16.0
	30	14.5	106.0	77.0	41.1	24.8	15.5
	40	10.3	100.9	73.8	39.3	23.6	14.7
	50	7.7	96.4	71.0	37.8	22.7	13.9
	60	6.0	92.6	68.5	36.4	21.8	13.3
	70	4.7	88.7	66.0	35.1	20.1	12.7
	80	3.6	84.3	63.2	33.5	19.9	12.0
	90	2.7	79.3	60.0	31.8	18.8	11.1
	100	1.0	-	-	-	-	-
	00	∞	-	-	-	-	-
10	1	995.5	165.5	115.9	62.4	38.6	25.5
	2	495.4	156.8	109.5	58.9	36.3	23.8
	5	195.5	143.6	101.0	54.2	33.3	21.6
	10	95.4	133.3	94.5	50.6	31.0	20.0
	15	62.0	127.1	90.5	48.5	29.6	19.0
	20	45.3	122.6	87.6	46.9	28.6	18.2
	25	35.3	119.0	85.3	45.6	27.7	17.6
	30	28.5	115.8	83.3	44.6	27.0	17.1
	40	20.1	110.8	80.1	42.8	25.9	16.3
	50	14.9	106.4	77.3	41.2	24.9	15.6
	60	11.4	102.4	74.7	39.8	24.0	14.9
	70	8.8	98.5	72.2	38.5	23.1	14.3
	80	6.7	94.3	69.6	37.0	22.2	13.6
	90	4.9	89.4	66.4	25.3	21.1	12.8
	100	1.0	-	-	-	-	-
	00						-
25	1	2 488.0	179.9	124.2	66.9	41.5	27.6
	2	1 238.0	169.9	117.9	63.4	39.3	26.0
	5	487.9	156.6	109.4	58.8	36.3	23.8
	10	237.8	146.4	102.8	55.2	33.9	22.1
	15	154.3	140.2	98.9	53.1	32.5	21.1
	20	112.5	135.6	96.0	51.5	31.5	20.4
	25	87.4	132.0	93.7	50.2	30.7	19.8
	30	70.6	129.0	91.7	49.1	30.0	19.3
	40	49.4	123.8	88.4	47.3	28.8	18.4
	50	36.6	119.5	85.7	45.8	27.9	17.7
	60	27.8	115.5	83.1	44.4	27.0	17.6
	70	21.3	111.6	80.6	43.1	26.1	16.4
	80	16.0	107.4	78.0	41.6	25.1	15.7
	90	11.4	102.4	74.7	39.8	24.0	14.9
	100	1.0	-	-	-	-	-

N is the period of consecutive years; *J* is the uncertainty; *Tr* is the return time.

Table 11. Maximum precipitation intensities transferred to the Jadibamba River micro-basin (mean altitude of 3 218 masl).

N	*J* (%)	*Tr* (años)	Maximum Intensities (mm/h)				
			5 min	10 min	30 min	60 min	120 min
	00	∞	-	-	-	-	-
5	1	498.0	199.3	139.2	74.8	46.1	30.2
	2	248.0	186.7	131.1	70.4	43.3	28.2
	5	98.0	169.8	120.3	64.5	39.5	25.4
	10	48.0	156.7	112.0	59.9	36.4	23.4
	15	31.3	148.8	106.9	57.2	34.8	22.0
	20	22.9	143.1	103.2	55.1	33.4	21.1
	25	17.9	138.6	100.3	53.6	32.4	20.3
	30	14.5	134.6	97.8	52.2	31.5	19.7
	40	10.3	128.1	93.7	49.9	30.0	18.7
	50	7.7	122.4	90.2	48.0	28.8	17.7
	60	6.0	117.6	87.0	46.2	27.7	17.0
	70	4.7	112.6	83.8	44.6	25.5	16.1
	80	3.6	106.9	80.3	42.5	25.3	15.2
	90	2.7	100.7	76.2	40.4	23.9	14.1
	100	1.0	-	-	-	-	-
	00	∞	-	-	-	-	-
10	1	995.5	210.2	147.2	79.2	49.0	32.4
	2	495.4	199.1	139.1	74.8	46.1	30.2
	5	195.5	182.4	128.3	68.8	42.3	27.4
	10	95.4	169.3	120.0	64.3	39.4	25.4
	15	62.0	161.4	114.9	61.6	37.6	24.1
	20	45.3	155.7	111.3	59.6	36.3	23.1
	25	35.3	151.1	108.3	57.9	35.2	22.4
	30	28.5	147.1	105.8	56.6	34.3	21.7
	40	20.1	140.7	101.7	54.4	32.9	20.7
	50	14.9	135.1	98.2	52.3	31.6	19.8
	60	11.4	130.0	94.9	50.5	30.5	18.9
	70	8.8	125.1	91.7	48.9	29.3	18.2
	80	6.7	119.8	88.4	47.0	28.2	17.3
	90	4.9	113.5	84.3	32.1	26.8	16.3
	100	1.0	-	-	-	-	-
	00						-
25	1	2 488.0	228.5	157.7	85.0	52.7	35.0
	2	1 238.0	215.8	149.7	80.5	49.9	33.0
	5	487.9	198.9	138.9	74.7	46.1	30.2
	10	237.8	185.9	130.6	70.1	43.0	28.1
	15	154.3	178.0	125.6	67.4	41.3	26.8
	20	112.5	172.2	121.9	65.4	40.0	25.9
	25	87.4	167.6	119.0	63.8	39.0	25.1
	30	70.6	163.8	116.5	62.4	38.1	24.5
	40	49.4	157.2	112.3	60.1	36.6	23.4
	50	36.6	151.8	108.8	58.2	35.4	22.5
	60	27.8	146.7	105.5	56.4	34.3	22.4
	70	21.3	141.7	102.4	54.7	33.1	20.8
	80	16.0	136.4	99.1	52.8	31.9	19.9
	90	11.4	130.0	94.9	50.5	30.5	18.9
	100	1.0	-	-	-	-	-

N is the period of consecutive years; *J* is the uncertainty; *Tr* is the return time.

sample (33, 10 and 6%, respectively), again indicating the large predominance of the hydraulic similitude in basins with an oblong oval shape.

The degree of approximation of the similitude is greater in basins with round oval shapes, followed by elongated oval and oblong oval, with respect to the limit established for each hydraulic similitude parameter.

Transfer of Hydrometeorological Information

In general, information about the intensity of maximum storms is very scarce, but it is highly useful for generating maximum runoffs for micro-basins without hydrometric data related to peak flows. For basins with hydraulic similitude, this methodology provides a simple solution to the problem.

The selection of the design variable (Tables 10 and 11)— in which a wide range of options exist in terms of useful life (N), uncertainty (J), return times (T_r) and duration, according to the concentration time of the receptor-collector surface— enables adapting it to the nature and importance of each hydraulic project.

Finally, precipitation intensity can be converted into runoff using another law of hydrological systems in the high Andes, given the dimensionless parameter expressed in equation (3), the basis of the Rational method.

Conclusions

The physical laws that govern hydrological systems in the high Andes, which are based on precipitation-runoff phenomena, are governed by dimensionless morphometry represented by equations (1), (2), (3), (4) and (5). This set constitutes the scientific basis for this methodology.

The trio that serves as the basis for the hydraulic similitude among hydrological systems in the high Andes is the Gravelius index, convergence ratio and orographic coefficient, to ensure geometric, kinematic and dynamic similitude, respectively, using previously established approximation levels.

In terms of approximation similitude levels that are acceptable for practical purposes, measured using the variation coefficient, reference values of 0.05, 0.20 and 0.30 can be used for the Gravelius index, convergence ratio and the orographic coefficient, respectively. Nevertheless, this depends on the decisions made by investigators, according to their interests.

Because of the dimensionless nature of the methodology developed herein, it can be applied to any region, or among regions, sub-nations and internationally, as long as the physical laws that govern the high Andes hydrological systems are met (equations (1), (2), (3), (4) and (5)).

The morphometric regionalization of studies can be quite helpful to solving problems resulting from a scarcity of hydrometeorological information, for the purpose of the integral management of pilot hydrographic basins, which can be replicated in similar basins and can help to respond to global climate change, including extreme phenomena such as El Niño.

The exchange of hydrometeorological information among similar hydrological systems using dimensionless morphometry techniques is a simple process, unlike other regional methodologies that require a lot of information distributed across space and time to obtain acceptable results.

This sample study of the dimensionless morphometry of the Cajamarca region reports a large predominance of hydrological systems with a high potential for hydraulic erosion (80%). This translates into excessive surface drainage capacity and sediment transport and, thus, a high risk of danger from flooding due to extreme rainfall events, which is even greater with the presence of extreme El Niño events.

References

Antigüedad, I. (1980). Estudio morfométrico de la cuenca del río Arratia (Viscaya). *Boletín de la Real Sociedad Geográfica*, *66*, 31-52.

Aparicio, M. (1997). *Fundamentos de hidrología de superficie* (303 pp.). Barcelona: Limusa, S. A.

Askoa-Ibizate, G. (2004). Análisis morfométrico de la cuenca y de la red de drenaje del río Zadorra y sus afluentes aplicado a la peligrosidad de crecidas. *Boletín de la AGE*, *38*, 311-329.

Chow, V. T. (1993). *Hidrología aplicada*. Santafé de Bogotá: McGraw Hill.

Cruz-Santillán, J., & Tamés, P. (1983). Análisis cuantitativo de la red de drenaje de la cuenca del río Deba. *Lurralde*, *6*, 95-117.

Docampo, B. G., De Vikeña, E., Rico, E., & Rallo, A. (2009). Morfometría de las cuencas de la red hidrográfica (País Vasco, España). España: Facultad de Ciencias, Universidad del País Vasco.

Gaspari, F. G. (2002). *Plan de ordenamiento territorial de cuencas degradadas*. Aplicación de SIG (179 pp.). Huelva, España/ Buenos Aires: Ediciones Cooperativas.

Gaspari, F. J., Rodriguez, A. M., Senisterra, G. E., Denegri, G., Deldado, M. I., & Besterio, S. (2012). Caracterización morfométrica de la cuenca alta del río Sauce Grande, Buenos Aires, Argentina. VII Congreso de Medio Ambiente AUGM, del 22 al 24 de mayo de 2012, UNLP, La Plata, Argentina.

Gravelius, H. (1914). *Morphometry of Drainage Bassins*. Amsterdan: Elsevier.

Ibáñez, S., Moreno, H., & Gisberbert, J. (2005). *Morfología de las cuencas hidrográficas*. Escuela Técnica Superior de Ingeniería Agronómica y del Medio Natural. Recuperado de ruinet.upv.es/bitstream/

Henaos, J. E. (1988). *Introducción al manejo de cuencas hidrográficas* (396 pp.). Bogotá: Universidad Santo Tomás, Centro de Enseñanza Desescolarizada.

Horton, R. E. (1945). Erosional Development of Streams and their Drainage Basins: Hydrophysical Approach to Quantitative Morphology. *Geological Society of America Bulletin*, *56*, 275-370.

ICOLD (2008). *International Commission of Large Dams*, ICOLD. Recuperado de http://www.icoldcigb.net/, http://www.dams.org.

Jimenez, O. & Farías, H. (2005). Problemática de la sedimentación del embalse Valdesia, República Dominicana. Santo Domingo: Instituto Nacional de Recursos Hidráulicos de la República Dominicana (INDRHI).

Martínez, J. (1986). Características morfométricas de la red de drenaje de algunas cuencas de la sierra de los Álamos (Moratalla, Murcia). *Papeles de Geografía Física*, *11*, 45-51.

Rocha, A. (2006). *Problemática de la sedimentación de embalses en el aprovechamiento de los ríos peruanos, aplicada al embalse de Poechos*. I Congreso Internacional de Hidráulica, Saneamiento y Medio Ambiente, Instituto de la Construcción y Gerencia (ICG), Lima, Perú. Recuperado de http://www.imefen.uni.edu.pe.

Rodríguez-Díaz, H. A. (2001). *Hidráulica experimental* (337 pp.). Santafé de Bogotá: Centro Editorial, Escuela Colombiana de Ingeniería.

Senciales, J. (2005). *El Análisis morfológico de las cuencas fluviales aplicado al estudio hidrográfico*. Málaga, España: Departamento de Geografía, Universidad de Málaga. Recuperado de dialnet.unirioja.es/descarga/artículo/109746.pdf.

Sotelo-Ávila, G. (1977). *Hidráulica general. Vol. I. Fundamentos* (551 pp.). México, DF: Limusa.

Streeter, V., & Wilie, E. (2000). *Mecánica de fluidos* (9a edición). Santafé de Bogotá: McGraw Hill Internacional, S.A.

Universidad Nacional de Colombia-Sede Medellín (s.f.) *HidroSIG*. Medellín: Escuela de Ciencias y Medio Ambiente. Recuperado de www.medellin.unal.edu.co/hidrosig.

Vergara, M. (1993). *Técnicas de modelación en hidráulica.* Buenos Aires: Ediciones Alfa Omega.

Institutional address of the author

Mg. Oswaldo Ortiz Vera

Universidad Nacional Agraria La Molina
Apdo. 456-La Molina, Lima, Perú
Teléfono: +51 (016) 3495 647
Fax: +51 (016) 3495 670
ingoov@gmail.com
pdrh@glamolina.edu.pe
pdrh.epg@gmail.com

Hydrological Modeling based on Rainfall Estimates using Hydrometeorological Sensors

• Iván Vilchis-Mata* • Khalidou M. Bâ • Roberto Franco-Plata •
• Carlos Díaz-Delgado •
Universidad Autónoma del Estado de México
*Corresponding Author

Abstract

Vilchis-Mata, I., Bâ, K. M., Franco-Plata, R., & Díaz-Delgado, C. (July-August, 2015). Hydrological Modeling based on Rainfall Estimates using Hydrometeorological Sensors. *Water Technology and Sciences* (in Spanish), 6(4), 45-60.

This work assesses the integration of daily rainfall data from hydrometeorological sensors in the Amacuzac River basin, Mexico, for the period 2003 to 2009. It includes data from automated weather stations (AWS), C-band weather radar from the Cerro Catedral and *PERSIANN* and *CMORPH* satellite systems, in the *CEQUEAU* distributed hydrological model, with a spatial resolution of 27 x 27 km^2. These estimates can be used to simulate daily flow. The performance of the hydrological modeling was evaluated with Nash-Sutcliffe efficiency criteria, graphic techniques, calibration and validation. The results indicate that the values of the criteria used are acceptable when compared with observed daily rainfall as well as flow simulations. The mean daily interannual Nash values obtained were 0.60 with radar, 0.81 with *PERSIANN*, 0.83 with AWS and 0.85 with *CMORPH*. The mean monthly interannual values obtained were 0.90 with radar, 0.91 with *PERSIANN*, 0.92 with AWS and 0.95 with *CMORPH*. Therefore, it can be stated that the combination of the technological tools is a useful solution when little rainfall data is available, providing real-time automated processes that contribute to analyses and decision-making.

Keywords: Rainfall estimate, weather radar, weather satellite, *CEQUEAU*, *PERSIANN*, *CMORPH*, hydrological modeling.

Resumen

Vilchis-Mata, I., Bâ, K. M., Franco-Plata, R., & Díaz-Delgado, C. (julio-agosto, 2015). Modelación hidrológica con base en estimaciones de precipitación con sensores hidrometeorológicos. Tecnología y Ciencias del Agua, *6(4), 45-60.*

En este trabajo se evalúa la integración de datos a nivel diario de precipitación estimada con sensores hidrometeorológicos, tales como estaciones meteorológicas automáticas (EMA), radar meteorológico banda C de Cerro Catedral y sistemas satélites PERSIANN y CMORPH, dentro del modelo hidrológico distribuido CEQUEAU, con una resolución espacial de 27 x 27 km^2, para el periodo comprendido del año 2003 a 2009, implementado en México, en la cuenca del río Amacuzac. Estas estimaciones permitieron simular caudales a nivel diario, cuyo desempeño de la modelación hidrológica fue evaluado mediante el criterio de eficiencia Nash-Sutcliffe, técnicas gráficas, calibración y validación. Los resultados indican que los valores de los criterios utilizados son aceptables tanto en la comparativa con las precipitaciones diarias observadas como en las simulaciones de caudales, obteniendo valores de Nash interanuales medios diarios en el caso del radar 0.60, PERSIANN 0.81, EMA 0.83 y CMORPH 0.85, respecto a los interanuales medios mensuales, para el radar 0.90, PERSIANN 0.91, EMA´s 0.92 y CMORPH 0.95. Por tal motivo es posible afirmar la utilidad de la combinación de estas herramientas tecnológicas como una solución a la escasez de datos de precipitación, estableciendo procesos automatizados y en tiempo real que permitan el desarrollo de análisis y toma decisiones.

***Palabras clave**: estimación de precipitación, radar meteoro-lógico, satélite meteorológico, CEQUEAU, PERSIANN, CMORPH, modelación hidrológica.*

Received: 08/04/2014
Accepted: 06/03/2015

Introduction

Distributed hydrological models have been extensively developed over the past two decades, while meteorological data continues to be limited due to insufficient measurement stations. Precipitation is the main input for a hydrological model, and the spatial distribu-

tion of precipitation is the main variable in hydrology, climatology and agriculture studies. Rain gauges are instruments traditionally used to measure precipitation. Nevertheless, they provide point information and have very limited coverage in many basins around the world, particularly in developing countries. While weather radar provides highly valuable information to estimate precipitation it does not cover many basins because of its cost. Nevertheless, estimating precipitation based on radar has been successfully used by many hydrological studies (Lee, Shin, Kim, & Park, 2014; Magaña-Hernández, Bâ, & Guerra-Cobián, 2013; Guerra-Cobián, Bâ, Quentin-Joret, Díaz-Delgado, & Cârsteanu, 2011; Eleuch *et al*., 2010; Bedient, Anthony, Benavides, & Vieux, 2003; Bedient, Hoblit, Gladwell, & Vieux, 2000). Fattorelli, Casale, Borga and Da Ros (1999) indicate that efficient and timely acquisition of information about precipitation from large areas is crucial to early and effective flood alerts. Images from land radar and satellites make it possible to simultaneously and frequently view large regions. In effect, the use of radar and satellite data in a hydrological forecasting systems offers the opportunity to produce alerts that are better and earlier than those produced by systems based only on rain gauge data.

Passive microwave and infrared sensors are the two most commonly applied satellite techniques used to estimate precipitation (Ebert, Janowiak, & Kidd, 2007).

Currently, an increasingly larger number of precipitation satellite products is available on the internet nearly in real-time. With the advances in high-speed internet communications digital precipitation maps provided by national weather centers, government institutions and university research groups can be downloaded in a matter of seconds.

For example, the International Precipitation Working Group (IPWG, http://www.isac. cnr.it/~ipwg/) compiled 23 algorithms to estimate precipitation using satellites from the United States, Europe, Japan and China, and developed a program to validate daily precipitation. To verify the quality of the satellite information they used precipitation recorded by rain gauges and weather radars in Australia, the United States and northern Europe. The CMORPH and PERSIANN algorithms were chosen from the available options because of their easy access to information related to Mexico. These were applied to a Mexican basin.

CMORPH (*Climate Prediction Center Morphing Technique*) is an algorithm which was developed in the United States by the National Oceanic and Atmospheric Administration (NOAA) to estimate precipitation. The product integrates measurements from passive microwave sensors, which are interpolated over time, using advection information from infrared heat sensors to interpolate between sweeps by satellites with microwave sensors (Joyce, Janowiak, Arkin, & Xie, 2004). Precipitation estimated by CMORPH is available from December 2002 at different special and temporal resolutions ((8 x 8 km2; 0.25° x 0.25°; 30 min, 3 h and daily) for regions located between 60° north and 60° south.

The PERSIANN algorithm (Hsu, Gao, Sorooshian, & Gupta, 1997; Sorooshian *et al*., 2000) was developed by the Center for Hydrometeorology and Remote Sensing (CHRS) at the University of California, Irvine. The algorithm uses measurements from infrared sensors which are fitted to measurements from microwave sensors and calibrated using TRMM radar (Tropical Rainfall Measuring Mission), when available. PERSIANN is an algorithm based on a neural network function with approximation and classification procedures to estimate the intensity of rainfall, with a pixel resolution of 0.25° x 0.25°. The data are available from March 2000 with temporal resolutions of 3 and 6 h and a 0.25° x 0.25° spatial resolution. Another version of this algorithm exists, called PERSIANN-CCS (Hong, Hsu, Sorooshian, & Gao, 2004), which

is based on a technique to classify clouds in order to determine relationships between the temperature at the top of the clouds and precipitation.

Joyce *et al*. (2004) validated precipitation estimated by the *CMORPH* and other algorithms (at a daily level with a resolution of 0.25° x 0.25°) in Australia and the United States using cells containing rain gauges. They reported that *CMORPH* provided better results. Dinku, Ceccato, Cressman and Connor (2010) showed that *CMORPH* provides slightly lower estimations of precipitation than other algorithms with which it was compared, for a period of 10 days with a resolution of 0.25° x 0.25°. Ebert *et al.*(2007) reported that *CMORPH* generally underestimates the number of days with rainfall in Australia when using a daily level and a spatial resolution of 0.25° x 0.25°. Nevertheless, the estimated daily precipitation has a higher correlation than other satellite algorithms used to estimate precipitation. Serrat-Capdevila *et al*. (2013) compared *CMORPH* and *PERSIANN* algorithms at a daily level for the Sensegal River in Africa and found that the *CMORPH* provides better results. In addition, several studies have used these algorithms in comparative analyses of precipitation estimations, including Behrangi *et al*. (2014); Habib, Haile, Tian and Joyce (2012a); Joyce and Xie (2011); Habib, Elsaadini and Haile (2012b), and Stisen and Sandholt (2010).

In Mexico, Bâ and Serrat-Capdevilla (2012), Vilchis-Mata (2013) and Magaña-Hernández *et al*. (2013) evaluated different methods to estimate precipitation using remote sensors, including *CMORPH* and *PERSIANN*, and concluded that *CMORPH* produces better results at the daily level. The objective of the present investigation is to use precipitation estimated by *CMORPH* and *PERSIANN* algorithms to evaluate the possibility of using this source of information to model daily runoff in a basin in Mexico.

CEQUEAU Hydrological Model

This model was developed by the National Institute for Scientific-Water Research (INRS-EAU, now INRS-ETE, French acronym) at the University of Quebec, Canada to reproduce runoff in a basin (Morin, Sochanski, & Paquet, 1998; Singh & Frevert, 2002; Morin & Paquet, 2007). It has been used in different countries for the continuous simulations of flows or for hydrological forecasting in order to manage reservoirs (Bâ *et al*., 2013; Bâ & Serrat-Capdevila, 2012; Eleuch *et al*., 2010; Llanos, Bâ, & Castiella, 1999; Ayadi & Bargaoui, 1998; Bâ, Díaz, & Rodríguez, 2001). In addition, the World Meteorological Organization (WMO, 1986, 1992) has compared this model to various hydrological models based on different basins worldwide. The Tinto Alcan River company (RTA, Spanish acronym) uses this model in operations in order to manage reservoirs and has financed the newest versions of this model (http://ete.inrs.ca/ete/publications/cequeauhydrological-model).

Given the model's distributed parameters, the basin is divided into elemental areas in the shape of squares (parcels) and the flows are calculated for each of these areas, taking into account spatial-temporal variations due to the physiographic characteristics. This discretization makes this type of model compatible for use with precipitation estimations by satellites.

It contains two components to simulate the vertical and horizontal flow of water in each square (Figure 1). The vertical component is called the product function and the horizontal component the transfer function.

The production function refers to the modeling of the vertical flow of water (rain, evapotranspiration, infiltration, etc.) and is aimed at obtaining a water volume for each of the three recipients included in the model: lakes and marshes, soil and aquifers. The water volume is calculated for each partial element by multiplying the water depth

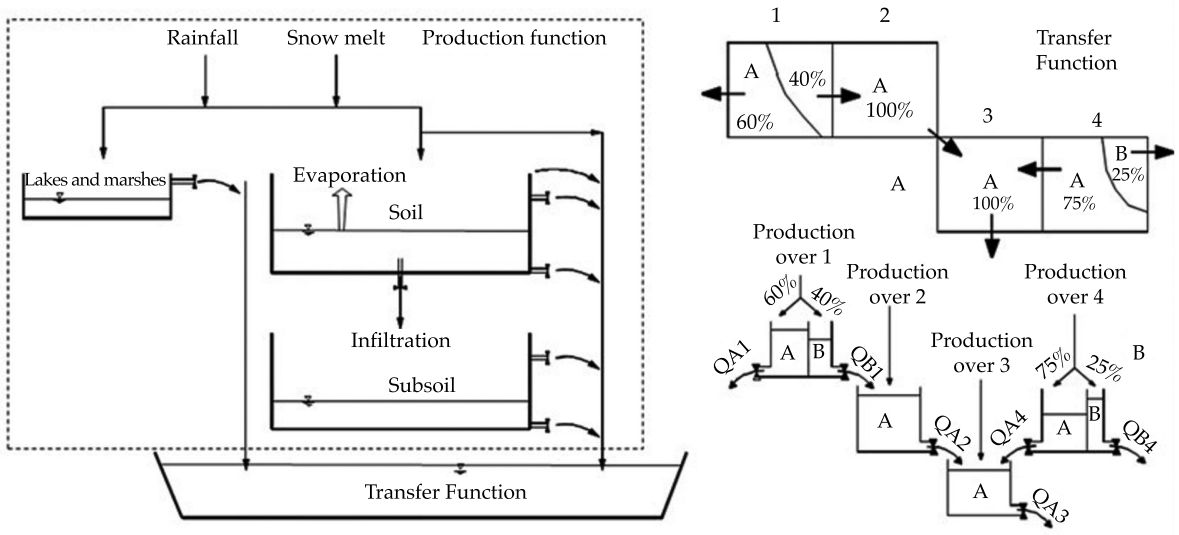

Figure 1. Production function (left) and transfer function (right) for the hydrological model with distributed *CEQUEAU* parameters (adapted from Morin & Paquet, 2007).

produced in the entire square by the area of the partial element under consideration. The transfer function analyzes the way in which the flow is transferred through the drainage network. It takes into account lakes, marshes, dams and bypasses. The model examines each parcel for defined time intervals, which can be one day or even one hour.

Evapotranspiration is calculated based on the modified Thornthwaite formula (Morin & Paquet, 2007). The calculations are performed according to the time intervals indicated by the user. As shown in the illustration in Figure 1, surface and delayed runoff depend on the water level in the recipients, conceptual drainage coefficients and the thresholds of the recipient. This is simulated with equations involving the parameters of the model. These parameters govern the behavior of the water flow in the three recipients (lakes and marshes, soil and aquifer), snow melting, evapotranspiration and transfer. Two types of input data are required by the model—physiographic and hydrometeorological .

The model contains an application to optimize its parameters. The algorithm is based on the Powell method (1964), whose objective function is the Nash coefficient (equation (1)) or the relative error between observed and simulated flows. The model also contains graphic criteria such as comparisons of hydrographs and classified flows, among others.

$$NTD = 1 - \frac{\sum_{i=1}^{n}\left(Q_{Ci} - Q_{Oi}\right)^2}{\sum_{i=1}^{n}\left(Q_{Oi} - \overline{Q_O}\right)^2} \qquad (1a)$$

$$NTD^* = 1 - \frac{\sum_{n=1}^{NNE}\sum_{i=1}^{365}\left(Q_{Ci} - Q_{Oi}\right)^2}{\sum_{n=1}^{NNE}\sum_{i=1}^{365}\left(Q_{Oi} - \overline{Q_O}\right)^2} \qquad (1b)$$

Where:

NTD = Annual, dimensionless Nash-Sutcliffe criterion, from -∞ to 1.
NTD^*= Inter-annual, dimensionless Nash-Sutcliffe criterion, from -∞ to 1.
Q_{Ci} = flows calculated on day i, in m^3/s.
Q_{Oi} = observed flows on day i, in m^3/s.
$\overline{Q_O}$ = average of observed flows in n days.
NNE = number of years..

Materials and Methods

The development of this work consists of a logical sequence of seven procedures to prepare the required inputs. These correspond to: acquisition and pre-processing; followed by validation of data measured on land by the automated weather stations (AWS) and estimated by remote sensing systems; generation of the *CEQUEAU* hydrological model's input parameters; hydrological modeling and its calibration at the hydrographic basin level; and lastly, the analysis of the results from the different types of scenarios (radar, satellites), as described in detail below.

1. **Data acquisition**: This consists of compiling and storing rain gauge data inputs obtained from the three main sources: automated weather stations (AWS), Cerro Catedral weather radar, and satellite sensors (*PERSIANN* and *CMORPH*), with an analysis of the availability and quality of this information.

2. **Pre-processing of data**: This involves the generation of databases accumulated at a daily level (24 h) derived from the AWS, as well as importation, validation, adaptation and analysis in GIS-IDRISI, in order to obtain daily accumulated precipitation estimates from raster images produced by weather radar and satellite images. This is supported by the importation and pre-processing module developed by CRI-Ecuador and the methodology developed by Vilchis-Mata, Quentin, Bâ y Díaz-Delgado (2011).

3. **Validation of rain gauge data**: This analysis is interpreted as a point validation between observed data(x) from rain gauges at the AWS and data (y) estimated by the remote sensors (*CMORPH* and *PERSIANN*). This procedure is based on a dimensionless measurement, such as the determination coefficient (r^2), to measure the degree of reliability or goodness-of-fit and variations in the data set (equation (2)):

$$r^2 = \left(\frac{\sum (x-\bar{x})(y-\bar{y})}{\sqrt{\sum (x-\bar{x})^2 \sum (y-\bar{y})^2}} \right)^2 \qquad (2)$$

4. **Preparation of physiographic parameters**: This involves delimiting the hydrographic basin and obtaining its parameters in an automated manner (Table 1) by applying the hydrogeomatic module implemented in GIS-IDRISIS by Franco-Plata (2008) and improved by Franco-Plata *et al*. (2013).This basin information (Figure 2) is obtained based on topographic information from the Radar Topography Mission's (SRTM-NASA) digital elevation model (DEM), with an initial spatial resolution of approximately 90 meters, which is adjusted to the spatial resolution of the precipitation data provided by the satellite images (27 km). The information about land use corresponding to the percentage of lakes, marshes and forest cover is obtained from data provided by the National Commission for the Knowledge and Use of Biodiversity (Conabio, Spanish acronym) or from the supervised classification of satellite images, when available. A grid is then created which divides the basin into complete squares, where each square is identified by the coordinates (I,J), and which in turn are divided into as many as 4 partial elements as defined by the delimitation of the watersheds within the complete square. In the case of the present investigation, these squares correspond to a spatial resolution of 27 km and indicate the direction of the flow from one square to its neighboring square, so that it coincides with the initial information obtained from satellites. The files with extension .PHY (physiographic) and .BV (basin information) are produced by this process.

Table 1. Physiographic characteristics of the basin.

Area and perimeter	***A* = 8 927.61 km²** ***P* = 755.46 km**
Compactness coefficient	*Kc* = 2.25
Circularity Ratio	*Rci* = 0.2
Hypsometric Relationship and Mean Elevation	*Rh* = 3.36 *H* = 1 708.2
Slope of the Basin	*S*° = 10.54 *S*% = 19.15
Characteristics of the Main River	*Lc* = 219.2 km *La* = 133.27 km *Sc* = 0.012 *Sh* = 1.64 *H*max = 3 179 masl *H*min = 627 masl
Concentration Time	*Tc*1 = 23.24 hours (Kirpich) *Tc*2 = 23.36 hours (CHPW)

5. **Preparation of hydrometeorological files**: This process analyzes and structures information regarding daily flow observed at the Atenango del Río hydrometric station (managed by the Federal Electric Commission), minimum and maximum temperature data from the AWS located in the basin and precipitation data contained in databases generated daily from radar and satellite sources (CMORPH and PERSIANN), in a database management program called SEDHIM (Chávez & Galicia, 2002) and available in the formats required by the CEQUEAU model. As a result, files are created per sensor (radar, CMORPH and PERSIANN) with a .MET extension (meteorological) and a .CAU extension (flow). It is important to mention that the file with a .DHM extension contains the definition of the period for preparing the hydrometeorological data for the simulations, as well as the routes for accessing the files mentioned.

6. **Hydrological Modeling**. This corresponds to the calculation of flows in the basin based on the files generated and required by the CEQUEAU (.PHY, .BV, .DHM, .CAU), as well as the editing of a parameters file with the extension .PAH, which contains some of the parameters determined by the physics of the phenomenon. Others depend on the hydrological and physiographic characteristics of the basin, while others are defined during the calibration process.

7. **Calibration and validation**: Calibration is a stage that enables attributing values to the conceptual parameters involved in the balance equations, as indicated in Figure 1. In this case, these parameters refer to the height of the recipients, the drainage coefficients, the Thornthwaite exponent and index, etc. This process can be carried out by: a) trial and error, b) optimization or c) a combination of both. In this process, the initial parameters included in the file with the .PAH extension change automatically (optimization), or by trial and error until finding the best NTD value closest to 1. The calibration is the most crucial of all the stages in the modeling. Sorooshian and Arfi (1982) emphasize that the art of modeling primarily lies in the calibration. And furthermore, with the best of models,

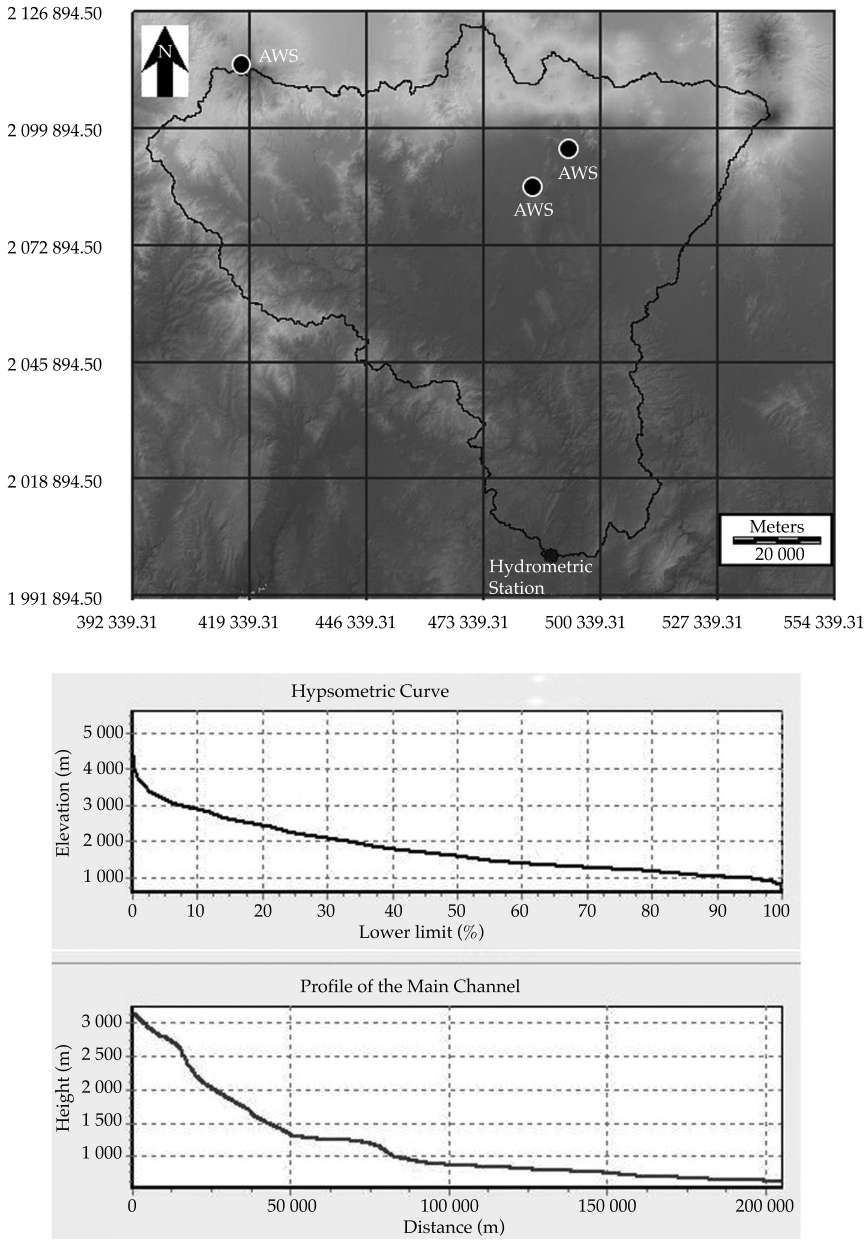

Figure 2. Delimitation, location of AWS, hypsometric curve and the profile of the basin up to the Atenango del Río hydrometric station.

no matter how sophisticated and realistic they may be, if the calibration is not done well they will always produce false results.

In addition, the quality of a model is measured by the validation results. This stage uses numerical criteria (NTD, in this case) or graphic criteria to compare the results from simulations with parameters obtained from the calibration process and the observed hydrographs.

Results

The physiographic parameters of the basin (Table 1) need to be calculated in order to model runoff. This process enables obtaining the area of the basin and its concentration time, which are physical parameters required by the *CEQUEAU* model. The model was calibrated using precipitation observed at the AWS and precipitation estimated from radar and from satellite (*CMORPH* and *PERSIANN*).

In the case of the Cerro Catedral radar, Vilchis- Mata *et al*. (2011) identified an orographic blocking of the radar beam from the volcanoes and mountains in the zone of influence, including the Jocotitlán, Nevado de Toluca, Popocatépetl and Iztaccíhuatl volcanoes, as well as the NW system of mountains corresponding to the Nevado de Toluca and the Ajusco volcanoes. These generate screens (under-detection) in the bottom portions and echoes from the ground due to secondary lobes, thereby resulting in an absence of data (Figure 3). To correct this, an interpolation process needs to be performed between the affected pixels and the values of their neighboring pixels, for each one of the images, with the supposition that the fields of precipitation are relatively homogenous. This results in an image product which represents the daily accumulated precipitation with orographic correction. This can be applied operationally in a distributed hydrological model when representing the spatial distribution of precipitation in the study area. In addition, a potential benefit of the information is its wide coverage of areas where it is difficult to install and operate manual devices (Hossain, Anagnostou, Dinku, & Borga, 2004).

Considering the limitations of the rain gauge and radar networks, satellite sensors represent the only viable means to estimate precipitation across the planet. In effect, techniques that integrate visible, infrared and microwave data make their use possible by solving problems that affect these techniques (microphysics of clouds and thermodynamic properties) when taken individually. Nevertheless, the quantitative estimates of precipitation using remote sensors present a degree of uncertainty associated with the nature of the measurements.

The r^2 values in the scenarios with underestimations and overestimations are complementary to the overall analysis. Underestimates correspond to a small percentage attributable to precipitations under 2.0 mm as well as local events which were not completely quantified by remote sensors. Meanwhile, overestimation reflect a generalized phenomenon seen in the results of hydrological modeling, which are most affected.

With respect to the results obtained from the hydrological model (Tables 2, 3, 4 and 5), a considerable variation can be seen among the different sources of information (AWS, radar, *PERSIANN* and *CMORPH*), considering the spatial variability in the precipitation and the non-linearity of the transfer of mass and energy to within the basin, which are considered reliable data.

High amounts of rainfall were observed from the Amacuzac River basin to the Atenango del Río hydrometric station between May and October, where the hydrograph peaks for this period did not present an adequate fit, while the flows remained uniform during the dry season. On a daily level, the simulations with AWS presented higher Nash-Sutcliffe criterion values than those obtained with the *PERSIANN*, which in turn were more accurate than those of radar. On a monthly level the order of the AWS values were the same, while the radar values exceeded those obtained with *PERSIANN*. It is worth mentioning that the simulations performed with *CMORPH* data at both daily and monthly levels were widely satisfactory, presenting the highest Nash-Sutcliffe criterion values in this analysis (Figures 4, 5, 6 and 7).

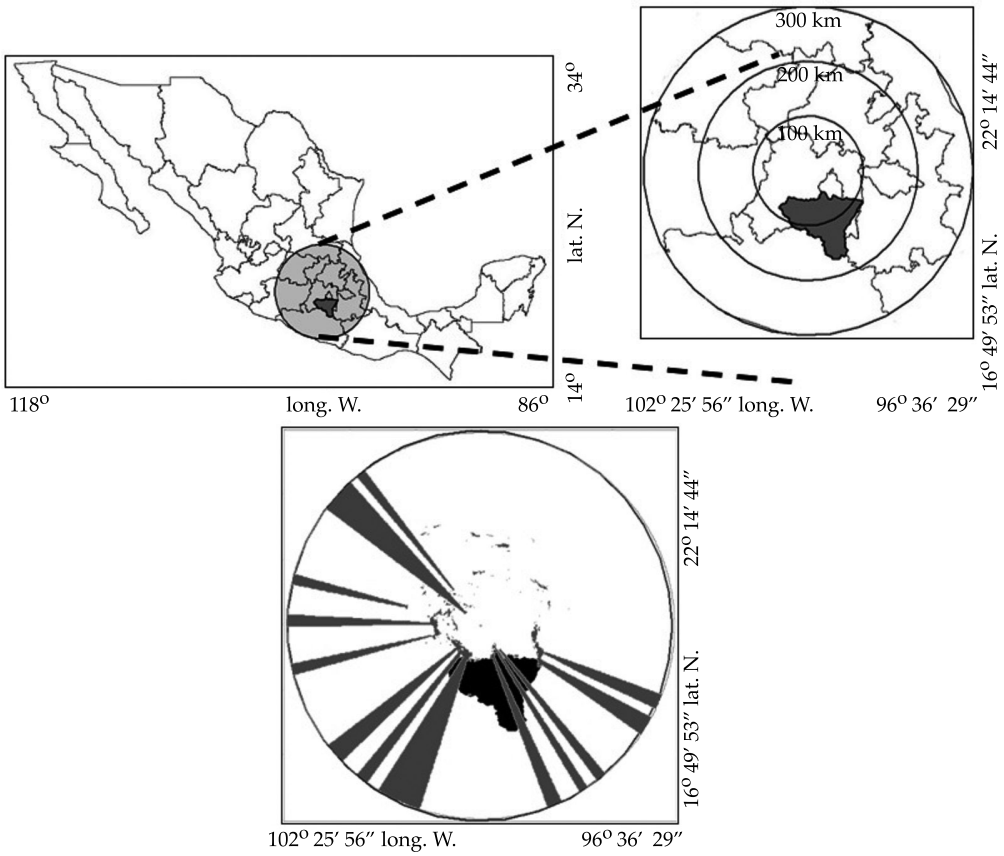

Figure 3. Location of the basin in the radius of influence of the Cerro Catedral radar and affects from orographic blocking.

Table 2. Mean daily inter-annual flows.

Source of Information	Observed flow (m^3/s)	Calculated flow (m^3/s)	Relative error (%)	Observed water depth (mm)	Calculated water depth (mm)	Relative error (%)	Nash-Sutcliffe Criterion
AWS	50.6	49.5	-2.2	193	189	-2.2	0.831
Radar	57.1	57.1	0.0	218	217	-0.5	0.600
PERSIANN	50.6	50.1	-1.0	193	191	-1.0	0.807
CMORPH	50.6	50.6	0.0	193	193	0.0	0.851

Table 3. Monthly mean inter-annual flows.

Scenario	Observed flow (m^3/s)	Calculated flow (m^3/s)	Relative error (%)	Observed water depth (mm)	Calculated water depth (mm)	Relative error (%)	Nash-Sutcliffe Criterion
AWS	50.6	49.5	-2.2	193	189	-2.2	0.923
Radar	57.1	57.0	-0.2	218	217	-0.5	0.902
PERSIANN	50.6	50.1	-1.0	193	191	-1.0	0.912
CMORPH	50.6	50.6	0.0	193	193	0.0	0.950

Table 4. Daily accumulated mean inter-annual flows.

Scenario	Observed flow (m^3/s)	Calculated flow (m^3/s)	Relative error (%)	Observed water depth (mm)	Calculated water depth (mm)	Relative error (%)	Nash-Sutcliffe Criterion
AWS	7 255.7	6 978.3	-3.8	27 654	26 597	-3.8	0.995
Radar	8 151.9	8 010.2	-1.8	31 070	30 530	-1.8	0.997
PERSIANN	7 255.7	6 628.6	-8.6	27 654	25 264	-8.6	0.986
CMORPH	7 255.7	6 883.0	-5.1	27 654	26 234	-5.1	0.994

Table 5. Monthly accumulated mean inter-annual flows.

Scenario	Observed flow (m^3/s)	Calculated flow (m^3/s)	Relative error (%)	Observed water depth (mm)	Calculated water depth (mm)	Relative error (%)	Nash-Sutcliffe Criterion
AWS	262.4	252.2	-3.9	1000	961	-3.9	0.995
Radar	294.2	289.1	-1.8	1121	1102	-1.7	0.997
PERSIANN	262.4	240.8	-8.2	1000	918	-8.2	0.986
CMORPH	262.4	249.8	-4.8	1000	952	-4.8	0.994

Note: In tables 2, 3, 4 and 5, the radar values cover only the period 2008-2009 and thus the difference between this observed flow and the other scenarios for the period 2003-2009.

Conclusions

The objective of this work was to analyze the use of precipitation information obtained from remote sensors as input for a distributed hydrological model. Without a doubt, this approach improves the perception of reality by providing a better spatial and temporal representation of precipitation in a region. The results reflect that, among the methods analyzed, the best flow simulations were those corresponding to the use of the CMORPH algorithm, even with the AWS stations. Nevertheless, this work presented only three AWS stations in a basin measuring 9 000 km^2 and therefore they do not accurately reflect the distribution of precipitation. Meanwhile, the specialized literature indicates that using radar to estimate daily precipitation produces satisfactory results compared to estimates based on satellites, though that was not the case in the study basin. This could be explained by the partial lack of information caused by orographic blocking of the radar signal, which was completed through interpolation.

It is worth mentioning that before using precipitation information estimated by remote sensors, validation needs to be performed with rain gauges and, when applicable, corrections made based on statistical criteria, the geographic zone and the regional behavior of the climate.

Lastly, the use of the information from Mexico's radar network needs to be systematized for hydrological studies.

Acknowledgements

The authors thank the State of Mexico Autonomous University (Universidad Autónoma del Estado de México) for financing the research project 3459/2013CH, as well as the reviewers for their insightful observations and recommendations.

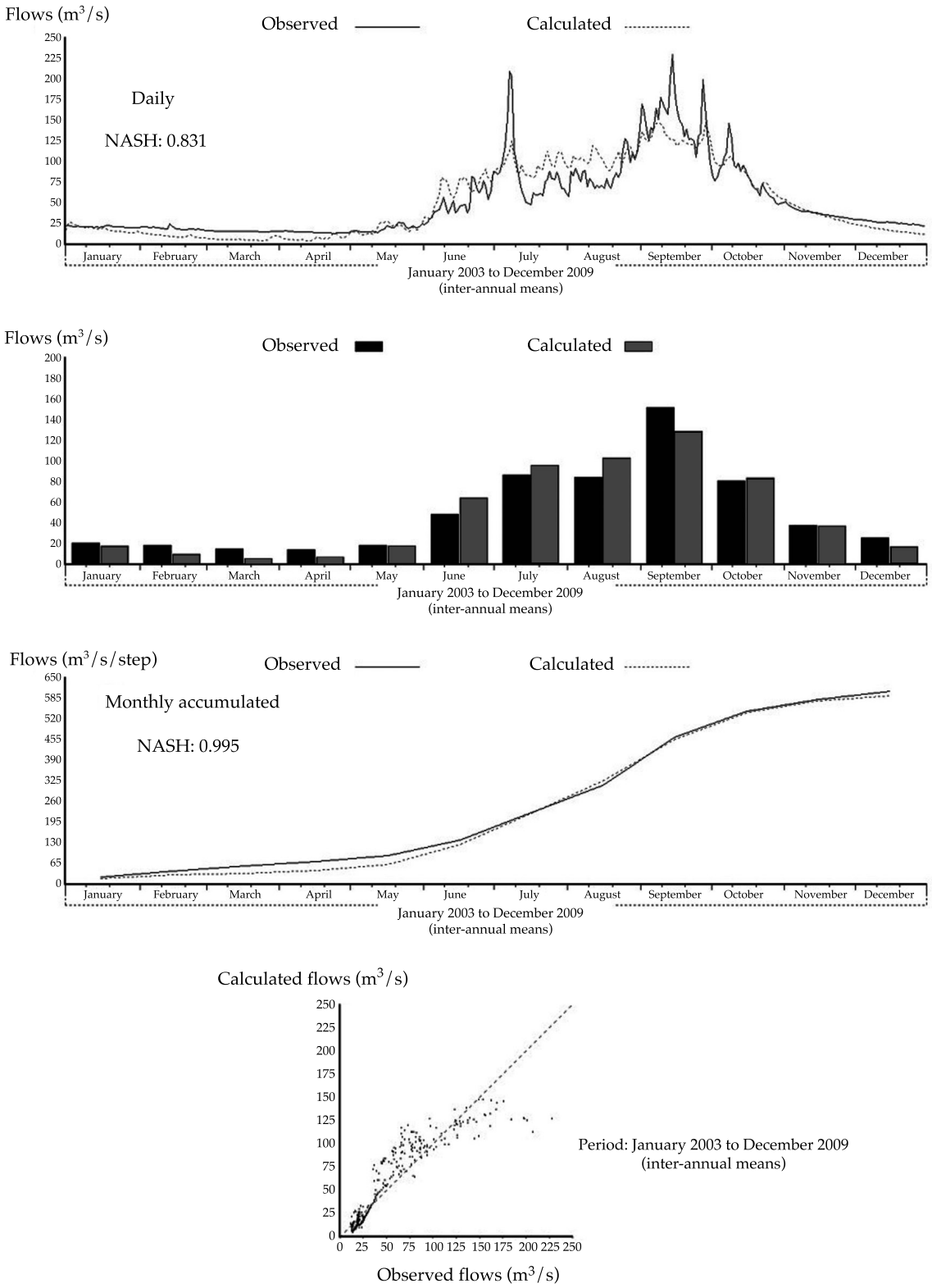

Figure 4. Hydrographs with AWS.

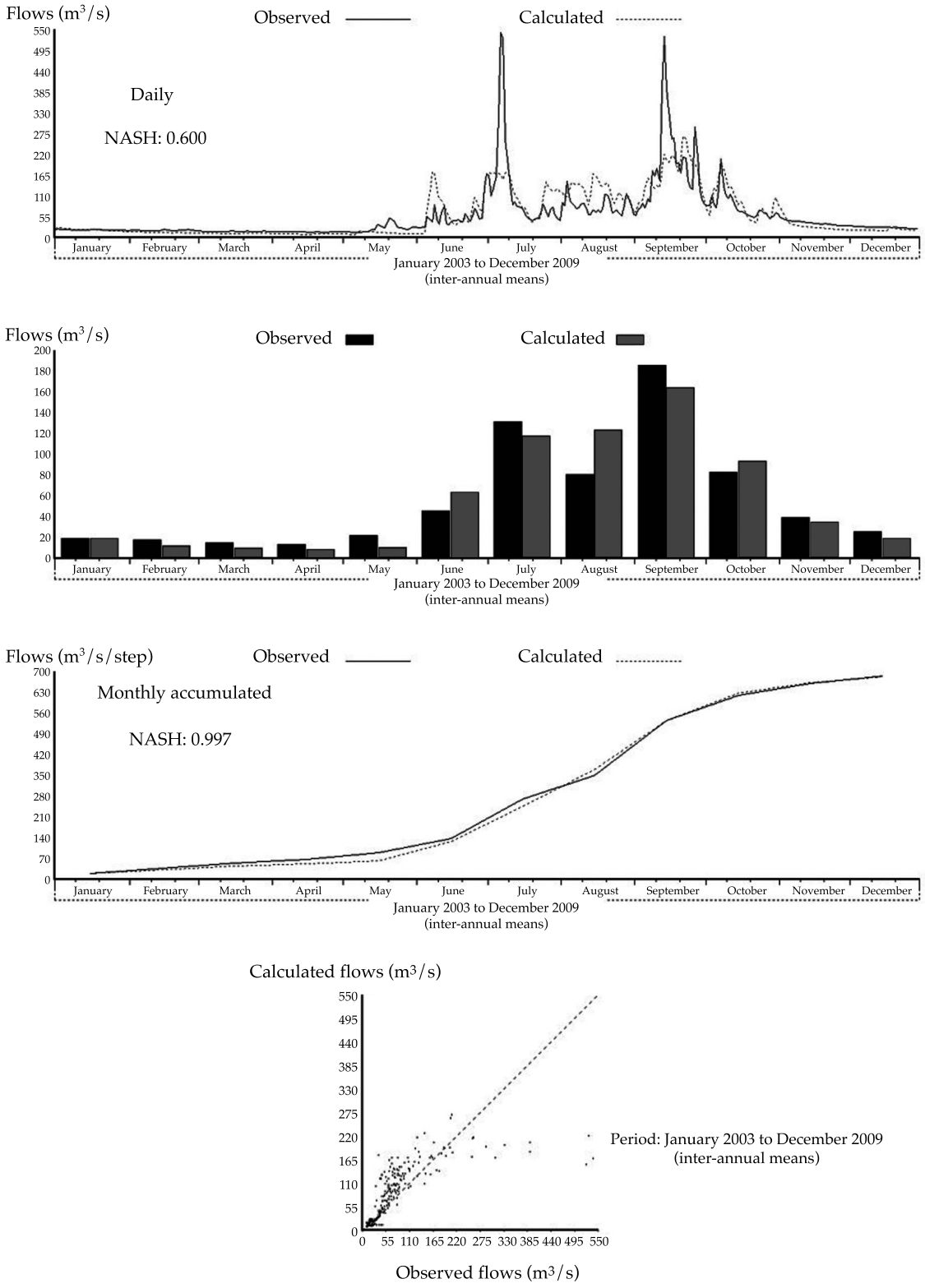

Figure 5. Hydrographs with radar images (inter-annual, 2008-2009).

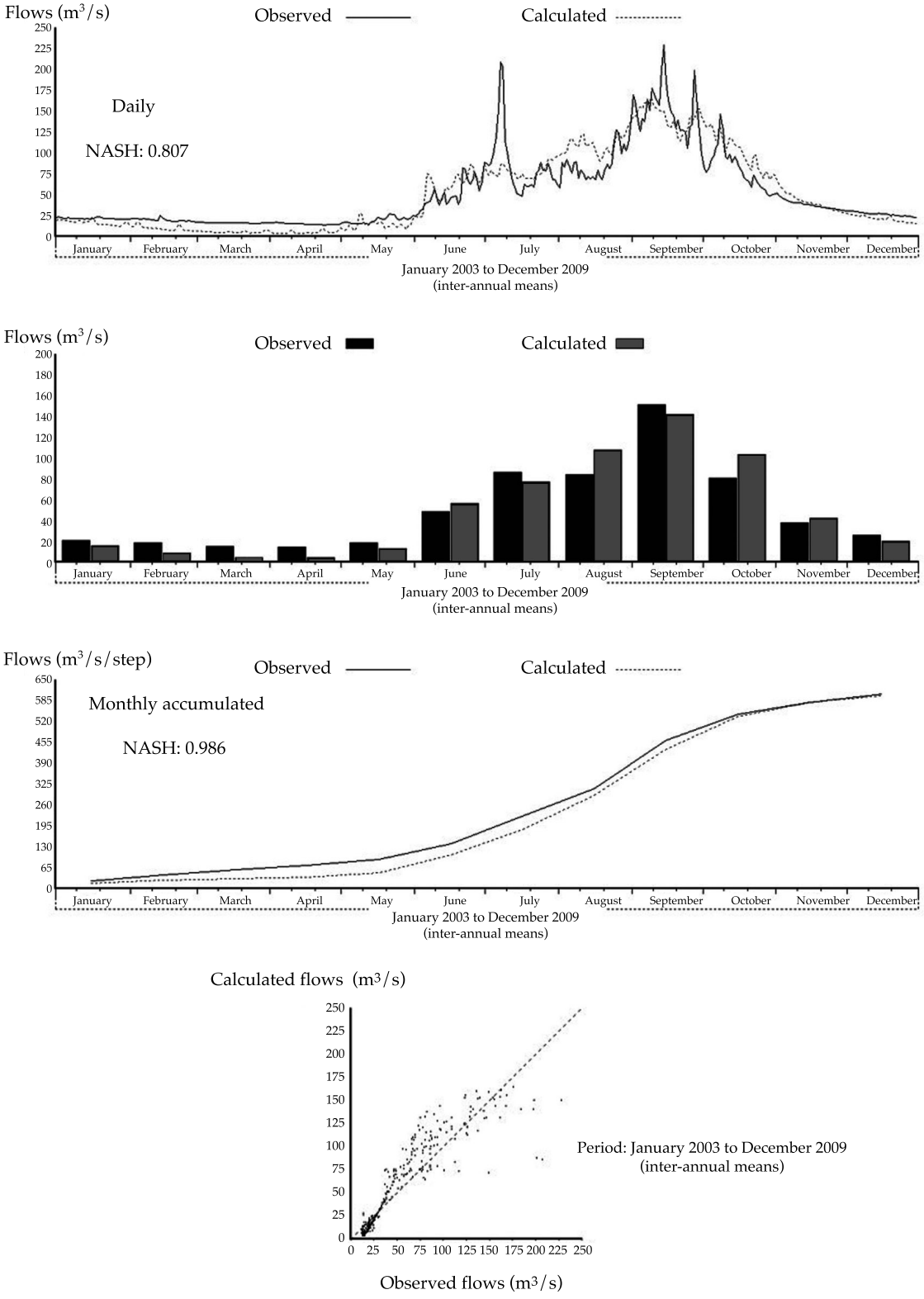

Figure 6. Hydrographs with PERSIANN images (inter-annual, 2003-2009).

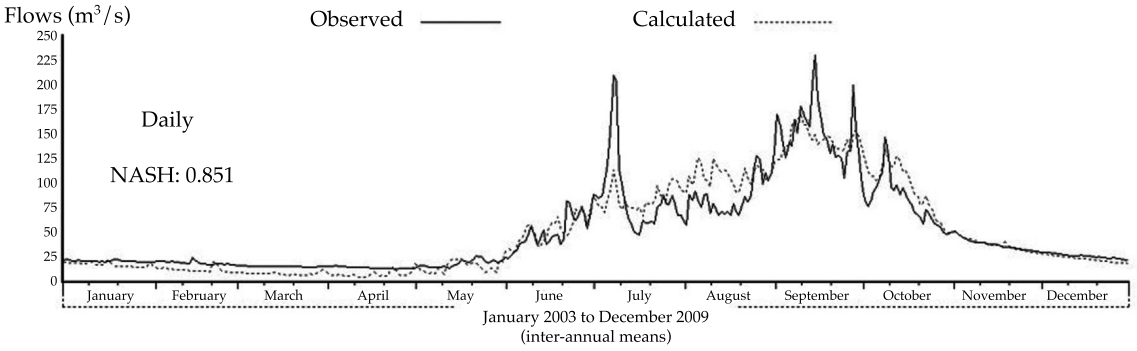

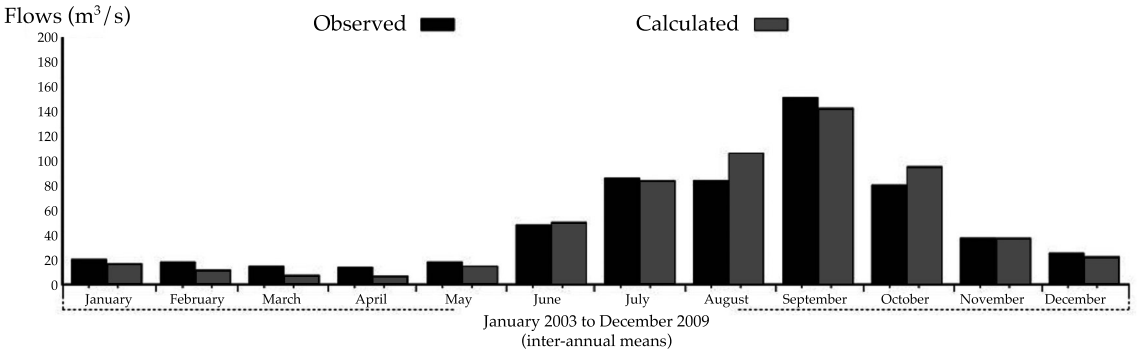

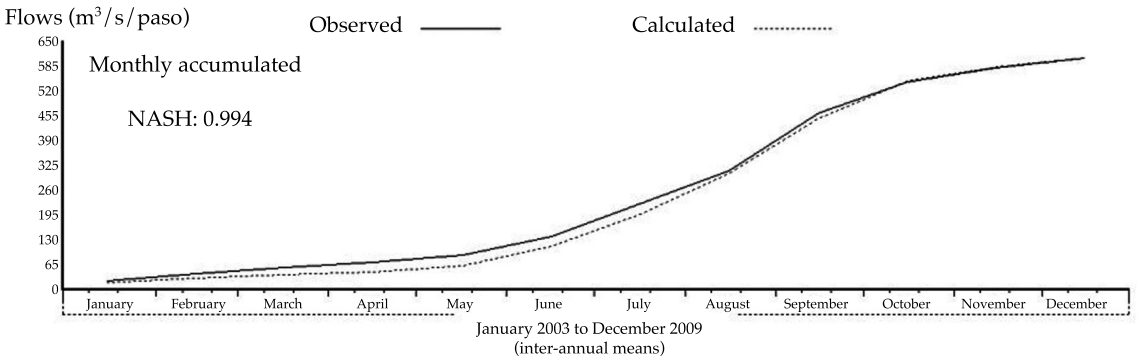

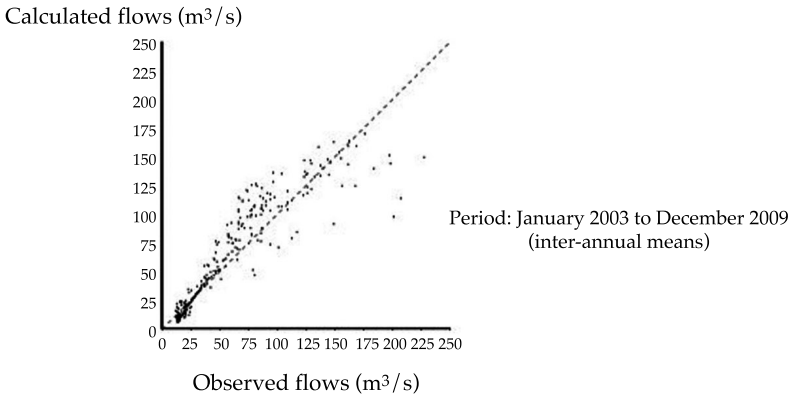

Figure 7. Hydrographs with CMORPH images (inter-annual, 2003-2009).

References

Ayadi, M., & Bargaoui, Z. (1998). Modélisation des écoulements de l'oued Miliane par le modèle CEQUeau. *Journal des Sciences Hydrologiques*, *43*(5), 741-758.

Bâ, K. M., Díaz-Delgado, C., Quentin, E., Ojeda, C. I., Guerra-Cobián, V. H., Carsteanu, A., & Franco, P. R. (2013). Modelación de grandes cuencas con *SIG-IDRISI* y *CEQUEAU*: caso de estudio del río Senegal, África Occidental. *Tecnología y Ciencias del Agua*, *4*(2), 129-136.

Bâ, K. M., & Serrat-Capdevila, A. (2012). Modelación hidrológica con precipitación estimada por imágenes satelitales: el caso del río La Sierra (México) (pp. 261-287). En *La importancia de las inundaciones en la gestión integrada de los recursos hídricos*. Querétaro, México: Universidad Autónoma de Querétaro.

Bâ, K. M., Díaz, C., & Rodríguez, V. (2001). Simulación de caudales de los ríos Amacuzac y San Jerónimo en el Estado de México, México. *Ingeniería Hidráulica en México*, *16*(4), 117-126.

Bedient, P. B., Anthony, H., Benavides, J. A., & Vieux, B. E. (2003). Radar-Based Flood Warning System Applied to Tropical Storm Allison. *Journal Hydrologic Engineering*, *8*(6), 308-318.

Bedient, P. B., Hoblit, B. C., Gladwell, D. C., & Vieux, B. E. (2000). NEXRAD Radar for Flood Prediction in Houston. *Journal Hydrologic Engineering*, *5*(3), 269-277.

Chávez, C. R., & Galicia, J. A. (2002). *Diseño e implementación de una herramienta computacional para el manejo de bases de datos hidrométricas y meteorológicas para el modelo hidrológico* CEQUEAU. Tesis de Licenciatura en Ingeniería de Computación. Toluca, México: Facultad de Ingeniería, Universidad Autónoma del Estado de México.

Behrangi, A., Andreadis, K., Fisher, J. B., Turk, F. J., Granger, S., Painter, T., & Das, N. (2014). Satellite-Based Precipitation Estimation and its Application for Streamflow Prediction over Mountainous Western U.S. Basins. *American Meteorological Society*, *53*, 2823-2842.

Dinku, T., Ceccato, P, Cressman, K., & Connor, S. J. (2010). Evaluating Detection Skills of Satellite Rainfall Estimates over Desert Locust Recession Regions. *J. Appl. Meteor. Climatol.*, *49*, 1322-1332.

Ebert, E. E., Janowiak, J. E., & Kidd, C. (2007). Comparison of Near-Real-Time Precipitation Estimates from Satellite Observations and Numerical Models. *Bull. Amer. Meteor. Soc. 88*, 47-64.

Eleuch, S., Carsteanu, A., Ba, K. M., Magagi, R., Goïtia, K., & Diaz-Delgado, C. (2010). Validation and Use of Rainfall Data to Simulate Water Flows in the Rio Escondido Basin. *Stochastic Environmental Research and Risk Assessment Journal*, *24*(5), 559-565. Online, September 3, 2009.

Fattorelli, S., Casale, R., Borga, M., & Da Ros, D. (1999). *Integración de técnicas radar y sensores remotos para la estimación de lluvias en aplicaciones hidrológicas y mitigación de riesgos de inundación*. Comisión Europea/Asociación Italiana de Hidronomía (AIDI)/Programa Europeo del Medio Ambiente/UNESCO/PHI. Recuperado de http://www.unesco.org.uy/phi/libros/Fattorelli.pdf.

Franco-Plata, R. (2008). *Concepción e implementación de un módulo hidrogeomático para la evaluación de disponibilidad de recursos hídricos* (185 pp.). Tesis doctoral. Toluca, México: Centro Interamericano de Recursos del Agua de la Facultad de Ingeniería de la UAEM.

Franco-Plata, R., Miranda, V. C., Solares, H. H., Manzano, L. R., Bâ, K. M., & Exposito, J. L. (2013). Implementing into GIS a Tool to Automate the Calculation of Physiographic Parameters of River Basins. *Open Journal of Modern Hydrology* (OJMH), *3*, 67-74. Published Online April, 2013. Recuperado de http://scirp.org/journal/ojmh.

Guerra-Cobián, V. H., Bâ, K. M., Quentin-Joret, E., Díaz-Delgado, C., & Cârsteanu, A. A. (julio-septiembre de 2011). Empleo de información NEXRAD en el modelado hidrológico para cuencas con pluviometría deficiente. *Tecnología y Ciencias del Agua*, antes Ingeniería hidráulica en México, *2*(3), 35-48.

Habib, E., Haile, A. T., Tian, Y., & Joyce, R. (2012a). Evaluation of the High-Resolution CMORPH Satellite Rainfall Product Using Dense Rain Gauge Observations and Radar-Based Estimates. *Journal of Hydrometeorology*, *13*, 1784-1798.

Habib, E., Elsaadini, M., & Haile, A. T. (2012b). Climatology-Focused Evaluation of CMORPH and TMPA Satellite Rainfall Products over the Nile Basin. *American Meteorological Society*, *51*, 2105-2121.

Hong, Y., Hsu, K. L., Sorooshian, S., & Gao, X. G. (2004). Precipitation Estimation from Remotely Sensed Imagery Using an Artificial Neural Network Cloud Classification System. *J. Appl. Meteor.*, *43*, 1834-1852.

Hossain, F., Anagnostou, E. N., Dinku, T., & Borga, M. (2004). Hydrological Model Sensitivity to Parameter and Radar Rainfall Estimation Uncertainty. *Hydrological Processes*, *18*, 3277-3291.

Hsu, K. L., Gao, X. G., Sorooshian, S., & Gupta, H. V. (1997). Precipitation Estimation from Remotely Sensed Information Using Artificial Neural Networks. *J. Appl. Meteor.*, *36*, 1176-1190. Recuperado de http://ete.inrs.ca/ete/publications/cequeau-hydrological-model (01/2015).

Joyce, R. J., Janowiak, J. E., Arkin, P. A., & Xie, P. (2004). CMORPH: A Method that Produces Global Precipitation Estimates from Passive Microwave And Infrared Data At High Spatial And Temporal Resolution. *J. Hydrometeor.*, *5*, 487-503,

Joyce, R., & Xie, P. (2011). Kalman Filter –Based CMORPH. *American Meteorological Society*, *12*, 1547-1563.

Lee, Y. R., Shin, D. B., Kim, J. H., & Park, H. S. (2014). Precipitation Estimation over Radar Gap Areas Based On

Satellite And Adjacent Radar Observations. *Atmos. Meas. Tech. Discuss*., *7*, 6299-6325.

Llanos, H., Bâ, K. M., & Castiella, A. (1999). Modelación hidrológica de la cuenca alta del río Ega (País Vasco y Navarra). *Ingeniería del Agua*, *6*(3), 241-250.

Magaña-Hernández, F., Bâ, K. M., & Guerra-Cobián, V. H. (diciembre, 2013). Estimación del hidrograma de crecientes con modelación determinística y precipitación derivada de radar. *Agrociencia*, *47*(8), 745-755.

Morin, G., Sochanski, W., & Paquet, P. (1998). *Le modèle de simulation de quantité CEQUEAU-ONU, Manuel de référence* (252 pp). Rapport de recherche No 519. Saint-Foy, Quebec: Organisation des Nations-Unies et INRS-Eau.

Morin, G., & Paquet, P. (2007). *Le modèle hydrologique CEQUEAU* (458 pp.). Rapport de recherche no R000926. Saint-Foy, Quebec: INRS-ETE.

Powell, M. J. D. (1964). An Efficient Method for Finding the Minimum of a Function of Several Variables without Calculating Derivatives. *Computer Journal*, *7*, 155-162.

Serrat-Capdevila, A., Valdes, J., Bâ, K. M., Durcik, M., Merino, M., & Demaria, E. M. (2013). *Hydrologic Simulations of Three Poorly Gauged Watersheds of the Senegal River Using a Lumped and a Distributed Model with Different Inputs*. American Geophysical Union, Meeting of the Americas, Cancun, Mexico, May, 14-17.

Singh, V. P., & Frevert, D. K. (2002). *Mathematical Models of Large Watershed Hydrology*. Highlands Ranch, USA: Water Resources Publications. LLC..

Sorooshian, S., Hsu, K., Gao, X., Gupta, H. V., Imam, B., & Braithwaite, D. (2000). Evaluation of PERSIANN System Satellite-Based Estimates of Tropical Rainfall. *Bulletin of American Meteorology Society*, *81*, 2035-2046.

Sorooshian, S., & Arfi, F. (1982). Response Surface Parameter Sensitivity Analysis Methods For Postcalibration Studies. *Water Resources Research*, *18*(5), 1531-1538.

Stisen, S., & Sandholt, I. (2010). Evaluation of Remote-Sensing-Based Rainfall Products through Predictive Capability in Hydrological Runoff Modeling. *Hydrol. Process*., *24*, 879-891.

Vilchis-Mata, I., Quentin, E., Bâ, K. M., & Díaz-Delgado, C. (octubre-diciembre de 2011). Estimación de precipitación diaria a través de un SIG con imágenes de radar meteorológico. *Tecnología y Ciencias del Agua*, *2*(4), 167-174.

Vilchis-Mata, I. (2013). *Estimación y validación de precipitación derivada de imágenes de satélite y radar para uso en modelos hidrológicos* (150 pp.). Tesis doctoral. Toluca, México: Centro Interamericano de Recursos del Agua de la Facultad de Ingeniería de la UAEM.

WMO (1992). *Simulated Real-Time Intercomparison of Hydrological Models*. Operational Hydrology Report No. 38. Genoa: World Meteorological Organization.

WMO (1986). *Intercomparison of Models of Snowmelt Runoff*. Operational Hydrology Report No. 23. Genoa: World Meteorological Organization.

Institutional Address of the Authors

Dr. Iván Vilchis-Mata
Dr. Roberto Franco-Plata

Universidad Autónoma del Estado de México
Facultad de Geografía
Cerro de Coatepec, Ciudad Universitaria
50110 Toluca, México, México
Teléfono: +52 (722) 215 0255
ivilchism@uaemex.mx
rfplata@gmail.com

Dr. Khalidou M. Bâ
Dr. Carlos Díaz-Delgado

Universidad Autónoma del Estado de México
Facultad de Ingeniería
Carretera Toluca Atlacomulco k. 14.5, Unidad San Cayetano
50200 Toluca, Estado de México, México
Teléfonos: +52 (722) (296) 555 051 y 1806 191 y 92 # 111
khalidou@uaemex.mx
cdiazd@uaemex.mx

Metal Concentrations in Water and Sediments in the Upper Grijalva River Basin, Mexico-Guatemala border

• Rafaela María Laino-Guanes* •
El Colegio de la Frontera Sur, México
*Corresponding Author

• Ricardo Bello-Mendoza •
University of Canterbury, New Zealand

• Mario González-Espinosa • Neptalí Ramírez-Marcial •
El Colegio de la Frontera Sur, México

• Francisco Jiménez-Otárola •
Centro Agronómico Tropical de Investigación y Enseñanza, Costa Rica

• Karim Musálem-Castillejos •
El Colegio de la Frontera Sur, México

Abstract

Laino-Guanes, R. M., Bello-Mendoza, R., González-Espinosa, M., Ramírez-Marcial, N., Jiménez-Otárola, F., & Musálem-Castillejos, K. (July-August, 2015). Metal Concentrations in Water and Sediments in the Upper Grijalva River Basin, Mexico-Guatemala border. *Water Technology and Sciences* (in Spanish), 6(4), 61-74.

This work presents an evaluation of heavy metal concentrations in the upper Grijalva River basin, in micro-basins with rivers that supply water to communities on the Mexico-Guatemala border, representing a possible risk to human health. In addition, given current prospecting activities and interest in developing mining in the near future, this study can provide reference values with which to evaluate the environmental impact of these activities in the region. Metal contents (As, Cd, Cr, Cu, Hg, Ni, Pb and Zn) were evaluated in surface water and in sediments during the rainy season (August 2011 and June 2012) as well as the dry season (January 2012 and December 2012) in the Xelaju and Bacanton River basins, as well as in the sub-basins of the Allende, Buenos Aires, Molino and Carrizal Rivers. The results were compared with norms corresponding to Mexico and Canada, and in the case of sediments, also with background reference levels in the United States. Concentrations of Hg exceeded the maximum allowable limits established by both norms and the reference levels mentioned, during both the rainy and dry seasons. The results suggest that wastewater from the city of Motozintla de Mendoza discharged into the Xelaju River partially explains the increase in Hg concentrations in the water and sediments. The concentrations of As, Cd, Cr, Cu, Ni, Pb and Zn detected were minimal and did not exceed maximum limits allowed by Mexican norms, although in some cases they exceeded those established by Canadian norms and the United States reference values.

Keywords: Mercury, rivers, mining, Motozintla de Mendoza.

Resumen

Laino-Guanes, R. M., Bello-Mendoza, R., González-Espinosa, M., Ramírez-Marcial, N., Jiménez-Otárola, F., & Musálem-Castillejos, K. (julio-agosto, 2015). Concentración de metales en agua y sedimentos de la cuenca alta del río Grijalva, frontera México-Guatemala. Tecnología y Ciencias del Agua, *6(4), 61-74.*

Se presenta una evaluación sobre la concentración de metales pesados en la cuenca alta del río Grijalva en microcuencas cuyos ríos abastecen de agua a comunidades de la región fronteriza México-Guatemala por sus posibles riesgos para la salud humana. Además, en virtud de las acciones actuales de prospección y del interés por el desarrollo de la minería en el futuro próximo, este estudio puede brindar valores de referencia sobre los cuales se pueda evaluar el impacto ambiental de tales actividades en la región. Se evaluó el contenido de metales (As, Cd, Cr, Cu, Hg, Ni, Pb y Zn) en agua superficial y en sedimentos durante la época de lluvias (agosto de 2011 y junio de 2012) y en época seca (enero de 2012 y diciembre de 2012) en las cuencas de los ríos Xelajú y Bacantón, así como en las subcuencas de los ríos Allende, Buenos Aires, Molino y Carrizal. Los resultados fueron contrastados con las normativas correspondientes de México y Canadá, y también, en el caso de los sedimentos, con los niveles de fondo de referencia para los Estados Unidos de América. Las concentraciones de Hg rebasaron los límites máximos permisibles (LMP) establecidos en ambas normas y niveles de referencia revisados tanto en época de lluvias como en la seca. Los resultados sugieren que la descarga de aguas residuales de la ciudad de Motozintla de Mendoza al río Xelajú explica parcialmente el incremento de la concentración de Hg tanto en las aguas como en los sedimentos. Las concentraciones detectadas de As, Cd, Cr, Cu, Ni, Pb y Zn fueron mínimas y no sobrepasaron los LMP en la norma mexicana; sin embargo, en algunos casos rebasaron los LMP establecidos en la norma canadiense y en los valores de referencia de los Estados Unidos.

***Palabras clave**: mercurio, ríos, minería, Motozintla de Mendoza.*

Received: 28/03/2014
Accepted: 31/03/2015

Introduction

Although some metals are crucial for living beings, high levels of exposure damage human health as well as flora and fauna (García-García, Pedraza-Garciga, Montalvo, Martínez, & Leyva, 2012; Jiménez-Cisneros, 2001; White & Rasmussen, 1998). Because of their high toxic potential, As, Cd, Cr, Hg and Pb are handled in a particular way and are considered highly dangerous pollutants. Nevertheless, other metals such as Cu and Zn can also be toxic if they exceed certain concentration levels (Esteves, Gil, & Harvey,1996; García-García *et al*., 2012; Soto-Cruz, Carrillo-Chávez, & Suárez-Sánchez, 2011). Some metals tend to accumulate in aquatic organisms ("bioaccumulation"), where concentrations increase when moving up the food chain, presenting a risk to the health of persons who consume them (Pérez-Cruz, Rangel-Ruiz, & Gamboa-Aguilar, 2013). For example, effects of Hg have been observed to intensify when this metal accumulates in the tissue of fish (Jiménez-Cisneros, 2001). Studies performed with marine species warn about this accumulated effect and its transfer through the food chain, and indicate that several heavy metals can be considered to be genotoxic agents (Haesloop & Schirmer, 1985; Sánchez-Galan, Linde, Ayllon, & García-Vázquez, 2001). An example of the transfer of heavy metals in the food chain is the middle Pilcomayo River Basin, in Bolivia, where high concentrations of metals were detected in the hair of the inhabitants living near the edges of the basin. This was attributed to the consumption of fish and water from the river. This river is polluted by the exploitation of minerals in the upper basin (Smolders, Archer, Stassen, Llanos-Cavero, & Hudson-Edwards, 2006).

Domestic, agricultural and industrial wastes represent the primary sources of heavy metal pollutants in water bodies (Castro & Valdés, 2012). The determination of natural concentrations of heavy metals and the contribution from anthropic sources makes it possible to evaluate the degree to which a particular zone is affected. To this end, an analysis of both water and sediments is indispensable (Villanueva & Botello, 1992), particularly since metals tend to be deposited in river sediments (Soto-Cruz *et al*., 2011) even when concentrations in water are low (Leal-Ascencio,Miranda, Sánchez, Prieto-García, & Gordillo, 2009; Szalinska, Haffner, & Drouillard, 2007).

Rivers are one of the primary means of metal transport in coastal regions. They are transported by the movement of materials from the middle and upper basins (Zhang *et al*.,1992). The effects of heavy metals on marine ecosystems are of particular interest because these pollutants are contained in sediments which can be released into the water, becoming available to the marine biota. This represents a potential threat to the functioning of an ecosystem (Visviki & Rachlin, 1991).

Studies performed in the middle and lower Grijalva River basin confirm the presence of heavy metals in both the water and sediments in the basin's rivers and lakes (Leal-Ascencio *et al*., 2009; Pérez-Cruz *et al*., 2013), as well as at the mouth of this river in the Gulf of Mexico (Rosales-Hoz,Carranza-Edwards, Santiago-Pérez, Méndez-Jaime, & Doger-Badillo, 1994; Vázquez, Elias,Aguayo, & Baeza, 1996; Villanueva & Botello,1992). Nevertheless, very few studies exist about the presence of metals in the upper basin (Alvarado-Arcia, Ilizaliturri-Hernández, Martínez-Salinas, & Torres-Dosal,2014), which is important to understanding the origins of these pollutants and the dynamics throughout the entire basin.

Meanwhile, mineral resources found in the upper Grijalva River basin in both Mexico and Guatemala are of great interest to mining companies (Copae, 2010; Robleto-Morales,2011). The 2001 – 2006 National Mining Development Program of Mexico, published in the *Official Journal of the Federation* on

November 24, 2003, states that Chiapas has a vast mining potential which has not been exploited. In 2010, a total of 112 mining licenses were granted in Chiapas (Roblero-Morales, 2011). According to the Mexican Mining Administration System, the licenses in the upper Grijalva River would be used to mine gold, silver, lead, copper and trisodium phosphate (SIAM, 2015). The extraction of these minerals could create pollution from mercury, arsenic, lead and other products associated with mining, depending on the process used and the management of the wastes (Alpers, Myers, Millsap, & Regnier,2014; Pinedo-Hernández, Marrugo-Negrete, & Diez, 2014; PNUMA, 2002; UNEP, 2013).

Given this panorama, Alvarado-Arcia *et al*.(2014) report the possibility of an increase in mining activity in the coming years, along with its inherent environmental consequences. Mining extraction presents a risk to human health and alters the environment, generating soils with physical, chemical and biological conditions that limit the establishment of vegetation and other organisms (Puga, Sosa,Lebgue, Quintana, & Campos, 2006). Open pit mining is one of the highest risk industries in the world, both for those who work there because of the materials used as well as for persons who live in nearby communities because of the irrational use of natural resources such as water and the severe impacts generated (Copae, 2010; Osores-Plenge, Rojas-Jaimes, & Manrique-Lara- Estrada, 2012). In addition, when mining activities cease the sites are often abandoned and negatively affect the quality of the water, soil and air in the ecosystems in which they are located. The environment is constantly affected when remediation and cleanup measures are not performed at the sites (Kirschbaum, Murray,Arnosio, Tonda, & Cacciabue, 2012).

This study is aimed at establishing a baseline concentration of heavy metals, which has been the subject of very few studies in the region. Since the presence of metals in ecosystems is also related to natural causes, the values presented in this study could contribute to understanding background levels and constructing a reference point that can be used in future investigations to determine whether or not a pollutant has been released, in anticipation of the possible mining exploitation.

The objectives of this study were: (1) to evaluate the presence of metals in water and sediments in six tributaries of the Grijalva River, in the upper basin (border between Mexico and Guatemala); and (2) identify whether the wastewater from Motozintla de Mendoza (Chiapas), the main urban population in the study area, contributes to heavy metal pollution in the river receiving these wastes, and if this could represent a potential risk to the communities downstream in the basin. To this end, the presence of metals in the largest tributaries of the Xelaju River was analyzed, three of which represent the main source of water for the city of Motozintla de Mendoza.

Methods

Study Area

The study area is composed of the Xelaju and Bacanton River basins, located on the Mexico-Guatemala border, in the upper Grijalva River basin (Figure 1). The Xelaju River basin is located in Mexico, in portions of the municipalities of Motozintla de Mendoza and Mazapa de Madero, in the state of Chiapas. The Bacanton River begins in Guatemala, in the municipality of Tacana, state of San Marcos. It crosses the Guatemala-Mexican border in the municipality of Mazapa de Madero, Chiapas. These rivers are tributaries of the Grijalva River, which empties into the Gulf of Mexico, in the state of Tabasco. The city of Mazapa de Madero is located in the middle Xelaju basin, whose main tributaries are the

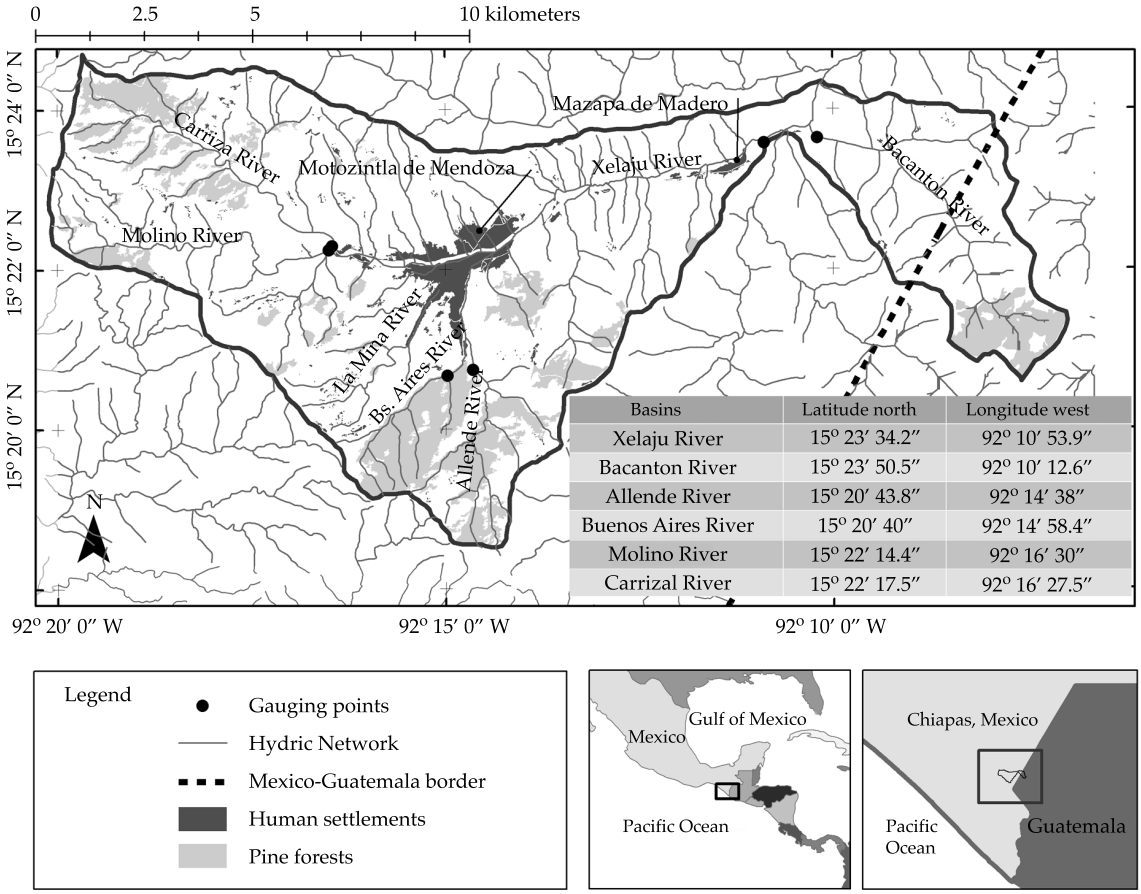

Figure 1. Location of the study area, geographic coordinates of the gauging points in the Xelaju and Bacanton river basins, and the Allende, Buenos aires, Molino and Carrizal sub-basins, on the Mexico-Guatemala border.

Allende, Buenos Aires and La Mina rivers, which begin south of the city. The Molino and Carrizal rivers begin west of that city. The Allende, Buenos Aires, Molino and Carrizal sub-basins are delimited within the Xelaju River in order to detect the presence of heavy metals in the sediments and water before and after the water courses pass though the city of Motozintla de Mendoza.

The Xelaju River basin has an area of 9 728 ectares and nearly 33 068 inhabitants (including the city of Motozintla de Mendoza with 23 755 inhabitants). The Bacanton River basin has 1 968 hectares and an estimated population of 2 321 inhabitants (746 in Mexico and 1 575 in Guatemala). The Allende, Buenos Aires, Molino and Carrizal sub-basins measure 884, 532, 1 146 and 1 693 hectares and have 563, 179, 1 498 and 1 751 inhabitants, respectively (Laino-Guanes, Musálem-Castillejos, González-Espinosa, & Ramírez-Marcial, 2014).

The city of Motozintla de Mendoza receives surface water primarily from the Allende, Buenos Aires and Carrizal rivers, and untreated municipal wastewaters are discharged into the Xelaju River. The other smaller communities also receive their water generally from surface sources and discharge their domestic wastes into land that is adjacent to their housing or in nearby streams. Their sanitary waste is deposited in septic

tanks. Most of the families in Motozintla de Mendoza and the rest of the rural populations in the study region live in conditions of extreme poverty and marginalization, with serious deterioration in natural resources (Caballero *et al*., 2006; Ordóñez, 2010).

The study region is highly seismic due to geological faults (Plascencia-Vargas,González-Espinosa, Ramírez-Marcial, Álvarez-Solis, & Musálem-Castillejos, 2014). The Polochic-Motagua fault system runs across the Motozintla valley, where a volcanic-plutonic outcropping tectonically lies on top of partially eroded Mesozoic sediments (Carfantan, 1977). The surface lithology of the area is made up of rocks that are sedimentary, volcanic-sedimentary, intrusive and extrusive igneous and metamorphic (INEGI,1980; MAGA, 2005).

The rainy season is from May to October and the dry season from November to April. Annual mean precipitation is 822 mm at the Motozintla de Mendoza weather station (15º 22′ 00′′ latitude north; 92º 15′30′′ longitude west; 1 210 m altitude) and 1 278 mm at the Buenos Aires station (15º 19′ 57′′latitude north; 92º 16′ 03′′ longitude west; 1 720 m altitude), according to historical data from 1978 for the Motozintla de Mendoza station and from 1982 for the Buenos Aires station (National Water Commission; Conagua, 2011).

Sample Collection and Determination of Heavy Metals

Concentrations of As, Cd, Cr, Cu, Hg, Ni, Pb and Zn in water and sediments were quantitatively determined at gauging points in the two basins and the four sub-basins. Their geographic coordinates are presented in the map of the study area (Figure 1). A total of 19 simple water samples were collected in 1-liter plastic (polypropylene) containers which were hermetically sealed. First, samples were taken during the rainy season (August 2011 and June 2012) and the dry season (January 2012) for the analysis of all metals. Then, since the results indicated the absence of all these metals or negligible quantities with the exception of Hg, only this element was analyzed one more time in December 2012. The samples taken in the rainy season were collected a minimum of 48 hours after the last precipitation in order to ensure base flows in all cases and to prevent measurements during peak flows in which sediment transport could distort the results.

The channels of two rivers (Molino and Carrizal) studied dried up completely during the dry season and therefore no water samples were obtained. At the edge of the sites where the water samples were collected, sediment samples were taken during the rainy season (June 2012) when all the rivers had flows. The samples obtained were those with a predominance of clay and silt, since metals tend to accumulate in the smaller particles deposited in the river beds (Pérez-Carreras, Moreno-García, & González-Parra, 1995; Singh, Hasnain, & Banerjee, 1999). The sediment samples were collected in borosilicate glass containers with hermetic seals. At each gauging point, a 1-liter sample of surface sediment was collected at a depth between 0 and 15 cm. This was composed of five sub-samples. The water and sediment samples were kept refrigerated while they were transported to the laboratories.

The analytic determination of Cr, Cu, Ni, Pb and Zn was performed according to Mexican Official Norm NMX-AA-051-SCFI-2001. Flame atomic absorption spectroscopy was used for the samples collected on August 2011 and January 2012. The quantification limits (QL) from the water analysis were 200 µg/l for Cr, Cu and Ni, 190 µg/l for Pb and 340 µg/l for Zn. A high-precision graphite furnace was used for the June 2012 sample, and the QL obtained were 10 µg/l for Cr, 5 µg/l for Cu and Pb and 20 µg/l for Ni. The determination of Zn was not performed since it did not have the sensitivity required by the equipment. The QL corresponding to the sedi-

ment analysis were 5 mg/kg for Cr and Ni, 10 mg/kg for Cu, 0.2 mg/kg for Pb and 2 mg/kg for Zn. A VARIAN brand atomic absorption spectrophotometry was used (SpectrAA220 model) and the graphite furnace was a VARIAN braned, model GTA110. Three procedures were used for quality control: (1) use of *Trace* Metals WasteWateR™ reference material, lot P192-500, ERA brand, (2) sample analysis in triplicate and (3) analysis of the target reagent.

The analysis of As, Cd and Hg were performed with a GBC brand, AVANTA PM model atomic absorption spectrophotometry and a GBC brand HG 3000 model flame and hydride generator. The samples were previously processed with a LABCONCO brand Six-Place Kjeldahl semi-micro digester. The QL obtained from the water analysis were 0.05 µg/l for As and Hg and 0.4 µg/l for Cd. The QL from the sediment analyses were 0.18 mg/kg for As, 1.73 mg/kg for Cd and 0.25 mg/kg for Hg. For each parameter, four target treatment were analyzed and one in triplicate for quality control. The certified reference material was also performed in triplicate. The EAA's ET-QU03 procedures for the determination of heavy metals were followed (2008).

In addition, water samples were collected from each sampling point to measure total hardness (mg $CaCO_3$/l) using a volumetric acid-base titration technique according to the APHA 2340 C method (1998).

Maximum permissible limits according to Mexican and Canadian norms and U.S.

Reference Levels

The concentrations of metals in water were compared to the Official Mexican Norm NOM-127-SSA1 (1994) which establishes the maximum permissible limits (MPL) for water quality for human use and consumption. This legislation does not include Ni. Canadian Environmental Quality Guidelines (CEQG) were also used, which establish water quality parameters for metals in continental waters for the protection of aquatic life. The Canadian guidelines do not include total Cr and propose using formulas based on total water hardness to calculate guideline values for Cu, Ni and Pb (see MPL and formulas in Table 1).

In Mexico, no MPL have been established for metals in sediments and, therefore, the results from this study will be compared to the Mexican Official Norm NOM-147-SEMARNAT/SSA1, 2004 , Criteria to Determine Contamination of Soils by Heavy Metals. This legislation does not include total Cr (only hexavalent), Cu or Zn values. Canadian CEQG guidelines were also used, which establish reference values for metals in sediments present in continental water bodies.

Although these guidelines do not include Ni, two values have been established for As, Cd, Cr, Cu, Hg, Pb and Zn: (1) those by the Interim Sediment Quality Guideline (ISGQ) which represent the concentrations below which no adverse biological effects are expected and (2) the Probable Effect Level, which is the concentration above which ad-

Table 1. Permissible limits for metals in water, established by Offical Mexican Norm (OMN) and Canadian guidelines (CEQG).

Norm	As	Cd	Cr	Cu	Hg	Ni	Pb	Zn
	(µg/l)							
OMN	50	5	50	2000	1	-	25	5 000
CEQG	5	0.09	-	$e^{0.8545}$ [ln(hardness)] - 1.465 * 0.2 µg/l	0.026	$e^{0.76}$ [ln(hardness)] + 1.06 µg/l	$e^{1.273}$ [ln(hardness)] - 4.705 µg/l	30

OMN: Official Mexican Norm 127-SSA1-1994 which establishes permissible water quality limits for human use and consumption.
CEQG: *Canadian Environmental Quality Guidelines*, which establish water quality parameters for the protection of aquatic life with respect to the presence of metals in continental waters.

verse biological effects often appear. Lastly, the results from metals in sediments were compared to background levels established by the reference table (Screening Quick Reference Table for Inorganics in Freshwater Sediment) issued by the National Oceanic and Atmospheric Administration (NOAA). See MPL and reference levels in Table 2.

Results and Discussion

The presence of Hg was detected in all the basins (Table 3). Concentrations were not quantifiable during the rainy season (August 2011). The QL (quantification limits) from the analysis was lower than the MPL (maximum permissible limits) established by Mexican norms but above the Canadian MPL. In June 2012, the Hg concentrations in all the rivers except the Molino River exceeded the MPL established by Mexican and Canadian norms. During the dry season, the Molino and Carrizal rivers did not have any flow, while the Hg in the Allende and Buenos Aires Rivers were not quantifiable by the method used by the analysis. In January 2012, higher concentrations were found in the Xelaju and Bacanton rivers, 3.26 μg/l and 2.58 μg/l, respectively. These values exceeded the MPL established by Mexican and Canadian norms. In December 2012, the Hg values found in the Xelaju and Bacanton rivers exceeded the MPL established by Canadian norms but not those by Mexican norms (see MPL in Table 1).

The Cu, Pb and Zn concentrations were not quantifiable in any of the basins with the analytical method used, except for: (1) June 2012 when 21 μg/l of Cu was detected in the Carrizal River, value which is lower than the MPL established by Mexican norms but higher than the Canadian MPL calculated based on total hardness; (2) June 2012, when 10 and 12 μg/l of Pb were detected in the Xelaju and Carrizal rivers, respectively, values which are lower than the Mexican MPL and higher than the Canadian MPL calculated based on water hardness. It is worth mentioning that the QL from the analytical method used for Pb in August 2011 and January 2012 exceeded the MPL established by Mexican norms; and (3) In August 2011, when 440 μg/l of Zn was detected in the Bacanton River, which is lower than the Mexican MPL but higher than the Canadian norm. For Zn, the QL from the analytical method used exceeded the Canadian MPL.

The Cd, Cr and Ni concentrations were not quantifiable in any of the basins with the analytical methods used. For Cd, the QL from the analytical method used exceeded

Table 2. Permissible limits for metals in sediments, established by Mexican norms (OMN) and Canadian guidelines (CEQG), and background levels for the United States (NOAA; 1999).

Norm		As	Cd	Cr	Cu	Hg	Ni	Pb	Zn
		(mg/kg)							
OMN		22	37	-	-	23	1 600	400	-
CEQG	ISQG	5.9	0.6	37.3	35.7	0.17	-	35	123
	PEL	17	3.5	90	197	0.486	-	91.3	315
NOAA		1.1	0.1-0.3	7-13	10-25	0.004-0.051	9.9	4-17	7-38

NOM: Official Mexican Norm-147-SEMARNAT/SSA1-2004, establishing criteria to determine contamination of soil by metals.
CEQG: *Canadian Environmental Quality Guidelines* for sediments from continental water bodies.
ISQG: *Interim Sediment Quality Guideline*.
PEL: *Probable Effect Level*.
NOAA: *National Oceanic and Atmospheric Administration*, background levels from the *Screening Quick Reference Table for Inorganics in Freshwater Sediment*.

Water *Technology and Sciences*. Vol. VI, No. 4, July-August, 2015, pp. 61-74

Table 3. As, Cd, Cr, Cu, Hg, Ni, Pg and Zn concnetrations in the water in the Xelaju, Bacanton, Allende, Buenos Aires, Molino and Carrizal rivers during the rainy season (August 2011 and June 2012) and the dry season (January 2012 and December 2012 for Hg).

Basin	As (µg/l)			Cd (µg/l)			Cr (µg/l)			Cu (µg/l)		
	Aug. 2011	Jan. 2012	Jun. 2012	Aug. 2011	Jan. 2012	Jun. 2012	Aug. 2011	Jan. 2012	Jun. 2012	Aug. 2011	Jan. 2012	Jun. 2012
Xelaju River	0.55	1.48	< 0.05	< 0.4	< 0.4	< 0.4	< 200	< 200	< 10	< 200	< 200	< 5
Bacanton River	0.42	0.70	< 0.05	< 0.4	< 0.4	< 0.4	< 200	< 200	< 10	< 200	< 200	< 5
Allende River	< 0.05	0.16	< 0.05	< 0.4	< 0.4	< 0.4	< 200	< 200	< 10	< 200	< 200	< 5
Buenos Aires River	0.21	0.96	< 0.05	< 0.4	< 0.4	< 0.4	< 200	< 200	< 10	< 200	< 200	< 5
Molino River	< 0.05	Dry channel	< 0.05	< 0.4	Dry channel	< 0.4	< 200	Dry channel	< 10	< 200	Dry channel	< 5
Carrizal River	< 0.05	Dry channel	< 0.05	< 0.4	Dry channel	< 0.4	< 200	Dry channel	< 10	< 200	Dry channel	21

Table 3 (continued). As, Cd, Cr, Cu, Hg, Ni, Pg and Zn concnetrations in the water in the Xelaju, Bacanton, Allende, Buenos Aires, Molino and Carrizal rivers during the rainy season (August 2011 and June 2012) and the dry season (January 2012 and December 2012 for Hg).

Basin	Hg (µg/l)				Ni (µg/l)			Pb (µg/l)			Zn (µg/l)	
	Aug. 2011	Jan. 2012	Jun. 2012	Dec. 2012	Aug. 2011	Jan. 2012	Jun. 2012	Aug. 2011	Jan. 2012	Jun. 2012	Aug. 2011	Jan. 2012
Xelaju River	< 0.05	3.26	2.17	0.07	< 200	< 200	< 20	< 190	< 190	10	< 340	< 340
Bacanton River	< 0.05	2.58	1.13	0.06	< 200	< 200	< 20	< 190	< 190	< 5	440	< 340
Allende River	< 0.05	< 0.05	1.51	< 0.05	< 200	< 200	< 20	< 190	< 190	< 5	< 340	< 340
Buenos Aires River	< 0.05	< 0.05	1.44	< 0.05	< 200	< 200	< 20	< 190	< 190	< 5	< 340	< 340
Molino River	< 0.05	Dry channel	0.73	Dry channel	< 200	Dry channel	< 20	< 190	Dry channel	< 5	< 340	Dry channel
Carrizal River	< 0.05	Dry channel	2.13	Dry channel	< 200	Dry channel	< 20	< 190	Dry channel	12	< 340	Dry channel

the Canadian MPL. For Cr, the QL from the analytical method exceeded the Mexican MPL in August 2011, nevertheless the method was more precise in June 2012 when the concentrations detected were below this limit.

During both the rainy and dry seasons, the As concentrations detected were below the Mexican and Canadian MPL or were not quantifiable with the analytical method used.

For sediments in the Xelaju, Bacanton, Allende, Buenos Aires, Molino and Carrizal rivers, the Hg concentrations detected did not exceed Mexican MPL (Table 4). Nevertheless, the values were over the PEL and ISQG established by Canadian guidelines, except for the Carrizal and Bacanton rivers which had Hg concentrations below the PEL (see MPL in Table 2). In the sediments from the Bacanton River, Hg was not quantifiable and the QL from the method used exceeded ISQG and NOAA values. The Hg concentrations detected in the sediments in all the basins exceeded NOAA levels.

The As, Cu and Cr concentrations in the sediments from all the rivers were lower than the Mexican and Canadian MPL, but exceeded NOAA levels in some cases.

The Cd and Pb concentrations in the sediments were not quantifiable in any of the basins. For Cd, the QL from the method exceeded the ISQG and NOAA values. The concentrations of Ni and Zn in the sediments in all the rivers were lower than the Mexican, Canadian and NOAA MPL.

The lack of norms for metals in sediments still needs to be addressed in Mexico and other Latin American countries. Legislation should take into account priorities based on the geographic and environmental conditions of the water bodies in the regions (Leal-Ascencio *et al.*, 2009).

Mercury and the City of Motozintla de Mendoza

The results from the analysis of heavy metals indicate that the Hg concentrations detected in the study area exceeded the Mexican and Canadian MPL for water, and exceeded the Canadian and NOAA MPL for sediments.

Meanwhile, the concentrations of the other metals analyzed (As, Cd, Cr, Cu, Ni, Pb and Zn) were lower than the Mexican MPL (although in some cases they exceeded Canadian and/or NOAA MPL) or were not quantifiable by the analytical method used. Therefore, this section analyzes only the presence of Hg in water and in the sediments from the above rivers after they passed through the city of Motozintla de Mendoza. The gauging points in the Allende, Buenos Aires, Molino and Carrizal rivers (tributaries of the Xelaju River) provide the results before the rivers passed through this city and the gauging point in the Xelaju River (Figure 1) corresponds to the results after passing through the city.

The results from four samples of Hg in water were analyzed, two in the rainy sea-

Table 4. Cd, As, Hg, Cu, Cr, Ni, Pb and Zn concentrations in sediments in the Xelaju, Bacanton, Allende, Buenos Aires, Molino and Carrizal rivers during the rainy season (June 2012).

Basin	As	Cd	Cr	Cu	Hg	Ni	Pb	Zn
	(mg/kg)							
Xelaju River	1.04	< 1.73	8.45	28.09	1.29	7.12	< 0.2	3.29
Bacanton River	0.37	< 1.73	5.62	21.96	< 0.25	9.36	< 0.2	2.25
Allende River	1.31	< 1.73	9.63	25.33	0.74	6.73	< 0.2	3.36
Buenos Aires River	0.53	< 1.73	32.58	23.13	0.52	7.58	< 0.2	2.72
Molino River	0.56	< 1.73	19.03	22.98	0.81	7.37	< 0.2	4.67
Carrizal River	0.92	< 1.73	24.08	29.68	0.31	7.10	< 0.2	2.61

son and two in the dry season. Two of the channels completely dried up during the dry season (Table 3). The data did not present a clear relationship between the presence of Hg and the dry period. Nevertheless, the results suggest the presence of higher Hg concentrations in the flow leaving the city of Motozintla de Mendoza, at least in quantities that exceeded the QL fro, the analytical method used. Due to the inconsistent behavior of the appearance of Hg in water during the different samplings, we focused on the results from June 2012 when the presence was detectable at all sampling points. This situation did not occur during any of the other three sampling periods.

The amount of Hg in water increased after passing through the city of Motozintla de Mendoza (Figure 2), although in both cases (before and after the city) the values detected exceeded Mexican (NOM-127) and Canadian (CEQG) MPL.

Likewise, the concentration of Hg in sediments in June 2012 were higher after the river passed through the city (Figure 3) and, in both cases, the values detected exceeded Canadian (ISGG and PEL) and NOAA MPL, although they were lower than the Mexican (NOM-147) MPL for soil contamination from metals (23 mg/kg).

The sources of Hg could be natural or anthropogenic. Natural sources include volcanic activities, evaporation from land and aquatic surfaces, degradation of minerals, forest fires and erosion of rocks that are natural sources of Hg (Pirrone *et al*., 2010; PNUMA, 2002). Several anthropogenic sources also exist, such as the use of carbon to generate energy and heat; production of cement; use of fluorescent lamps, headlights, manometers, thermostats, thermometers, and other instruments and their accidental breakage; electrical switches; dental fillings; incineration of wastes (municipal, medical and toxic); garbage dumps; crematories; and mining, which includes the extraction of Hg as a main product or as a byproduct from the extraction of other metals, such as gold, silver or zinc (Pirrone *et al*., 2010; UNEP, 2013).

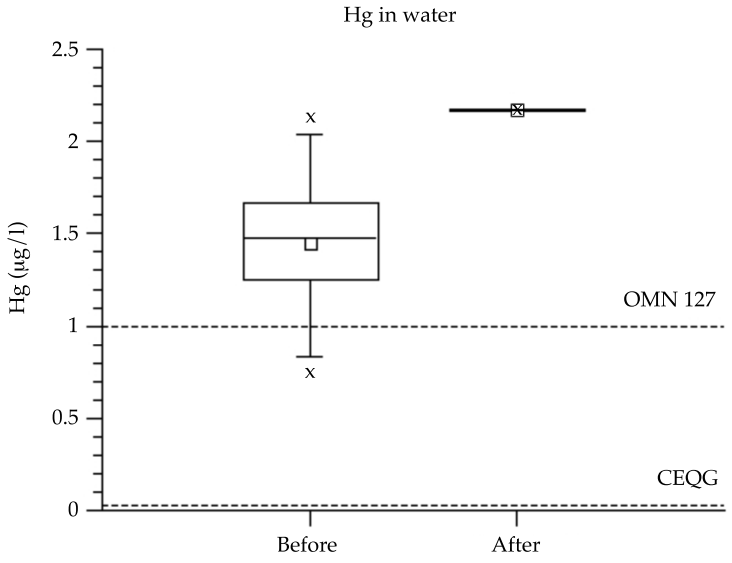

Figure 2. Hg concentrations in water in June 2012) median+lower and upper quartiles) before (including the tributaries of the Allende, Buenos Aires, Molino and Carrizal rivers) and after (gauging point in the Xelaju River) passing through the city of Motozintla de Mendoza. Maximum permissible limits according to Mexcian norm (NOM-127) and Canadian guidelines (CEQG)..

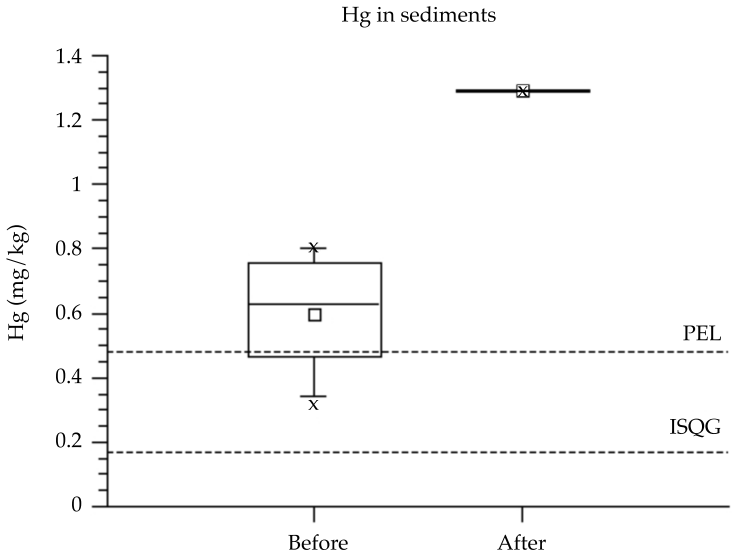

Figure 3. Hg concentrations in water in June 2012 (median+lower and upper quartiles) before (including the tributaries of the Allende, Buenos Aires, Molino and Carrizal rivers) and after (gauging point in the Xelaju River) passing through the city of Motozintla de Mendoza. Canadian environmental quality guidelines (ISGG and PEL).

Considering the presence of volcanoes in the region, some other candidates for the Hg detected in the study area may be related to the geology, especially in regards to the lower amount detected before the river passes through the city of Motozintla de Mendoza. After the city, the increase in Hg concentrations may be from both natural and anthropogenic sources, such as the discharge of untreated municipal wastewater and the dislodging and transport of sediments. Nevertheless, more data are needed to confirm the above.

Conclusions

The metal detected most frequently and with the highest concentration was Hg in water as well as in sediments. Concentrations of Hg increased after the Xelaju River passed through the city of Motozintla de Mendoza. Other potentially toxic elements were detected (As, Cd, Cr, Cu, Ni, Pb and Zn) but in very low concentrations or below the MPL established by Mexican and Canadian norms. More information is needed in order to conclude whether these metals negatively affect the ecosystem and health of the communities downstream in the basin.

Acknowledgements

We thank those in charge of the laboratories at the El Colegio de la Frontera Sur, Juan Jesús Morales, in San Cristóbal de Las Casas, and Adriana Zavala Mendoza, in Chetumal, for the heavy metal determinations. We would like to recognize Anahí Hernández García, Abel Roblero Vázquez, Hugo Santacreu, Juan Suárez, Diana Noriero, Romeo Jiménez, Alejandro Alcudia and Pedro Santiago for their help collecting the water and sediment samples. We thank Andrés Sierra-Soler for helping to collect samples and for obtaining the relevant geographic information for the study area, as well as for processing the boundaries of the sub-basins in the initial stage of this investigation. This work was made possible by the support of the Fondo Institucional de Fomento Regional para el Desarrollo Científico, Tecnológico y de

Innovación (Fordecyt) of the National Council on Science and Technology (Consejo Nacional de Ciencia y Tecnología; Conacyt, Spanish acronym), through grant 143303 "Measures and strategies for sustainable management for the regional development of the cross-border Grijalva hydrographic basin." This project was simultaneously supported in 2010 and 2012 by the Secretary of Natural Resources and Environmental Protection (Sernapam; Spanish acronym) of the state of Tabasco.

References

Alpers, C. N., Myers, P. A., Millsap, D., & Regnier, T. B. (2014). Arsenic Associated with Gold Mining in the Sierra Nevada Foothills: Case Study and Field Trip Guide for Empire Mine State Historic Park, California. *Reviews in Mineralogy and Geochemistry*, *79*, 553-587.

Alvarado-Arcia, A., Ilizaliturri-Hernández, C. A., Martínez-Salinas, R. I., & Torres-Dosal, A. (2014). Riesgos ambientales y de salud por metales (cadmio y mercurio) presentes en suelos y sedimentos del río Grijalva (pp. 240-256). Cap. 9. En M. González-Espinosa, & M. C. Brunel-Manse (Eds.). *Montañas, pueblos y agua. Dimensiones y realidades de la Cuenca Grijalva*. Vol. 1. México, DF: El Colegio de la Frontera Sur y Editorial Juan Pablos.

APHA Standard Methods (1998). *Método 2340 C* (pp. 2-37) (20 ed.). Washington, DC: APHA.

Caballero, L., Macías J. L., García-Palomo, A., Saucedo, G. R., Borselli, L., Sarocchi, D., & Sánchez, J. M. (2006). The September 8-9, 1998 rain-triggered flood events at Motozintla, Chiapas, Mexico. *Natural Hazards*, *39*, 103-126.

CEQG (2003). *Canadian Council of Miners of the Environment*. Canadian Environmental Quality Guidelines. Recuperado de www.st-ts.ccme.ca.

Carfantan, J.Ch. (1977). La cobijadura de Motozintla - Un paleoarco volcánico en Chiapas. Universidad Nacional Autónoma de México, *Instituto de Geología, Revista*, *1*(2), 133-137.

Castro, G., & Valdés, J. (2012). Concentración de metales pesados (Cu, Ni, Zn, Cd, Pb) en la biota y sedimentos de una playa artificial, en la bahía San Jorge 23°S, norte de Chile. *Latin American Journal of Aquatic Research*, *40*(2), 267-281.

Conagua (2011). *Atlas del agua en México 2011*. México, DF: Comisión Nacional del Agua, Secretaría de Medio Ambiente y Recursos Naturales.

Copae (2010). *Situación actual del agua de los ríos Tzalá y Quivichil en el área de influencia de la mina Marlin, ubicada en los municipios de San Migue Ixtahuacan y Sipacapa, departamento de San Marcos, Guatemala. Tercer informe anual del monitoreo y análisis de la calidad del agua*. Comisión Pastoral Paz y Ecología. Recuperado de http://goldcorpoutofguatemala.files.wordpress.com/2010/07/tercer20informe20anual20del20monitoreo.pdf

Esteves, J. E., Gil, M., & Harvey, M. (1996). *Evaluación de la contaminación por metales en sedimentos y materiales en suspensión de la cuenca Turbio - Gallegos*. Puerto Madryn, Argentina: Fundación Patagonia Natural.

García-García, N., Pedraza-Garciga, J., Montalvo, J. F., Martínez, M., & Leyva, J. (2012). Evaluación preliminar de riesgos para la salud humana por metales pesados en las bahías de Buenavista y San Juan de los Remedios, Villa Clara, Cuba. *Revista Cubana de Química*, *24*(2), 126-135.

Haesloop, U., & Schirmer, M. (1985). Accumulation of Orally Administered Cadmium by the Eel (Anguilla anguilla). *Chemosphere*, *14*(10), 1627-1634.

INEGI (1980). *Conjunto de datos vectoriales de las cartas temáticas de Geología*. México, DF: Instituto Nacional de Estadística y Geografía.

Jiménez-Cisneros, B. E. (2001). *La contaminación ambiental en México: causas, efectos y tecnología apropiada*. México, DF: Editorial Limusa, Colegio de Ingenieros Ambientales de México, A.C., Instituto de Ingeniería de la UNAM y FEMISCA.

Kirschbaum, A., Murray, J., Arnosio, M., Tonda, R., & Cacciabue, L. (2012). Pasivos ambientales mineros en el noroeste de Argentina: aspectos mineralógicos, geoquímicos y consecuencias ambientales. *Revista Mexicana de Ciencias Geológicas*, *29*(1), 248-264.

Laino-Guanes, R. M., Musálem-Castillejos, K., González-Espinosa, M., & Ramírez-Marcial, N. (2014). El uso del agua en Motozintla de Mendoza, Chiapas: conflictos, contaminación y posibles soluciones (pp. 445-462). Cap. 17. En M. González-Espinosa, & M. C. Brunel-Manse (Eds.). *Montañas, pueblos y agua. Dimensiones y realidades de la Cuenca Grijalva*. Vol. 2. México, DF: El Colegio de la Frontera Sur y Editorial Juan Pablos.

Leal-Ascencio, M. T., Miranda, S., Sánchez, E., Prieto-García, F., & Gordillo, A. (2009). Metals Pollution in the El Limon Lagoon, Chiapas, Mexico. *Tropical and Subtropical Agroecosystems*, *10*(3), 415-421.

MAGA (2005). *Mapa geológico*. Ciudad de Guatemala: Ministerio de Agricultura, Ganadería y Alimentación.

NOAA (1999). *United States. Screening Quick Reference Tables*. National Oceanic and Atmospheric Administration. Recuperado de http://response.restoration.noaa.gov/cpr/sediment/squirt/squirt.html

NMX-AA-051-SCFI Norma Oficial Mexicana – Análisis de agua – Determinación de metales por absorción atómica en aguas naturales, potables, residuales y residuales tratadas – Método de prueba (2001). México, DF: Secretaría de Economía.

NOM-127-SSA1 Norma Oficial Mexicana - Salud Ambiental, agua para uso y consumo humano - Límites Permisibles

de Calidad y Tratamientos a que debe someterse el agua para su potabilización (1994). México, DF: Secretaría de la Salud.

NOM-147-SEMARNAT/SSA1 Norma Oficial Mexicana que establece criterios para determinar las concentraciones de remediación de suelos contaminados por arsénico, bario, berilio, cadmio, cromo hexavalente, mercurio, níquel, plata, plomo, selenio, talio y/o vanadio (2004). México, DF: Secretaría de Medio Ambiente y Recursos Naturales.

Ordóñez, C. E. (2010). Modos de vida de la población rural en microcuencas de las partes altas de los ríos fronterizos de México y Guatemala (pp. 14-17). En *Red de espacios de innovación socioambiental. Innovación socioambiental y desarrollo en la frontera sur de México*. México, DF: El Colegio de la Frontera Sur.

Osores-Plenge, F., Rojas-Jaimes, J. E., & Manrique-Lara-Estrada, C. H. (2012). Minería informal e ilegal y contaminación con mercurio en Madre de Dios: un problema de salud pública [versión electrónica]. *Acta méd. Peruana*, *29*(1), 38-42. Recuperado de http://www.scielo.org.pe/scielo.php?script=sci_arttext&pid=S1728-59172012000100012&lng=es&nrm=iso.

Pérez-Carreras, L., Moreno-García, A. M., & González-Parra, J. (1995). Influencia de las fracciones arcilla y arena en el contenido y disponibilidad de metales pesados en suelos. *Revista de la Sociedad Española de la Ciencia del Suelo*, *1*, 83-89.

Pérez-Cruz, Y. G., Rangel-Ruiz, L., & Gamboa-Aguilar, J. (2013). Metales en almejas y sedimentos en la Reserva de la Biosfera "Pantanos de Centla" Tabasco, México. *Hidrobiológica*, *23*(1), 1-8.

Pinedo-Hernández, J., Marrugo-Negrete, J., & Diez, S. (2014). Speciation and Bioavailability of Mercury in Sediments Impacted by Gold Mining in Colombia. *Chemosphere*, *119*, 1289-1295.

Pirrone, N., Cinnirella, S., Feng, X., Finkelman, R. B., Friedli, H. R., Leaner, J., Mason, R., Mukherjee, A. B., Stracher, G. B., Streets, D. G., & Telmer, K. (2010). Global Mercury Emissions to the Atmosphere from Antropogenic and Natural Sources. *Atmospheric Chemistry and Physics*, *10*, 5951-5964.

Plascencia-Vargas, H., González-Espinosa, M., Ramírez-Marcial, N., Álvarez-Solis, D., & Musálem-Castillejos, K. (2014). Características físico-bióticas de la cuenca del río Grijalva (pp. 29-79). Cap. 1. En M. González-Espinosa, & M. C. Brunel-Manse (Eds.). *Montañas, pueblos y agua. Dimensiones y realidades de la Cuenca Grijalva*. Vol. 1. México, DF: El Colegio de la Frontera Sur y Editorial Juan Pablos.

PNUMA (2002). *Evaluación mundial sobre el mercurio. Productos químicos - División de Tecnología, Industria y Economía*. Ginebra: Programa de las Naciones Unidas para el Medio Ambiente.

Programa Nacional de Desarrollo Minero 2001-2006 [en línea]. *Diario Oficial de la Federación*, 24 de noviembre de 2003. Recuperado de http://www.economia.gob.mx/files/transparencia/PRG4.pdf.

Puga, S., Sosa, M., Lebgue, T., Quintana, C., & Campos, A. (2006). Contaminación por metales pesados en suelo provocada por la industria minera. *Ecología Aplicada*, *5*(1-2), 149-155.

Roblero-Morales, M. (2011). *El despertar de la serpiente, la Sierra Madre de Chiapas en riesgo: extracción minera y comunidades en resistencia en Chicomuselo, Chiapas*. Tesis de maestría. San Cristóbal de Las Casas, México: Universidad Autónoma Chapingo.

Rosales-Hoz, L., Carranza-Edwards, A., Santiago-Pérez, S., Méndez-Jaime, C., & Doger-Badillo, R. (1994). Study of Anthropogenically Induced Trace Metal on the Continental Shelf in the Southeastern Part of the Gulf of Mexico. *Revista Internacional de Contaminación Ambiental*, *10*(1), 9-13.

Sánchez-Galan, S., Linde, A., Ayllon, F., & García-Vázquez, E. (2001). Induction of Micronuclei in Eel (Anguilla anguilla L.) by Heavy Metals. Ecotoxicology and Environmental Safety, 49(2), 139-143.

Singh, A. K., Hasnain, S. I., & Banerjee, D. K. (1999). Grain Size and Geochemical Partitioning of Heavy Metals in Sediments of the Damodar River – A Tributary of the Lower Ganga, India. *Environmental Geology*, *39*(1), 90-98.

SIAM (2015). Sistema de Administración Minera [en línea]. Secretaría de Economía de México. Recuperado de http://www.cartografia.economia.gob.mx/cartografia/#.

Smolders, A., Archer, J., Stassen, M., Llanos-Cavero, J. C., *& Hudson-Edwards, K. (2006).* Concentraciones metálicas en cabellos de habitantes de las orillas de la cuenca media del río Pilcomayo. *Revista Boliviana de Ecología y Conservación Ambiental*, *19*, 13-22.

Soto-Cruz, O., Carrillo-Chávez, J., & Suárez-Sánchez, J. (2011). Concentraciones de metales y metaloides en sedimentos del río Zahuapan, Tlaxcala, México. En R. Jiménez-Guillen, & M. L. Hernández-Rodríguez (Eds.). *Zahuapan: río-región-contaminación* (pp. 57-78). Tlaxcala, México: El Colegio de Tlaxcala, A.C.

Szalinska, E., Haffner, G., & Drouillard, K. (2007). Metals in the Sediments of the Huron-Erie Corridor in North America: Factors Regulating Metal Distribution and Mobilization. *Lakes and Reservoirs: Research and Management*, *12*(4), 217-236.

UNEP (2013). *Mercury, Time to Act. Chemical Branch - Division of Technology, Industry and Economics*. Geneva: United Nations Environment Programme.

Vázquez, G. F., Elias, D. M., Aguayo, J. E., & Baeza, A. (1996). Trace Metal Species in Aquatic Samples of the Tabasco Lagoons, Mexico. *Environment International*, *22*(3), 377-382.

Villanueva, F. S., & Botello, A. V. (1992). Metales pesados en la zona costera del Golfo de México y Caribe mexicano: una revisión. *Revista Internacional de Contaminación Ambiental*, *8*(1), 47-61.

Visviki, I., & Rachlin, J. W. (1991). The Toxic Action and Interactions of Copper and Cadmium to the Marine Alga *Dunaliella minuta*, in Both Acute and Chronic Exposure. *Archives of Environmental Contamination and Toxicology*, *20*(2), 271-275.

White, P. A., & Rasmussen, J. B. (1998). The Genotoxic Hazards of Domestic Wastes in Surface Waters. *Mutation Research/Reviews in Mutation Research*, *410*(3), 223-236.

Zhang, J., Huang, W., Liu, S., Liu, M., Yu, Q., & Wang, J. (1992). Transport of Particulate Heavy Metals towards the China Sea: A Preliminary Study and Comparison. *Mar. Chem.*, *40*, 161-178.

Institutional Address of the Authors

M.C. Rafaela María Laino-Guanes

El Colegio de la Frontera Sur (Ecosur)
Departamento de Conservación de la Biodiversidad
Carretera Panamericana y Periférico Sur s/n, Barrio María Auxiliadora
29290 San Cristóbal de Las Casas, Chiapas, México
Teléfono: +52 (595) 2122 4845
rafilaino@gmail.com

Dr. Ricardo Bello-Mendoza

University of Canterbury
Department of Civil and Natural Resources Engineering
8140 Christchurch, New Zealand

El Colegio de la Frontera Sur (Ecosur)
Departamento de Conservación de la Biodiversidad
Carretera Panamericana y Periférico Sur s/n, Barrio María Auxiliadora
29290 San Cristóbal de Las Casas, Chiapas, México
Teléfono: +52 (962) 6289 800, extensión 5440
rbello@ecosur.mx

Dr. Mario González-Espinosa

El Colegio de la Frontera Sur (Ecosur)
Departamento de Conservación de la Biodiversidad
Carretera Panamericana y Periférico Sur s/n, Barrio María Auxiliadora
29290 San Cristóbal de Las Casas, Chiapas, México
Teléfono: +52 (967) 6749 000, extensión 1100
mgonzale@ecosur.mx

Dr. Neptalí Ramírez-Marcial

El Colegio de la Frontera Sur (Ecosur)
Departamento de Conservación de la Biodiversidad
Carretera Panamericana y Periférico Sur s/n, Barrio María Auxiliadora
29290 San Cristóbal de Las Casas, Chiapas, México
Teléfono: +52 (967) 6749 000, extensión 1321
neptalirm@gmail.com

Dr. Francisco Jiménez-Otárola

Centro Agronómico Tropical de Investigación y Enseñanza (CATIE)
30501 Cartago, Turrialba, Costa Rica
Teléfono: +506 2558 2651
fjimenez@catie.ac.cr

Dr. Karim Musálem-Castillejos

El Colegio de la Frontera Sur (Ecosur)
Departamento de Conservación de la Biodiversidad
Carretera Panamericana y Periférico Sur s/n, Barrio María Auxiliadora
29290 San Cristóbal de Las Casas, Chiapas, México
Teléfono: +52 (595) 98122 3778
k.musalem@gmail.com

Land Use Changes and their Effects on GHG Dynamics in the State of Durango

• Palmira Bueno-Hurtado* •
Instituto Nacional de Investigaciones Forestales Agrícolas y Pecuarias, México
*Corresponding Author

• Armando López-Santos •
Universidad Autónoma Chapingo, México

• Ignacio Sánchez-Cohen • Miguel Agustín Velásquez-Valle •
• José Luis González-Barrios •
Instituto Nacional de Investigaciones Forestales Agrícolas y Pecuarias, México

Abstract

Bueno-Hurtado, P., López-Santos, A., Sánchez-Cohen, I., Velásquez-Valle, M. A., & González-Barrios, J. L. (July-August, 2015). Land Use Changes and their Effects on GHG Dynamics in the State of Durango. Water Technology and Sciences (in Spanish), 6(4),
75-84.

Actions are being taken worldwide to evaluate greenhouse gas (GHG) emissions in different countries. According to reports by the National Development Plan in Mexico, several national GHG inventories have been performed by different sectors. The present work quantifies the emissions and absorption of GHG resulting from land use changes in the state of Durango. The IPCC method was applied using the Greenhouse Gas Inventory Software, version 1.3.1. Emissions of gases other than CO_2 produced by burning were calculated. Coniferous vegetation lost the largest amount of biomass and therefore emitted the most CO_2, while abandoned agricultural land resulted in a capture of CO_2, mostly from the recuperation of xeric shrubs and hardwoods. Most of the GHG emissions (other than CO_2 produced by burning) were emitted in regions containing coniferous vegetation.

Keywords: Conversion, forest, agriculture, burning.

Resumen

Bueno-Hurtado, P., López-Santos, A., Sánchez-Cohen, I., Velásquez-Valle, M. A., & González-Barrios, J. L. (julio-agosto, 2015). Cambios de uso de suelo y sus efectos sobre la dinámica de GEI en el estado de Durango, México. Tecnología y Ciencias del Agua, 6(4), 75-84.

En el mundo se están tomando acciones para evaluar las emisiones de gases efecto invernadero (GEI) en distintos países. Acorde a lo indicado en el Plan Nacional de Desarrollo en México se han realizado ya varios inventarios nacionales de GEI en distintos sectores. En el presente trabajo se realizó una cuantificación de las emisiones y absorciones de GEI debido al cambio de uso de suelo en el estado de Durango. Se aplicó la metodología del IPCC, mediante el programa Greenhouse Gas Inventory Software versión 1.3.1. Se calcularon las emisiones de gases distintos al CO_2 producto de quema. El grupo de vegetación que perdió la mayor cantidad de biomasa y por ende emitió mayor CO_2 fue coníferas, por otro lado, el abandono de tierras agrícolas provocó la captura de CO_2 en mayor medida por la recuperación de matorral xerófilo y latifoliadas. En cuanto a las emisiones de GEI distintas al CO_2 producto de quema, las mayores cantidades se emiten en las zonas donde se encuentran coníferas.

Palabras clave: *conversión, bosques, agricultura, quema.*

Received: 14/05/2014
Accepted: 09/04/2015

Introduction

The Clean Development Mechanism (CDM) is found in Article 12 of the Kyoto Protocol (United Nations Framework Convention on Climate Change (UNFCCC)). Its objective is to aid countries not in Annex I, which are essentially developing countries. There are over 7 450 CDM projects, 53 of which are related to forestation and reforestation, which are much

fewer than projects involving agriculture (219), waste management (944) and fossil fuel emissions (236) (UNFCCC, 2014). CDM projects are aimed at reducing the greenhouse effect (GE), which first involves quantifying gases released into the atmosphere. The Intergovernmental Panel on Climate Change (IPCC) has created methodologies for this purpose, one of which is presented in the IPCC guidelines for greenhouse gas (GHG) inventories, revised in 1996. These guidelines contain 5 modules for GHG inventories, one of which is land use change and forestry.

Land use changes contribute to GHG emissions, and deforestation in particular (Mas and Flamenco-Sandoval, 2011). In the land use change and forestry sector, roughly 1.6 Gt of carbon (C) is emitted annually (CGE, 2005). It is worth mentioning that activities involving land use changes not only produce emissions but also sequestration (Rootzén *et al*., 2010). In addition to CO_2, land use changes release methane (CH_4), nitrous oxide (N_2O), nitrogen oxides (NO_x) and carbon monoxide (CO) (EPA, 2010; Manso, 2003; PNUMA, 2005).

In Mexico, the General Law on Climate Change (2012) stipulates the creation and updating of GHG inventories at national and state levels for the different emissions categories, including forests and land uses. Thus, the objective of the present study is to create an inventory of GHG emissions and capture resulting from land use changes in the state of Durango, based on the IPCC methodology.

Materials and Methods

The present work covers the state of Durango, located between the parallels 22° 19′ and 26° 48′ latitude north and the meridians 107° 11′ and 102° 28′ longitude west. *Greenhouse Gas Inventory Software* version 1.3.1 was used. The calculation method used was that proposed by the IPCC guidelines for greenhouse gases, version 1996 (IPCC, 1996).

Land use changes involve both the emission and capture of GHG. Emissions are caused by forests and jungles being converted into induced crops and pastures. Capture occurs when farmlands are abandoned and woody vegetation regenerates.

To calculate the area of existing vegetation, the following INEGI Land Use and Vegetation charts were processed using ARCMAP 9.3: series IV (2007), series III (2002), series II (1993) and series I (1985), at a scale of 1:250000.

Some of the default values shown in Table 1 were used for the calculation, obtained from INEGI 2006 and the IPCC Good Practice Guidance (SEMARNAT and INE, 2006; GPG-LULUCF, 2003).

The IPCC methodology calculates the GHG dynamics as described below:

CO_2 Released from Conversion of Forests into Other Land Uses

Estimation of loss in biomass:

$$LB = AC * (BBC - BAC)$$

Where *LB* = annual loss in biomass (kt ms); *AC* = area converted annually (kha); BBC = biomass before conversion (t ms ha^{-1}); *BAC* = biomass after conversion (t ms ha^{-1}).

The estimation of carbon released from burning aerial biomass *in-situ* is given by:

$$\Delta AC = ((LB * FBI) * FOI) * CF$$

Where ΔAC = amount of carbon released from burning biomass *in-situ* (kt C); *LB* = annual loss in biomass (kt ms); *FBI* = fraction of biomass burned *in-situ*; *FOI* = fraction of biomass oxidized *in-situ*, *CF* = carbon fraction of the aerial biomass.

Estimation of carbon released from burning aerial biomass outside the forest:

$$BBO = LB * fbb$$

Table 1. Default values from IPCC (GPG-LULUCF, 2003) and the National GHG Inventory (Semarnat & INE, 2006).

Default value	Vegetation Group	
Biomass before conversion		**t ms* ha**
	Coniferous	93
	Hardwood	61.6
	Semi-deciduous forest	104.1
	Low forest	37.31
	Xerix shrub	37
Biomass after conversion		**t ms ha**
	Coniferous	28.2
	Hardwood	28.0
	Semi-deciduous forest	32.4
	Low forest	23.3
	Xerix shrub	17.2
		Dimensionless
Fraction of biomass burned in situ	All	0.5
Fraction of biomass oxidized in situ	All	0.9
Fracton of carbon burned undergound	All	0.5
Fraction of biomas burned off-site	All	0.5
Fraction of biomass oxidized off-site	All	0.9
Fraction of carbon from biomass undergound	All	0.5

*Dry material.

Where BBO = amount of biomass burned outside the forest (kt ms); *LB* = annual loss in biomass (kt ms); *fbb* = fraction of biomass burned outside the forest.

Carbon released due to burning outside the forest:

$$\Delta CO = \left(BBO * fbo\right) + CF$$

Where ΔCO = amount of carbon released from burning biomass outside the forest (kt C); BBO = amount of biomass burned outside the forest (kt ms); *fbo = fraction of biomass oxidized outside the forest*; *CF* = carbon fraction of burning of aerial biomass outside the forest.

Estimation of total carbon released from burning aerial biomass *in-situ* and outside the forest:

$$\Delta CBIO = \Delta CBI + \Delta CBO$$

Where ΔCBIO= total carbon released from burning *in-situ* and outside the forest (kt C); ΔCBI = amount of carbon released from burning *in-situ* (kt C); ΔCBO = amount of carbon released from burning biomass outside the forest (kt C).

Estimation of CO_2 released from decomposition of aerial biomass:

$$\Delta CD = \left(\left(MA * \left(BBC - BAC\right)\right) * FAD\right) * CF$$

Where ΔCD = carbon emitted from decomposition of aerial biomass (kt C); MA = mean area converted (10-year average) (kha); BBC = biomass before conversion (t ms ha^{-1}); BAC; biomass after conversion (t ms ha^{-1}); FAD = fraction abandoned that decomposed; CF = carbon fraction of the aerial biomass.

Estimation of total CO_2 emissions from conversion of forests and prairies:

$$\Delta TCC = (\Delta CBIO + \Delta CD) * (44/12)$$

ΔTCC = total annual CO_2 released from conversion of forests and prairies (Cg of CO_2); $\Delta CBIO$ = carbon released from burning *in-situ* and outside the forest (kt C); ΔCD = carbon released from decomposition of aerial biomass (kt C); 44/12 represents the molecular weight of CO_2 / C.

CO_2 Captured from Conversion of Abandoned Agricultural Land

Since regeneration rates decrease over time, a 20-year period prior to the inventory and a period of 20 to 100 years prior were used.

The calculation of annual carbon absorption by the aerial biomass (abandoned land during the prior 20 years):

$$\nabla BA = (AA * GR) * CF$$

Where ∇BA = annual absorption of carbon by the aerial biomass (kt C); AA = total abandoned area which has been in the regeneration stage during the prior 20 years (k ha); GR = annual growth rate of the aerial biomass (t ms ha^{-1}); CF = carbon fraction of the aerial biomass.

To calculate the area abandoned during the prior 20 years, the vegetation areas from series II and IV of the INEGI Land Use and Vegetation charts were compared. The annual growth rate of the biomass from natural regeneration was obtained from INEGI (2010) (Semarnat & INE, 2009) and is shown in Table 1.

Calculation of annual carbon absorption by the aerial biomass (land abandoned for more than 20 years):

$$\nabla BA_{>20} = (AA_{>20} * GR) * CF$$

Where $\nabla BA_{>20}$ = annual absorption of carbon by the aerial biomass in land that has been abandoned for more than 20 years (kt C); $AA_{>20}$ = total abandoned area which has been in the regeneration stage for more than 20 years (k ha); GR = annual growth rate of the aerial biomass (t ms ha^{-1}); CF = carbon fraction of the aerial biomass.

For lands abandoned for more than 20 years, vegetation areas in series I and IV of the INEGI Land Use and Vegetation charts were used as a reference. The annual growth rate is shown in Table 1.

Calculation of total CO_2 removal in abandoned lands.

The results from the previous formulas are summed, as shown as follows:

$$\nabla TCA = \nabla BA + \nabla BA_{>20}$$

Where ∇TCA = total carbon absorbed by the abandoned lands (kt C); ∇BA = annual absorption of carbon by the aerial biomass during the first 20 years (kt C); $\nabla BA_{>20}$ = annual absorption of carbon by the aerial biomass for more than 20 years (kt C).

Gases other than CO_2 released from burning

The estimation of nitrogen released:

$$\Delta N = \Delta CBIO * N:C$$

Where ΔN = total nitrogen released (kt N); $\Delta CBIO$ = total carbon released from burning *in-situ* and outside the forest (kt C); N:C = ratio of nitrogen to carbon, which is 0.01 according to vapor, default value proposed by the IPCC workbook (IPCC, 1996).

Estimation of emissions of gases other than CO_2:

$$\Delta GO = \Delta CBIO * RE$$

Where ΔGO = emissions of gases other than CO_2 (kt C); $\Delta CBIO$ = total carbon released from burning *in-situ* and outside the

forest (kt C); RE = ratio of the emission of gases other than CO_2.

The emissions ratios were obtained from the IPCC workbook (IPCC; 1996) and are 0.012 for CH_4, 0.06 for CO, 0.007 for N_2O and 0.121 for NO_x.

Lastly, to calculate emission for gases other than CO_2, a conversion was performed according to different conversion ratios for each type of gas.

$$\Delta B = \Delta GO * CR$$

Where ΔB = emissions from burning of forests (Gg CH_4, Gg CO, Gg N_2O, NO_x); Δ GO = emissions from gases other than CO_2 (Kt C); CR = conversion ratio; CO (28/12), CH_4 (16/12 N_2O (44/28), NO_x (46/12).

Uncertainty Analysis

The percentage of uncertainty was calculated using the equations below. The first was applied to uncertain amounts that were combined through multiplication and the second when the uncertain amounts were combined through addition and without correlating them:

$$U_{total} = \sqrt{U_1^2 + U_2^2 + \cdots + U_n^2}$$

Where U_{total} = percentage of uncertainty in the product of the amounts (the half-length of the 95% confidence interval divided by the total); U_i = percentage of uncertainty associated with each one of the amounts:

$$U_{total} = \frac{\sqrt{(U_1 \bullet x_1)^2 + (U_2 \bullet x_2)^2 + \cdots + (U_n \bullet x_n)^2}}{x_1 + x_2 + \cdots + x_n}$$

Where U_{total} = percentage of uncertainty in the product of the amounts (half-length of the 95% confidence interval divided by the total); X_i = uncertain amounts and U_i = percentage of uncertainty associated with them.

It is important to mention that the uncertainties pertaining to default values correspond to those cited by the IPCC Good Practice Guidance (GPG-LULUCF, 2003), in terms of the uncertainty of the data using the national level as a reference. These were obtained from the National Greenhouse Gas Inventory (Semarnat & INE, 2006). With respect to the uncertainty in the calculation of land use areas, this was obtained with the following equation:

$$\% \text{ of uncertainty} = \frac{\frac{1}{2}(4\sigma)}{\mu}(100)$$

Where σ = standard deviation and μ = mean of the distribution.

Results and Discussion

CO_2 Released by Conversion of Forest Land into Other Uses

The area of wooded vegetation that converted into agricultural use in the state of Durango is shown in Figure 1. It is equal to an annual loss in biomass of 8 292.52 kt of dry matter (ms). Of this total, 146.25 kt ms was burned and 3 731.65 kt ms was oxidized *in-situ*. The vegetation group with the highest loss in biomass was coniferous, whereas semi-deciduous represented the smallest loss (Table 2).

The loss in biomass mentioned in the above paragraph corresponds to total carbon emissions of 2 067.7 kt C (7 581.52 Gg of CO_2) from decomposition and 3 731.65 kt C (13 682.67 Gg of CO_2) from burning (Figure 2).

The emissions from burning and decomposition of biomass nationally was 52 180 Gg of CO_2 from burning and 62 321 Gg of CO_2 from decomposition (Semarnat & INE, 2009). That is, the state of Durango represented 26.22% of the national emissions produced by burning and 12.16% produced by decomposition. Meanwhile, the state of Sinaloa emitted 664.47 Gg of CO_2 from burning and 1 993.38 Gg of CO_2 from decomposition (IEGEIE-

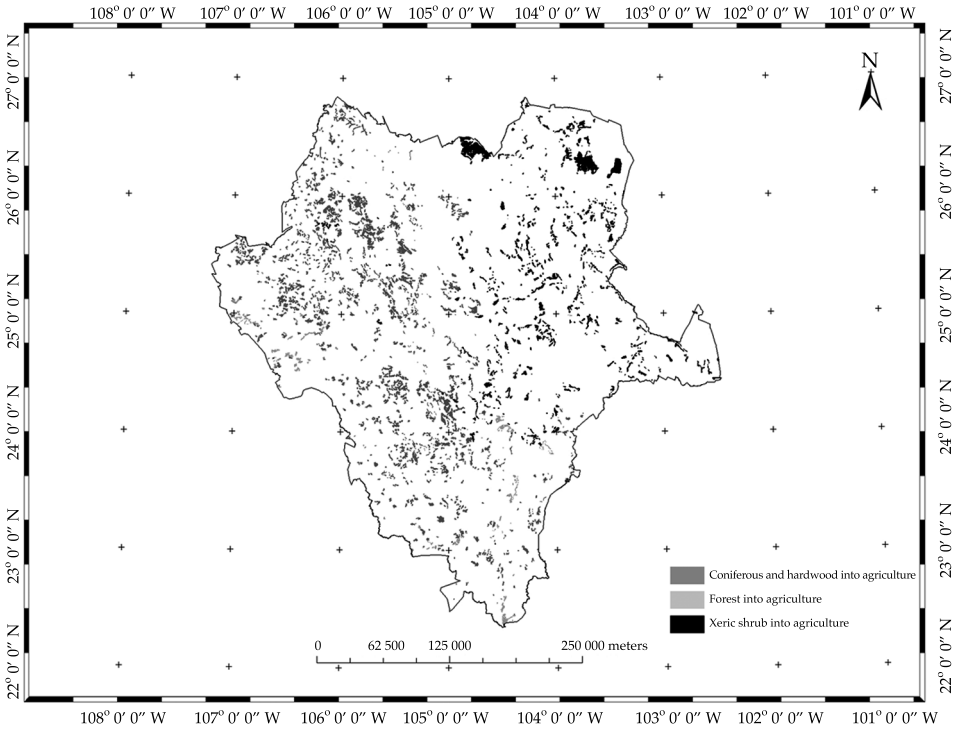

Figure 1. Loss in vegetation from 1993 to 2007.

Table 2. Carbon emissions from burning of biomass *in situ* and outside the forest.

Vegetation in 2002	ALB (kt ms)	BBI (kt ms)	BOI (kt ms)
Coniferous	6 623.79	3 311.90	2 980.71
Hardwood	366.37	183.19	164.87
Low Forest	103.08	51.54	46.39
Semi-deciduous Forest	60.90	30.45	27.41
Xeric shrub	1 138.38	569.19	512.27
Total, Durango	8 292.52	4 146.25	3 731.65

ALB Annual Loss in Biomass; BBI Biomass burned *in situ*; BOI Biomass oxidized *in situ*.

Sinaloa, 2005), that is, 4.85% and 26.29% of the emissions released in Durango. Chiapas is another state with findings from CO_2 emissions caused by changes in land use, where 2 133 Gg was released from the conversion of agricultural land and prairies into forests (IEGEIC, 2011), representing 10% of the total emissions in Durango.

It is important to take into account in the above paragraphs that the proportions of vegetation vary among the states. In Durango, 31% is state land made up of forests, conifer and oak, while dry forests are predominant in Sinaloa and wet jungles are predominant in Chiapas (INEGI, 2014).

Gases Released from Burning, Other than CO_2

Gases other than CO_2 that were released from the burning of biomass were: 261.21 Gg of CO, 0.21 Gg of N_2O, 7.42 Gg of NO_x and

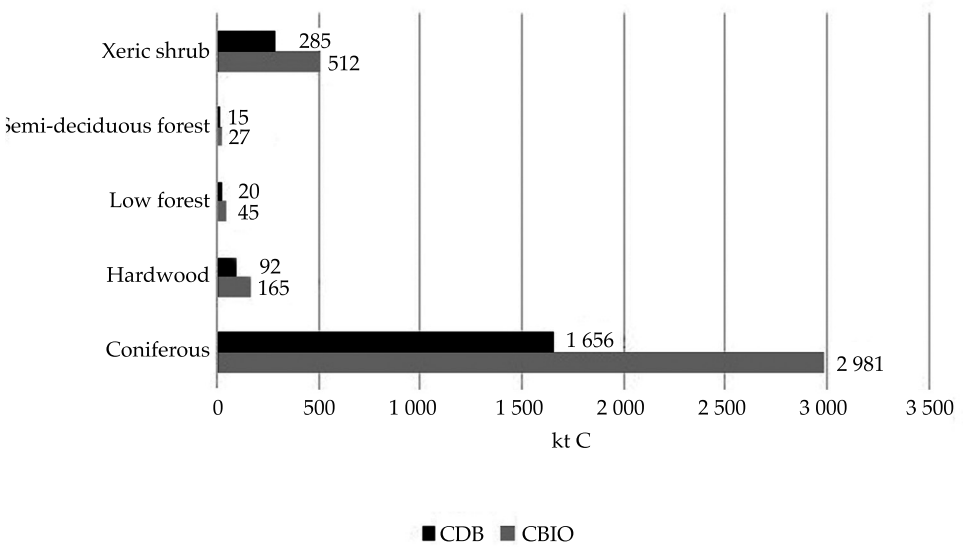

Figure 2. Carbon released by burning *in situ* and outside the forest (CBIO), carbon released by decomposition of biomass on the soil (CDB).

29.85 Gg of CH_4 (Figure 3). When comparing these results, the state of Sinaloa emitted 10% of the CH_4, 10% of the CO, 9.52% of the N_2O and 10.24% of the NO_x emitted by Durango (IEGEI-Sinaloa, 2005). The state of Guanajuato emitted 2.88 % of the CH_4, 2.87 % of the CO, 4.76 % of the N_2O and 2.83 % of the NO_x emitted by Durango (IEGEI-Guanajuato). Thus, there appears to be more burning in Durango than in the other states.

CO_2 Capture from Conversion of Abandoned Agricultural Land

Vegetation groups that are regenerating because of land abandoned as of 1985 were xeric shrub (324.44 kha) and hardwood (85.57 kha), and as of 1993, hardwood (117.76 kha) followed by xeric shrub (70.95 kha) (Table 3).

The total CO_2 absorption in Durango was 872.06 Gg of CO_2, which was 52% less in the state of Chiapas and 200% and 300% more in Guanajuato and Sinaloa, respectively (IEGEIC, 2011; IEGEI Guanajuato, 2005; IEGEIE-Sinaloa, 2005).

Summary of CO_2 Dynamics

In terms of changes in the use of forest and agricultural land in the state of Durango, 872.06 Gg of CO_2 was captured and 21 264.2 Gg of CO_2 was released into the atmosphere annually (Figure 4). Uncertainty in the results from abandoning agricultural land and the conversion into forests were 20.57% and 36.94%, respectively.

Conclusions

Estimations were generated of GHG emissions and capture resulting from changes in forest and agricultural land use in the state of Durango. The vegetation group that lost the most biomass and therefore released the largest amount of CO_2 was coniferous, followed by xeric shrub, hardwoods, low forest and semi-deciduous forests. Most of the CO_2 was emitted from burning and lesser amounts from the decomposition of biomass. The abandonment of agricultural lands was the primary cause of CO_2 capture and resulted

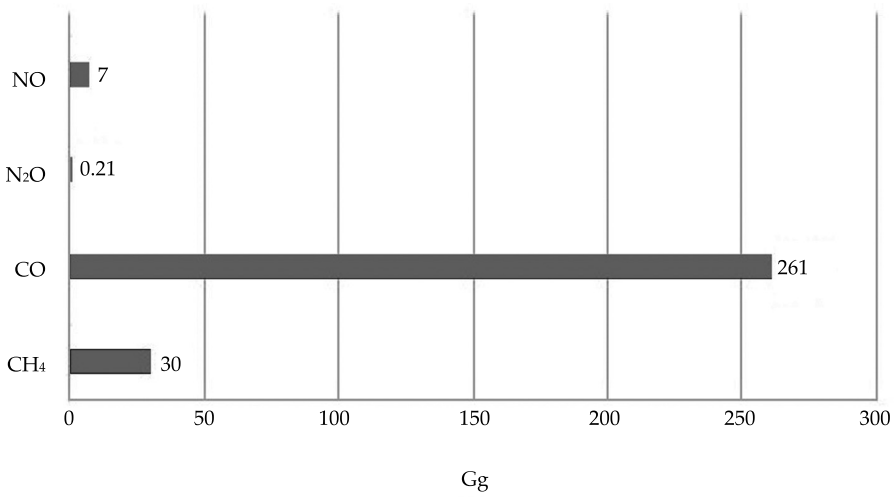

Figure 3. Emissions of gases other than CO_2 as a result of burning in the state of Durango.

Table 3. Conversion of agriculture and pasture areas in 1985 and 1993 (losses) into vegetation groups in 2007 (gains).

Vegetation group	AAO (kha)	ACC* (kt C)	AAF (kha)	ACC• (kt C)
Coniferous	14.83	9.63	42.45	27.59
Hardwood	85.57	55.62	117.76	76.54
Semi-deciduous forest	16.72	2.17	5.18	2.85
Low forest	53.49	6.95	9.2	5.06
Xeric shrub	324.44	42.17	70.95	9.22
Total carbon (kha)				237.83
Total CO_2 capture (Gg)				872.06

*For over 20 years; • for the first 20 years; AAO abandoned area for over 20 years; AAF abandoned area in the first 20 years; ACC annual carbon capture.

from the regeneration of xeric shrubs and hardwoods. In terms of the emission of GHG other than CO_2 as a result of burning, most were released in regions with coniferous.

References

CGE (2005). *Handbook on Land-Use Change and Forestry Sector* (600 pp.). Consultative Group of Experts on National Communications from Parties not included in Annex I to the Convention. United Nations Framework Convention on Climate Change.

EPA (2010). Methane and Nitrous Oxide Emissions from Natural Source [on line]. Washington, DC: United States Environmental Protection Agency. Office of Atmospheric Programs. Citado el 1 de septiembre de 2011. Recuperado de World Wide Web: http://www.epa.gov/outreach/pdfs/Methane-and-Nitrous-Oxide-Emissions-From-Natural-Sources.pdf.

GPG-LULUCF (2003). *Good Practice Guidance for Land Use, Land-Use Change and Forestry* (600 pp.). Intergovernmental Panel on Climate Change.

IEGEI (2005). *Guanajuato. Inventario Estatal de Gases de Efecto Invernadero del Estado de Guanajuato*. Guanajuato.

IEGEIC (2011). *Inventario Estatal de Gases de Efecto*

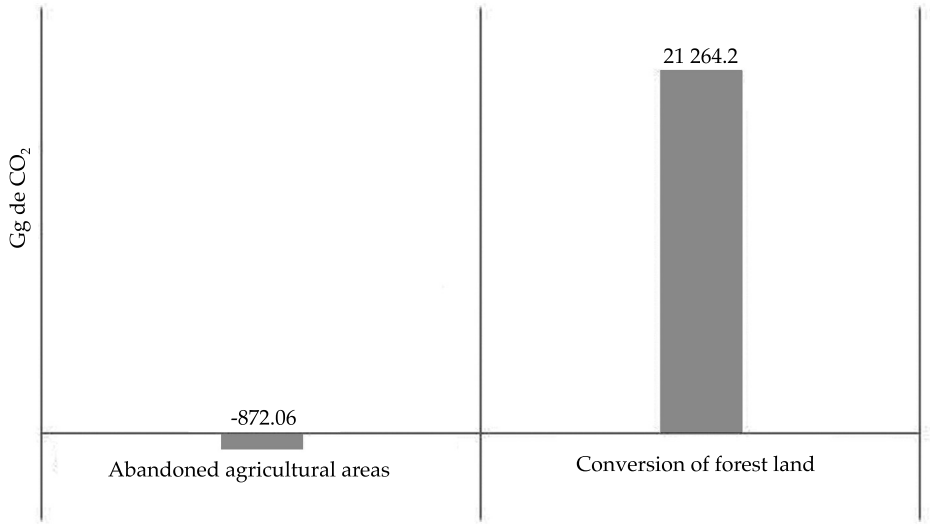

Figure 4. CO2 emissions and capture in the state of Durango.

Invernadero del Estado de Chiapas. Programa de Acción ante el Cambio Climático del Estado de Chiapas (72 pp.). México, DF: Universidad de Ciencias y Artes de Chiapas, El Colegio de la Frontera Sur, Colegio de Posgraduado, Instituto Tecnológico de Tuxtla Gutiérrez, Universidad Nacional Autónoma de México, Secretaría de Medio Ambiente Vivienda e Historia Natural, Secretaría de Medio Ambiente y Recursos Naturales, Conservation International Mexico A.C.

IEGEIE (2005). *Sinaloa. Inventario Estatal de Emisiones de Gases de Efecto Invernadero del Estado de Sinaloa* (196 pp.). Culiacán, México: Instituto Nacional de Ecología, Universidad Autónoma de Sinaloa, Dirección General de Educación en Ciencia y Tecnología del Mar, Universidad Politécnica de Sinaloa.

INEGI (2011). *Flora y fauna de Durango*. Citado el 3 de mayo 2011. Recuperado de http://cuentame.inegi.gob.mx/monografias/informacion/dur/territorio/recursos_naturales.aspx?tema=me&e=10.

INEGI (2014). *Información por entidad*. Citado el 15 de mayo 2014. Recuperado de http://cuentame.inegi.gob.mx/monografias/informacion/dur/.

IPCC (1996). *Directrices del IPCC para los inventarios de gases de efecto invernadero, versión revisada en 1996: Libro de trabajo*. Panel Intergubernamental de Cambio Climático.

Kaul, M., Dadhwal, V. K., & Mohren, G. M. J. (2009). Land Use Change and Net C flux in Indian Forests. *Forest Ecology and Management*, *258*, 100-108.

Mas, J. F., & Flamenco-Sandoval, A. (2011). Modelación de los cambios de coberturas/uso del suelo en una región tropical de México. *GeoTrópico*, *5*(1), 1-24.

Manso, J. R. (2003). Emisiones de gases y partículas producto de los incendios forestales en Cuba entre 1989 y 1999. Sitio Argentino de Producción Animal. Citado el 1 de mayo de 2011. Recuperado de http://www.produccion-animal.com.ar/incendios_y_uso_del_fuego/41-gases.pdf.

PNUMA (2005). *Emisiones de dioxinas y furanos por quema incontrolada de biomasa* (42 pp.). Ginebra: Programa de Naciones Unidas para el Medio Ambiente, Inter-Organization Programme for the Sound Management of Chemicals.

Rootzén, J. M., Berndes, G., Ravindranath, N. H., Somashekar, H. I., Murthy, I. K., Sudha, P., & Ostwald, M. (2010). Carbon Sequestration versus Bioenergy: A Case Study from South India Exploring the Relative Land-Use Efficiency of Two Options for Climate Change Mitigation. *Biomass and Bioenergy*, *34*, 116-123.

Semarnat-INE (2006). *México Tercera Comunicación Nacional ante la Convención Marco de las Naciones Unidas sobre el Cambio Climático* (254 pp.). México, DF: Secretaría de Medio Ambiente y Recursos Naturales, Instituto Nacional de Ecología.

Semarnat-INE (2009). *Cuarta Comunicación Nacional ante la Convención Marco de las Naciones Unidas sobre el Cambio Climático* (274 pp.). Secretaría de Medio Ambiente y Recursos Naturales. México, DF: Instituto Nacional de Ecología.

Semarnat (2009). *Cambios en el uso del suelo en México*. Citado el 1 de septiembre de 2011. Recuperado de http://app1.semarnat.gob.mx/dgeia/resumen_2009/02_ecosistemas/cap2_2.html.

UNFCCC (2014). *Clean Development Mechanism (CDM)*. Citado el 1 de septiembre de 2014. CDM Project Search. Recuperado de http://cdm.unfccc.int/.

Institutional Address of the Authors

M.C. Palmira Bueno Hurtado

Instituto Nacional de Investigaciones Forestales Agrícolas y Pecuarias
Centro Nacional de Investigación Disciplinaria en Relaciones Agua-Suelo-Planta-Atmósfera
Km 6.5 margen derecha Canal Sacramento
Gómez Palacio, Durango, México
bueno.palmira@inifap.gob.mx

Dr. Armando López Santos

Universidad Autónoma Chapingo
Unidad Regional Universitaria de Zonas Áridas
25330 Bermejillo, Durango, México
armando.lopezsantos@gmail.com

Dr. Ignacio Sánchez Cohen

Instituto Nacional de Investigaciones Forestales Agrícolas y Pecuarias
Centro Nacional de Investigación Disciplinaria en Relaciones Agua-Suelo-Planta-Atmósfera
Km 6.5 margen derecha Canal Sacramento
Gómez Palacio, Durango, México
sanchez.ignacio@inifap.gob.mx

Dr. Miguel Agustín Velásquez Valle

Instituto Nacional de Investigaciones Forestales Agrícolas y Pecuarias
Centro Nacional de Investigación Disciplinaria en Relaciones Agua-Suelo-Planta-Atmósfera
Km 6.5 margen derecha Canal Sacramento
Gómez Palacio, Durango, México
velasquez.agustin@inifap.gob.mx

Dr. José Luis González Barrios

Instituto Nacional de Investigaciones Forestales Agrícolas y Pecuarias
Centro Nacional de Investigación Disciplinaria en Relaciones Agua-Suelo-Planta-Atmósfera
Km 6.5 margen derecha Canal Sacramento
Gómez Palacio, Durango, México
gonzalez.barrios@inifap.gob.mx

Short-and Long-Term Price Elasticity of Residential Water Demand in an Arid Region. Case Study of La Paz, BCS, Mexico

• Gerzaín Avilés-Polanco* •
Universidad Autónoma de Baja California Sur, México
*Corresponding Autohr

• Marco A. Almendarez-Hernández •
Centro de Investigaciones Biológicas del Noroeste, México

• Víctor Hernández-Trejo •
Universidad Autónoma de Baja California Sur, México

• Luis Felipe Beltrán-Morales •
Centro de Investigaciones Biológicas del Noroeste, México

Abstract

Avilés-Polanco, G., Almendarez-Hernández, M. A., Hernández-Trejo, V., & Beltrán-Morales, L. F. (July-August, 2015). Short-and Long-Term Price Elasticity of Residential Water Demand in an Arid Region. Case Study of La Paz, BCS, Mexico. *Water Technology and Sciences* (in Spanish), 6(4), 85-99.

Overexploitation, saline intrusion and limited water supplies are the main problems faced by coastal arid zones. Since these conditions occur in the city of La Paz, we have proposed that the short- and long-term price elasticity of residential water demand be estimated in order to measure the impact of block pricing on efficient use. The results demonstrate that long-term elasticity is greater than short-term. This work contributes to the empirical evidence regarding adjustments in consumption in response to permanent increases in prices.

Keywords: Residential water demand, block prices, price elasticity, short-term and long-term.

Resumen

Avilés-Polanco, G., Almendarez-Hernández, M. A., Hernández-Trejo, V., & Beltrán-Morales, L. F. (julio-agosto, 2015). Elasticidad-precio de corto y largo plazos de la demanda de agua residencial de una zona árida. Caso de estudio: La Paz, B.C.S., México. Tecnología y Ciencias del Agua, *6(4), 85-99.*

La sobrexplotación, intrusión salina y limitaciones en la oferta hídrica constituyen los principales problemas de zonas áridas costeras. Considerando que la ciudad de La Paz, Baja California Sur, México, presenta estas condiciones, nos hemos propuesto estimar la elasticidad-precio de corto y largo plazos de la demanda de agua residencial para medir el impacto que tiene la estructura de precios en bloque en el uso eficiente. Los resultados revelan una elasticidad de largo plazo mayor a la de corto plazo. Este trabajo contribuye con evidencia empírica sobre el ajuste en el consumo ante incrementos permanentes en los precios.

***Palabras clave**: demanda de agua residencial, precios en bloque, elasticidad precio, corto y largo plazos.*

Recibido: 30/10/2013
Aceptado: 24/04/2015

Introduction

One of the main challenges facing large urban areas located in arid coastal zones is the sustainability of services that supply water, since increasingly larger volumes are needed to meet demands that often exceed the supply capacity (Soto & Bateman, 2006). The lack of adequate economic market instruments, such as block pricing structures that contribute to managing demand, can lead to an inefficient use of the resource and its depletion. The evident need

for these instruments has brought about a rapid growth in investigations about pricing structures (Howe & Linaweaver, 1967; Cavanagh, Hanemann, & Stavins, 2001).

The entities responsible for providing local water services in Mexico are Municipal Drinking Water and Sewer Operating Entities (OOMSAPAS, Spanish acronym). According to Elnaboulsi (2009), they should design fee structures according to four basic criteria: efficiency, equity, financial viability and simplicity. In conditions of scarcity and limited capacities to increase the water supply, the OOMSAPAS should encourage efficient use through prices that provide incentives to conserve water in order to avoid its depletion (Bartoszczuk & Nakamori, 2004). In this regard, Klawitter (2003) indicates that the design of a sustainable price for urban water should satisfy the needs of current and future generations through the efficient use of the resource as well as recuperate total costs (including supply and opportunity costs and economic externalities). It should also be equitable for all the different users. Dalhuisen, Florax, De Groot and Nijkamp (2001) also suggest that the price structure should be fair, encourage efficient use and be administratively feasible. It is therefore important to evaluate whether or not price structures meet these objectives. If they do meet them, it is also important to analyze to what degree. To this end, it is necessary to estimate the percentage change in the water demand as a result of a percentage change in the price, known as the price elasticity of water demand. This will be inelastic if the percentage change in the amount demanded is less than proportional to the percentage change in price. It is unitary when the change is equally proportional and elastic when it is more than proportional. It is also important to determine whether differences exist between short-term and long-term elasticity in order to know whether long-term changes in consumption occur as a result of permanent increases in the pricing structure over time. This would imply that users adjust consumption one or more periods after the current bill. It is useful for the OOMSAPAS to estimate short- and long-term elasticity because this makes it possible to identify the parameters needed to design fee structures that will contribute to accomplishing specific goals to reduce water demand.

Background

In many countries, market price structures for residential water and electricity are based on block pricing systems. This has come about due to income distribution policies with progressive pricing systems, where poor homes that consume less pay the lowest prices. The entities responsible for supplying water services not only seek economic efficiency but other objectives as well, such as equity and local acceptance (Ruijs, 2009). There is currently an extensive amount of literature about estimating demand functions for these systems. There is also consensus that residential water demand is inelastic, as shown by Dalhuisen *et al*. (2003) in a meta-analysis of price elasticity from studies dating back to 1963 and 1998, in which a mean elasticity of -0.41 was found. Elasticity differs according to place, time and estimation techniques. Methods used include ordinary least squares (OLS), instrumental variables and discrete continuous choice models (DCC) in order to address simultaneity problems presented by block prices (Hewitt & Hanemann, 1995). The data used by these techniques basically consists of micro-data applied in cross-section or data panels.

For studies that use macro-data, or aggregate data, estimation techniques consist of OLS, the Generalized Method of Moments (GMM) (Ruijs, 2009) and cointegration models with error correction. Using this method, Martínez-Espiñeira (2005) found that consumption, price and virtual income levels were not stationary, unlike first-differences. This indicates an order of integration, *I*(*1*), which is important to consider in the process

of generating information at the time of the econometric specification. In addition to prices, the literature also considers other factors as determinants of demand, including climate, demographics (make-up and size of households), socioeconomics (income level) and culture (Howe & Linaweaver, 1967; Billings & Agthe, 1980; Renzetti, 1992), among others. Recently in Mexico, interest has grown in the study of the water demand function for residential use. Using micro-data, Jaramillo (2005) estimated price demand sensitivities of -0.22 using the discrete continuous choice method and -0.58 with instrumental variables (IV). García-Salazar and Mora (2008) found elasticities of -0.18 and -0.2 for the Torreon Coahuila region using IV. In another study, developed by Sisto (2010) in La Laguna metropolitan area, elasticities between -0.47 and -0.53 were found with ordinary least squares models. Meanwhile, with the IV and OLS methods, Salazar and Pineda (2010) determined an elasticity of -0.33 using aggregate data on a local scale with 134 localities— the highest price demand elasticity, in absolute terms, of those reported with micro-data by the empirical literature on residential water demand in Mexico.

The empirical evidence suggests that measurements and a block pricing structure reduce water usage. Nevertheless, there is considerable differences between developed and developing countries in measuring instruments. Yepes and Dianderas (1996) found 85 to 90% usage in developed countries, while 50% was found in developing countries. In the case of Mexico, micro-measurements are limited. Nevertheless, an important statistic is that only 46% of water intakes are measured while 54% are not (based on a sample of 39 cities with populations over 50 000 inhabitants), according to the National Water Commission (Conagua, 2008). This lack of investment in micro-measuring instruments brings into question the principles of economic efficiency and equity in the supply of water in Mexico, with its discriminatory pricing between homes with measurements and those without. This situation could result in subsidiaries for the consumer, in which the price per cubic meter for homes without micro-measurements may be lower than the price paid by homes with measurements, bringing about inequity and lowering incentives to efficiently use the resource. The lack of measurements also affects financial operating deficits. This has encouraged the estimation of short- and long-term water demanded for residential use in the city of La Paz, Baja California Sur (BCS). In this city, micro-measurements are low (40%) and the operating entity has a financial deficit (two characteristics which are representative of the national situation). Problems also exist related to the sustainability of the water supply due to overexploitation of the aquifer (the only supply source), which is subject to seawater intrusion. For these reasons, the objective of this work was to estimate the short- and long-term price elasticity of the residential water demand in the city of La Paz, in order to measure the impact of a block pricing structure on the efficient use of water. To this end, the hypothesis proposed was that, with an increase in micro-measurements, an adequately designed block pricing fee structure can contribute to managing water demand through pricing signals that result in the efficient use of the resource (decreasing its consumption) and thereby attain the objectives related to equity, economic efficiency and sustainable use of residential water.

Materials and Methods

Study Area and Description of the Data

The urban area of the city of La Paz was selected because: a) it is located in a semi-arid region where no surface water bodies exist and precipitation is scarce, which has resulted in the need to extract groundwater through pumping of coastal wells, resulting in overexploitation of the aquifer and indirectly

causing the intrusion of seawater; b) homes represent the sector with the highest demand, with 60.86% of the total water extracted from the aquifer (30 018 597 m^3). According to Cruz-Falcón (2007), the aquifer has an area of 200 km^2, the water deficit is 9 million cubic meters annually and the infiltration of seawater ranges from 150 to 200 meters annually. Figure 1 shows the location.

Schematic Description of the Methodology

Figure 2 presents a flow diagram of the methodology used.

Determination of the Sample Size and Description of Variables

The distribution of demand at the La Paz OOMSAPAS, by type of user, was 94.28% domestic, 5.47% commercial and 0.24% industrial in the year 2008. Increases in the fee structure from 2003 to 2008 can be seen in Figure 3 (OOMSAPAS, 2009).

Cross-sectional and time series data were used to estimate elasticity. The cross-sectional data were obtained from a survey administered in 2008. For the time series estimation, official data were obtained containing individual identification codes from household consumer bills. This information was used to calculate average monthly consumption and the average marginal price. The strategy to obtain the cross-sectional information was to analyze the distribution of water household consumption within 11 consumption ranges in order to estimate the optimal sample size based on the consumption estimator. The analysis of the distribution showed that 93.96% of the homes with

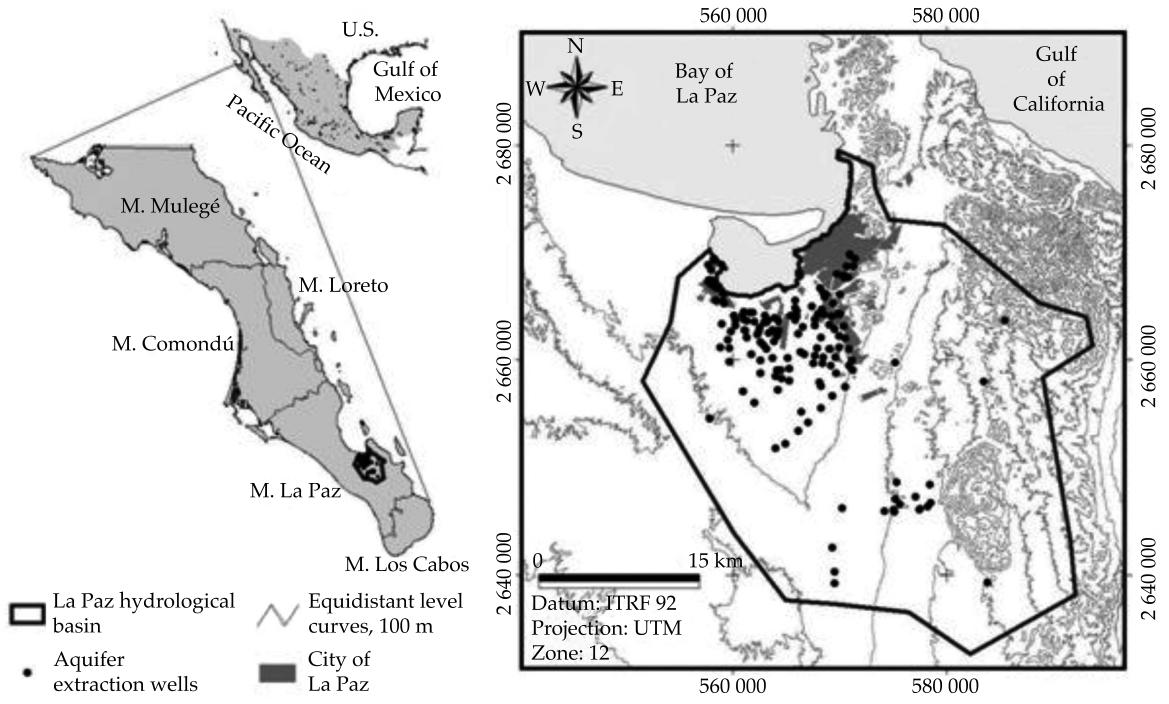

Source: Laboratory Services unit and Support, CIBNOR (ULSA), 2011.

Figure 1. Location of the study area, delimitation of the basin, distribution of extraction wells and City of La Paz, Baja California Sur, Mexico.

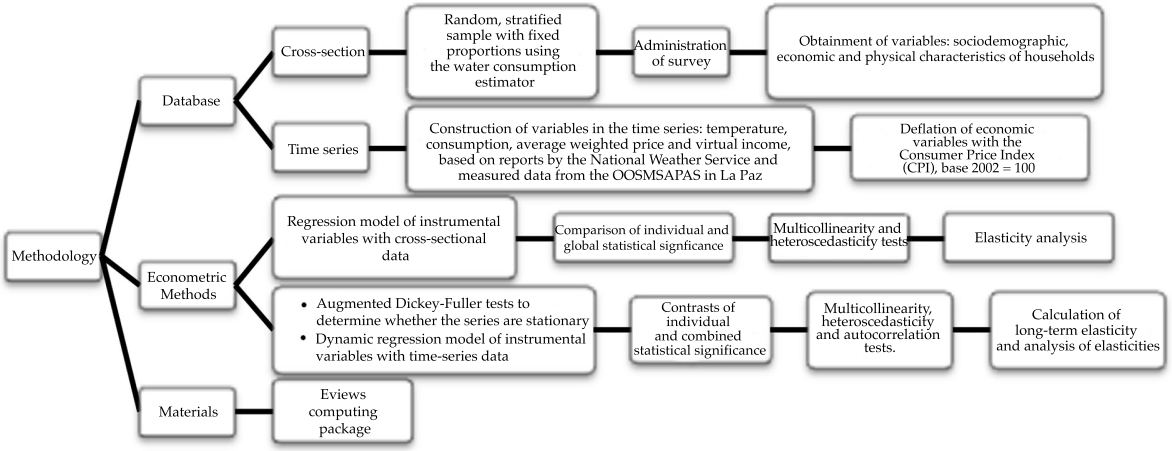

Fuente: elaboración propia.

Figure 2. Flow diagram of the methodology.

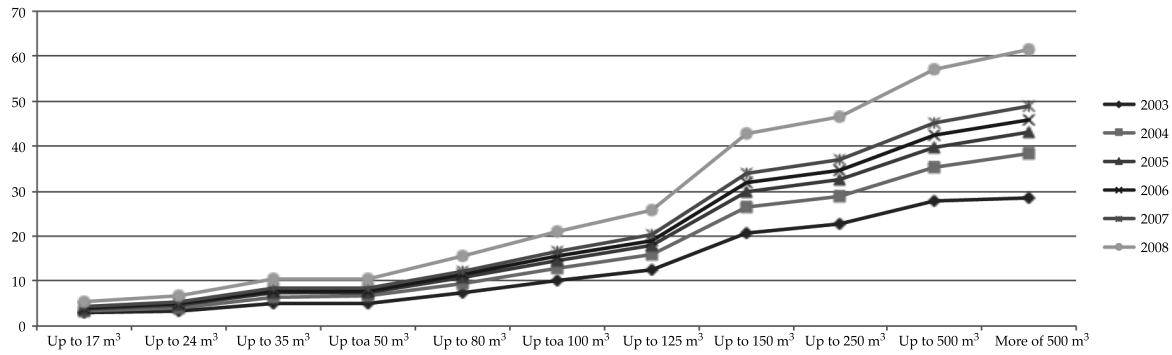

Source: OOMSAPA, La Paz. The prices per cubic meter include treatment and sewer, 2009.

Figure 3. Block fee structure for domestic usage, La Paz, Baja California Sur, period 2003- 2008.

micro-measurements fell into the first three blocks, 27 568 of which had a consumption range between 0 and 17 m^3 monthly, 9 515 had a range of over 17 to 24 m^3 monthly and 5 485 were in the range of over 24 to 35 m^3. The optimal size of the sample was obtained using a stratified random method with proportionate allocation , with an error of 4% and a 95% confidence interval. This resulted in a sample size of 594 homes, which was adjusted to 600. Table 1 shows the description and descriptive statistics of the variables obtained from the survey.

Given that 93% of the homes with micro-measurements fell in the 35 m^3 consumption block, the econometric strategy was limited to working with data from homes with micro-measurements that consumed up to 50 cubic meters during the period 2003 to 2008, since these represented over 95%. This avoided problems with statistical interference by eliminating atypical consumption data. The time series database contained monthly variables from 2003 to 2008, including: a) aggregate consumption by households with micro-measurements (thousands of cubic

Table 1. Description of sociodemographic and economic variables and physical characteristics of the households surveyed.

Variable	Description	Units	Mean	Standard error	Variable	Descripción	Units	Mean	Standard error
Income	Monthly family income	$ 000 / mes	8 364.5	7 702.05	*p*4	Marginal price block 4	pesos/m³	8.4	-
Education	Education of head of household	Categorical	3.67	1.17	*p*5	Marginal price block 5	pesos/m³	12.2	-
Age	Age of head of household	Ordinal	39.32	12.61	*p*6	Marginal price block 6	pesos/m³	16.6	-
Members	Number of members	Ordinal	4.12	1.47	*p*7	Marginal price block 7	pesos/m³	20.31	-
Cm³	Water consumption	m³ / day	0.7	0.31	*p*8	Marginal price block 8	pesos/m³	33.84	-
Lnprice	Log of price	$/m³	1.72	0.29	*p*9	Marginal price block 9	pesos/m³	23.11	-
M²construction	Square meters of building	m²	84.73	23.67	*p*10	Marginal price block 10	pesos/m³	45.26	-
Yard	Homes with yard	Binary	0.63	0.48	*p*11	Marginal price block 11	pesos/m³	48.81	-
Bathrooms	Number of bathrooms	Ordinal	1.53	0.74	*y*virtual2	Virtual income in block 2	$000/year	109	124.65
Cistern	Homes with cistern	Binary	0.71	0.45	*y*virtual3	Virtual income in block 3	$000/year	109.77	124.74
Faucets	Number of faucets	Ordinal	3.7	1.5	*y*virtual4	Virtual income in block 4	$000/year	109.77	124.74
Rationed allocations	Supply restriction	Binary	0.51	0.5	*y*virtual5	Virtual income in block 5	$000/year	110.23	124.8
Storage	Homes with water storage	Binary	0.79	0.4	*y*virtual6	Virtual income in block 6	$000/year	111.86	125
Length of time	Age of home	Ordinal	14.46	13.17	*y*virtual7	Virtual income in block 7	$000/year	112.81	125.12
Information	Knowledge of the aquifer condition	Binary	0.67	0.46	*y*virtual8	Virtual income in block 8	$000/year	116.25	125.56
*p*1	Marginal price block 1	pesos/m³	4.31	-	*y*virtual9	Virtual income in block 9	$000/year	117.05	125.66
*p*2	Marginal price block 2	pesos/m³	5.34	-	*y*virtual10	Virtual income in block 10	$000/year	119.16	125.95
*p*3	Marginal price block 3	pesos/m³	8.37	-	*y*virtual11	Virtual income in block 11	$000/year	120.06	126.07

Source: authors.

meters, in logarithms); b) average marginal price per cubic meter; c) maximum average temperature and d) virtual income. These were expressed in logarithms and shown in Figure 4.

The economic variables were deflated based on the National Consumer Price Index (NCPI), obtained from the Bank of Mexico (base 2002 = 100). Income was based on weighted mean monthly salaries according to the Salario Medio de Cotización (SMCIMSS) of the population of permanent workers enrolled in the Mexican Social Security Institute in Baja California Sur. This was obtained from the National Minimum Salary Commission (CONASAMI). This variable is included as

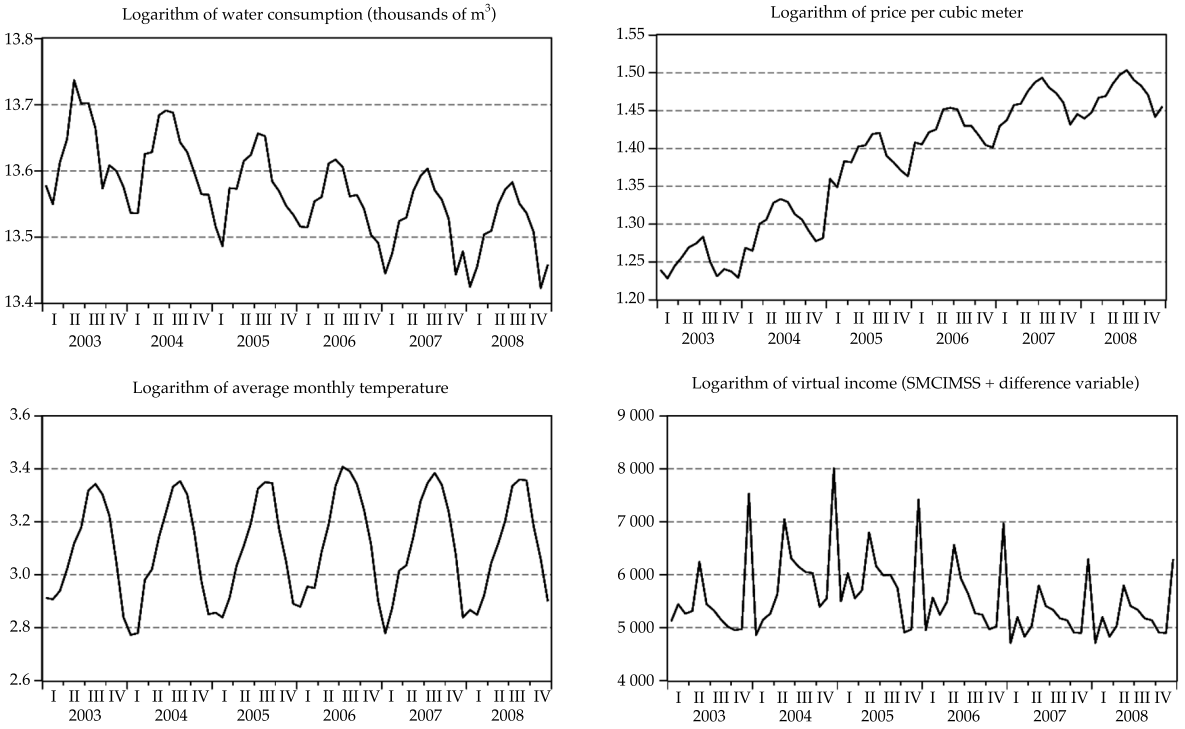

Source: authors.

Figure 4. Time series corresponding to domestic consumption, price, temperature and income in logarithms registered in La Paz, Baja California Sur, 2003-2008.

an indicator of family income in the state since it has the advantage of being available monthly and has also been used previously in empirical studies in Mexico as a proxy for family income (Islas & Moreno, 2011). Temperature corresponds to the average monthly temperature in the city of La Paz, obtained from the National Weather System (Conagua, 2010).

Análisis estadístico de series de tiempo

Statistical Time Series Analysis

Based on the non-stationary history of consumption and prices reported by Martínez-Espiñeira (2005), the process of generating information (PGI) was analyzed using the Augmented Dickey-Fuller (ADF) test (Dickey & Fuller, 1981), applying the procedure from the general to the specific. This included constants and trends and an evaluation of its statistical significance. The results are presented in Table 2.

Based on the values from the ADF tests, the null hypothesis that the series have unit roots was rejected (at a 5% statistical significance), confirming the stationarity of levels, which provides information for an adequate econometric specification.

Theoretical Framework for Block Pricing Structures

The theoretical framework on which the present empirical study was based is described in the literature related to block pricing structures and segmented budget constraints (Hausman, 1985; Moffitt, 1986; Hewitt & Hanemann, 1995; Olmstead, Hanemann, &

Table 2. Descriptive statistics and unit root tests for consumption, price, income and temperature, in logarithms. Period 2003-2008 with monthly frequency.

Unit root tests in levels				
Variable	**ADF**			
Consumption log	-4.31 (1)***			
Price log	-3.60 (2)**			
Income log	-8.21 (1)***			
Temperature log	-			
Mackinon critical value 5% = -3.47 [***] rejects the null hypothesis at 5%, [**] rejects the null hypothesis at 1% (*n*) indicates lags.				
Variable	**Mean**	**Standard deviation**	**Minimum**	**Maximum**
Consumption log	13.57	0.07	13.42	13.74
Price log	4.08	0.21	3.75	4.50
Income log	3.84	0.14	3.66	4.19
Temperature log	3.10	0.19	2.77	3.41

Source: authors.

Stavins, 2005) in supply industries (water, energy, gas etc.) where it is common to have non-linear fees with increasing or decreasing pricing structures. Non-linear prices are often used by the authorities responsible for urban water supplies. Prices are selected at constant rates up to a certain consumption level, with increasing or decreasing rates per block. With constant rates, consumers always pay an equal amount per unit of consumption. With increasing (decreasing) rates per block, as consumption increases a higher (lower) amount is charged for the last unit consumed in each block. With block pricing rates the demand function is not linear and includes discrete jumps. To show a simple case of non-linear structures with two blocks, the following suppositions are considered: a consumer with Y income maximizes the quasi-concave utility function $U(q,z)$, where q represents the amount of water expressed in cubic meters and z another good. The price of z is normalized at 1 and water is sold based on a two-block fee which may be increasing or decreasing. With p_j, $j = 1, 2$, the price of water in the j^{th} block, and $\bar{x}$ as the cutoff of the first block, the budget constraint is defined by two linear segments and can be described by the following conditions:

$$l = \begin{matrix} p_1 q + zq < \bar{x} \\ p_1\bar{x} + p_2\left(q - \bar{x}\right) + zq > \bar{x} \end{matrix} \quad (1)$$

Or also:

$$l = \begin{matrix} p_1 q + zq < \bar{x} \\ l + \left(p_1 - p_2\right)\bar{x} = p_2 q + zq > \bar{x}^{(2)} \end{matrix} \quad (2)$$

In this sense, virtual income is denoted by $\tilde{y} = y + (p_1 - p_2)\bar{x}$ and the term $(p_1 - p_2)\bar{x}$ is equal to the implicit subsidy that the consumer receives. This notion was introduced by Taylor (1975). Later, Nordin (1976) adapted this approach by including a difference variable $d = \sum_{j=1}^{i-1}\left(p^{j+1} - p^j\right)\bar{x}^j$, which indicates the difference in payment if all the units are charged the marginal price of the last block and the current consumption payment. The difference variable is positive with increasing block rates and negative with decreasing rates. The effects of the block pricing structure is interpreted as an implicit tax when block prices decrease and as an implicit subsidy when they increase, as shown in Figure 5.

The multi-block fees generate budgetary sets that are different than traditional constraints in that they are non-linear and may or may not be convex. Unlike the classic maximization scheme in which the consumer would have to equal the marginal price only once for a marginal benefit, block prices have a marginal price in each block, which in a two-block structure increases the number of consumption options to 3 (as seen in Figure 5), that is, one inside each block and another one at the cutoff between them. To analyze the behavior of the consumer in a block structure, the choice made by the consumer needs to be represented, which will be discrete and continuous. This results in an estimation of demand with conditional and unconditional functions. The demand function is conditioned and given by the choice the consumer makes within a particular block. The equation is expressed algebraically as follows:

$$q = \begin{cases} q(p_1, y_1) & siq < \bar{x} \\ \bar{x} & siq = \bar{x} \\ q(p_2, y_2) & siq > \bar{x} \end{cases} \quad (3)$$

where (p_1, p_2) and $(\tilde{y}_1, \tilde{y}_2)$ represent the prices and virtual income, respectively, in blocks 1 and 2. The unconditional demand model is obtained using the combination of the discrete and continuous choices:

$$q = \begin{cases} q(p_1, y_1) & siq(p_1, y_1) < \bar{x} \\ \bar{x} & siq(p_2, y_2) \leq \bar{x} \geq q(p_1, y_1) \\ q(p_2, y_2) & siq > \bar{x} \end{cases} \quad (4)$$

Both increasing and decreasing block pricing pose difficulties for empirical modeling due to the endogeneity between price and consumption.

Econometric Modeling for Cross-sectional Data

The instrumental variables (IV) method was used to estimate water demand. This consists of two parts. First, the regression of the average marginal price observed in the characteristics of the block pricing structure is estimated, with all the other exogenous variables. Second, the predicted prices are used in order to take into account the simultaneous determination of price and quantity, or more accurately, the price and the block in which it is consumed. This addresses the endogeneity problem with estimators that theoretically correspond to the relationship between price and consumption level. The following model

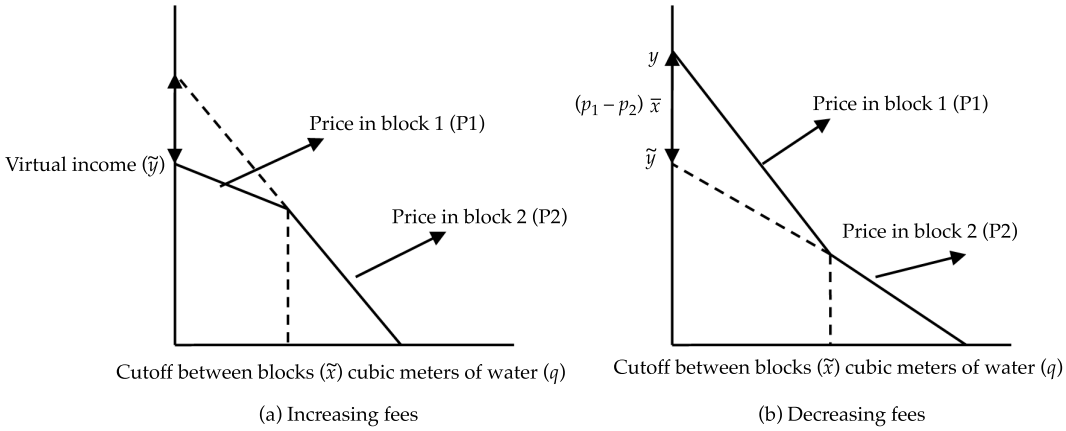

Source: developed based on Cavanagh, Hanemann and Stavins (2001).

Figure 5. Budgetary restriction with two-block pricing fees with increasing and decreasing fees.

was used to estimate short-term demand:

$$Cm^3 = \exp(z\delta)p^{\alpha}\tilde{y}^{\beta}\exp(\varepsilon) \quad (5)$$

taking the logarithms, we get:

$$\ln Cm^3 = z\delta + \alpha \ln p + \ln \tilde{y} + \varepsilon \quad (6)$$

where the theoretically expected sign of the coefficient of the price logarithm (*lnp*) is negative, while the amount ($\ln Cm^3$) and the income level ($\tilde{y}$) should be positively related. The matrix contains the physical and socioeconomic characteristics described in Table 2 and ε, the stochastic term. This instrument corresponds to this same pricing structure (variable amounts of marginal prices) as Hewitt and Hanemann (1995) and Cavanagh, Hanemann and Stavins (2001). The contribution by this work is the incorporation of the information variable as a dichotomic variable, which indicates whether the head of household is aware of the overexploitation of the aquifer and the problem with the intrusion of seawater. A very important aspect is that the *lnp* and *lny* coefficients cannot be directly interpreted as elasticities due to the non-linear budget constraint, since they do not reflect the probability that the households will change blocks in response to a change in price or income level because the reaction of households to increases in price and income level depends on the consumption block. Therefore, the coefficients will be interpreted as a measurement of sensitivity. The coefficients corresponding to the physical characteristics of the households and their make-up will be interpreted as a proportional change in water consumption given unit increases, since these are exponentially included in the demand function.

Econometric Modeling of Time Series Data

Long-term demand is estimated based on the econometric contributions developed by Cavanagh *et al*. (2001). The econometric specification is:

$$x_t = \alpha p_t + \beta(y_t + d_t) + \delta x_{t-1} + \gamma z_t + \varepsilon_t \quad (7)$$

Where x_t is aggregate consumption; y_{pt} is the average price; $y_t + d_t$ corresponds to virtual income with y_t = income, $yd_t = \sum_{j=1}^{i-1}\left(p^{j+1} - p^j\right)\bar{x}^j$, the consumption lag x_{t-1} is included since the households are expected to adjust their consumption level according to changes in the marginal price per cubic meter one period after the water bill payment (one month); z_t is the average temperature and ε_t is the error term. It is important to note that the instrument used in this time series estimation is the same as the one used for the cross-sectional estimation. Another important aspect is that only short-term elasticities are considered in equation (7). To obtain long-term elasticities, the following equation needs to be calculated:

$$\varepsilon_{lp} = \frac{\beta}{1-\delta} \quad (8)$$

Where β is the price coefficient and δ is the autoregressive parameter. It is worth mentioning that this elasticity takes into account temporality in terms of the process of adjusting consumption over time in response to changes in prices, that is, the statistical significance of δ. Its sign and magnitude indicate the sensitivity of current household consumption to the consumption and prices billed one or more periods earlier. In order to obtain robust estimators, the econometric strategy applied the White test to detect heteroscedasticity, and the Durbin-*h* test to detect serial correlation with the inclusion of x_{t-1}.

Results

Results from the Cross-Sectional Model

Table 3 shows the short-term coefficient estimated using the ordinary least squares (OLS) and IV methods.

Most of the estimators generated by the OLS method were statistically significant.

Of these, the positive sign of the *ln*price coefficient and its significance are notable. This is more representative of the slope of the data in the block pricing structure than the demand curve. This occurred due to the model's endogeneity problem, which results in biased and inconsistent coefficients. In terms of the results from the IV method, they confirm that the use of instruments corrects the endogeneity problem related to price and the amount demanded in the block pricing structures. Thus, theoretically expected signs are obtained at a statistical significance level of 1%, as shown by the *ln*price coefficient (n_p = –0.56), indicating that the households subject to block pricing structures react by adjusting consumption when the price increases. In addition, the price inelasticity of residential water demand is confirmed. The income variable was not statistically significant. The interpretation of the coefficients of the household characteristics requires a transformation, since they are exponentially included in the demand function. The transformation of the coefficients with antilogarithms makes it possible to interpret them as proportional changes in water consumption in response to unit increases. After performing this transformation, it was found that adding one more bathroom results in an increase in water consumption of 16%, on average. The households that have water storage as one of their consumption habits consume roughly 1% less water than those without storage. The effect of increasing one member in the household represents an increase in water consumption of 6.5%. The age of the home is a determinant of consumption level, as it indicates, and is squared since each yearly increase in a home's age corresponds to an increase in water demand of 1.6%; although older homes consume less than newer ones. In terms of the effect of information about the overexploitation of the aquifer, the coefficient indicates that households with this knowledge consume roughly 1% less water than those that do not know about the overexploitation of the aquifer and the intrusion of seawater.

Results from the Time Series Model

The results from the long-term estimation can be seen in Table 4.

In the estimation of the time series, all the coefficients had theoretically expected signs

Table 3. Results from the cross-sectional estimation using the instrumental variables method.

Variable	MCO		VI	
	Coefficient	Standard error	Coefficient	Standard Error
*Ln*price	0.85	0.044454	-0.56 ***	0.0575
*Ln*income	0.02	0.01814	4.73E-07	2.53E-07
*L*bathrooms	0.08	0.031702	0.14***	0.0417
Storage	-0.01	0.023803	-0.07*	0.0467
*L*members	0.04	0.027821	0.06***	0.015
*L*age	0.03	0.015599	0.016***	0.0047
*L*age^2	-0.0000633	0.0000358	-0.0003***	0.00009
Information	0.015	0.019168	-0.097**	0.0403
Constant	-2.205	0.229326		

Note: (*) indicates a 10% significance; (**) a 5% significance; (***) a 1% significance. Estimations of robustness in heteroscedasticity by the White method.
Source: authors.

Table 4. Results from the estimation of the time series using the instrumental variables method.

Variable	Coeficiente	Error estándar	Estadístico-*t*	Prob.
Log of constant	7.33	1.34	5.48	0.00
Log of consumption (-1)	0.44	0.10	4.29	0.00
Log of price	-0.51	0.08	-6.11	0.00
Log of temperature	0.11	0.02	4.99	0.00
log of income	0.17	0.05	3.70	0.00
Adjusted *R*-squared	0.85	*F-statistic* 93.18		
White test	13.61	(Prob.(0.00))		
Durbin-*h* Test	0.20	$T = 72$		

Source: authors.

and were statistically significant at a level of 1%. The short-term price elasticity is inelastic and indicates that the increase in the marginal price has the effect of a decrease in demand which is less than proportional to the increase in the price. That is, when increasing the price 10%, the consumption decreases 5.1% monthly, on average. The consumption coefficient with a lag indicates that the households adjust their consumption one period after paying the water bill. The virtual income coefficient shows that increases in income and the implicit subsidy result in an increase in demand. The temperature variable affects demand, that is, an increase of 1% in average maximum temperature will have the effect of increasing the monthly water demand by 0.11%.

The price elasticity of long-term demand was -0.90, higher than short-term elasticity (-0.51) in absolute terms. This result is consistent with the empirical literature and suggests that households adjust their long-term consumption level in response to permanent increases in the pricing structure. The result from the Durbin-*h* serial correlation test was 0.20, less than the normal distribution (1.64), and therefore the null hypothesis of a lack of a serial correlation cannot be rejected (5% significance level).

Discussion

The short- and long-term elasticity estimators presented above demonstrate consistency between the cross-sectional and time series estimations (-0.56 and -0.51, respectively). This was the case with previous studies in Mexico related to the inelasticity of demand. Nevertheless, the results from this work differ from the others in terms of the magnitude of the elasticity. This can be seen when comparing this work with other studies, for example, with García-Salazar and Mora (2008) who studied the Torreon region (-0.2 to -0.18), which indicates that an average increase of 100% in the price per cubic meter of water will result in a 20% decrease in demand. Meanwhile, in La Paz, a 100% increase in the price will result in a 51% decrease in demand. Another contribution by this study is the inclusion of the information variable in the cross-sectional estimation. The results show that households with knowledge about the overexploitation of the aquifer and the intrusion of seawater consumed less water than those without this information. This is significant to managing demand, since information campaigns by the OOMSAPAS could more efficiently affect consumption and thereby decrease the pressure to overexploit aqui-

fers. In addition, it is important to consider that the elasticities represented in this work and the studies described above show how demand responds to price changes but do not indicate the amount of water demanded that would not respond to prices (that is, the level of water consumption that is indispensable to survival and, therefore, does not respond to price). There is an evident need for future investigations about this subject since this is crucial to the design of mixed fee structures that include a fixed consumption level with no charges and block prices after a certain consumption level. The implementation of this type of fee structure would explicitly address equity and access to water as a human right.

Conclusion

This study is the first of its kind to estimate the long-term price elasticity of residential water demand in Mexico using a chronological data series. The results are consistent with the literature on demand functions pertaining to block pricing and they contribute to the study of the impact of pricing policies on household consumption in developing countries where the water supply is limited by the geological characteristics of reservoirs as well as by climatic factors. The results show the importance of pricing structures and permanent fee increases to adequately manage water demand, which achieves the efficient use of the resource. The long- and short-term demand elasticities were greater than the average reported in the national empirical literature. This indicates that the magnitude of the adjustment in water consumption in response to sustained increases in prices is greater in homes in the city of La Paz than in other regions in Mexico, while increases in temperature and income result in a higher monthly water demand. These results have implications for water use and management policies in semi-arid regions where the water supply is limited, as well as for areas where the hydrological cycle may be altered (overexploitation and intrusion of seawater in coastal zones).

Plans to manage water resources in regions with limited water supplies should consider applying pricing instruments to manage urban water demand, since households adjust their water consumption level when block pricing structures are used to impose sustained price increases. This would achieve the efficient use of the resource. The results of the estimations of short-term price elasticity in the cross-sectional and time series models resulted in -0.56 and -0.51, respectively, while long-term price elasticity was -0.90, demonstrating consistency between the estimators. In addition, it is important to mention that both estimations were performed with real consumption and price data provided by the operating entity. Thus, the study fulfills the proposed objective and corroborates the hypothesis that, along with the use of measurements, the adequate design of fee structures using block pricing contributes to managing residential water demand, resulting in the efficient use of the resource by decreasing consumption in response to permanent price increases in the fee structure over time.

Acknowledgments

The authors wish to thank the Municipal Drinking Water, Sewage and Water Treatment Operating Entity of La Paz (Organismo Operador Municipal del Sistema de Agua Potable, Alcantarillado y Saneamiento de La Paz (OOMSAPAS, Spanish acronym) for providing consumption and pricing data containing "individual codes," without which this work would not have been possible. In addition, we thank the valuable comments from the anonymous reviewers.

References

Banxico (2010). *Banco de México. Estadísticas de inflación*. Recuperado de http://www.banxico.org.mx/politica-monetaria-e-inflacion/estadisticas/inflacion/indices-precios.html.

Bartoszczuk, P., & Nakamori, Y. (2004). *Modelling Sustainable Water Prices. Handbook of Sustainable Development Planning: Studies in Modelling and Decision Support*. En M. Quaddus & A. Siddique (Eds.). Cheltenham: Edward Elgar. Recuperado de http://www.jaist.ac.jp/~bpawel/BARTOSpopr8niew.pdf.

Billings, R., & Agthe, D. (1980). Price Elasticities for Water: A Case of Increasing Block Rates. *Land Economics*, *56*, 73-84.

Cavanagh, S. M., Hanemann, W. M., & Stavins, R. N. (2001). *Muffled Price Signals: Household Water Demand Under Increasing-Block Price*. Recuperado de http://www.hks.harvard.edu/fs/rstavins/Papers/Cavanagh_Hanemann_Stavins_ASSA_Paper.pdf.

Cibnor (2011). *Mapa de la Cuenca de La Paz, B.C.S., México*. La Paz, México: Unidad de Laboratorios de Servicios y Apoyo (ULSA) del Centro de Investigaciones Biológicas del Noroeste.

Conagua (2008). *Estadísticas del agua en México*. México , DF: Comisión Nacional de Agua.

Conagua (2010). *Temperatura por entidad federativa*. México, DF: Servicio Meteorológico Nacional,. Recuperado de http://smn.cna.gob.mx/climatologia/temperaturas/tmaximas.html.

Cruz-Falcón, A. (2007). *Caracterización y diagnóstico del acuífero de La Paz, B.C.S., mediante estudios geofísicos y geohidrológicos*. La Paz, México: Instituto Politécnico Nacional-Centro Interdisciplinario de Ciencias Marinas.

Dalhuisen, J., Florax, R., De Groot, H., & Nijkamp, P. (2003). Price and Income Elasticities of Residential Waterdemand: A Meta-Analysis. *Land Economics*, *79*, 292-308.

Dickey, D. A., & Fuller, W. A. (1981). Likelihood Ratio Statistics for Autoregressive Time Series with a Unit Root. *Econométrica*, *49*, 1057-1072.

Elnaboulsi, J. C. (1999). A Model for Constrained Peak-Load Water and Wastewater Pricing and Capacity Planning Can. *Water Resources Journal*, *24*(2), 87-96.

García-Salazar, J. A., & Mora, J. S. (2008). Tarifas y consumo de agua en el sector residencial de la Comarca Lagunera. *Región y Sociedad*, *40*, 119-132.

Hausman, J. (1985). The Econometrics of Non-Linear Budget Sets. *Econometrica*, *53*, 1255-1282.

Hewitt, J. A., & Hanemann, W. M. (1995). A Discrete/Continuous Choice Approach to Residential Water Demand under Block Rate Pricing. *Land Economics*, *71*, 173-192.

Howe, C. W., & Linaweaver, F. P. (1967). The Impact of Price on Residential Water Demand and its Relation to System Demand and Price Structure. *Water Resources Research*, *3*, 13-32.

Islas, C. A., & Moreno, G. (2011). Determinantes del flujo de remesas en México, un análisis empírico. *EconoQuantum*, *7*, 9-36.

Jaramillo, L. A. (2005). Evaluación econométrica de la demanda de agua de uso residencial en México. *El Trimestre Económico*, *286*, 267-390.

Klawitter, S. A (2003). *Methodical Approach for Multi Criteria Sustainability Assessment of Water Pricing in Urban Areas*. Paper presented at the 2003 Berlin Conference on the Human Dimensions of Global Environmental Change. Recuperado de http://www.fu-berlin.de/.

Martínez-Espiñeira, R. (2005). *An Estimation of Residential Water Demand Using Co-Integration and Error Correction Techniques. Munich Personal RePEc Archive*. Recuperado de http://mpra.ub.uni-muenchen.de/615/.

Moffitt, R. (1986). The Econometrics of Piecewise-Linear Budget Constraints. *Journal of Business and Economic Statistics*, *4*, 317-328.

Nordin, J. A. (1976). A Proposed Modification on Taylor's Demand-Supply Analysis: Comment. *The Bell Journal of Economics*, *7*, 719-721.

Olmstead, S. M., Hanemann, M. W., & Stavins, R. N. (2005). *Do Consumers React to the Shape of Supply? Water Demand under Heterogeneous Price Structures Resources for the Future*. Recuperado de: http://www.rff.org.

OOMSAPAS (2009). *Base de datos internos sobre facturación por clave de usuario*. Proporcionados por la dirección general del H. XII Ayuntamiento de La Paz, Baja California Sur. Organismo Operador Municipal del Sistema de Agua Potable y Alcantarillado de La Paz, B.C.S. México.

Renzetti, S. (1992). Evaluating the Welfare Effects of Reforming Municipal Water Prices. *Journal of Environmental Economics and Management*, *22*, 147-163.

Ruijs, A. (2009). Welfare and Distribution Effects of Water Pricing Policies. *Environment Resources Economics*, *43*, 161-182.

Salazar, A., & Pineda, N. (2010). Factores que afectan la demanda de agua para uso doméstico en México. *Región y Sociedad*, *49*, 3-16.

Sisto, N. (2010). Manejo sustentable del uso de agua y crecimiento urbano. *Ensayos Revista de Economía*, *1*, 23-38.

Soto, G., & Bateman, I. (2006). Scope Sensitivity in Households' Willingness to Pay for Maintained and Improved Water Supplies in a Developing World Urbana Area: Investigating the Influence of Baseline Supply Quality and Income Distribution Upon Stated Preferences in México City. *Water Resources Research*, *42*, 1-15.

Taylor, D. (1975). The Demand for Electricity: A Survey. *The Bell Journal of Economics*, *6*, 74-110.

Yepes, G., & Dianderas, A. (1996). *Water & Wastewater Utilities*. Washington, DC: World Bank.

Institutional Address of the Authors

Gerzaín Avilés-Polanco
Víctor Hernández-Trejo

Universidad Autónoma de Baja California Sur (UABCS)
Departamento Académico de Economía
Carretera al sur, km 5.5
Apartado Postal 19-B
23080 La Paz, Baja California Sur, México
Teléfono: +52 (612) 1238 800, extensión 3210
gaviles@uabcs.mx
victorh@uabcs.mx

Marco A. Almendarez-Hernández
Luis Felipe Beltrán-Morales

Centro de Investigaciones Biológicas del Noroeste (Cibnor)
Instituto Politécnico Nacional 195
Playa Palo de Santa Rita Sur
23096 La Paz, Baja California Sur, México
Teléfono: +52 (612) 1751 230, extensión 5123
malmendarez@cibnor.mx
lbeltran04@cibnor.mx

Wet soil surface.

Photo: Fidencio Cruz Bautista

Estimate of the Impact of Climate Change on Soil Fertility and Coffee Production in Veracruz, Mexico

• Juan Gabriel Brigido* • Iourii Nikolskii • Liliana Terrazas •
• Sergio Santiago Herrera •
Colegio de Postgraduados, México
*Corresponding Author

Abstract

Brigido, J. B., Nikolskii, I., Terrazas, L., & Herrera, S. S. (July-August, 2015). Estimate of the Impact of Climate Change on Soil Fertility and Coffee Production in Veracruz, Mexico. *Water Technology and Sciences* (in Spanish), 6(4), 101-116.

Estimates of the vulnerability of crops to climate change typically ignore the possible alterations in the fertility of the soil caused by this phenomenon. The primary objective of the present work was to estimate the role of alterations in soil fertility in the predictions of coffee production (*Coffea Arabica L.*) for the end of the 21st century in 6 of the largest coffee producing regions in the state of Veracruz, Mexico. Three global circulation models were used with two radiative forcing scenarios. A crop development model was applied according to the biological and climate characteristics proposed by IIASA/FAO. The model is extensively used worldwide. The calculations of cherry coffee production based on current climate conditions and their comparison with data reported by SAGARPA indicate that the yields calculated are reliable. The correlation coefficient between the calculated and observed yields is 0.93 with a standard error of 0.08. By the end of 21st century, as much as a 34% reduction in coffee production is expected. This varies among coffee regions primarily due to changes in rainfall , and to a lesser extent to increases in air temperature. A lack of knowledge about alterations in soil fertility caused by climate change can create errors as high as 40% in the estimation of coffee production. This factor should therefore not be overlooked.

Keywords: Vulnerability, agriculture, local hydrothermal index, integral soil fertility index, climate change scenarios, state of Veracruz of Mexico.

Resumen

Brigido, J. B., Nikolskii, I., Terrazas, L., & Herrera, S. S. (julio-agosto, 2015). Estimación del impacto del cambio climático sobre fertilidad del suelo y productividad de café en Veracruz, México. Tecnología y Ciencias del Agua, *6(4), 101-116.*

*La estimación de la vulnerabilidad de los cultivos agrícolas al cambio climático se hace principalmente ignorando la alteración posible de la fertilidad del suelo atribuible al mismo cambio climático. El objetivo principal del presente trabajo fue estimar el papel de la alteración de la fertilidad del suelo en las predicciones sobre la productividad del cultivo de café (*Coffea Arabica L.*) al final del siglo XXI para seis de las regiones cafetaleras productoras más importantes del estado de Veracruz, México. Se han considerado tres modelos de circulación global bajo dos escenarios de forzamiento radiativo. Se ha aplicado un modelo de desarrollo del cultivo en función de sus características biológicas y las características climáticas propuesto por IIASA/FAO y utilizado ampliamente en el mundo. Los cálculos de la productividad de café cereza para las condiciones climáticas actuales y su comparación con los datos reportados por la SAGARPA señalan que los rendimientos calculados son confiables. El coeficiente de correlación entre los rendimientos calculados y observados es igual a 0.93 con error estándar de 0.08. Al final del siglo XXI se espera hasta un 34% de reducción en la productividad de café, variando entre regiones cafetaleras debido principalmente al cambio al cambio en la precipitación y, en menor grado, al incremento de la temperatura del aire. La ignorancia de la alteración de la fertilidad del suelo atribuible al cambio climático puede causar errores en la estimación de la productividad de café de hasta un 40%, por lo que este factor no debe ser desestimado.*

***Palabras clave**: vulnerabilidad, agricultura, índice hidrotérmico local, índice integral de fertilidad del suelo, escenarios de cambio climático, estado de Veracruz, México.*

Received: 27/01/2014
Accepted: 06/03/2015

Introduction

Several recent studies have indicated that climate changes recorded over recent years are particularly unusual (Jacoby & D´Arrigo, 1997; Mann, Bradley, & Hughes, 1998, 1999; Rodney & Freddy, 2002; Caballero, Lozano-García, Vázquez-Selem, & Ortega, 2010). Some factors that can produce changes in the climate are known, although not precisely. While some believe we are experiencing a natural event which is part of a cycle, most suggest that climate changes is entirely or partially caused by human activities, especially carbon emitted into the atmosphere from the use of fossil fuels and deforestation (Gonzalez *et al*., 2003; Magaña, 2004).

The climate changes that are currently being observed are expected to inevitably affect natural resources in the future and, in turn, agricultural yields, including coffee crops. Investigations performed around the world and in Mexico about the vulnerability of coffee to climate change consider only the direct effect of changes in solar radiation, air temperature and precipitation, neglecting the indirect effect of a possible alteration in the fertility of soil due to climate change.

Veracruz is the second largest coffee producing state in the country, with 153 000 hectares, directly benefiting 300 000 families who work in this industry (Contreras, 2010). Several studies have been performed about the vulnerability of coffee crops (mostly with *Coffea arabica* L.) to climate changes expected during the 21st century. Most of these studies have been qualitative (Camargo, 2010; Villers, Arizpe, Orellana, Conde, & Hernández, 2009; Haggar & Schepp, 2012) and indicate how some of the physiological processes related to the crop will be affected, but do not contribute to identifying the percentage change in coffee yields. Other studies have quantitatively estimated the potential impact of climate change on coffee yields based on empirical regression models of the relationship between coffee yields and climate factors, and even certain economic factors related to managing this crop (Fontagro, 2011; Haggar & Schepp, 2012; Laderach *et al*., 2011; Lin, Perfecto, & Vandermeer, 2008; Paavola, 2008; Heakin, Gay, Estrada, & Conde, 2004; Jaramillo *et al*., 2011). Theoretical models (mainly the IIASA-FAO, 2012) have also been used to study the relationship of coffee production to the biological factors and climate conditions expected over the 21st century (Bunn *et al*., 2013; Davis, Gole, Baena, & Moat, 2012; Rivera-Silva *et al*., 2013). These have determined a reduction in coffee yields (*Coffea arabica* L.) of 10 to 25% in the state of Veracruz during the 21st century, depending on the climate change scenario and models used for the analysis.

Nevertheless, these studies have ignored another possible factor— the potential altering of the fertility of the soil due to long-term climate change. Over recent years, several studies have been conducted in Mexico to quantitatively estimate the role of climate change on soil fertility and its effect on crop yields (Nikolskii, Bakhlaeva, Contreras, & Ordaz, 2001; Contreras *et al*., 2002; Castillo *et al*., 2007; Terrazas, Nikolskii, Heerera, Castillo, & García, 2010). Nevertheless, these works only estimated the vulnerability of wheat, corn and beans to climate change.

The objective of the present study was to evaluate the vulnerability of coffee crops (*Coffea arabica* L.) in the state of Veracruz to climate change by the end of the 21st century. The theoretical IIASA/FAO (2012) model was used, taking into account not only the physiological processes involved in the growth of the crop but also the effect of possible changes in the soil's fertility as a result of climate change.

Materials and Methods

The present study was conducted in the central region of the state of Veracruz, in 20 municipalities distributed throughout the

six principal coffee-producing regions in the state: Atzalan, Coatepec, Córdoba, Huatusco, Misantla and Tezonapa. Ninety percent of the state's coffee producers and 93% of the state's total crop area is located in this area (Moguel & Toledo, 1999; López, Díaz, & Martínez, 2007).

These regions are located between latitudes 18° 36' and 20° 4'with altitudes ranging from 600 to 1 500 masl. Annual mean precipitation is 1 717.3 mm and annual mean temperature is 20.2 °C. The predominant soil types are andisols, cambisols, lithosols and luvisols. The slopes of the terrain range from 0 to 30% (SMN, 2013; INIFAP, 2012).

The typical climate conditions at the beginning of the 21st century were obtained from climatological normals corresponding to each of the weather stations selected, published in the National Weather Service webpage (SMN, 2013). The climate conditions for the end of the century were obtained from estimations by the Atmospheric and Environmental Sciences Information Unit, at the Center for Atmospheric Sciences, National Autonomous University of Mexico (UNAM, Spanish acronym). These were generated from 3 of the 15 global circulation models available from the interoperability models project, phase 5: MPI-ESM-LR (Max-Plank Institute), GFDL-CM3 (Geophysical Fluid Dynamics Laboratory) and HADGEM2-ES (Met Office Hadley) (Fernández, Zavala, & Romero, 2014).

Two radiative forcing scenarios were used: RCP 4.5 (650 ppm of CO_2) and RCP 8.5 (1370 ppm); the RCP 6.0 (720 ppm) forcing was not analyzed because it was considered to be an intermediate value between the selected values.

These three models were used for the following reasons:

— Although the simulation of monthly temperature and precipitation values by the various models are not very different, the three models selected correspond to the group with the best performance results, according to the evaluation by Cavazos *et al.* (2013).
— The 15 models in the final report containing updated climate change scenarios for Mexico (one of the products from the Fifth National Communication) had a spatial resolution of 0.5° x 0.5° (approximately 55 x 55 km) (Cavazos *et al.*, 2013). Nevertheless, the models were restructured at 30" x 30" (approximately 926 x 926 m) using a scale reduction process with the 1950-2000 scenario developed by Hijmans, Cameron, Parra, Jones and Jarvis (2005) as a reference. This incorporated the effect of topography and therefore provided a better spatial distribution of the climate change variables studied. It is very important to use models with these characteristics to calculate coffee yields in mountainous regions in the state of Veracruz, where the climates in the coffee-producing regions vary greatly.
— The purpose of the present work was to estimate the possible degree of change in soil fertility and coffee yields in function of the expected changes in temperature and precipitation in the state of Veracruz at the end of the 21st century. The hypothesis is that the vulnerability of coffee production to climate change can be ignored if there are no significant differences in the yields calculated. On the other hand, if the yields significantly depend on the changes in temperature and precipitation simulated by the models selected, then it will be necessary to perform a more in-depth and detailed investigation of this type.

The current climate characteristics of the coffee-producing regions in Veracruz are shown in Table 1. The impact of climate change on cherry coffee production (*Coffea Arabica* L.) by the end of the 21st century was estimated.

Table 1. Average annual temperature (T^{2000}), precipitation (Pr^{2000}), net radiation (Nr^{2000}) values and the climate index (HTI^{2000}) for the beginning of the 21st century at the coffee-producing (*Coffea Arabica* L.) sites mentioned in the state of Veracruz.

Coffee-producing region	Municipality	T^{2000} (°C)	Pr^{2000} (mm year^{-1})	Rn^{2000} (MJ m^{-2} year^{-1})	HTI^{2000} (dimensionless)
Atzalán	Atzalán	16.1	1 947.32	3 900.42	0.8
	Jalacingo	15.7	1 678.52	4 116.88	0.98
	Las Minas	17.9	1 492.89	2 886.38	0.77
	Martínez de la Torre	23.6	1 986.44	3 958.62	0.79
Coatepec	Naolinco	22.6	1 046.63	5 056.40	1.92
	Coatepec	19.6	1 746.85	4 917.40	1.12
	Jalcomulco	24.5	1 090.12	5 334.82	1.95
	Teocelo	20.6	2 026.2	4 191.41	0.82
	Jilotepec	19.4	1 663.32	3 191.18	0.76
	Cosautlán de Carvajal	19.8	2 111.96	3 880.33	0.73
	Emiliano Zapata	23.2	935.6	4 102.23	1.75
Cordoba	Ixhuatlán del café	20.2	1 900.15	4 820.26	1.01
	Atoyac	24.5	2 116.74	4 039.01	0.76
Huatusco	Comapa	23.1	1 078.74	4 373.95	1.61
	Tenampa	19.8	1 681.69	3 457.04	0.82
	Huatusco	17.2	1 960.59	3 870.28	0.79
Misantla	Vega de Alatorre	24.2	1 578.69	3 967.41	1
	Misantla	24.7	1 715.56	4 407.86	1.02
	Acatlán	15.3	1 442.24	3 171.50	0.88
Tezonapa	Tezonapa	24.1	2 755.07	5 292.12	0.76

Note: the HTI climate index is described by equation (1).

As can been seen, precipitation ranged from 935.6 mm year^{-1} to 2 755.07 mm. Mean annual temperature ranged from 15 to 25°C.

According to Budyko (1974), Volobuev (1974), Aydarov (1985), Nikolskii *et al*. (2001), Contreras *et al*. (2002), Castillo *et al*. (2007) and Terrazas *et al*. (2010), the annual climate conditions for year *j* can be characterized by the local hydrothermal index (*HTI*):

$$IHT^j = \frac{Rn^j}{\lambda . Pr^j} \qquad (1)$$

Where Rn^j is the average annual net radiation (MG m^{-2} year^{-1}); λ is the latent heat from water evaporation (2.512 MJ m^{-2} mm^{-1}) and Pr^j is annual mean precipitation (mm year^{-1}).

The HTI^j values are dimensionless and range from 0.4 to 1 in humid tropical regions in Mexico, 1 to 3 in semi-humid and semi-arid regions, and 3 to 8 in arid regions in northern Mexico. As seen in Table 1, the HTI^{2000} values for the reference regions for coffee production in the state of Veracruz range from 0.73 to 1.95, which corresponds to a semi-arid climate.

Estimation of Coffee Yields (Coffea arabica L.)

Cherry coffee yields were calculated for the climate scenarios mentioned previously and for climate conditions at the beginning of this century, using an equation proposed by IIASA/FAO (2012):

$$Y^{j}_{cal} = Y^{j}_{max} * INSH^{j} * F^{j}_{a} \quad (2)$$

Where Y^{j}_{cal} is the coffee yield (*Coffea arabica* L.) (in kg ha^{-1} year^{-1} of cherry coffee) corresponding to the reference sites for the base scenario at the beginning of the 21st century (j = 2 000) and at the end of the 21st century (j = 2 075-2 099); Y^{j}_{max} is the potential maximum yield, or the agro-climate of the economically attainable yield of dry matter, in which healthy plants can be produced with an adequate water and nutrient supply (in kg ha^{-1} year^{-1}) for the base scenario (j = 2 000) at the beginning of the 21st century and at the end of the century (j = 2 075-2 099); F^{j}_{s} = integral soil fertility index for the base scenario at the beginning of the 21st century (j = 2000) and the end of the 21st century (j = 2 075-2 099), which can be presumed to be different at the end of the century due to a certain dependency of the fertility of the soil on climate conditions (Contreras *et al*., 2002; Castillo *et al*., 2007; Terrazas *et al*., 2010).

Of course the model does not consider the potential effect of infestations or disease (which can also be presumed to be dependent on climate change) since existing mathematical models used to predict the effect of climate change on diseases and/or infestations are empirical (Van der Vossen, 2005). That is, they were developed based on observations related to particular reference sites and are therefore not representative of other regions or climatic zones. In addition, these models contain a large number of empirical parameters and it is not known how to apply these to the case of Veracruz. Thus, the present investigation did not use these models.

Estimation of Potential Yields (Y^{j}_{max})

The biomass and potential or maximum yield (Y^{j}_{max}) of the crops were calculated using a model based on eco-physiological principles (IIASA/FAO, 2012):

$$Y^{j}_{max} = Bn * CI \quad (3)$$

Where Bn is the net biomass of the total dry matter (in kg ha^{-1}) and CI is the crop index or the fraction of Bn corresponding to the agricultural product (dimensionless). The value of Bn (in kg ha^{-1}) is calculated by the following equation:

$$Bn = \frac{0.36 b_{gm} L}{(1/n) + 0.25 C_t} \quad (4)$$

Where b_{gm} is the maximum brute biomass production of a reference crop with a Leaf Area Index (LAI) equal to 5 (in kg ha^{-1} day^{-1}); b_{gm} primarily depends on the photosynthetically active radiation and the concentration of CO_2 in the atmosphere; L is the fraction of the maximum growth rate of the crop with incomplete land cover when the leaf area index (LAI) is under 5 (LAI<5, dimensionless); n is the duration (in days) of the normal crop cycle for coffee (*Coffea Arabica* L.) (which is 270 days) (IIASA/FAO, 2012); C_t is the fraction of the brute biomass production rate (as CH_2O) that is lost due to maintenance respiration, which depends on the type of crop (leguminous versus non-leguminous) and mean air temperature (kg day^{-1}).

To obtain the values of b_{gm}, the maximum biomass production rate (Pm) was estimated (in kg CH2O ha-1 h-1) using the following expressions:

For $Pm^3 \geq 20$ kg CH_2O ha^{-1} h^{-1}:

$$b_{gm} = N(0.8 + 0.01 P_m) b_O + (1\text{-}N)(0.5 + 0.025 P_m) b_C \quad (5)$$

For $Pm < 20$ kg CH_2O ha^{-1} h^{-1}:

$$b_{gm} = N(0.8 + 0.01 P_m) b_O + (1 - N)(0.5 + 0.025 P_m) b_C \quad (6)$$

Where N is a dimensionless parameter dependent on the theoretical photosynthetically active radiation (Ac), or daily potential, cn, with a completely clear sky (in MG m^{-2} day^{-1}) and the global shortwave radiation (Rg, in m^{-2} day^{-1}). This equation assumes that the real photosynthetically active radiation (RFA) is half of the global radiation and is 20% of the theoretical Ac on a cloudy day:

$$N = \frac{Ac - 0.5Rg}{0.8Ac} \qquad (7)$$

b_O is the brute rate of dry matter production for a hypothetical reference crop (kg CH_2O ha^{-1} h^{-1}) on completely cloudy days, with a canopy covering the entire land and a maximum biomass production rate of 20 kg ha^{-1} h^{-1}; b_C is the brute production rate of dry material for a hypothetical reference crop (kg CH_2O ha^{-1} h^{-1}) on completely clear days, with canopy entirely covering the land and a maximum biomass production rate of 20 kg ha^{-1} h^{-1}.

The correction factor for partial land coverage (L) is calculated as follows:

$$\text{If } IAF < 5$$

$$L = 0.3424 + 0.9051 Log_{10}(LAI) \qquad (8)$$

$$\text{If } IAF \geq 5, \text{ then } L = 1$$

The values of C_t can be calculated with the following equation:

$$C_t = C_{30}\left(0.0044 + 0.0019\,T + 0.0010\,T^2\right) \qquad (9)$$

Where T is the mean monthly air temperature during the crop cycle; C_{30} is the rate of loss in the brute biomass production due to maintenance respiration at 30° C (0.0108 for non-leguminous plants, as is the present case).

The information regarding CI, N, LAI, photosynthetic route, Pm, b_O, b_C and regional data about the beginning and end of the crop cycle for coffee in Mexico were obtained from publications by IIASA/FAO (2012) and De Wit (1965).

The following considerations were included in the calculation according to the period corresponding to the climate change scenarios for the for the end of the 21st century (j = 2 075 - 2 099): 1) The CI was practically independent of climate change and therefore no change was considered. In addition, no change in the LIA was considered (Cure & Acock, 1986; Anthony & Ziska, 2000); 2) No change was considered in the duration of the crop cycle (N) since the methodology did not consider changes in coffee crops because of a lack of reference research about this factor in our country; 3) No significant change in the transmissivity of the atmosphere was considered because of its diathermal property and, therefore, the parameters b_O and b_c did not change.

Estimation of the Soil Water Availability Index (SWAI^j)

The Water Demand Satisfaction^j Index (WDSI) was calculated according to the annual water balance in the plants' radicle area (accumulative). To this end, a monthly scale was used based on the equation proposed by Frère and Popov (1986):

$$WDSI_i^j = WDSI_{i-1}^j \left(\frac{MD_i^j}{\sum_i^n WD^j} \right) * 100 \qquad (10)$$

Where $WDSI^j_i$ is the Water Demand Satisfaction Index for month i during year j, $WDSI^j_{i-1}$ is the Water Demand Satisfaction Index for the month prior to that same year, MD^j_i is the absolute moisture deficiency for month i of year j; $\sum_{i=1}^{n} WD^j$ is the sum of the water demanded by the crop during year j from month i to n, during its crop cycle (270 days, from February 15 to November 15)

when the biomass of the plant is produced (IIASA/FAO, 2012). The evapotranspiration of the crop (ETc^{j}_{i}) for month i of year j was included when calculating the $WDSI^{j}_{i}$ and MD^{j}_{i} values as well as water infiltration into the soil (Inf^{j}_{i}) for month i of year j.

Allen, Santos, Raes and Smith (2006) defined the water demanded (WD) or needed by the crops as the amount of water required to compensate for loss due to the evapotranspiration (ETc) by the crop. For the present case, the evapotranspiration of the crop (ETc^{j}_{i}) was calculated based on their recommendations using minimum climatological values. Reference evapotranspiration (ET_0) was calculated per month using the CROPWAT 8.0 program (FAO, 2013). The value obtained was then multiplied by the transfer coefficient $Kc = 1.1$ (Allen *et al.*, 2006).

Water infiltration into the soil was obtained according to the difference between monthly precipitation and surface runoff (SARH, 1991; CNA, 2002). The depth of the water stored that is usable and available for the crops was determined according to soil texture at a depth of 70 cm, which corresponds to the radicle area of coffee plants.

Of course some coffee plants are located in the shade, in which case a possible effect from the reduction of evapotranspiration needs to be considered using the pertinent calculations found in the literature for the distribution of net radiation under tree canopies (Chang, 2001). Nevertheless, according to experimental observations related to changes in microclimates and coffee yields in shade (Siles, Harmand, & Vaast, 2010), while the temperature of the leaves is lower competition for water from the soil also occurs, resulting in similar coffee yields for plants with full exposure and those in the shade. Since the main objective of the calculations was to estimate the relative change in yields at the end of the 21st century ($Y^{2075\text{-}2099}$) as a fraction of the yield at the beginning of the century (Y^{2000}), the following relative values were calculated: $WDSI^{2075\text{-}2099}/WDSI^{2000}$, $ET^{2075\text{-}2099}/ET^{2000}$ and $Pr^{2075\text{-}2099}/PR^{2000}$. The final conclusion was that the effect of the shade can be ignored, while assuming that the structure of the vegetation will significantly change over time.

Estimation of the Integral Soil Fertility Index (F^{j}_{s})

The Integral Soil Fertility Index (F^{j}_{s}) for the base scenario was calculated according to the formula proposed by Pegov and Jomyakov (1991), and adapted by Bakhlaeva, Román-Calleros and Maslov (2006):

$$F_s^j = 0.46\frac{MO}{MO_{\max}} + 0.28\sqrt{\frac{P}{P_{\max}}\frac{K}{K_{\max}}} + 0.26e^{-\left(\frac{pH-6}{2}\right)^2} \quad (11)$$

Where F^{j}_{s} is the soil fertility for the base scenario at the beginning of the 21st century ($j = 2000$); MO, K and pH are the modal values of the organic matter, phosphorous and potassium contents in the soil that are available to the crop and the pH values typical of soils in coffee fields, with the same HTI index for the base scenario at the beginning of the 21st century ($j = 2000$); MO_{max}, P_{max} and K_{max} are maximum observed MO, P and K values in the study area ($j = 2000$).

The value of F_s is dimensionless and ranged from 1 to 0.1, corresponding to soil that is potentially most fertile (where 0 is completely degraded and infertile soil). Equation (11) is useful because it uses a small amount of information about some of the soil properties in Mexico from data from INEGI (1988, 2004) and INIFAP (2012).

The change in soil fertility due to climate change was estimated based on the Law of Geographic Zonality for Soil (Budyko, 1974; Volobuyev, 1974). According to this law, the regional modal values of some of the chemical, physical and biological properties of geomorphologically homogeneous (same topography, geological and hydrogeological

conditions, texture, mineralogy of the subsoil and formation time) virgin soils depend primarily on the typical HTI^j index for the base scenario at the beginning of the 21st century (j = 2000) and at the end of the century (j = 2 075 - 2 099) (Volobuyev, 1974; Aydarov, 1985; Nikol'skii *et al*., 2006; Castillo *et al*., 2007).

Equation (12) was used to calculate net radiation (R_n) in the calculation of the HTI^j:

$$R_n = (1-\alpha)R_s - R_{nl} \qquad (12)$$

Where α is the albedo or the crop's reflection coefficient (dimensionless), with a value of 0.15 (Jaramillo & Gómez, 1989; Jaramillo, 2005); R_s and R_{nl} are the incoming solar radiation (or global radiation) and the net longwave radiation for year j (MJ m^{-2} day^{-1}), respectively.

The *HTI* values were spatially interpolated for the base scenario (j = 2000) for the entire coffee-producing region using the Kriging method with ArcGis version 10 software (ESRI, 2010).

The quantitative relation of the modal values of F_s^{2000} in function of the HTI^{2000} index was determined based on the existing database of the current distribution of soil properties for virgin soil and coffee fields in Mexico. According to the Law of Geographic Zonality for Soil it can be presumed that the relation of F_s^{2000} (HTI^{2000}) will remain the same at the end of the 21st century when regional climate index values change ($HTI^{2075\text{-}2099}$). This considered an annual average climate change that is slow enough for the F_s^{2000} (HTI^{2000}) relation to remain the same. Then, knowing the values of $HTI^{2075\text{-}2099}$ corresponding to the coffee production at the reference sites, the change in the fertility factor F_s^{2000} can be estimated for these sites using the relation represented by the graph of F_s^{2000} (HTI^{2000}).

Figure 1 shows the schematic explanation of the existing relation between fertility and the *HTI* currently and for possible changes in the future.

The procedure to determine the F_s^{2000} (HTI^{2000}) relation has been described by Nikolskii *et al*. (2001, 2006) and Contreras *et al*. (2002). The present work mainly includes the following stages:

1. Selecting and systematizing geographic sites and data related to the properties of the virgin soils and those from coffee fields in Mexico, as mentioned, using the set of charts from the INEGI (2004) and INIFAP (2012). In the present work, the processing of the edaphological information was automated using ArcGis 10.0 software. The analysis used the INEGI Continuous Mexican Elevations 3.0 (CEM 3.0) with a resolution of 15 m, and georeferenced databases of soil properties from auger holes (INEGI, 2004, 2013; INIFAP, 2012).
2. Processing of the data related to the soil properties, obtaining modal values (X) of the fertility index and determining confidence intervals ($X \pm 2\sigma$, where σ corresponds to the standard deviation of the natural logarithms of partial values for each property) for each of the intervals in the HTI^{2000}scale. Previous investigations established that the statistical distribution of each property is lognormal (Nikolskii *et al*.,2001; Contreras *et al*., 2002).
3. Determining the best fit of the F_s^{2000} (HTI^{2000}) curves to the modal values for this property using the CurveExpert 1.4 program (Hyams, 2010) and calculating confidence intervals.
4. Estimating the $HTI^{2075\text{-}2099}$ climate index value for each reference site and the corresponding fertility index value $F_s^{2075\text{-}2099}$.

The direct effect from the increase in concentrations of CO_2 in the atmosphere at the end of the 21st century on changes in organic matter contents and the fertility index was not included because it was not significant (Bazzaz & Sombroek, 1996; Knorr, Prentice, Holland, & House, 2005).

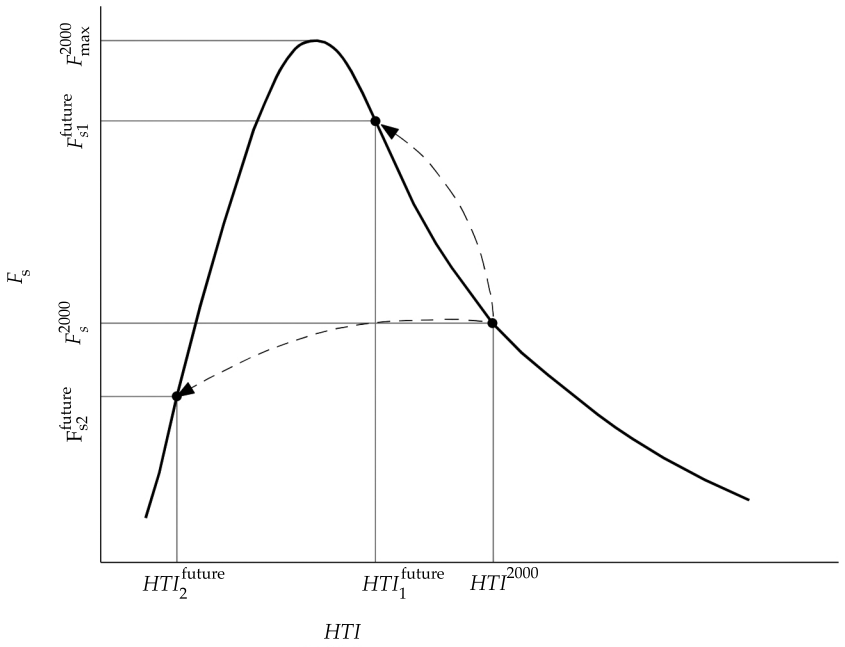

Figure 1. Prediction of change in the Integral Fertility Soil Index F_s in the reference coffee-producing region in funciton of the climate change index *HTI* during the course of the 21st century. The graph of $F_s(HTI)$ corresponds to the dependency between regional modal values of F_s on regional average annual *HTI* values at the beginning of the 21st century. HTI^{2000} and HTI^{future} correspond to a reference site at the beginning of the century. The pair $HTI_1^{2075\text{-}2099}$ and $F_{s1}^{2075\text{-}2099}$ and the pair $HTI_2^{2075\text{-}2099}$ and $F_{s2}^{2075\text{-}2099}$ correspond to possible climate change scenarios $HTI_1^{2075\text{-}2099}$ or $HTI_2^{2075\text{-}2099}$) at the same reference site for the end of the 21st century and the respective soil fertility index values ($F_{a1}^{2075\text{-}2099}$ or $F_{a2}^{2075\text{-}2099}$).

Lastly, the relative change in the coffee yield at the end of the 21st century (ΔY, in %) was estimated based on the selected scenarios with the following equation:

$$\Delta Y = \left(\frac{Y_{calc}^{2075-2099} - Y_{calc}^{2000}}{Y_{calc}^{2000}} \right) 100$$

$$= \left(\frac{Y_{max}^{2075-2099}}{Y_{max}^{2000}} \frac{SWAI^{2075-2099}}{SWAI^{2000}} \frac{F_s^{2075-2099}}{F_s^{2000}} - 1 \right) 100 \qquad (13)$$

Relative changes in the models' yield components were also estimated: ΔY_{max}, $\Delta WDSI$ and ΔF_s using the following equations:

$$\Delta Y = \left(\frac{Y_{max}^{2075-2099} - Y_{max}^{2000}}{Y_{max}^{2000}} \right) 100 \qquad (14)$$

$$\Delta Y = \left(\frac{SWAI^{2075-2099} - SWAI^{2000}}{SWAI^{2000}} \right) 100 \qquad (15)$$

$$\Delta Y = \left(\frac{F_s^{2075-2099} - F_s^{2000}}{F_s^{2000}} \right) 100 \qquad (16)$$

Results and Discussion

In order to verify reliability of the model's prediction of coffee yields, the annual average cherry coffee production during the period 2003-2011 was compared to the mean of the municipalities in the study (SIAP, 2013).

The regression equation obtained with the CurveExpert 1.3 program (Hyams, 2010) is:

$$\frac{Y_{real}^{2\,000}}{Y_{real\ max}^{2\,000}} = 0.07 + 0.99\frac{Y_{calc}^{2\,000}}{Y_{calc\ max}^{2\,000}} \qquad (17)$$

Where $Y_{real}^{2\,000}$ and $Y_{calc}^{2\,000}$ are the observed and calculated annual average yields, respectively, at the beginning of the 21st century for the references sites in the state of Veracruz: $Y_{real\ max}^{2\,000}$ of 2 471.1 kg ha^{-1} year^{-1} and $Y_{calc\ max}^{2\,000}$ of 2 059.5 kg ha^{-1} year^{-1}.

The difference between $Y_{real\ max}^{2\,000}$ and $Y_{calc\ max}^{2\,000}$ can be explained by not having included several factors in the process to calculate the yields, such as economic and technological aspects involved in managing the crops, daily fluctuation in air temperature and risk of infestation and disease, among others. Nevertheless, for our analysis it is important to compare the relative yields, that is, the fraction of maximum yields at the end of the 21st century. Since there is a good correlation between relative values $Y_{calc}^{2\,000}$ and $Y_{calc\ max}^{2\,000}$ and $Y_{real}^{2\,000}$ and $Y_{real\ max}^{2\,000}$ (Figure 2), we considered the estimations of the relative change in productivity expected in the future to be reliable.

Figure 3 shows the dependence of the modal values of the soil fertility index F_s^{2000} on the climate index HTI^{2000}, which is typical for coffee-producing soils in the state of Veracruz and for virgin soils in different climatic regions in Mexico in flat and hilly terrain with different slopes ranging from 0 to 30%. The 95% confidence intervals (±2σ) of the modal values are also shown.

The preliminary comparison shows similarity between the regional graphs of $F_s^{2000}(HTI^{2000})$ representing coffee-producing soils in the state of Veracruz and those of the virgin soils located on flat and hilly terrain with forest vegetation and slopes between 0 and 30%. The distribution of the values of the fertility index, F_s^{2000}, for coffee-producing soils

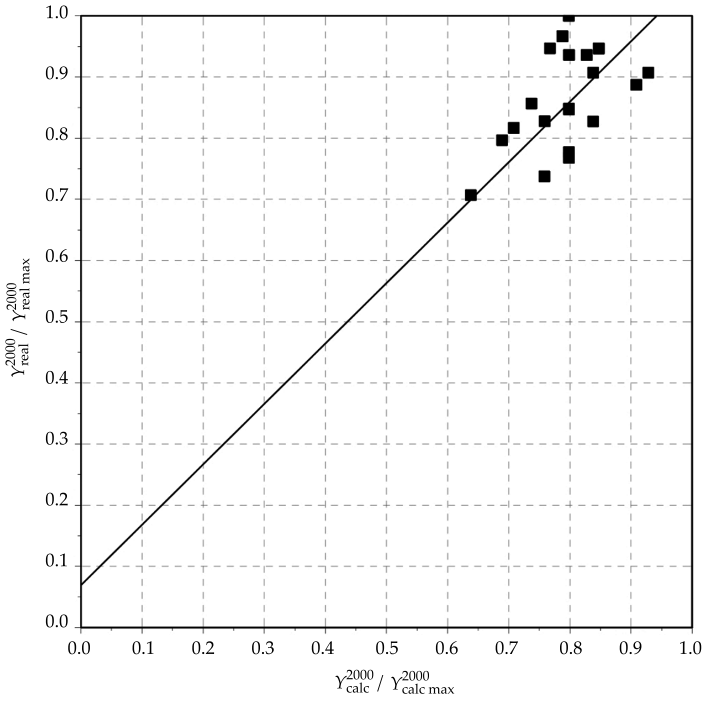

Figure 2. Comparison of observed yield fractions and estimate with the IIASA/FAO model for climate conditions from 2003 - 2011.

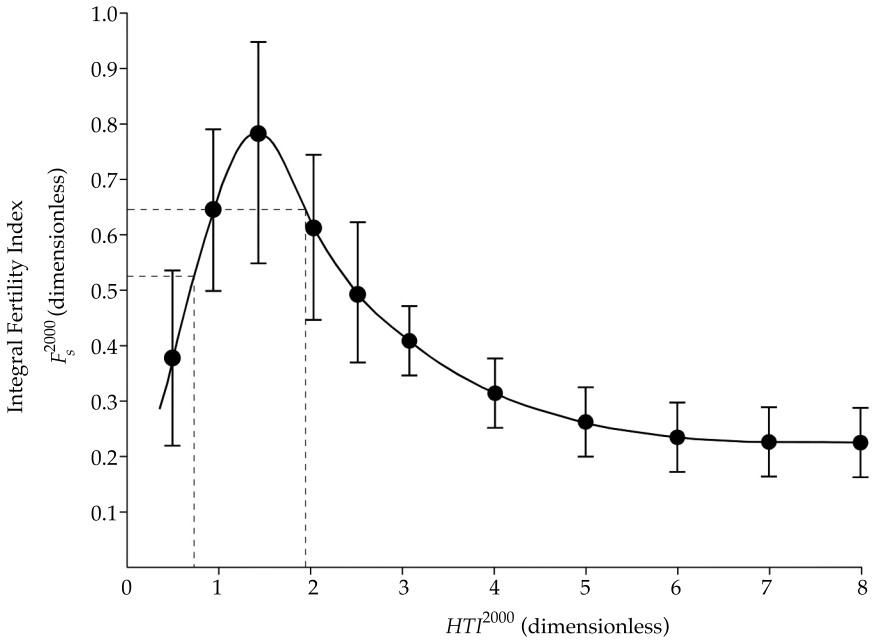

Figure 3. Dependence of the modal values of the soil fertility index in function of the typical climate index for coffee-producing soils in the state of Veracruz and virgin soils located in different climatic regions in Mexico, in flat and hilly terrains with forest vegetation and diffferent slopes within a range of 0 30%. Confidence intervals (± 2σ are also shown for the modal values at 95%. The average annual climate indices for the coffee-producing regions of Veracruz are $0.73 \leq HTI^{2000} \leq 1.95$.

in Veracruz in function of the $HTI^{2000}$are within the F_s^{2000} ranges found for virgin soils. Figure 3 presents a general distribution graph. The generalized graph of $F_s^{2000}(HTI^{2000})$ is presented to obtain more certainty in the estimation of the relative change in the fertility index, F_s, for coffee-producing soils in Veracruz in function of the climate change index *HTI* at the end of the 21st century.

The coffee-producing soils studied in the state of Veracruz correspond to average climate indices of $0.73 \leq HTI^{2000} \leq 1.95$, which according to Figure 3 represents very fertile soil.

The climate change scenarios indicate the following predictions: an average annual increase in temperature of 11 to 25% (from 2 to 4°C) at the end of the 21st century, a decrease in precipitation of 10% (100 to 250 mm year^{-1}) depending on the scenario and the reference site; and an increase in global radiation from 4 to 10% (200 to 400 Mj m^{-2} year^{-1}).

Table 2 shows the results expected from the changes indicated by the modeling of climate change. This presents the estimation of the relative change in yields (ΔY_{calc}) and in the yield components (ΔY_{max}, ΔWDSI and ΔF_s) of the coffee crop (*Coffea arabica* L) at the end of the 21st century (2075-2099).

The analysis of the information in Table 2 shows that the change in coffee yields estimated (ΔY_{calc}) for the end of the 21st century depends on the climate change scenario and the scenarios related to the increase in CO_2 concentrations in the atmosphere. The coffee yield at the end of the 21st century is expected to be less than current yields, with losses from 10% to 34%. The different models show an overall difference of 30% in the estimations of the coffee's vulnerability to climate change.

Table 2. Estimate change in coffee yields (*Coffea arabica L.*) ($\Delta Y_{calc.}$) and its components ($\Delta Y_{máx.}$, $\Delta SWAI$ and ΔF_s) in coffee-producing region in the state of Veracruz for the end of the 21st century (period 2075-2099) considering climate change scenarios developed by the GFDL CM3, HADGEM2 and MPI ESM LR models for two trajectories in the increase in CO2 in the atmosphere at the end of this century: up to 650 ppm and 1370 ppm.

Coffee-producing region	Climate model	*RCP* 4.5					*RCP* 8.5				
		$\Delta Y_{max.}$ (%)	Δ *WDSI* (%)	ΔF_s (%)	$\Delta Y_{calc.}$ (%)	φF (%)	$\Delta Y_{max.}$ (%)	Δ *WDSI* (%)	ΔF_s (%)	$\Delta Y_{calc.}$ (%)	φF (%)
Atzalán	GFDL CM3	-2.19	-4.57	5.54	-12.59	35.88	-6.15	-4.39	7.85	-17.89	35.31
	HADGEM2	-2.38	-8.86	5.14	-15.14	31.50	-6.91	-3.36	5.94	-11.94	20.76
	MPI ESM LR	-1.34	-0.80	1.70	-9.50	42.82	-4.35	-0.77	3.65	-11.75	30.07
Coatepec	GFDL CM3	-5.75	-12.20	0.28	-25.71	38.78	-9.84	-14.18	-0.45	-33.65	36.38
	HADGEM2	-5.99	-14.51	0.96	-25.94	37.17	-10.37	-11.94	1.70	-25.55	30.53
	MPI ESM LR	-4.12	-9.49	2.69	-20.54	35.63	-8.04	-10.31	0.99	-24.63	28.7
Córdoba	GFDL CM3	-0.94	-7.38	-0.68	-18.86	38.79	-5.21	-5.88	3.14	-21.98	35.07
	HADGEM2	-1.19	-10.53	-0.82	-20.17	36.01	-5.91	-11.12	1.64	-21.36	17.2
	MPI ESM LR	0.68	-5.99	-4.51	-16.19	34.81	-3.49	-5.99	0.82	-17.69	19.37
Huatusco	GFDL CM3	-9.10	-9.13	1.96	-25.03	21.97	-11.39	-12.10	2.29	-31.57	24.73
	HADGEM2	-7.57	-10.87	1.90	-23.62	24.03	-11.94	-11.74	3.53	-25.49	11.64
	MPI ESM LR	-5.74	-6.52	1.57	-17.76	11.79	-9.63	-6.95	1.96	-22.74	14.34
Misantla	GFDL CM3	-4.76	-2.14	4.64	-13.30	14.51	-9.15	-6.00	4.76	-23.73	8.17
	HADGEM2	-4.85	-14.24	4.64	-22.31	7.27	-9.85	-1.58	4.60	-14.56	22.51
	MPI ESM LR	-3.67	-0.44	3.11	-10.41	39.68	-6.42	-0.42	4.64	-12.37	34.82
Tezonapa	GFDL CM3	-9.34	-10.39	14.75	-16.90	14.04	-14.40	-10.39	18.03	-23.06	16.31
	HADGEM2	-9.59	-12.99	13.11	-18.89	18.66	-16.36	-14.29	16.39	-22.67	0.88
	MPI ESM LR	-7.81	-9.09	9.84	-14.66	8.43	-11.92	-9.09	14.75	-17.20	0.51

Note: φF is the potential error in the prediction of coffee yields when neglecting changes in the soil's fertility due to climate change.

The vulnerability of the coffee crops (*Coffea arabica* L) to climate change is expected to be greatest in the regions of Coatepec and Huatusco where a decrease in yields (ΔY) of 25 to 30% is expected. A deficiency in the water needed to grow the crop was found to have the greatest impact on changes in yield. The expected change in the water demand satisfaction index (ΔWDSI) due to a decrease in precipitation and an increase in evapotranspiration in some regions is estimated to be 10 to 15%. Meanwhile, maximum potential yields are expected to be 2 to 6% less than the current yields in the same regions due to an increase in temperature and solar radiation.

The analysis indicates that climate change will alter the fertility of the soil. The changes in the integral soil fertility index (F_s) will range from a 5% decrease to a 15% increase depending on the region, CO_2 concentrations in the atmosphere and the corresponding climate.

The potential error in the prediction of changes in coffee yields (φF) when neglecting changes in soil fertility due to climate change was estimate as follows:

$$\phi F = \left(\frac{\Delta Y_{calc}^{2075-2099}\left(\text{with } F_a\right) \Delta Y_{calc}^{2075-2099}\left(\text{without } F_a\right)}{\Delta Y_{calc}^{2075-2099}\left(\text{with } F_s\right)} \right) 100 \quad (18)$$

Where $\Delta Y_{cal}^{2075\text{-}2099}$ (with F_s) is the value of the estimated change in yields when including

fertility in the model and $\Delta Y_{cal}^{2\,075\text{-}2\,099}$ (without F_s) is the change when not including fertility in the model.

The estimations indicate an error of as much as 50% in coffee yields calculations for the end of the 21st century when not including changes in soil fertility due to climate change. Furthermore, even the sign of ΔY could change, indicating that this factor should not be ignored.

Conclusions

1. Cherry coffee (*Coffea arabica* L.) yields in the central portion of the state of Veracruz are estimated to decrease between 10 and 34% by the end of the 21st century. This range depends on the coffee-producing region, scenarios for increases in CO_2 concentration in the atmosphere and the model used to predict the climate change scenario.
2. The coffee crops most vulnerable to climate change in this state are located in the regions of Coatepec and Huatusco.
3. The analysis of the vulnerability of the components of coffee yields (potential yield (Y_{max}), water needs satisfaction index (WNSI) and integral soil fertility index (F_s) showed that each one influences the total calculated yield and they are essential to more accurately determining changes in yield based on climate change scenarios.
4. Neglecting modifications in the fertility of the soil due to climate change can cause errors of as much as 40% in coffee yield predictions for the end of the 21st century and, therefore, this factor should not be ignored.

Acknowledgements

The authors would like to thank the National Institute for Forestry, Agricultural and Livestock Research (Instituto Nacional de Investigaciones Forestales, Agrícolas), in Xalapa, Veracruz, and in particular Gabriel Díaz Padilla for help with the information regarding the soil properties sampled in the coffee-producing zones in the state of Veracruz.

References

Allen, G. R., Santos, L., Raes, D., & Smith, M. (2006). *Evapotranspiración del cultivo. Guías para la determinación de los requerimientos de agua de los cultivos* (298 pp.). Riego y Drenaje 56. Roma: FAO.

Anthony, E. H., & Ziska, L. H. (January, 2000). Crop Breeding Strategies for the 21st Century. *Journal of Experimental Botany*, *51*(342), 1-8.

Aydarov, I. P. (1985). *Manejo de los regímenes hídrico, salino y de nutrientes en suelos bajo riego* (en ruso) (204 pp.). Moscú: Ed. Agropromizdat.

Bazzaz, F. & Sombroek, W. (Eds.). (1996). *Global Climate Change and Agricultural Production Direct and Indirect Effects of Changing Hydrological, Pedological and Plant Physiological Processes* (146 pp.). Rome: FAO.

Budyko, M. (1974). *Climate and Life* (508 pp.). New York: Publ. Academic Press.

Bunn, C., Ovalle-Rivera, O., Laderach, P., Mosnier, A., Obersteiner, M., & Kirschke, D. (2013). T*he Utility of an Agroecological Niche Model of Coffee Production for Future Change Scenarios*. Impacts World 2013, International Conference on Climate Change Effects, May 27-30, Potsdam, Brandenburg, Germany.

Caballero, M., Lozano-García, S., Vázquez-Selem, L., & Ortega, B. (2010). Evidencias de cambio climático y ambiental en registros glaciales y en cuencas lacustres del centro de México durante el último máximo glacial. *Boletín de la Sociedad Geológica Mexicana*, *62*(3), 359-377.

Camargo, M. B. P. (2010). The Impact of Climatic Variability and Climate Change on Arabic Coffee Crop in Brazil. *Bragantia*, *69*(1), 239-247.

Castillo, A. M., Nikolskii, I., Ortiz, C., Vaquera, H., Cruz, G., Mejía, E., & González, A. (junio, 2007). Alteración de la fertilidad del suelo por el cambio climático y su efecto en la productividad agrícola. *Interciencia*, *32*(6), pp. 368-376.

Cavazos, T., Salinas, J. A., Martínez, B., Colorado, G., De Grau, P., Prieto-González, R., Conde-Álvarez, A. C., Quintanar-Isaías, A., Santana-Sepúlveda, J. S., Romero-Centeno, R., Maya-Magaña, M. E., Rosario de la Cruz, J. G., Ayala-Enríquez, Ma. del R., Carrillo-Tlazazanatza, H., Santiesteban, O., & Bravo, M. E. (2013). *Actualización de escenarios de cambio climático para México como parte de los productos de la quinta comunicación nacional. Informe Final del Proyecto al INECC* (150 pp.). México, DF: INECC.

Chang, J. H. (2001). *Climate and Agriculture: An Ecological Survey* (304 pp.). Chicago: Transaction Publisher.

CNA (17 de abril, 2002). Norma Oficial Mexicana NOM-011-CNA-2000. Conservación del recurso agua, que establece las especificaciones y el método para determinar la

disponibilidad media anual de las aguas nacionales. *Diario Oficial de la Federación*, México, D.F.

Contreras, B. A., Nikolskii, I., Aceves, L., Arteaga, R., Escalona, M., & Fernández, D. (mayo-junio, 2002). Pronóstico del cambio en algunas propiedades de los suelos agrícolas al modificarse las condiciones microclimáticas. *Agrociencia*, *36*(3), 267-277.

Contreras, H. A. (septiembre-diciembre, 2010). Los cafetales de Veracruz y su contribución a la sustentabilidad. *Estudios Agrarios*, *16*(45), 143-161.

Cure, J. D., & B. Acock (1986). Crop Responses to Carbon Dioxide Doubling: A Literature Survey. *Agricultural and Forest Meteorology*, *38*(1), 127-145.

Davis, A. P., Gole, T. W., Baena, S., & Moat, J. (November, 2012). The Impact of Climate Change on Indigenous Arabica Coffee (*Coffea arabica*): Predicting Future Trends and Identifying Priorities. *PLoS ONE*, *7*(11), 1-13.

De Wit, C. T. (1965). Photosynthesis of Leaf Canopies. *Agricultural Research Reports*, *663*, 1-56.

ESRI (2010). ArcGis. *An Easy Mapping and Geographic Analysis Platform (Computer Program), Version 10*. Redlands, USA: Enviromental Systems Research Institute.

FAO (2013). *CROPWAT 8.0 for Windows (Computer Program)*. Rome: Natural Resources and Environment Department.

Fernández, E. A., Zavala, H. J., & Romero, C. R. (2014). *Atlas Climático Digital de México. Ejemplos de modelos y escenarios de la 5ª Comunicación Nacional de México para la Convención Marco de Naciones Unidas para el Cambio Climático*. Recuperado de http://atlasclimatico.unam.mx/atlas/Docs/f_escenarios.html#ModelosGlobales5ta.

Fontagro (2011). *Sensibilidad y adaptación del café al cambio climático en Centroamérica (CafAdapt)*. San José, Costa Rica: Fondo Regional de Tecnología Agropecuaria.

Frère, M., & Popov, G. F. (1986). *Pronóstico agrometeorológico del rendimiento de los cultivos* (194 pp.). Roma: FAO.

Heakin, H., Gay C., Estrada, F., & C. Conde (2004). Impactos potenciales del cambio climático en la agricultura: escenarios de producción de café para el 2050 en Veracruz (México) (pp. 651-660). En L. C. Diego, C. J. C. García, A. D. F. Rasilla, H. P. F. Fernández de Arroyabe, & P. C. Garmendia (Coords.). *El clima entre el mar y la montaña*. IV congreso de la Asociación Española de Climatología, Santander, España.

Gonzalez, E. M., Jurado, E., González, E. S., Aguirre, C. O., Jiménez, P. J., & Navar, J. (julio-septiembre, 2003). Cambio climático mundial: origen y consecuencias. *Ciencia UANL*, *6*(3), 377-385.

Haggar, J., & Schepp, K. (2012). *Coffee and Climate Change. Impacts and Options for Adaption in Brazil, Guatemala, Tanzania and Vietnam* (50 pp.). NRI Working Paper Series: Climate Change, Agricultura and Natural Resources No. 4. Publ. Greenwich, UK: University of Greenwich.

Hijmans, R. J., Cameron, S. E., Parra, J. L., Jones, P. G., & Jarvis, A. (December, 2005). Very High Resolution Interpolated Climate Surfaces for Global Land Areas. *International Journal of Climatology*, *25*(15), 1965-1978.

Hyams, D. A. (2010). *Comprehensive Curve Fitting System for Windows (Computer Programme). Version 1.4*. San Francisco, USA: Microsoft Corp.

IIASA/FAO (2012). *Global Agro-Ecological Zones (GAEZ v3.0)*. Rome: IIASA Publ./FAO.

INEGI (1988). *Conjunto de las cartas de topografía, geología, uso de suelo y edafología (escala 1:250 000 y 1:50 000) de la República Mexicana*. Aguascalientes, México: Instituto Nacional de Estadística, Geografía e Informática.

INEGI (2004). *Información Nacional sobre Perfiles de Suelo. Ver. 1.2* (24 pp.). Aguascalientes, México: Instituto Nacional de Estadística, Geografía e Informática.

INEGI (2013). *Continuo de elevaciones mexicano 3.0 (CEM 3.0)*. México, DF: Instituto Nacional de Estadística, Geografía e Informática.

INIFAP (2012). *Muestreo de las propiedades del suelo en zonas cafetaleras de Veracruz*. Xalapa, México: INIFAP Campo Experimental.

Jacoby, G. C., & D'Arrigo, R. D. (August, 1997). Tree Rings, Carbon Dioxide, and Climatic Change. *Proceedings of the National Academy of Sciences of the United States of America*, *94*(16), 8350-8353.

Jaramillo, R. A., & Gómez, G. L. (julio-septiembre, 1989). Microclima en cafetales a libre exposición solar y bajo sombrío. *Cenicafé* (Colombia), *40*(3), 65-79.

Jaramillo, R. A. (septiembre, 2005). La redistribución de la radiación solar y la lluvia dentro de plantaciones de café (*Coffea arabica* L.) *Revista de la Academia Colombiana de Ciencias Exactas, Fisicas y Naturales*, *29*(112), 371-382.

Jaramillo, J., Muchugu, E., Vega, F. E., Davis, A., Borgemeister, Ch., & Chabi-Olaye, A. (September, 2011). Some Like it Hot: The Influence and Implications of Climate Change on Coffee Berry Borer (*Hypothenemus hampei*) and Coffee Production in East Africa. *PLoS ONE*, *69*(9), 1-14.

Knorr, W., Prentice, I., Holland, E., & House, J. (2005). Long-Term Sensitivity of Soil Carbon Turnover to Warming. *Nature*, *433*(7023), 298-301.

Laderach, P., Lundy, M., Jarvis, A., Ramirez, J., Perez-Portilla, E., Schepp, K., & Eitzinger, A. (2011). Predicted Impact of Climate Change on Coffee-Supply Chains (pp. 703-723). In F. W. Leal (Ed.). *The Economic, Social and Political Elements of Climate Change*. Berlin: Springer Berlin Heidelberg.

Lin, B. B., Perfecto, I., & Vandermeer, J. (octubre de 2008). Synergies between Agricultural Intensification and Climate Change could Create Surprising Vulnerabilities for Crops. *BioScience*, *58*(9), 847-854.

López, M. R., Díaz, P. G., & Martínez, R. J. (2007). *Potencial productivo y tipología de productores de café en la zona centro del estado de Veracruz* (25 pp.). México, DF: INIFAP.

Magaña, R. V. O. (2004). El cambio climático global: comprender el problema (2004). En *Cambio climático:*

una visión desde México (525 pp.). México, DF: Secretaría de Medio Ambiente y Recursos Naturales e Instituto Nacional de Ecología.

Mann, M. E., Bradley, R. S., & Hughes, M. K. (April, 1998). Global-Scale Temperature Patterns and Climate Forcing over the Past Six Centuries. *Nature*, *392*, 779-787.

Mann, M. E., Bradley, R. S., & Hughes, M. K. (March, 1999). Northern Hemisphere Temperatures during the Past Millennium: Inferences, Uncertainties, and Limitations. *Geophysical Research Letters*, *26*(6), 759-762.

Moguel, P., & Toledo, V. M. (febrero, 1999). Conservación de la biodiversidad en los tradicionales sistemas de café de México. *Biología de la Conservación*, *13*(1), 11-21.

Nikolskii, G. I., Bakhlaeva, O., Contreras, A., & Ordaz, V. (2001). Assessment of Changes in Soil Properties as Dependent on Hydrotermic Conditions of Plowlands (by the Example of Mexico). *Eurasian Soil Science*, *35*(10), 1031-1036.

Nikolskii, Y. U. N., Castillo-Álvarez, M., Bakhlaeva, O. S., Román-Calleros, X. A., & Maslov, B. S. (2006). The Influence of the Possible Global Climate Change on the Properties of Mexican Soils. *Eurasian Soil Science*, *39*(11), 1164-1169.

Paavola, J. (November, 2008). Livelihoods, Vulnerability and Adaptation to Climate Change in Morogoro, Tanzania. *Environmental Science & Policy*, *11*(7), 642-654.

Pegov, S. A., & Jomyakov, P. (1991). *Modelación del desarrollo de los sistemas ecológicos* (en ruso) (223 pp.). San Petersburgo, Rusia: Ed. Gidrometeoizdat.

Rivera-Silva, M. R., Nikolskii-Gavrilov, I., Castillo-Álvarez, M., Ordaz-Chaparro, V. M., Díaz-Padilla, G., & Guajardo-Panes, R. A. (octubre-diciembre, 2013). Vulnerabilidad de la producción del café (*Coffea arabica* L.) al cambio climático global. *Terra Latinoamericana*, *31*(4), 305-313.

Rodney, M. J. J. N., & Freddy, H. J. R. (2002). Análisis de tendencia de series de tiempo oceanográficas y meteorológicas para determinar evidencias de cambio climático en la costa del Ecuador. *Acta oceanográfica del Pacífico*, *11*(1), 17-21.

SMN (2013). *Normales climatológicas* [en línea]. México, DF: Servicio Meteorológico Nacional de la Comisión Nacional del Agua. Citado el 18 de marzo de 2013. Recuperado de http://smn.cna.gob.mx/index.php?option=com_content&view=article&id=164:veracruz&catid=14&Itemid=2.

SARH (1991). *Manual de conservación del suelo y agua. Instructivo* (33 pp.). (3a ed.). Chapingo, México: SARH.

SIAP (2013). *Proyecciones para el sector agropecuario en México* [en línea]. México, DF: SAGARPA, Servicio de Información Agroalimentaria y Pesquera. Citado el 6 de marzo de 2013. Recuperado de http://www.siap.gob.mx/cierre-de-la-produccion-agricola-por-cultivo/.

Siles, P., Harmand, J. M., & Vaast, P. (March, 2010). Effects of *Inga densiflora* on the Microclimate of Coffee (*Coffea arabica* L.) and Overall Biomass under Optimal Growing Conditions in Costa Rica. *Agroforestry Systems*, *78*(3), 269-286.

Terrazas, M. L., Nikolskii, G. I., Herrera, G. S., Castillo, A. M., & García, E. A. (enero-marzo, 2010). Alteración de la fertilidad del suelo y vulnerabilidad de maíz y trigo bajo riego debido al cambio climático. *Tecnología y Ciencias del Agua*, *1*(1), 87-102.

Van Der Vosen, H. A. M. (October, 2005). A Critical Analysis of the Agronomic and Economic Sustainability of Organic Coffee Production. *Experimental Agriculture*, *41*(4), 449-473.

Villers, L., Arizpe, N., Orellana, R., Conde, C., & Hernández, J. (mayo, 2009). Impactos del cambio climático en la floración y desarrollo del fruto del café en Veracruz, México. *Interciencia*, *34*(5), 322-329.

Volobuev, V. R. (1974). *Introducción a la energía de formación de suelos* (127 pp.) (en ruso). Moscú: Nauka Publ.

Institutional Address of the Authors

M. en C. Juan Gabriel Brigido

Colegio de Postgraduados
Programa de Hidrociencias
kilómetro 36.5 de la carretera México-Texcoco
56230 Montecillo, Estado de México, México
Teléfono: +52 (595) 9520 200, extensión 1175
Fax: +52 (595) 9520 237
brigido.juan@colpos.mx

Dr. Iourii Nikolskii

Profesor-investigador titular
Colegio de Postgraduados
Programa de Hidrociencias
kilómetro 36.5 de la carretera México-Texcoco
56230 Montecillo, Estado de México, México
Teléfono: +52 (595) 9520 200, extensión 1175
Fax: +52 (595) 9520 237
nikolski@colpos.mx

M.C. Liliana Terrazas

Colegio de Postgraduados
Programa de Hidrociencias
kilómetro 36.5 de la carretera México-Texcoco
56230 Montecillo, Estado de México, México
Teléfono: +52 (595) 9520 200, extensión 1175
Fax: +52 (595) 9520 237
termely@colpos.mx

M.C. Sergio Santiago Herrera

Colegio de Postgraduados
Programa de Hidrociencias
kilómetro 36.5 de la carretera México-Texcoco
56230 Montecillo, Estado de México, México
Teléfono: +52 (595) 9520 200, extensión 1175
Fax: +52 (595) 9520 237
hserch@colpos.mx

Validation of the *ClimGen* Model to Estimate Climate Variables when Lacking Data for Modeling Processes

• Gerardo Esquivel* •
Instituto Nacional de Investigaciones Forestales, Agrícolas y Pecuarias, México
*Corresponding Author

• Julián Cerano •
Universidad Nacional Autónoma de México

• Ignacio Sánchez •
Instituto Nacional de Investigaciones Forestales, Agrícolas y Pecuarias, México

• Armando López •
Universidad Autónoma Chapingo, México

• Oscar G. Gutiérrez •
Universidad Estatal de Sonora, México

Abstract

Esquivel, G., Cerano, J., Sánchez, I., López, A., & Gutiérrez, O. G. (July-August, 2015). Validation of the ClimGen Model to Estimate Climate Variables when Lacking Data for Modeling Processes. *Water Technology and Sciences* (in Spanish), *6*(4), 117-130.

Many hydrological and environmental models often require meteorological information corresponding to different time intervals as input data. This information is often not available at the sites of interest. At most weather stations, data registry periods are frequently insufficient for a good modeling of processes. A series of restrictions exist in their application when meteorological data is not directly available. The present study evaluated the use of the ClimGen weather generator to estimate missing temperature and rainfall data for three sites with low, medium and high rainfall. The parameterization and calculation of the missing data performed for the Riito weather station, which represents dry conditions, resulted in r^2 values for maximum temperature of $r^2 = 0.96$, minimum temperature $r^2 = 0.95$ and rainfall $r^2 = 0.98$. The Tepehuanes and El Tarahumar stations represent medium rainfall conditions, and resulted in r^2 values for maximum temperature of $r^2 = 0.98$, minimum temperature $r^2 = 0.90$ and $r^2 = 0.99$, and rainfall $r^2 = 0.96$ and $r^2 = 0.93$, respectively. Lastly, The Francisco Rueda stations represented high rainfall conditions and resulted in r^2 values for maximum temperature of $r^2 = 0.96$, minimum temperature $r^2 = 0.98$ and rainfall $r^2 = 0.97$. The results indicate that the data estimated by the weather generator are representative of historical climate data at the study sites.

Keywords: Process modeling, weather generators, precipitation, temperature, ClimGen.

Resumen

Esquivel, G., Cerano, J., Sánchez, I., López, A., & Gutiérrez, O. G. (julio-agosto, 2015). Validación del modelo ClimGen en la estimación de variables de clima ante escenarios de datos faltantes con fines de modelación de procesos. Tecnología y Ciencias del Agua, *6(4), 117-130.*

Diversos modelos hidrológicos y ambientales con frecuencia requieren información meteorológica, como datos de entrada a intervalos de tiempo variable, que a menudo no están disponibles en los sitios de interés. En la mayoría de las estaciones meteorológicas, el periodo de registro de datos es a menudo insuficiente para permitir una buena modelación de procesos, por lo tanto existe una seria restricción en su aplicación si no se dispone de manera directa de los datos meteorológicos. En este estudio, el generador climático ClimGen fue evaluado para la estimación de datos faltantes de temperatura y precipitación para tres sitios con baja, media y alta ocurrencia de precipitación. Se realizó la parametrización y cálculo de datos faltantes para la estación meteorológica Riito, que representa la condición seca, obteniendo valores bajo el criterio de r^2 *para la variable temperatura máxima de* $r^2 = 0.96$*, temperatura mínima* $r^2 = 0.95$ *y precipitación* $r^2 = 0.98$*. Las estaciones Tepehuanes y El Tarahumar, que representan la condición media de humedad, obtuvieron valores para la variable temperatura máxima de* $r^2 = 0.98$*; temperatura mínima* $r^2 = 0.90$ *y* $r^2 = 0.99$*; y precipitación* $r^2 = 0.96$ *y* $r^2 = 0.93$*, respectivamente. Por último, la estación Francisco Rueda, que representa la condición húmeda, obtuvo* $r^2 = 0.96$ *para temperatura máxima;* $r^2 = 0.98$ *para temperatura mínima, y* $r^2 = 0.97$ *para precipitación. Los resultados indican que los datos estimados por el generador climático son representativos de los datos históricos del clima en los sitios de estudio.*

Palabras clave*: modelación de procesos, generadores climáticos, precipitación, temperatura, ClimGen.*

Received: 12/05/2014
Accepted: 24/04/2015

Introduction

Climate variables such as precipitation and temperature have a large influence on the hydrological cycle. Changes in these variables can affect evaporation and runoff patterns and the amount of groundwater and water stored in glaciers, wetlands lakes and lakes (Sarangi & Kumar, 2006). They are determinants in agriculture, especially in cultivation systems commonly found in arid and tropical regions (Tingem, Rivington, Azam- Ali, & Colls, 2008). Therefore, their variability contributes to hydrological processes that can generate extreme events such as floods and/or droughts.

In terms of simulation processes, hydrological and environmental models have become important tools for the planning, management and administration of natural resources. Nevertheless, these models require several types of input data (maximum and minimum temperatures, precipitation, solar radiation, wind speed and runoff, among others) corresponding to different time intervals. This information is often not available from the sites of interest (Safeq & Fares, 2011). Most weather stations often have an insufficient period of records for good modeling processes. Therefore, a series of limitations exist in the application of models when meteorological data is not directly available (Hoogenboom, 2000). This situation highlights the importance of expanding data registries by generating climate data from short-term observations using various statistical procedures.

Mathematical models known as stochastic generators have addressed this problem (Richardson & Wright, 1984). These models simulate time-series corresponding to climate variables. They provide data to expand a registry at a site as well as climate information when measured data are not available, by interpolating the model parameters. These models have several interconnected components and generally simulate multiple variables using observed historical meteorological information as input data. They generate estimated meteorological data that is statistically similar to observed weather records (Hoogenboom & Soltani, 2003).

WGEN was one of the first weather generators developed to model soil erosion and water quality (Richardson & Wright, 1984), and others have been developed since then. The CLIGEN weather generator, part of the Water Erosion Prediction Procedure model (Flanagan & Livingston, 1995), is based on WGEN's weather generation methods (Nicks, Richardson, & Williams, 1990). Additional weather generators include *USCLIMATE* (Johnson, Hanson, Hardegree, & Ballard, 1996), *CLIMAK* (Danuso & Della, 1997) and *ClimGen* (Stöckle, Campbell, & Nelson, 1999).

Databases of climate records in Mexico generally do not contain large enough series to analyze climate variability on a time scale of more than 60 years. In addition, the records have a high percentage of missing data (IMTA, 2009), creating a large problem with reliability when used in climatological, hydrological, environmental and paleoclimatological studies. Thus, the objectives of the present study were to: 1) evaluate the capacity of the ClimGen weather generator (version 4.06.06) (Stöckle, Nelson, Donatelli, & Castellvì, 2001) to estimate data that is missing from weather stations and 2) improve and expand the weather records from the stations.

Materials and Methods

Study Area

The present work was based on three sites in Mexico subject to different environmental conditions (low, medium and high rainfall) (Figure 1). The Riito station, in the municipality of San Luis Rio Colorado, state of Sonora, is located between 32° 08′ 00″ latitude north and 114° 54′ 05″ longitude west. Average annual precipitation is 52.5 mm and annual

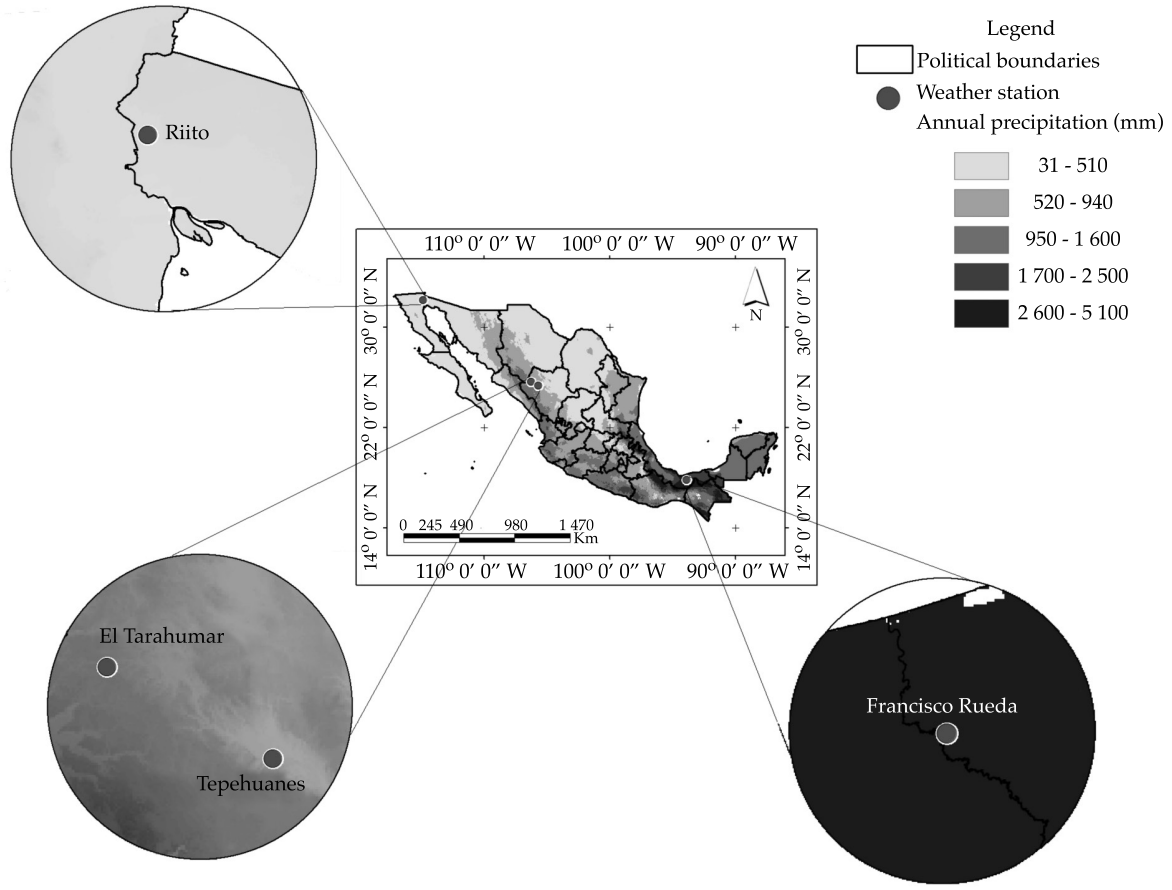

Figure 1. Geographic location of the weather stations studied.

mean temperature is 22.1°C. The altitude is 13 meters above sea level (masl). The Tepehuanes and El Tarahumar weather stations are located in the Sierra Madre Occidental, in the state of Durango, between 25° 20′ 00″ and 25° 37′ 01″ latitude north and 105° 43′ 00″ and 106° 19′ 28″ longitude west, respectively. The altitudes range from 1 680 to 3 120 masl, with an annual precipitation of 676 mm and an annual mean temperature of 13.5°C. Lastly, the Francisco Rueda station, in the municipality of Huimanguillo, Tabasco, is located at 17° 50′ 12″ latitude north and 93° 56′ 30″ longitude west, with an average annual precipitation of 2 414 mm, annual mean temperature of 26.3 °C and an altitude of 7 masl (IMTA, 2009; Conagua, 2012).

Climatological Information

The historical weather records were obtained from the Rapid Weather Information Extractor III, version 2.0 (*Extractor Rápido de Información Climatológica; ERIC, Spanish acronym*) (IMTA, 2009). Each of the data series was analyzed for consistency in the information in order to detect atypical data due to errors in data entry or from other sources (for example, maximum temperature with values of 0, maximum temperature under the minimum, months with duplicate records, etc.). This was aimed at improving the quality of the input data and, thus, decreasing errors in the validation process. Descriptive statistics were also obtained for each of the stations studied (Table

1). The methodology by Castro and Carbajal (2010) was used to discard inconsistencies in each variable: maximum temperature (*t*max), minimum temperature (*t*min) and precipitation (PP).

Description of *ClimGen*

ClimGen is a stochastic weather generator used to estimate data series at the daily level, including precipitation, maximum temperature, minimum temperature, solar radiation, relative humidity and wind speed. The statistical results from ClimGen are similar to historical weather data (Tingem, Rivington, Azam-Ali, & Colls, 2007) and each station can be parameterized (Safeeq & Fares, 2011). ClimGen uses the Weibull distribution (Weibull, 1951) to represent daily precipitation, and the approximation curve is an improvement over the Fourier series used by other weather generators (for example, CLIGEN) to simulate seasonal variations in weather data.

Precipitation

The number of precipitation events was generated with a second-order Markov chain model (Nicks *et al*., 1990). The combination of conditional probabilities for the two states in the Markov chain (α=rainy day followed by a dry day, β=dry day followed by rainy day) was calculated on a monthly scale and individually for each station based on observed historical data (Nicks *et al*., 1990):

$$P(W/D) = \alpha$$

$$P(D/D) = 1 - \alpha$$

$$P(D/W) = \beta$$

$$P(W/W) = 1 - \beta$$

Where:

$P(W/D)$ = the probability of a day with rain when it does not rain the previous day.

Table 1. Descriptive statistics for the weather stations in the study.

	Station	Riito	Tepehuanes	El Tarahumar	Francisco Rueda
	Years of data	1949-2008 (59 years)	1922-1988 (66 years)	1964-2009 (45 years)	1965-2007 (42 years)
Temperature maximum (*t*max)	Mean	31.2	26.4	19.1	31.6
	Standard deviation	8.5	5.5	4.6	4.2
	Variance	72.9	30.4	21.1	17.8
	Maximum	50	40	32.5	45
	Minimum	8	7.5	4	15
Temperature minimum (*t*min)	Mean	12.9	7	1	20.7
	Standard deviation	7.8	6.2	6.7	2.8
	Variance	61.4	38.9	44.3	8.1
	Maximum	33	20	17	27
	Minimum	-6.5	-11.2	-19	9
Precipitation (PP)	Mean	0.14	1.3	2.5	6.5
	Standard deviation	1.7	4.3	6.9	15.5
	Variance	2.9	18.9	47.7	240.1
	Maximum	80	78.5	120	187.5
	Minimum	0	0	0	0

P (D/D) = the probability of a day without rain when it does not rain the previous day.
P (D/W) = the probability of a day without rain when it does rain the previous day.
P (W/W) = the probability of day with rain when it does rain the previous day.

ClimGen uses a two-parameter Weibull distribution to calculate the magnitude of the precipitation on rainy days. In terms of daily precipitation, the Weibull distribution has been shown to be superior to other probability distribution functions (Selker & Haith, 1990).

Temperature

According to Richardson (1981), temperature and solar radiation data are easier to statistically model than precipitation since a smaller proportion of their values are equal to 0 and the distribution of these values is much less biased than with precipitation data. ClimGen's technique to generate maximum and minimum temperatures is similar to that of WGEN and is based on the supposition that temperature is a weak stationary process (Matalas, 1967).

This approach considers maximum and minimum temperatures to be a continuous stochastic multivariate process with daily means and standard deviations that depend on the precipitation (rainy or dry) during the day (Richardson, 1981). The time-series of the residuals of the maximum and minimum temperatures are obtained by eliminating the periodic means and adjusting the standard deviations. The residuals are analyzed for dependency on time and with cross-correlation (Castellvi & Söckle, 2001; Stöckle & Nelson, 2003; Stöckle *et al.*, 2001).

Calibration and Validation of ClimGen

Generally for the weather stations in Mexico contained in the ERIC III, maximum and minimum temperatures, precipitation and evaporation data cover considerable time periods, unlike other variables such as wind speed, solar radiation and relative humidity, among others. Therefore, ClimGen was validated and calibrated specifically using temperature and precipitation data (Table 1). This computing tool is free and can be obtained by registering at the website http://sites.bsyse.wsu.edu/cs_suite/ClimGen/documentation/demos.html.

The *ClimGen* interface used to generate weather data involves two main procedures: 1) the site to be analyzed and 2) the generation of the data. For the first procedure, an output directory is selected to which the results will be directed. Once this is done, the site to be analyzed is parameterized by inputting the following information: a) geographic location of the site, that is, its coordinates (latitude-longitude, decimal degrees or UTM) and altitude; b) the location of the region with respect to altitude above sea level (ClimGen contains a global database from which the country can be chosen) and c) brief description of the weather station.

In this section, historical data must be entered manually for each year until the historical record is complete. This is the part of the computing process that takes the most time, since the information to be inputted is reiterated. The advantage of this process is that after inputting the records (complete or incomplete) for one year, the data can be viewed in table format or graphically (timeline) and a second exploratory graphic analysis of the information can be performed. Once all the historical records are inputted, ClimGen performs a statistical analysis (mean, standard deviation, maximum value, minimum value, sum) to determine whether or not the data can be generated. A minimum of 10 years is needed for the estimation of temperature and 25 years for precipitation.

After the above is completed, the second procedure is the generation of data. The file

generated by the previous procedure and the period to be generated are selected. *ClimGen* offers two simulation options: a) generate the missing data while keeping historical data and estimating only the missing values and b) completely replace all the *ClimGen* records. The output data can be generated in different formats depending on the users' interest (*CropSyst*/*SWAT*, *LARSWG*, among others). The LARS-WG format was used by the present work since it generates data tables, which helps to manipulate the information.

The model was validated by parameterizing the Tepehuanes weather station (Figure 1). Years with the historically highest and lowest precipitations were identified (1923 with 756 mm and 1929 with 242.6 mm) and records were randomly deleted in order to evaluate the predictive capacity of the missing data in the series. Both of the options offered by *ClimGen* were used: a) generating the missing data while keeping historical data and estimating only the missing values and b) completely replacing all the *ClimGen* records. The corresponding simulations were run and only the observed data versus calculated data were graphed. In addition, the statistical parameters of the observed versus calculated data were obtained as well as those generated by the SPSS v. 17.0 statistical program, in order to validate the efficiency of the weather data estimation for a one-year period (1923, the year considered to have the highest precipitation and 1929 which had the lowest precipitation according to the historical records).

A longer period of time was consecutively parameterized —66 years of observed data for the Tepehuanes station (10084) and 45 years for El Tarahumar station (10026). Stockle *et al*. (1999) suggest a minimum of 20 years of historical weather data to complete the parameterization of meteorological variables to be produced by a weather generator, and preferably 30 to 45 years. Therefore, the available records fulfilled the requirements needed to estimate the missing temperature and precipitation data for the two stations.

The previously validated stations reflected the mean precipitation (676 mm). To evaluate the efficiency of the model under different environmental conditions, the Riito station in Sonora (average annual precipitation of 52.5 mm) and the Francisco Rueda station in Tabasco (2 414 mm annual average precipitation) were analyzed (IMTA, 2009). For the stations analyzed, the period with the largest amount of missing information was 3 months, with one month of missing data inter-annually. Lastly, scatter plots were generated and the statistical parameters of the observed historical values and those calculated by ClimGen were obtained.

Results

Estimation of Missing Data from One Year

A notable similarity was found between the trends in the observed and calculated data for two years with different climate conditions—the year with the largest precipitation records (Figure 2a) and the one with the smallest records (Figure 2b), both corresponding to the Tepehuanes weather station in the state of Durango.

The statistical parameters of the observed data versus the calculated data and data generated by ClimGen for the year 1923 showed that the variances of the observed data and the calculated data remained the same, but not for the data generated by ClimGen (Table 2). Meanwhile, the variance of the generated data decreased (Table 3).

Estimation of Missing Data for More than One Year

The r^2 criterion was calculated for longer periods of missing data (66 years for Tepehuanes and 45 years for El Tarahumar station). The findings for the Tepehuanes station were: r^2

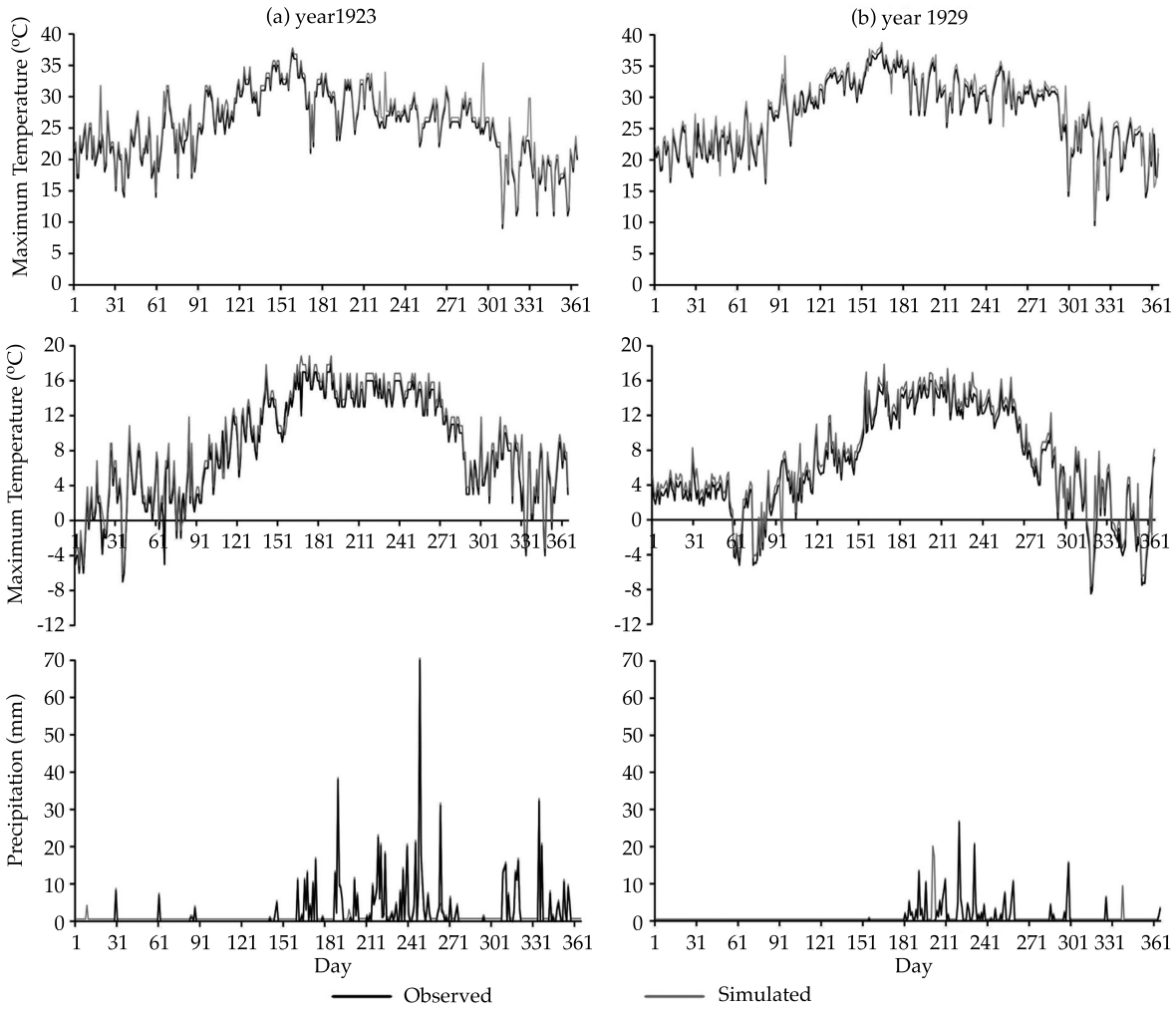

Figure 2. Annual temperature and precipitation series, observed and simulated by GlimGen for the T epehuanes station.

= 0.98 for maximum temperature, r^2 = 0.90 for minimum temperature and r^2 = 0.96 for precipitation (Figure 3). For the El Tarahumar station: r^2 = 0.98 for maximum temperature, r^2 = 0.99 for minimum temperature and r^2 = 0.93 for precipitation (Figure 3). When keeping the historical records and only calculating missing values, the variance of the observed data remained the same as the that of the data calculated by the weather generator (Table 4).

Based on the scatter plots of the Riito station (state of Sonora) and the Francisco Rueda station (state of Tabasco), which are the two stations with environmental conditions different than those of Tepehuanes and El Tarahumar: at the Riito station r^2 = 0.96 for maximum temperature, r^2 = 0.95 for minimum temperature and r^2 = 0.99 for precipitation, and at the Francisco Rueda station r^2 = 0.96 for maximum temperature, r^2 = 0.98 for minimum temperature and r^2 = 0.97 for precipitation (Figure 4). For all four of these stations, when keeping the historical records in the database and only generating missing

Table 2. Statstical parameters of the observed data versus both the calculated and generated data for year 1923.

	N	Mean	Variance	Standard Deviation	Maximum	Minimum	*R*	R^2
Tmax_o	365	25.26	29.65	5.44	37	9		
Tmax_c	365	25.45	30.36	5.51	37	9	0.97	0.95
Tmax_g	365	26.71	33.91	5.82	44	12	0.52	0.27
Tmin_o	365	8.38	33.87	5.82	18	-7		
Tmin_c	365	8.36	34.31	5.85	18	-7	0.98	0.97
Tmin_g	365	7.27	42.40	6.51	20	-7	0.78	0.61
PP_o	365	2.1	37.55	6.12	70	0		
PP_c	365	2.12	37.53	6.12	70	0	0.99	0.98
PP_g	365	0.99	12.23	3.49	42	0	0.07	0.005

[1]"o" refers to observed data..
[2]"s" refers to data calculated by ClimGen.
[3]"g" refers to data generated by ClimGen.

Table 3. Statstical parameters of the observed data versus both the calculated and generated data for year 1929.

	N	Mean	Variance	Standard Deviation	Maximum	Minimum	*R*	R^2
Tmax_o	365	25.26	29.65	5.44	37	9		
Tmax_c	365	25.45	30.36	5.51	37	9	0.97	0.95
Tmax_g	365	26.71	33.91	5.82	44	12	0.54	0.30
Tmin_o	365	8.38	33.87	5.82	18	-7		
Tmin_c	365	8.36	34.31	5.86	18	-7	0.98	0.97
Tmin_g	365	7.27	42.40	6.51	20	-7	0.71	0.50
PP_o	365	2.10	37.55	6.13	70	0		
PP_c	365	2.12	37.53	6.13	70	0	0.86	0.75
PP_g	365	0.99	12.23	3.50	42	0	0.16	0.026

[1]"o" refers to observed data..
[2]"s" refers to data calculated by ClimGen.
[3]"g" refers to data generated by ClimGen.

data, the variance of the observed data and that of the data calculated by the weather generator remained roughly the same (Tables 4 and 5).

Discussion

The use of ClimGen was successful due to its multiple applications to generate time series, as a step prior to the application of other models (for example, *CROPWAT*) (Sarangi & Kumar, 2006; Bal, Choudhury Sood, Jalota, & Singh, 2008; Tingem *et al*., 2007; McKague, Rudra & Ogilvie, 2003) used to estimate climate variables (Sarangi, Madramootoo, & Koundal, 2008; Carbajal *et al*., 2010; Safeq & Fares, 2011). Nevertheless, few works have focused on evaluating the efficiency of the model when estimating missing data in a data series (Moradi, Nosrati, & Eslamian, 2007; Carbajal *et al*., 2010).

In Iran, Moradi *et al*. (2007) evaluated the estimation of maximum and minimum temperatures at five weather stations. The

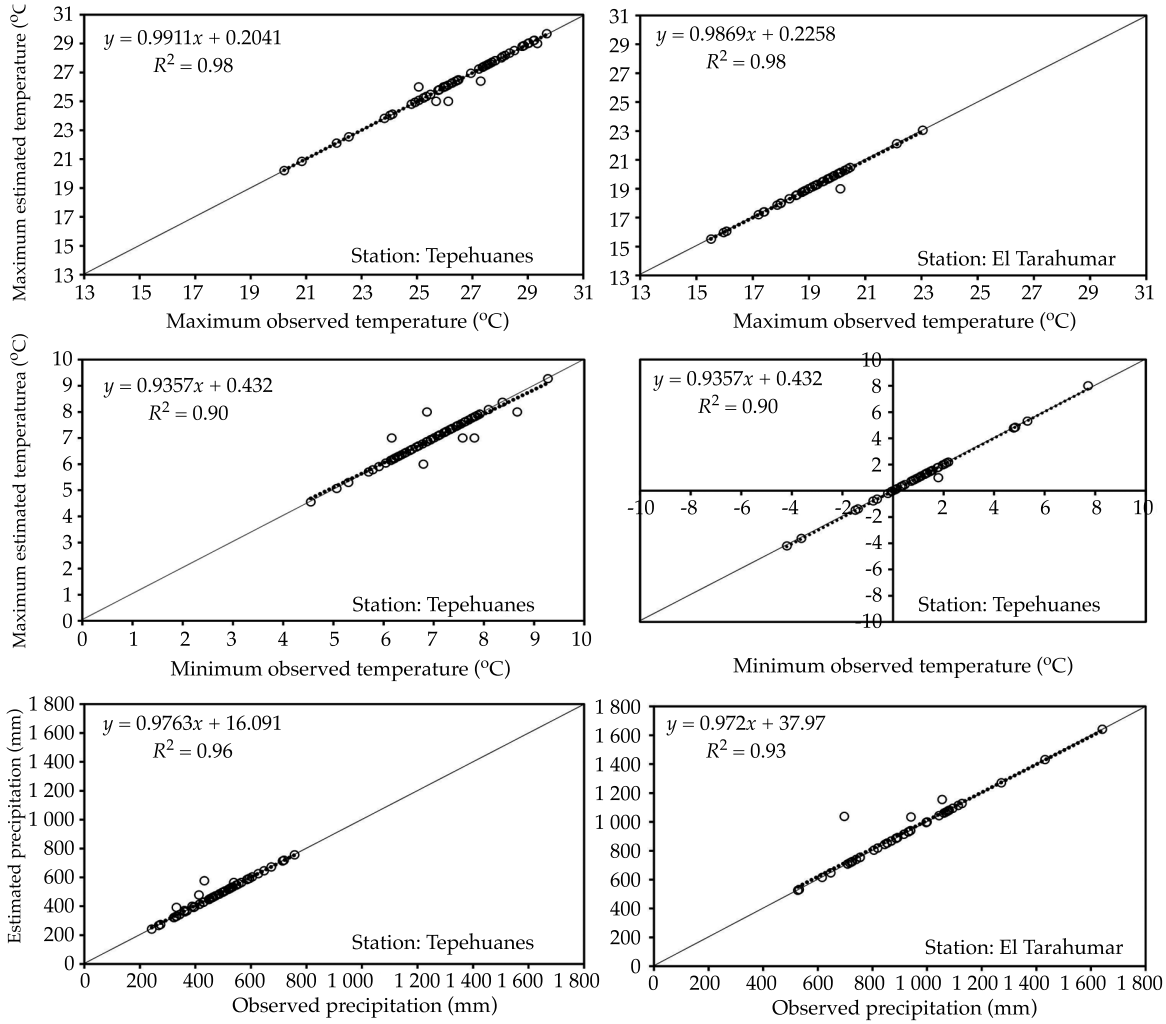

Figure 3. Observed climate variables (maximum temperature, minimum temperature and precipitation) and those setimated by ClimGen based on the r^2 criterion.

Table 4. Descriptive statistics of the observed data versus data calculated by ClimGen for the El Tarahumar and Tepehuanes weather stations.

	Tepehuanes					
	Maximum Temperature		Minimum temperature		Precipitation	
	Observed	Calculated	Observed	Calculated	Observed	Calculated
Mean	26.5	26.4	6.9	6.9	472	477
Standard Deviation	1.95	1.94	0.83	0.82	110.86	110.23
Variance	3.79	3.78	0.69	0.67	12 289.74	12 151.19
	El Tarahumar					
Mean	19.1	19.1	1.0	1.0	914	926
Standard Deviation	1.43	1.43	2.02	2.04	218.09	218.83
Variance	2.06	4.08	47 565.33	2.03	4.16	47 888.62

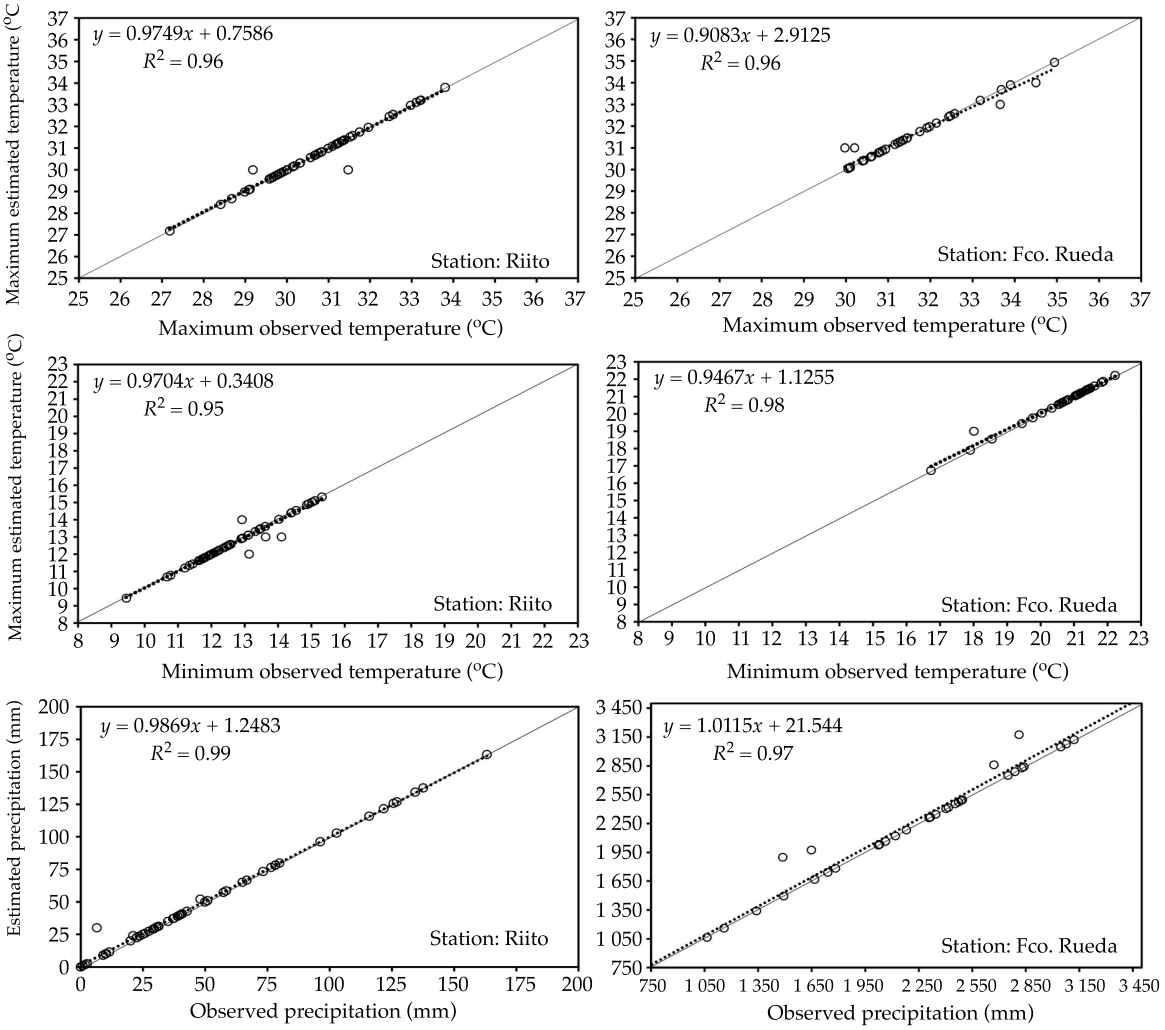

Figure 4. Observed climate variables (maximum temperature, minimum temperature and precipitation) and those setimated by ClimGen based on the r^2 criterion.

Table 4. Descriptive statistics of the observed data versus data calculated by ClimGen for the El Tarahumar and Tepehuanes weather stations.

	Riito					
	Maximum Temperature		**Minimum temperature**		**Precipitation**	
	Observed	**Calculated**	**Observed**	**Calculated**	**Observed**	**Calculated**
Mean	31.2	31.2	13.0	12.9	49	50
Standard Deviation	1.73	1.67	1.40	1.40	39.63	39.28
Variance	3.00	2.78	1.97	1.95	1 570.50	1 543.12
	Francisco Rueda					
Mean	31.6	31.6	20.6	20.6	2 189.2	2 235.8
Standard Deviation	1.32	1.22	1.17	1.12	755.24	773.44
Variance	1.74	1.49	1.38	1.26	570 388.82	598 213.57

correlation coefficients indicated a good fit between the observed and estimated data ($r = 0.82$, $r = 0.72$, $r = 0.79$ and $r = 0.78$, except for minimum temperature at one station, $r = 0.10$). Nevertheless, they recommended its use to estimate missing data in regions with medium to low precipitation.

Safeq and Fares (2011) evaluated the model with four stations under tropical conditions, finding that its estimation efficiency varied according to the site and the weather variable (for example, precipitation, wind speed, temperature). Of the four sites, *ClimGen* was able to reproduce observed precipitation for only one station and it underestimated this variable for two stations. On the other hand, its estimations of maximum temperature, minimum temperature and wind speed were reasonable.

In the case of the Tepehuanes weather station, the analyses of a one-year period showed that ClimGen is able to produce statistically significant estimations of maximum temperature, minimum temperature and precipitation for the year with the highest precipitation (in 1923, where $r^2 = 0.95$, $r^2 = 0.97$ and $r^2 = 0.98$, respectively) as well as the year with the lowest precipitation (in 1929 according to historical records, where $r^2 = 0.97$, $r^2 = 0.95$ and $r^2 = 0.75$, respectively). These estimations were obtained by keeping the historical data in the time series. When not keeping the observed data, the variability differed significantly for all the variables corresponding to the year 1923 ($r^2 = 0.27$ for maximum temperature, $r^2 = 0.61$ for minimum temperature and $r^2 = 0.005$ for precipitation) and the year 1929 ($r^2 = 0.30$ for maximum temperature, $r^2 = 0.50$ for minimum temperature and $r^2 = 0.026$ for precipitation).

Even though the two years analyzed had the highest and lowest historical precipitation, the model satisfactorily estimated these two environmental conditions and the variances of the observed data and calculated data remained the same. Nevertheless, the estimation efficiency decreased when not including existing data and generating the complete 365 days. This corroborates the results found by Moradi *et al.* (2007) and Safeq and Fares (2011), who reported obtaining good estimations with some climate parameters and substantial errors for particular study sites.

When considering periods of over one year, the scatter plots and the corresponding r^2 values indicated good predictive efficiency for maximum temperature ($r^2 = 0.98$ for both stations), minimum temperature ($r^2 = 0.90$ for Tepehuanes and $r^2 = 0.99$ for El Tarahumar) and precipitation ($r^2 = 0.96$ for Tepehuanes and $r^2 = 0.93$ for El Tarahumar). These values show that the weather generator estimated good quality values for regions with medium precipitation, which represents the climate in the study area.

For the Riito weather station (state of Sonora) in northern Mexico, with annual average precipitation of 52.5 mm, representative of arid conditions in the country: $r^2 = 0.96$ for maximum temperature, $r^2 = 0.95$ for minimum temperature and $r^2 = 0.99$ for precipitation. For the Francisco Rueda station in the state of Tabasco, with average annual precipitation of 2 414 (representing rainy conditions), good efficiency was obtained in the estimation of maximum temperature ($r^2 = 0.96$). For both stations, $r^2 = 0.98$ for minimum temperature and $r^2 = 0.97$ for precipitation. These results show the viability of the climate generator in the estimation of missing data, regardless of the environmental conditions at the stations studied. Nevertheless, it is important to remember that the estimations were primarily attributable to two factors: a) amount of historical information in the databases and b) amount of missing data. The maximum periods for which data was missing was 3 consecutive months, with one month of missing data inter-annually, found at the beginning, middle and end of the year. The generator was not evaluated for one or more years with information missing since this did

not correspond to the objectives of the study. Nevertheless, it is important to remember that according to the results, the variance decreased when generating a complete year.

The results are quite acceptable when compared to other works that evaluated the efficiency of the weather generator. For example, an evaluation the ClimGen's capacity to estimate missing data in the Peruvian high plains obtained values of $r^2 = 0.70$ and $r^2 = 0.71$ for two stations and $r^2 = 0.40$ for a third station (Carbajal *et al*., 2010). Safeq and Fares (2011) demonstrated that the performance of the generator varied even among stations in the same geographic region and with certain climate variables, and obtained reliable estimations with other climate variables (for example, maximum temperature, minimum temperature and wind speed).

A strength of having an extensive and complete series of historical weather records is the ability to parameterize models that do not permit missing data in data series (Esquivel *et al*., 2013a; Esquivel, Bueno, Sánchez, Velásquez, & Delgado, 2013b). It also helps to calibrate studies in which weather stations perform a key role (Cerano, Villaueva, Cervantes, Trucios, & Guerrero, 2013). The comparison between observed and calculated data is crucial to the validation of the model since this provides valuable information about the behavior of the data and determines whether or not it can function adequately. Overall, ClimGen demonstrated that it functioned well for the stations studied. A larger amount of observed data and a smaller amount of missing data in the database was found to strengthen the parameterization of the model and increase the quality of the data estimations.

Conclusions

ClimGen mostró un buen desempeño al calcular datos faltantes de la serie de tiempo histórica, lo cual indica que los datos estimados por el generador climático son representativos de los datos históricos del clima. Al calcular datos faltantes, es importante conservar los datos históricos observados de la estación y sólo calcular los datos faltantes; esto permite conservar la varianza de los datos calculados (temperatura máxima; ClimGen was shown to perform well when calculating missing data from a historical time series. This indicates that the data estimated by the weather generator are representative of the historical climate data. When calculating missing data, it is important to keep the station's observed historical data and only calculate the missing data, rather than completely generating all the data. Keeping the historical data makes it possible to preserve the variance of the calculated data ($r^2 = 0.95$ for maximum temperature *versus* $r^2 = 0.27$ for maximum temperature when completely generating all the data). This type of procedure makes it possible to expand the observed historical records from a particular station which increases the ability to use weather stations for hydrological, ecological, paleoclimatological and agricultural studies, among others. Nevertheless, it is important to mention that the data generated by the model should be used with care and analyzed graphically to identify data that significantly overestimate or underestimate historical records before using them as input data in a particular application. Another important aspect of the algorithm presented in this study is the prior validation of the climate information used, since the quality of this data affects the information generated. The study also demonstrates the ability to use annual records of climate variables when data is missing. Thus, the common practice of discarding this data can be abandoned and the information can be expanded for the purpose of modeling processes.

References

Bal, S. K., Choudhury, B. U., Sood, A., Jalota, S. K., & Singh, H. (2008). Evaluation of climgen model to generate

weather parameters under different climatic situations in Punjab. *Journal of Agrometeorology*, *1*(1), 39-45.

Carbajal, C. M., Yarlequé, C., Posadas, A., Silvestre, E., Mejía, A., & Quiroz, R. (2010). Reconstrucción de datos faltantes de precipitación pluvial diaria mediante la Transformada Wavelet. *Revista peruana geo-atmósferica RPGA*, *2*, 76-88.

Castellvi, F., & Stöckle, C. O. (2001). Comparing the performance of WGEN and ClimGen in the generation of temperature and solar radiation. *Transactions of American Society of Agricultural and Biological Engineers (ASABE)*, *44*, 1683-1687.

Cerano, P. J., Villaueva, D. J., Cervantes, M. R., Trucios, C. R., & Guerrero, S. J. L. (2013). Reconstrucción de sequías fuertes en el parque nacional "Pico de Tancítaro, Michoacán". *Revista Chapingo Serie Zonas Áridas*, *12*(2), 57-62.

Conagua (2012). *Climatología estadística*. Comisión Nacional del Agua. Agosto 28 de 2012. Citado el ocho de enero de 2014. Recuperado de http://smn.cna.gob.mx/climatologia/Estadistica/10084.pdf; http://smn.cna.gob.mx/climatologia/Estadistica/10026.pdf; http://smn.cna.gob.mx/climatologia/Estadistica/26076.pdf; http://smn.cna.gob.mx/climatologia/Estadistica/27015.pdf.

Danuso, F., & Della, M. V. (1997). *CLIMAK Reference manual* (pp. 148). DPVTA. Udine, Italy: University of Udine, Italy.

Esquivel, A. G., Sánchez, C. I., Velásquez, V. M. A., Lopez, S. A., Lopez, L. R., & Bueno, H. P. (2013a). Modelación del escurrimiento en una subcuenca del trópico húmedo de México y su análisis mediante índices de eficiencia predictiva. *Agrofaz*, *13*(2), 113-118.

Esquivel, A. G., Bueno, H. P., Sánchez, C. I., Velásquez, V. M. A., & Delgado, R. G. (2013b). Eficiencia predictiva de modelos hidrológicos para cuencas poco instrumentadas. *Memoria III Congreso Nacional de Manejo de Cuencas Hidrográficas*. Morelia, Michoacán México.

Flanagan, D. C., & Livingston, S. J. (1995). *WEPP User Summary*. NSERL Report No. 11. West Lafayette, USA: USDA-ARS National Soil Erosion Research Laboratory.

Hoogenboom, G. (2000). Contribution of Agro-Meteorology to the Simulation of Crop Production and its Applications. *Agricultural and Forest Meteorology*, *103*, 137-157.

Hoogenboom, G., & Soltani, A. (2003). Minimum Data Requirements for Parameter Estimation of Stochastic Weather Generators. *Climate Research*, *25*, 109-119.

IMTA (2009). *Extractor Rápido de Información Climatológica v. 3.0 (ERIC III). Base de datos y software*. Jiutepec, México: Instituto Mexicano de Tecnología del Agua.

Johnson, G. L., Hanson, C L., Hardegree, S. P., & Ballard, E. B. (1996). Stochastic Weather Simulation: Overview and Analysis of Two Commonly Used Models. *Journal of Applied Meteorology and Climatology*, *35*, 1878-1896.

Matalas, N. C. (1967). Mathematical Assessment of Synthetic Hydrology. *Water Resources Research*, *3*(4), 937-945.

Mckague, K., Rudra, R., & Ogilvie, J. ClimGen - A Convenient Weather Generation Tool for Canadian Climate Stations. Paper No. 03-118. *Proc. CSAE/SCGR 2003 Meeting*, 6-9 July, Montreal, Québec.

Moradi, I., Nosrati, K., & Eslamian, S. (2007). Evaluation of the RadEst and Climgen Stochastic Weather Generators for Low-Medium Rainfall Regions. *Journal of Applied Sciences*, *7*(19), 2900-2903.

Nicks, A. D., Richardson, C. W., & Williams, J. R. (1990). Evaluation of the EPIC Model Weather Generator (pp. 105-124). In A. N. Sharpley & J. R. Williams (Eds.). *EPIC – Erosion/Productivity Impact Calculator, 1. Model Documentation, USDA Technical Bulletin 1768*. Washington, DC: Government Printing Office.

Richardson, C. W. (1981). Stochastic Simulation of Daily Precipitation, Temperature, and Solar Radiation. *Water Resources Research*, *17*(1), 182-190.

Richardson, C. W., & Wright, D. A. (1984). *WGEN: A Model for Generating Weather Variables*. US Department of Agriculture, Agricultural Research Service, ARS-8.

Sarangi, A., & Kumar, A. (2006). *Trend Analysis of long Term Rainfall Data for Crop Planning as an Adaptation Measure to Climate Change* (pp. 1-6). 60th International Executive Council Meeting & 5th Asian Regional Conference, New Delhi, India.

Sarangi, A., Madramootoo, C. A., & Koundal, K. R. (2008). *Generation of Regional Water Harvesting Potential Scenarios using ClimGen Model* (pp. 139-142). International Symposium Water Harvesting, Brining Green Revolution to Rainfed Areas, New Delhi, India.

Safeeq, M., & Fares, A. (2011). Accuracy Evaluation of ClimGen Weather Generator and Daily to Hourly Disagregation Methods in Tropical Conditions. *Theoretical and Applied Climatology*, *106*, 321-341.

Selker, J. S., & Haith, D. A. (1990). Development and Testing of Single Parameter Precipitation Distribution. *Water Resources Research*, *26*(11), 2733-2740.

Stöckle, C. O., & Nelson, R. (2003). *Cropping System Simulation Model user's Manual* (p. 235). Washington, DC: Washing State University.

Stöckle, C. O., Nelson, R., Donatelli, M., & Castellvì, F. (2001). *ClimGen: A Flexible Weather Generation Program*. 2nd International Symposium Modelling Cropping Systems, Florence, Italy, 16-18 July.

Stöckle, C. O., Campbell, G. S., & Nelson, R. (1999). *ClimGen Manual* (28 pp.). Pullman, USA: Biological Systems Engineering Department, Washington State University.

Tingem, M., Rivington, M., Azam-Ali, S. N., & Colls, J. J. (2008). Climate Variability and Maize Production in Cameroon: Simulating the Effects of Extreme Dry and Wet Years. *Singapore Journal of Tropical Geography*, *29*(3). 357-370.

Tingem, M., Rivington, M., Azam-Ali, S. & Colls, J. (2007). Assessment of the Climgen stochastic weather generator at Cameroon sites. *African Journal of Environmental Science and Technology*, *1*(4), 86-92.

Weibull, W. (1951). A Statistical Distribution Function of Wide Applicability. *Journal of Applied Mechanics – Transactions ASME*, *18*(3), 293-297.

Institutional Address of the Authors

M.C. Gerardo Esquivel Arriaga

Instituto Nacional de Investigaciones Forestales, Agrícolas y Pecuarias
km 6.5 margen derecha canal Sacramento
35140 Gómez Palacio, Durango, México
Teléfono: +52 (871) 1590 104
esquivel.gerardo@inifap.gob.mx

M.C. Julián Cerano Paredes

Universidad Nacional Autónoma de México
Instituto de Geografía
Departamento de Geografía Física
Circuito de la Investigación Científica, Ciudad Universitaria, Coyoacán
04510 México, D.F., México
Teléfono: +52 (871) 1590 104
cerano.julian@inifap.gob.mx

Dr. Ignacio Sánchez Cohen

Instituto Nacional de Investigaciones Forestales, Agrícolas y Pecuarias
km 6.5 margen derecha canal Sacramento
35140 Gómez Palacio, Durango, México
Teléfono: +52 (871) 1590 104
sanchez.ignacio@inifap.gob.mx

Dr. Armando López Santos

Universidad Autónoma Chapingo
Unidad Regional Universitaria de Zonas Áridas
Dom. Conocido s/n Bermejillo
35230 Durango, México
Teléfono: +52 (872) 7760 190, 60
armando.lopezsantos@gmail.com

Dr. Oscar Gerardo Gutiérrez Ruacho

Universidad Estatal de Sonora
Rosales núm. 189. Col. Centro
83001 Hermosillo, Sonora, México
Teléfono: +52 (662) 2153 778
ruachogr@hotmail.com
oscar.gutierrez@ues.mx

Modeling to Estimate the Dimensions of the Wet Bulb in Trickle Irrigation

• Fidencio Cruz-Bautista* •
Universidad de Sonora, México
*Corresponding Author

• Alejandro Zermeño-González • Vicente Álvarez-Reyna • Pedro Cano-Ríos •
Universidad Autónoma Agraria Antonio Narro, México

• Miguel Rivera-González •
Instituto Nacional de Investigaciones Forestales, Agrícolas y Pecuarias, México

• Mario Siller-González •
Instituto Politécnico Nacional, México

Abstract

Cruz-Bautista, F., Zermeño-González, A., Álvarez-Reyna, V., Cano-Ríos, P., Rivera-González, M., & Siller-González, M. (July-August, 2015). Modeling to Estimate the Dimensions of the Wet Bulb in Trickle Irrigation. *Water Technology and Sciences* (in Spanish), *6*(4), 131-140.

The shape and volume of the wet soil resulting from the application of water by emitters is the most important factor in the design of trickle irrigation systems. The wet soil volume represents the amount of stored water, and the extension, depth and diameter should coincide with the radicle system of the plants and the spacing between emitters and irrigation lines. Therefore, the objective of this work was to develop equations to describe the advance of water in the wet bulb with a trickle irrigation system. Information related to soil wetting patterns and physical and hydraulic characteristics were used with three different textures to develop two equations. The results show that these equations describe the lateral and vertical advance of the water in the wet bulb of sandy-loam, clay-loam and silty-loam soils with a reliability of 90 to 94%. These equations show that the extension of the wet bulb depends on the volume of water applied, the flow of the emitter, the saturated hydraulic conductivity, initial and residual moisture contents of the soil and the silt content. The results demonstrate that these equations can be used to estimate the extension of the wet bulb in the soil with a localized irrigation system, and thereby determine the number of emitters needed to moisten the volume of soil required.

Keywords: Mathematical model, wetted soil volume, drip irrigation, wetting-pattern.

Resumen

Cruz-Bautista, F., Zermeño-González, A., Álvarez-Reyna, V., Cano-Ríos, P., Rivera-González, M., & Siller-González, M. (julio-agosto, 2015). Modelo para estimar la extensión del bulbo de humedecimiento del suelo en riego por goteo. Tecnología y Ciencias del Agua, *6(4), 131-140.*

La forma y el volumen de suelo mojado que se obtiene cuando los emisores aplican el agua es la característica más importante en el diseño de los sistemas de riego por goteo. El volumen de suelo mojado representa la cantidad de agua almacenada, mientras que su extensión, profundidad y diámetro deben coincidir con el sistema radicular de la planta y espaciamiento entre emisores y líneas regantes. Por esta razón, el objetivo del presente estudio fue desarrollar ecuaciones para describir el avance del agua en el bulbo de humedecimiento del suelo en un riego por goteo. Se usó información de patrones de humedecimiento de suelo y características físicas e hidráulicas de tres diferentes texturas para el desarrollo de dos ecuaciones. Los resultados mostraron que estas ecuaciones describen el avance lateral y vertical del agua en el bulbo de humedecimiento de suelos de textura franco-arenoso, franco-arcilloso o franco-limoso, con una confiabilidad de 90 y 94%. Estas ecuaciones muestran que la extensión del bulbo de humedecimiento es función del volumen de agua aplicada, caudal del emisor, conductividad hidráulica saturada, contenido de humedad inicial y residual del suelo, y contenido de limo en el suelo. Los resultados demostraron que estas ecuaciones pueden utilizares para estimar la extensión del bulbo de humedecimiento del suelo en un sistema de riego localizado, así como el número de emisores necesarios para humedecer el volumen de suelo requerido.

Palabras clave: *modelo matemático, volumen de suelo mojado, riego por goteo, patrón de humedecimiento.*

Received: 05/09/2012
Accepted: 30/04/2015

Introduction

The design and operations of trickle or drip irrigation systems requires knowing the distribution of the water under the emitters, given that the shape and volume of wet soil resulting from the application of water by the emitters are the most important characteristics in the design of this type of system. The volume of wet soil represents the amount of water stored in the soil, while the dimension, depth and diameter should coincide with the depth of the root system of the plants and the spacing among emitters and irrigation lines (Zur, 1996; Maia, Luiz, Francismar, & Dantas, 2010). The volume of wet soil and its dimension depends on the soil's texture and structure, the saturated hydraulic conductivity and the initial moisture content, in addition to the flow of the emitter and the total volume of water applied (Kandelous & Simunek, 2010; Nafchi, Mosavi, & Parvanak, 2011). Other factors affect the movement of water in the soil, such as the relative position of the emitters, the amount and frequency of irrigation and temporal and spatial changes in the moisture content of the soil, among others (Mmolawa & Or, 2000; Ruiz-Canales, Plana, Ruiz-Sánchez, Franco, & Abrisqueta, 2005; Kandelous & Simunek, 2010). If the distribution of the water in the wet soil is known, then the emitter or emitters can be arranged and operated in such a way as to guarantee the precise placement of the water and nutrients in the root zone of plants (Ruiz-Canales *et al*., 2005; Amin & Ekhmaj, 2006; Elmaloglou & Diamantopoulos, 2009). Nevertheless, few field studies exist that show the dynamics of water distribution in soil using trickle irrigation.

Therefore, the objective of this study was to develop equations to describe the lateral and vertical advance of water in the wet bulb in soil located under an emitter using a surface trickle irrigation system.

Theoretical Considerations

The water distribution pattern in soil significantly affects the design of local irrigation systems. Several studies have been performed using sophisticated analytical and numerical models to determine the distribution and pattern of moistening of the soil by water (Dasberg & Or, 1999). Many empirical, analytical and numerical models have also been developed to predict wetting patterns in soil with trickle irrigation using experimental observations and by solving the Richards equation (Cook, Fitch, Thorburn, Charlesworth, & Bristow, 2006; Kandelous & Simunek, 2010). Nevertheless, most of these models make predictions based on variables such as the flow of the emitter, volume of water applied and the hydraulic properties of the soil. Many of these models do not directly apply to the design and management of local irrigation systems and are based on highly limited solutions (Kandelous & Simunek, 2010; Nafchi *et al*., 2011, Ramírez de Cartagena & Sáinz-Sánchez, 1997). Meanwhile, empirical and semi-empirical models typically developed through regression analyses or field observations are more convenient for the design and operation of these irrigation systems (Ramírez de Cartagena & Sáinz-Sánchez, 1997; Amin & Ekhmaj, 2006; Kandelous & Simunek, 2010; Nafchi *et al*., 2011).

Given the background provided above and in accordance with the approaches introduced by Shwartzman and Zur (1986) and Amin and Ekhmaj (2006), equations (1) and (2) were proposed to identify the explanatory variables related with the advance of water in wet bulbs. These equations comes from a selection of variables using the Stepwise method and the non-linear relationship among them can be expressed as:

$$r = \beta_0 V^{\beta_1} K_s^{\beta_2} \theta_v^{\beta_3} \quad (1)$$

$$Z = \beta_0 V^{\beta_1} Q^{\beta_2} \theta_v^{\beta_3} \theta_r^{\beta_4} S_i^{\beta_5} \quad (2)$$

where r = lateral advance (L); Z = vertical advance (L); β_0, β_1, β_2, β_3, β_4 and β_5 are the regression coefficients; V = volume of water applied (L^3); Q = flow of the emitter ($L^3\ T^{-1}$); K_s = saturated hydraulic conductivity ($L\ T^{-1}$); θ = initial moisture content of the soil ($L^3\ T^{-3}$); θ_r = residual moisture content of the soil ($L^3\ T^{-3}$); S_i = silt content (%).

Materials and Methods

This study was performed with three soil textures located in the lagoon regions of Coahuila, Mexico. One texture was silty-loam located in an experimental field at the Antonio Narro Autonomous Agrarian University-Lagoon Unit, the other was clay-loam at the Technological Institute of Torreon and a third was sandy-loam at the National Research Institute for Forestry, Agricultural and Livestock, in Matamoros, Coahuila.

Surface trickle irrigation equipment was installed in the field to perform the wetting tests. It included a water container, irrigation head and irrigation line. The irrigation system was composed of a polyethylene hose 12.7 mm in diameter, a 6.35 mm diameter polyethylene tubing and emitters. The tubing was placed on the irrigation lines 1.5 m apart. An emitter was installed at the end of each tube.

Three wetting tests were performed with each soil texture to obtain the wetting pattern of the bulbs that formed under the emitters. The tests consisted of applying three different water volumes to the soil with the irrigation equipment described. The first test was conducted with emitters having a nominal flow of 2 liters per hour (lph) and an irrigation time of 0.5, 1.0, 1.5, 2.25, 3.0, 4.0, 5.0, 6.5 and 8.0 hours. The other two tests were performed with the same procedure using emitters with nominal flows of 4 and 8 lph.

Variables Measured

Physical and Hydraulic Soil Parameters

The proportion of solid particles from each of the soils was determined with the Bouyoucos hydrometric method and the texture was classified according to the soil texture triangle. The moisture content of the soils was also determined before each test using the gravimetric method at the depths shown in Table 1. The Guelph permeameter was used to calculate saturated hydraulic conductivity *in situ* using hydraulic loads of 5 and 10 cm according to the procedure described by Reynolds and Elrick (1985) and Reynolds *et al.* (2002). In addition, the parameters of the water retention curve and the saturated hydraulic conductivities used (Table 2) were modeled with the ROSETTA program, version 1.2 (Schaap, Leij, & Van Genuchten, 2001) based on the Van Genuchten (1980) and Mualem (1976) equations (Skaggs, Trout, Simunek, & Shouse, 2004; Kandelous & Simunek, 2010):

$$\theta(h)=\begin{cases}\theta_r+\dfrac{\theta_s-\theta_r}{\left(1+|\alpha h|^n\right)^m} & h<0\\ \theta_s & h\geq 0\end{cases} \qquad (3)$$

where $\theta(h)$ represents the water contents for a determined hydraulic potential (h); θ_s and θ_r are the saturated and residual water contents, respectively; α and n are parameters that affect the shape of the water retention function:

$$K(h)=K_s S_e^L\left[1-\left(1-S_e^{1/m}\right)^m\right]^2 \qquad (4)$$

and $K(h)$ is the unsaturated hydraulic conductivity, where L is the connectivity among pores, K_s is the saturated hydraulic conductivity and S_e is the effective saturation, defined as:

$$S_e=\frac{\theta-\theta_r}{\theta_s-\theta_r},\quad m=1-1/n \qquad (5)$$

Wetting Pattern of the Bulb

The wetting pattern of the bulb under the emitters was obtained in the field by directly measuring the wetting front (lateral and vertical advance) in the soil immediately after irrigation was finished, according to the following procedure:

a) The wet area of the soil under each emitter was measured after completing irrigation times of 0.5, 1.0, 1.5, 2.25, 3.0, 4.0, 5.0, 6.5 and 8.0 hours.
b) A quarter-circle of the wet soil area was excavated and a grid was laid out on the (x, z) and (y,z) coordinates and centered at the tip of the emitter.
c) The length of the wetting front was then measured in the horizontal and vertical directions.

Analysis of Data

The field measurements of the lateral and vertical advance of the water in the wetting bulb were used to determine the coefficients of equations (1) and (2). Physical and hydraulic data from the three types of soil in the wetting tests (Tables 1 and 2) were also used. As previously mentioned, the variables in equations (1) and (2) and the dependent variable presented a non-linear relationship and, therefore, they were log-transformed to make them intrinsically linear in order to facilitate the analysis and obtain coefficients using multiple linear regression (Amin & Ekhmaj).

Results

Equations to Predict the Distribution of Water in Wet Bulbs

Equations (6) and (7) present the coefficients obtained for the variables proposed in equations (1) and (2). These variables affect the advance of the water in the wet bulbs, with a confidence level of 90 and 94%, respectively, expressed by:

$$r = 0.14\ V^{0.353} K_s^{-0.110} \theta_v^{-0.387} \quad (6)$$

$$Z = 7.906\ V^{0.458} Q^{-0.152} \theta_v^{0.386} \theta_r^{0.349} S_i^{-0.421} \quad (7)$$

where r = lateral advance (m); Z = vertical advance (m); V = volume of water applied (m^3); Ks = saturated hydraulic conductivity ($m\ s^{-1}$); Q = emitter flow ($m^3\ s^{-1}$); θ_v = initial moisture content of the soil ($m^3\ m^{-3}$); θ_r = residual moisture content of the soil ($m^3\ m^{-3}$); S_i = silt content (%).

Equation (6) shows that the lateral advance (r) depends on the volume of water applied, the saturated hydraulic conductivity and the initial moisture contents of the soil. The significant partial coefficients (t- test) for these variables were 24.85, -3.93 and -7.45, respectively, with a multiple determination coefficient of 0.90 and $P(F > 209.26) <= 0.01$. The vertical advance (Z) of the water in the wet bulb is explained by the volume of water applied, the flow of the emitter, the initial and residual moisture contents of the soil and the silt content, according to equation (7). The partial correlation coefficients for these variables were 20.06, -4.55, 4.10, 3.92 and -8.31,respectively, with a multiple determination coefficient of 0.94 and $P(F > 194.74) < = 0.01$.

Shape and Dimension of the Wet Bulbs under the Emitter

With respect to the shape and dimension of the wet bulbs, only one side of the wetting front is shown (Figure 2) since the advance of the front is assumed to be symmetrical. Table 3 shows the variation in the lateral and vertical advance of the water in the wet bulbs according to the soil textures and volume of water applied.

Table 1. Physical and hydraulic properties of the soils where the wetting pattern tests were performed.

Textural class	Depth	Clay	Silt	Sand	Initial moisture	Apparent density	Saturated Hydraulic Conductivity
	(cm)	(%)	(%)	(%)	($cm^3\ cm^{-3}$)	($g\ cm^{-3}$)	($cm\ h^{-1}$)
Silty loam	0 – 20	28	46	26	0.098	1.146	2.050
	20 – 40	24	54	22	0.105	1.154	
	40 – 60	30	52	18	0.127	1.241	
Clay loam	0 – 20	26	22	52	0.066	1.139	3.283
	20 – 40	36	32	32	0.075	1.113	
	40 – 60	44	30	26	0.103	1.362	
Sandy loam	0 – 20	11	12	77	0.030	1.468	2.803
	20 – 40	11	9	80	0.048	1.538	
	40 – 60	8	8	84	0.063	1.526	

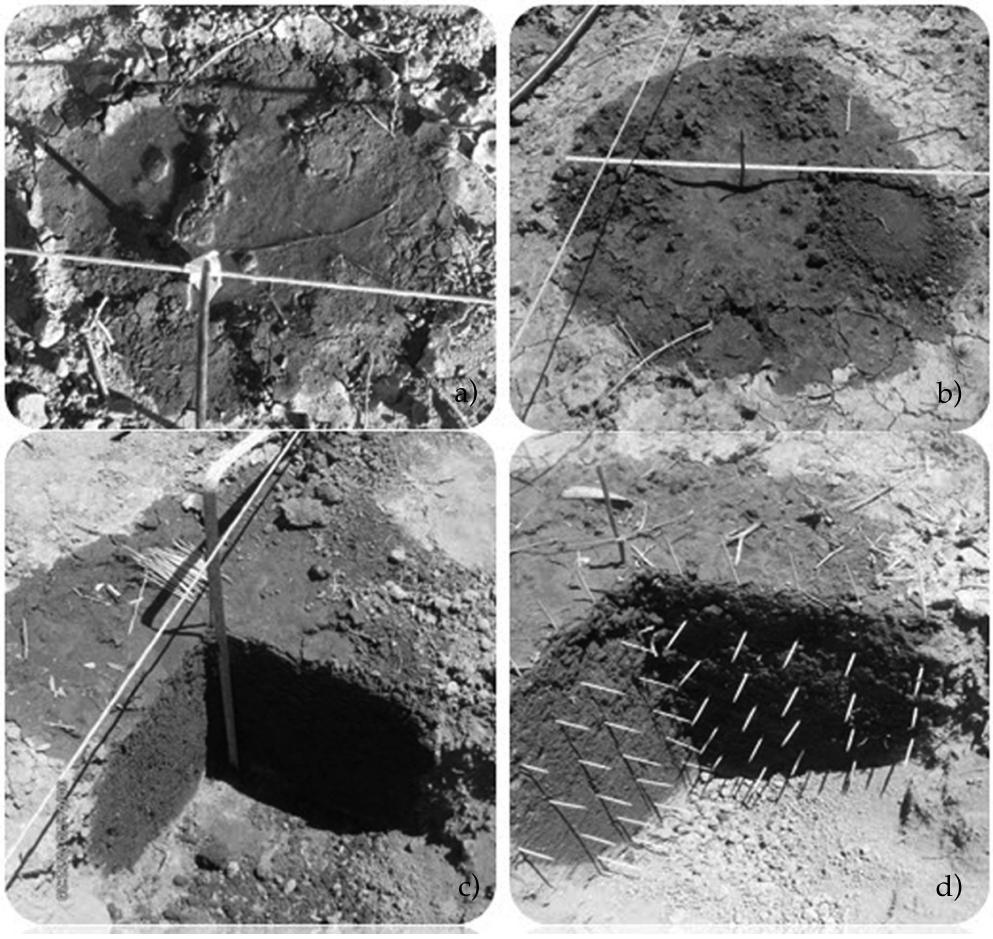

Figure 1. Shape and size of the wet bulb under an emitter: a) application of wter by the emitter; b) surface of the wet soil; c) profile of the wet soil; d) extension of the wet soil (*x*, *y*, *z* grid with separations of 5 cm) centered at the tip of the emitter.

Table 2. Hydraulic parameters of the soils where the wetting pattern tests were performed, obtained using the *ROSETTA* program, version 1.2 (Schaap *et al.*, 2001).

Textural class	Depth (cm)	θ_r ($cm^3\ cm^{-3}$)	θ_s ($cm^3\ cm^{-3}$)	K_s $cm\ h^{-1}$	α cm^{-1}	*n*	*L*
Silty loam	0-20	0.071	0.495	1.928	0.013	1.351	-0.357
	20-40	0.062	0.480	2.210	0.009	1.413	0.207
	40-60	0.075	0.482	1.173	0.008	1.384	-0.046
Clay loam	0-20	0.071	0.507	3.944	0.034	1.294	-1.611
	20-40	0.087	0.531	2.183	0.022	1.271	-1.472
	40-60	0.081	0.483	0.434	0.014	1.227	-1.439
Sandy loam	0-20	0.041	0.401	5.152	0.050	1.416	-1.337
	20-40	0.043	0.386	4.797	0.051	1.435	-1.359
	40-60	0.037	0.386	7.336	0.056	1.499	-1.212

θ_s and θ_r represent the saturated and residual water contents; k_s, represents the saturated hydraulic conductivity, α the inverse relationship between the entrance of air and the soil; *n* the measurement of the distribution of the size of the soil pores and *L* is the connectivity among pores. These are the parameters that affect the retention of water.

Discussion

Equations (6) and (7) present the variables that affect the advance of the water in the wet bulb, with a confidence level of 90 and 94%, respectively. The lateral and vertical advance (*r* and *Z*) of the water is explained by the relationships among the volume of water applied (*V*), the flow from the emitter (*Q*), saturated hydraulic conductivity (*Ks*), initial and residual moisture content of the soil (θ_v and θ_r) and the silt content (S_i). The volume of water applied (*V*) is the variable that most contributed to the lateral and vertical movement of water in the wet bulbs, as indicated by the partial correlation coefficients (*t*- test) for *V*, which were the highest (24.85 and 20.06, respectively). In addition, the correlation coefficients of *V* with respect to the dependent variables *r* and *Z* were 0.905 and 0.910. These results agree with information reported by Schwartzman and Zur (1986), Gil-Marín (2001), Amin and Ekhmaj (2006) and Nafchi *et al*. (2011). Therefore, the dimension of the wet bulb obtained when emitters apply water to soils with sandy-loam, clay-loam and silty-loam textures depends, in order of importance, on the volume of water applied, irrigation time, emitter flow, saturated hydraulic conductivity, initial and residual moisture contents and the silt content of the soil.

The variables shown in equations (6) and (7) are significant for a total of 9 variables that were considered to explain the lateral and vertical advance (*r* and Z) of water in the bulb. Other variables also included in the selection process were apparent density and sand and clay contents. The physical and hydraulic properties of the soils (Tables 1 and 2) were analyzed for each soil profile stratum separately, as suggested by Ramírez de Cartagena and Sáinz- Sánchez (1997).

The Stepwise method did not consider saturated hydraulic conductivity (Ks) to be a variable that affects the vertical advance of water in the wet bulb, as proposed by Schwartzman and Zur (1986), Amin and Ekhmaj (2006) and Kandelous, Liaghat and Abbasi (2008) in their models, which is also expected. Nevertheless, a detailed analysis detected that Ks is inversely proportional to the initial and residual moisture contents (θ_v and θ_r), and the silt content (S_i), which were considered since the hydraulic and physical properties of soil vary according to depth.

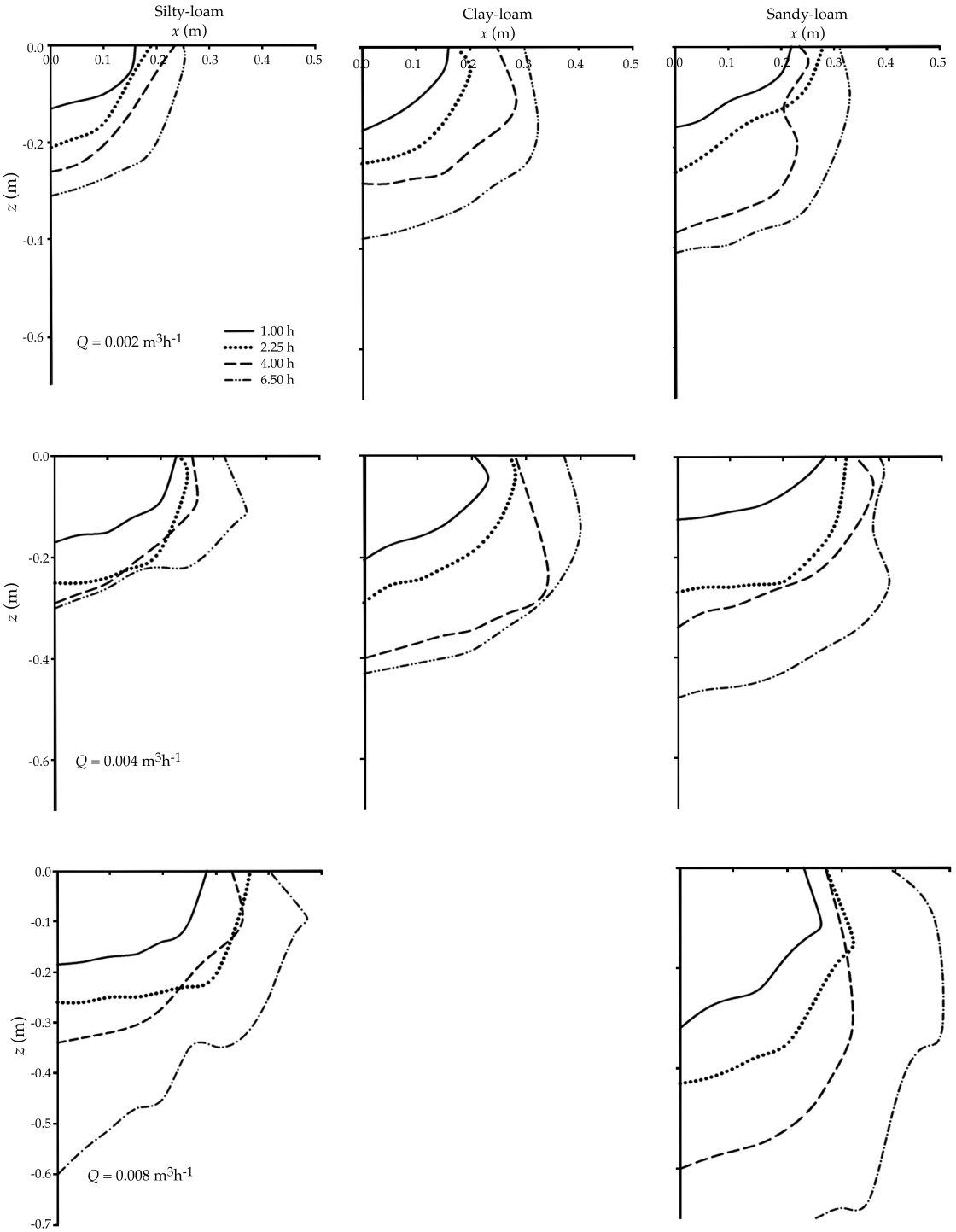

Figure 2. Advance of the wet front in the soil bulbs after 1.0, 2.25, 4.0 and 6.5 hours of irrigation.

The contrary occurs with the lateral or radial advance of the water when the soil has a certain amount of homogeneity and infiltration is presumed to be vertical.

Furthermore, the water applied by the emitters generally creates truncated ellipsoi-

Table 3. Differences in the lateral and vertical advance of water in the wet bulb according to soil texture and the water volume applied.

Q	Silty-clay Loam		Silty-sandy Loam		Clay-sandy Loam	
(m^3h^{-1})	(%)		(%)		(%)	
	Lateral	Vertical	Lateral	Vertical	Lateral	Vertical
0.002	0.3	7.3	0.5	10.8	0.8	3.9
0.004	0.8	9.1	1.0	10.2	0.8	5.6
0.008			1.0	16.6		

dal bulbs. The dimensions of these increase until the water absorption capacity of the soil, a function of *r* and *Z*, equals the velocity of water applied by the emitter. At first, when the soil is dry the penetration speed is quicker but if water continues to be applied, and as the porous spaces are filled and the clays expand, this penetration speed stabilizes. In this case, if the speed at which the water is applied exceeds the infiltration capacity of the soil, the lateral or radial advance of the water in the bulb increases. Figure 2 shows elliptical bulbs with horizontal elongations when applying low water volumes or flows, even with sandy-loam soil. But if the water is applied for a longer period of time— that is, the applied water volume (*V*) is increased —the vertical advance becomes more pronounced and the bulbs become vertically elongated in all three soil textures. This is consistent with findings by Cote, Bristow, Charlesworth, Cook and Thorburn(2003); Lazarovitch, Warrick, Furman and Simunek (2007) and Hao, Marui, Haraguchi and Nakano (2007). That is, as the application time of the water increases the lateral advance stabilizes and the vertical advance increases (Li, Zhang, & Li, 2003). This increase in the vertical advance can also be seen in Table 3, where the lateral advance in the bulb is roughly 1% and the vertical advance ranges from 4 to 17% when applying the same volume of water to each soil. With this process of penetration and redistribution of water in the soil, a wet bulb is obtained from different combinations of lateral and vertical advances. It is therefore important to mention that knowledge about the shape and dimension of the wet bulbs obtained under an emitter will enable determining the number of emitters needed to wet a given volume of soil.

Conclusions

The equations developed by this work describe the lateral and vertical distribution of water in a wet bulb in sandy-loam, clay-loam and silty-loam soils at a confidence level of 90% for lateral and 94% for vertical distribution.

The dimension of the wet bulbs obtained when the emitter applies water on any of these soils depends on, in order of importance, the volume of water applied, the emitter flow, saturated hydraulic conductivity, initial and residual moisture contents of the soil and the silt content of the soil.

When applying a small volume of water, elliptical bulbs with a horizontal elongation are obtained. The ellipse elongates in the vertical direction when increasing the application time of the water or the flow of the emitter.

Knowledge about the shape and dimension of the wet bulb obtained under an emitter will make it possible to determine the number of emitters needed to wet a given volume of soil.

References

Amin, M. S. M., & Ekhmaj, A. I. M. (2006). *DIPAC-Drip Irrigation Water Distribution Pattern Calculator*. 7th International Micro Irrigation Congress, 10-16 Sept. Pwtc, Kuala Lumpur, Malaysia.

Cook, F. J., Fitch, P., Thorburn, P., Charlesworth, P. B., & Bristow, K. L. (2006). Modelling Trickle Irrigation: Comparison of Analytical and Numerical Models for Estimation of Wetting Front Position with Time. *Environmental Modelling & Software*, *21*(9), 1353-1359.

Cote, C. M., Bristow, K. L., Charlesworth, P. B., Cook, F. J., & Thorburn, P. J. (2003). Analysis of Soil Wetting and Solute Transport In Subsurface Trickle Irrigation. *Irrig. Sci*., *22*, 143-156.

Dasberg, S., & Or, D. (1999). *Drip Irrigation* (162 pp.). New York: Springer-Verlag.

Elmaloglou, S., & Diamantopoulos, E. (2009). Simulation of Soil Water Dynamics under Subsurface Drip Irrigation from Line Sources. *Agricultural Water Management*, *96*, 1587-1595.

Gil-Marín, J. A. (2001). Forma y dimensiones del bulbo húmedo con fines de diseño de riego por goteo en dos suelos típicos de sabana. *Revista UDO Agrícola*, *1*(1), 42-47.

Hao, A., Marui, A., Haraguchi, T., & Nakano, Y. (2007). Estimation of Wet Bulb Formation in Various Soil during Drip Irrigation. *J. Fac. Agr., Kyushu Univ*., *52*(1), 187-193.

Kandelous, M. M. K., & Simunek, J. (2010). Comparison of Numerical, Analytical, and Empirical Models to Estimate Wetting Patterns for Surface and Subsurface Drip Irrigation. *Irrig. Sci*., *28*, 435-444.

Kandelous, M. M., Liaghat, A., & Abbasi, F. (2008). Estimation of Soil Moisture Pattern in Subsurface Drip Irrigation Using Dimensional Analysis Method. *J. Agri. Sci*., *39*(2), 371-378.

Lazarovitch, N., Warrick, A. W., Furman, A., & Simunek, J. (2007). Subsurface Water Distribution from Drip Irrigation Described by Moment Analyses. *Vadose Zone Journal*, *7*(6), 116-123.

Li, J., Zhang, J., & Li, R. (2003). Water and Nitrogen Distribution as Affected by Fertigation of Ammonium Nitrate from a Point Source. *Irrig Sci*., *22*, 19-30.

Maia, C. E., Luiz, S., Francismar, A. L., & Dantas, J. (2010). Dimensões de bulbo molhado na irrigação por gotejamento superficial. *Revista Ciência Agronômica*, *41*(1), 149-158.

Mmolawa, K., & Or, D. (2000). Root Zone Solute Dynamics under Drip Irrigation: A Review. *Plant and Soil*, *222*, 163-190.

Mualem, Y. (1976). A New Model for Predicting the Hydraulic Conductivity of Unsaturated Porous Media. *Water Resources Research*, *12*, 513-522.

Nafchi, R. F., Mosavi, F., & Parvanak, K. (2011). Experimental Study of Shape and Volume of Wetted Soil in Trickle Irrigation Method. *African Journal of Agricultural Research*, *6*(2), 458-466.

Ramírez De Cartagena, B. F., & Sáinz-Sánchez, M. A. (1997). Modelo de distribución de agua en suelo regado por goteo. *Ingeniería del Agua*, *4*(1), 57-70.

Reynolds, W. D., & Elrick, D. E. (1985). Measurement of Field-Saturated Hydraulic Conductivity, Sorptivity and the Conductivity-Pressure Head Relationship Using The "Guelph Permeameter". *Proc. National Water Well Association Conference on Characterization and Monitoring of the Vadose* (Unsaturated) Zone, Denver, Co. , USA.

Reynolds, W. D., Elrick, D. E., Youngs, E. G., Amoozegar, A., Booltink, H. W. G., & Bouma, J. (2002). Saturated and Field-Saturated Water Flow Parameters (pp. 797-878). In *Methods of Soil Analysis*. Part 4-Physical Methods. Madison, USA: Soil Science Society of America.

Ruiz-Canales, A., Plana, V., Ruiz-Sánchez, M. C., Franco, J. A., & Abrisqueta, J. M. (2005). Modelo de distribución temporal y espacial del balance de agua en el suelo para riego localizado en parcela. *Estudios de la zona no saturada del suelo*, *7*, 263-268.

Schaap, M. G., Leij, F.J., & Van Genuchten, M. Th. (2001). Rosetta: A Computer Program for Estimating Soil Hydraulic Parameters with Hierarchical Pedotransfer Functions. *Journal of Hydrology*, *251*, 163-176.

Schwartzman, M., & Zur, B. (1986). Emitter Spacing and Geometry Of Wetted Soil Volume. *J. Irrig. Drain. Eng*., *112*(3), 242-253.

Skaggs, T. H., Trout, T. J., Simunek, J., & Shouse, P. J. (2004). Comparison of HYDRUS-2D Simulations of Drip Irrigation with Experimental Observations. *Journal of Irrigation and Drainage Engineering*, *130*(4), 304-310.

Van Genuchten, M. Th. (1980). A Closed-Form Equation for Predicting the Hydraulic Conductivity of Unsaturated Soils. *Soil Sci. Am. J*.. *44*, 892-898.

Zur, B. (1996). Wetted Soil Volume as a Design Objective in Trickle Irrigation. *Irrig. Sci*., *16*, 101-105.

Institutional Address of the Authors

Dr. Fidencio Cruz-Bautista

Universidad de Sonora
Departamento de Agricultura y Ganadería
Blvd. Luis Encinas y Rosales s/n, Col. Centro
83000 Hermosillo, Sonora, México
Teléfono: +52 (662) 2592 100 y 2592 200
fidencio.cruz@guayacan.uson.mx

Dr. Alejandro Zermeño-González

Universidad Autónoma Agraria Antonio Narro Calz.
antonio Narro 1923, Buenavista
25084 Saltillo, Coahuila, México
Teléfono: +52 (884) 4172 474 y 4110 200
azermeno@uaaan.mx

Dr. Vicente Álvarez-Reyna
Dr. Pedro Cano-Ríos

Universidad Autónoma Agraria Antonio Narro Unidad Laguna, Periférico Raúl López Sánchez s/n
Colonia Valle Verde, 27059 Torreón, Coahuila, México
Teléfono: +52 (871) 7297 613, 7297 614 y 7297 610
vicpall@hotmail.com
canorp49@hotmail.com

M.C. Miguel Rivera-González

Centro Nacional de Investigación Disciplinaria en Relación Agua, Suelo, Planta, Atmosfera (CENID RASPA-INIFAP)
Km. 6.5 margen derecha canal Sacramento
35140 Gómez Palacio, Durango, México
Teléfono: +52 (871) 1590 104, 1590 105 y 1590 107
rivera.miguel@inifap.gob.mx

Dr. Mario Ángel Siller González Pico

Centro de Investigación y de Estudios Avanzados del Instituto Politécnico Nacional (Cinvestav-IPN)
Unidad Guadalajara
Av. Científica 1145. Colonia El Bajío
45019 Zapopan, Jalisco, México
Teléfono: +52 (33) 3777 3600
mario_siller@gdl.cinvestav.mx

Comparison of Venturi Tube-Meter Experimental Data with Computational Fluid Dynamics Simulations

• Mauro Iñiguez-Covarrubias • Jorge Flores-Velazquez* •
• Waldo Ojeda-Bustamante •
Instituto Mexicano de Tecnología del Agua
*Corresponding Author

• Carlos Díaz-Delgado •
Universidad Autónoma del Estado de México

• Roberto Mercado-Escalante •
Instituto Mexicano de Tecnología del Agua

Abstract

Iñiguez-Covarrubias, M., Flores-Velazquez, J., Ojeda-Bustamante, W., Díaz-Delgado, C., & Mercado-Escalante, R. (July-August, 2015). Comparison of Venturi Tube-Meter Experimental Data with Computational Fluid Dynamics Simulations. *Water Technology and Sciences* (in Spanish), 6(4), 141-152.

Irrigation systems require defining the total energy line of the water flow in order to prevent variations in pressure and flow at delivery and control points. Special equipment are installed at these points, including Venturi gauges. These devices have not been widely studied in terms of sizes, shapes, materials or functioning conditions, and the operating recommendations are derived from experimentally obtained characteristics. Thus, modeling their functioning with computational fluid dynamics (*CFD*) simulations would be practical, economical and reliable. The objective of this work was to validate the *CFD* simulation of the functioning of a Venturi device based on laboratory observations. The comparison of the experimental results and those obtained with the *CFD* were highly satisfactory for the mean velocity (1.53 m s^{-1}), flow (0.027 m^3 s^{-1}) and pressure in the differential manometer (15 cm de Hg). After the model was validated, 8 operating scenarios were simulated with variations in flow from 0.005 m^3 s^{-1} to 0.040 m^3 s^{-1} which simplified the modeling of the head loss flow rate relationship of the Venturi, with a quadratic equation, thereby eliminating the uncertainty related to the discharge coefficient required by the experimental analysis. The characteristic values of the device were a minimum hydraulic head of 0.4 kg cm^{-2} at the contraction of the Venturi and a total pressure loss of 0.075 kg cm^{-2} in the Venturi for a Q_{max} of 0.040 m^3 s^{-1}. Lastly, the design of Venturi devices using *CFD* is recommended to obtain reliable information for its installation in irrigation systems.

Keywords: Computational Fluid Dynamics (CFD), venturimeters, irrigation systems.

Resumen

Iñiguez-Covarrubias, M., Flores-Velazquez, J., Ojeda-Bustamante, W., Díaz-Delgado, C., & Mercado-Escalante, R. (julio-agosto, 2015). Comparación de resultados experimentales de un Venturi con simulación de dinámica de fluidos computacional. Tecnología y Ciencias del Agua, *6(4), 141-152.*

En los sistemas de riego es necesario definir la línea de energía total del flujo de agua para evitar variaciones de presión y gasto en los puntos de entrega y control. En estos puntos se instalan equipos especiales, entre los que se encuentran los aforadores Venturi. Estos dispositivos han sido poco estudiados en relación con tamaños, formas, materiales o condiciones de funcionamiento, y las recomendaciones de operación provienen de características obtenidas de modo experimental. Así, modelar su funcionamiento a través de simulación con dinámica de fluidos computacional (DFC) resultaría práctico, económico y confiable. El objetivo del trabajo consistió en validar la simulación de funcionamiento con DFC de un dispositivo Venturi con base en observaciones de laboratorio. La comparación de los resultados experimentales y mediante DFC fueron altamente satisfactorios para los valores de velocidad media (1.53 m s^{-1}), gasto (0.027 m^3 s^{-1}) y presión en el manómetro diferencial (15 cm de Hg). Una vez validado el modelo, se simularon ocho escenarios de operación, con variación de gasto desde 0.005 m^3 s^{-1} hasta 0.040 m^3 s^{-1}, lo cual simplificó el modelo de la relación gasto-pérdida de carga del Venturi, con una ecuación cuadrática y así eliminar la incertidumbre del coeficiente de descarga requerido en los análisis experimentales. Los valores característicos del dispositivo fueron un requerimiento de carga hidráulica mínima en la contracción del Venturi de 0.4 kg cm^{-2}, y una pérdida de carga total en el Venturi de 0.075 kg cm^{-2} para $Q_{máx}$ de 0.040 m^3 s^{-1}. Por último se recomienda diseñar dispositivos Venturi con DFC y con ello obtener información confiable para su instalación en sistemas de riego.

***Palabras clave**: dinámica de fluidos computacional (DFC), aforador Venturi, sistemas de riego.*

Received: 01/07/2014
Accepted: 28/04/2015

Introduction

When designing and operating hydraulic structures for many types of facilities (pumping and treatment plants, hydroelectric and micro-hydroelectric plants and irrigation systems, among others), in order to prevent undesired fluctuations in pressure and flow at delivery and control points the total energy line must be known as accurately as possible, and controlled when applicable. In effect, these points are hydraulically suitable for the installation of special devices that measure flow, including Venturi meters. Nevertheless, few studies have been conducted about these devices in terms of their size, shape, operating conditions and materials, particularly because of the high cost of laboratory experiments for each one of the various options.

Concepts and models involving fluid mechanics can be used to design gauges installed in pipes (Levy, 1957; White, 1994). This requires first defining the discharge or volumetric flow rate of the fluid through the pipes (SARH, 1973). Then, the appropriate lengths need to be selected and the site and operating conditions of the device defined. This process involves reviewing the size of the gauge based on the kinetic currents, the characteristics of the material and the internal speed of the water.

The velocity of a fluid through a pipe can be determined when the flow is constricted, or choked, and pressure from the increase in velocity at the constricted site is measured. The flow gauges that operate based on this principle are known as differential pressure flow meters. These measuring devices include Venturi, orifice plates and nozzles, among others. They basically consist of an element that constricts the flow and creates a change in the piezometric head, which translates into a loss in energy.

Chow (1959) reported that in order to define the operating recommendations for hydraulic equipment, particularly when studying special devices such as Venturi meters (White, 1994), losses in head between the points of interest must be determined. These calculations use the conservation of energy equation:

$$z_1 + \frac{p_1}{\gamma} + \frac{v_1^2}{2g} = z_2 + \frac{p_2}{\gamma} + \frac{v_2^2}{2g} + \sum_1^2 h_{f_{1-2}} \qquad (1)$$

Donde v = velocidad del agua (m s^{-1});

Where v = velocity of the water (m s^{-1}); g = acceleration of gravity (m s^{-2}); z = elevation head (m); $\sum_1^2 h_{f_{1-2}}$ = total loss in energy between sections 1 and 2 (m); $\frac{p_n}{\gamma}$ = pressure head at point n (m): $\frac{v_n^2}{2g}$ = velocity head at point n (m); and γ specific weight of the fluid (kg m^{-3}).

In the majority of flow applications the equation is solved in its integral form, with average variables such as the mean velocity (m s^{-1}) in the section studied. This model has been applied to all types of hydraulic structures used in engineering (SARH, 1973).

The Venturi meter can be divided into four zones for its analysis (Figure 1): (a): the inlet, which provides a uniform distribution of the flow lines inside the unit and uniform velocity when it reaches the constricted section (b): the convergence zone (converging cone) is the part of the structure where diameter is reduced to a size less than the inlet diameter to produce the choked flow (c): the divergence zone is a transition section between the smaller diameter and a diameter equal to or larger than the inlet diameter (d): the outlet zone is straight, with no changes in diameter and directs the flow to the pipe being used.

The components of the Venturi meter are designed with different sizes, shapes, operating conditions and type of material. The convergence and divergence zones can be curved or straight depending on the proposed design. An angle is defined for each device which determines the minimum length of the divergence needed to normalize the flow

at the outlet of the device. One of the most critical ratios in the Venturi meters is the degree of choking (m) represented by the ratio of the contracted section (throat) (A_2) to the inlet (A_1); that is, $m = A_2/A_1$. Measuring the loss in energy from the choked flow between two zones is recommended (Figure 1)— one measurement right at the end of the inlet, D_1, and the other right between where the constriction ends, D_2, and the divergence begins (ASME,1983). A methodology exists using available laboratory equipment to measure the fall in the energy line between these two zones. Nevertheless, the use of a differential mercury manometer installed at the points mentioned is the most recommended method.

On the other hand, the ASME (1983) presents a mathematical model derived using equation (1) to determine the volumetric flow rate based on the discharge coefficient, with knowledge of the pressure distribution line or piezometric line beginning at the center tube. In addition, given that the loss in energy between the inlet and convergence zones is represented by $h = (z_1 + v_1^2/2g) - (z_2 + v_2^2/2g)$ and when substituting h in the conservation of mass equation $A_1 = A_2\, v_2/v_1$,, equation (2) is obtained:

$$Q = C_d A_2 \sqrt{\frac{2gh}{1-(m)^2}} \qquad (2)$$

Where the coefficient C_d is the known discharge coefficient which is determined by experimental laboratory tests. Sotelo-Avila (1979) reported two tables presented by Smetana (1957) to determine the C_d coefficient— one based on the choked flow equation $m = A_2/A_1$ and the other based on the Reynolds number corresponding to the throat section.

Ranald (1978) and ASME (1983) present different tables and figures to calculate flow measurements in pipes when using a Venturi device. It is worth mentioning here that both present very similar discharge coefficient values. Meanwhile, the USDI (1979) and the IOS (1991) present standardized procedures to be followed to correctly measure flows with Venturi meters.

Traditionally, to calculate the parameters that are characteristic of flow and because of the complexity of hydraulics, it was necessary to discretize the system of equations while leaving some of the flow characteristics fixed. General balance of mass and energy equations were then applied and, in particular, the equation that describes its movement. Nevertheless, in the majority of these cases this description would be punctual and not permit the spatial representation of the system. This inconvenience was solved with computational fluid dynamics (*CFD*) (Anderson, 1995). *CFD* makes it possible to spatially view the study phenomena by obtaining a numerical solution to problems involving the movement of fluids. A high degree of accuracy has been found when validating the proposed model with experimental data, which has improved the understanding of hydraulics and of fluid mechanics in general.

In actuality, *CFD* and experimental analyses are complementary, in which the use of *CFD* reduces the number of experimental laboratory analyses needed. For example, valves (Davies & Stewart, 2002), pumps (Zheng, 2000) and open canals (Wu, Rodi, & Wenka, 2000) have been analyzed in hydraulic engineering. In protected agriculture, *CFD* has been used to model climates inside greenhouses and thereby suggest management strategies involving auxiliary cooling or heating systems (Flores-Velázquez, Mejia, Rojano, & Montero, 2011). For pressured irrigation systems, applications can be found to analyze irrigation emitters (Palau, Arviza, & Frankel, 2004) and fertilizer injection devices (Manzano & Palau, 2005).

Various authors have simulated the hydraulic behavior of weirs and gauges using *CFD* techniques after validating them with ex-

perimental data. Gharahjeh, Aydin and Altan-Sakarya (2015) simulated flow of water for a thin-crested weir , while Naghavi, Esmaili, Yazdi and Vahid (2011) simulated a circular weir. Temeepattanapongsa, Merkley, Barfuss and Smith (2014) validated a *CFD* model and fitted generic algebraic equations for a variety of gauges without throats (cutthroat flumes) based on simulated head-discharge data under free and submerged discharge conditions.

With *CFD*, equations that define the movement of a fluid are solved by combining fluid dynamics, programming and numerical methods. In general, the movement of a fluid is primarily based on physical processes that can be described in mathematical terms by a series of partial derivative equations that numerically represent flow components. Given an incompressible fluid (water) in the domain $\Omega \subset Rn$ over a time interval [0, t], the dynamic of the flow at each point (x, y) at a specific moment t is determined according to the state, density of mass ρ(x, t), velocity field u (x, t) and its energy e (x, t). The differential approach applies the principles of conservation of mass, momentum and energy to a control volume , which are characteristics included in the Navier-Stokes (N-S) equations. Solving for this results in its differential form. Continuity momentum equations are expressed by equations (3) and (4), which are generalized for x, y, z (White, 1994; Çengel & Cimbala, 2012) :

Continuity equation:

$$\frac{\partial u}{\partial x}+\frac{\partial v}{\partial y}+\frac{\partial w}{\partial z}=0 \qquad (3)$$

Momentum at x:

$$\rho\left(\frac{\partial u}{\partial t}+\frac{\partial u}{\partial x}u+\frac{\partial u}{\partial y}v+\frac{\partial u}{\partial z}w\right) = \rho g_x-\frac{\partial p}{\partial x}+\mu\left(\frac{\partial^2 u}{\partial x^2}+\frac{\partial^2 u}{\partial y^2}+\frac{\partial^2 u}{\partial z^2}\right) \qquad (4)$$

Where $\frac{\partial u}{\partial x}, \frac{\partial v}{\partial y}, \frac{\partial w}{\partial z}$ is the volumetric deformation of the finite volume analyzed ($V = uvw$) with respect to the x¸ y and z axes; ρ is the density (kg m^{-3}); v is the kinetic viscosity $\left(v=\frac{\mu}{\rho}\right)$ when μ is the dynamic viscosity; t is the time (s) and g the acceleration of gravity.

The objective of the present work is to provide information about the functioning of a Venturi device by obtaining differential and integral equations using devices with specific characteristics and experimental laboratory data reported by Sotelo-Ávila (1979). An additional objective was to compare the experimental data with those obtained by *CFD* simulations to determine operating and installation parameters for irrigation systems.

Materials and Methods

The Venturi Device Studied

El dispositivo descrito por Sotelo-Ávila (1979) corresponde al estudio reportado por Smetana (1957) y esquematizado en la figura 1. Tiene un diámetro en la zona inicial de $D_1 = 0.15$ m y un diámetro en la zona de estrangulamiento de The device described by Sotelo-Ávila (1979) corresponds to the study reported by Smetana (1957), shown in Figure 1. The diameter of the inlet zone is $D_1 = 0.15$ and the diameter of the throat section is $D_2 = 0.075$ m. The transition between these diameters is represented by the convergence zone which is conical. The divergence zone widens from the end of the convergence zone until again reaching the value of diameter D_1. Sotelo-Ávila (1979) propose an angle (θ) of 2.5 to 7° in order to determine the length needed for the divergence leading to the outlet in order to normalize the flow. In the deflection of the differential manometer between diameters D_1 and D_2, $\Delta h = 0.15$ m of Hg, as shown in Figure 1, where the specific weight of mercury is γ_{Hg} = 13 595 kg m^{-3} and the kinematic viscosity of the water at 10°C is $\upsilon = 0.013$ cm^2 s^{-1}.

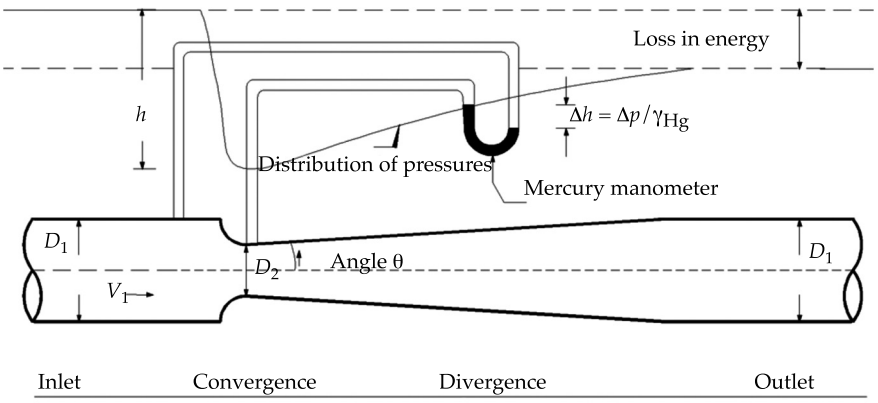

Figure 1. Venturi meter in a tuve with fow under pressure.

The kinetic current is the main variable studied by this work because of its affect on the functioning of the Venturi meter. An inadequate design of the inlet and outlet zones would be reflected by excessive flow velocity and the generation of dead zones or turbulence. According to Webber (1971), the diameter D_2 of the constriction should be large enough so that the pressure does not fall more than 2 water column meters below the absolute pressure, since air bubbles tend to be created at that pressure which presents the risk of cavitation in the walls of the device.

The Venturi shown in Figure 1 has a differential mercury manometer. The experimental laboratory observation provided the value of Δh and the volumetric flow rate (Q) can be determined with equation (5) (Sotelo-Ávila, 1979):

$$Q = C_d A_2 \sqrt{2g\Delta h\left(\frac{\gamma_{Hg}}{\gamma} - 1\right)} \qquad (5)$$

Where A_2 is the area of the convergence zone (m^2); g is the acceleration of gravity (m s^{-2}), γ_{Hg} is the specific weight of mercury (kg m^{-3}); γ is the specific weight of water (kg m^{-3}); Δh is the deflection of the mercury manometer (m); and C_d is the discharge coefficient (dimensionless).

Table 1 shows the geometric characteristics of the meter as reported by Sotelo Ávila (1979) and Smetana (1957), where the lengths of the inlet and outlet are over four times the value of D_1.

The volumetric flow rate is then determined based on the experimental results from the Venturi meter with the characteristics mentioned above. To this end, the information reported by Sotelo-Ávila (1979) was used indicating an initial velocity of V_i = 1.533 m s^{-1} and a throat constriction of m = 0.25, with which the values of the Reynolds number remain over 1 x 10^5. It is worth mentioning

Table 1. Geometric characteristics of the Venturi studied (Sotelo-Ávila, 1979).

Diameter (m)		Ratio	Area (m^2)		Relation	Convergence		Length (m)
Inlet = D_1	Constriction (throat) = D_2	D_2/D_1	A_1	A_2	$m = A_1/A_2$	Radius (m)	Angle (degrees)	Divergence
0.150	0.075	0.50	0.01767	0.0044	0.25	0.0375	3.5	0.6131

that for the installation of Venturi meters in irrigation systems, the important operating parameters that need to be known are the loss in total energy generated by the device and the absolute pressure in the convergence zone. According to Webber (1971), it is recommended that the line of energy be measured at a distance of $4D_1$ before the convergence and up to $4D_1$ after the divergence, at the point at which the flow behaves as a fully developed flow.

Computational Fluid Dynamics (CFD)

As mentioned, numerical tools such as CFD have been show to be efficient in the design and simulation of flows using modeling techniques with approximate solution methods for equations that govern the mechanics of fluids (equations (1), (3) and (4)) and numerical solution methods (finite volume), with their corresponding processing algorithms. Thus, *CFD* follows a series of steps that can be described by three overall stages:

a) **Preprocessing**. Generation of 3D digital representations of the geometry of the physical model of the device studied (Figure 2a). This step is crucial to define the mesh for the analysis (Figure 2b), in which the computational domain is divided into a finite number of prismatic elements to which the equations for the conservation of energy, mass and linear momentum are applied.

b) **Process**. After the geometry is generated, it is imported into the processor, where the values are assigned of the boundary conditions (Figure 2c), the left side of the inlet and the right side of the outlet. The corresponding hypotheses with respect to the Solver to be used are also established and the solution is obtained with the Reynolds-Averaged Navier-Stokes Simulations and the Pressure-Based method. The momentum equations for u, v and w are solved separately, followed by the energy equations. The most commonly used K-ε turbulence model is then solved and the attributes from the processing are incorporated into the CFD software (Table 2).

c) **Post-processing**. The results are graphically shown to scale in Figure 2d. It is worth noting that the *CFD* used by the present work was the commercial program *ANSYS Workbench v 14.5* (Fluent, 1998), which contains the interfaces needed to generate the geometry of the device (*Design Model*), the *Meshing* and the corresponding numerical simulator (*Fluent*).

Results and Discussion

Review Method for the Venturi tested in the laboratory

The discharge coefficient C_d was determined according to the methodology proposed by Sotelo-Ávila (1979) and the laboratory information related to initial velocity $v_i = 1.533$ m s^{-1}

Table 2. Initial conditions and calculation hypothesis.

Simulation Hypothesis	
Solver	Segregated *Pressure-Based*
Formulation	Implicit
Time condition	Stationary
Turbulence model	*K*-ε of two equations
Simulation scenarios	
Flow Velocity	Constant (velocity)
Simulation Scenarios	

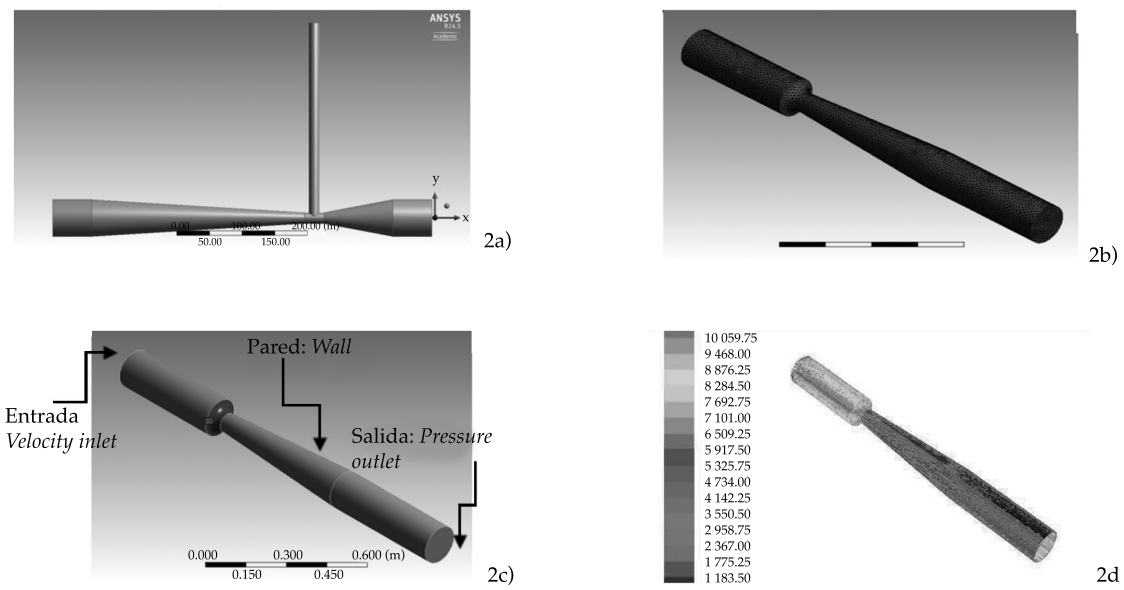

Figure 2. Stages in the construction of the computational model.

(Figure 3). This value was obtained based on the ratio of the constriction of $m = 0.25$ (Table 1) to the discharge coefficient $C_d = 1.009$. As reported by Sotelo-Avila (1979), the laboratory observation of the height of the mercury column in the deflection of the differential manometers was $\Delta h = 0.15$ m, and equation (5) was used to determine the volumetric flow rate $Q = 0.02698$ m^3 s^{-1}. The conservation of mass equation was used to determine the velocity in the convergence zone $V_2 = 6.13$ m^3 s^{-1}. Lastly, the Reynolds number $R_e = \frac{D_2 v_2}{\nu}$ was used to obtain the value $R_e = 3.54 \times 10^5$, which meets the recommendation that it be larger than $R_e = 1 \times 10^5$.

Figure 3 is a substitute for the graphs reported by Smetana (1957). The objective of this graph is to show the mathematical model of the ratio of the degree of constriction (m) to the discharge coefficient (C_d). Note that the model resulted in a determination coefficient $R^2 = 0.9972$.

The conventional experimental procedure described shows that each time there is a change in the initial velocity at the inlet of the Venturi, it is necessary to measure the corresponding change in the height of the column of the differential mercury manometer and calculate the volumetric flow rate with

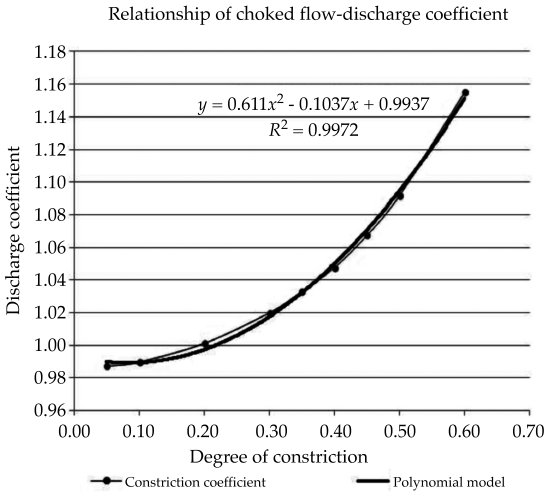

Figure 3. C_d coefficient in relation to the degree of constriction (m).

the new conditions. That is, the volumetric flow rate is related to the Δh of the column of mercury, which results in only one equation with two unknowns. Therefore, with this experimental procedure it necessary to know the initial velocity (at the inlet of the device), the value of Δh in the differential manometer and the value of the constriction (throat) m, in order to graphically obtain the corresponding value of the discharge coefficient C_d and, lastly, calculate the value of the volumetric flow rate. The main inconvenience of the experimental procedure described is that any change in flow conditions requires obtaining new experimental and observed data.

Review Method for the Venturi with CFD

Figure 4 shows the results obtained from the CFD simulation for the magnitude of the flow velocity vectors corresponding to each point (identified by circles) in the different zones in the Venturi meter: point D_1, convergence, divergence and the outlet of the device. The magnitudes of the velocity are represented by a colored graphic scale. Figure 5 shows punctual values of the flow velocity and pressure in relation to their location in the section of the tube in the inlet zone; that is, null velocity in the device walls up to a maximum of V = 1.8 m s^{-1} in the center of the cross-section of the pipe and pressure values of P = 78.7 cm of Hg in the wall of the pipe and P = 78.4 cm of Hg in the center of its cross-section. This information was used to determine the mean flow velocity and pressure at the inlet point with the help of equations (6) and (7):

$$V_m = \frac{V_1A_1 + V_2A_2 + \ldots + V_nA_n}{A_{\text{total}}} \qquad (6)$$

Where V_m = mean velocity of the flow in the section; V_n = punctual velocity in circle 1 up to n; A_n = area in circle 1 up to n; A_{total} = total area of the cross-section of the pipe:

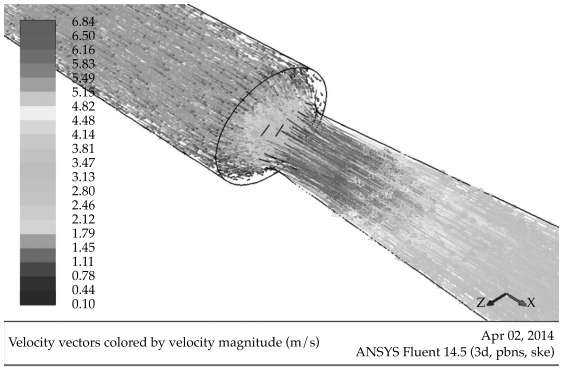

Figure 4. Distribution of velocities.

$$P_m = \frac{P_1A_1 + P_2A_2 + \ldots + P_nA_n}{A_{\text{total}}} \qquad (7)$$

Where P_m = mean flow pressure in the section; P_n = punctual pressure in circle 1 up to n; A_n = area in circle 1 up to n; A_{total} = total area of the cross-section of the pipe.

This procedure is repeated for the sections corresponding to the convergence and outlet zones of the device. The average flow velocity in the zones studied are presented in Table 3.

According to the calculation of the absolute relative error $|e_r|$ (equation (8)), the values obtained from the experimental values reported by Sotelo-Ávila (1979) and those obtained using the *CFD* (Table 3) were virtually the same: mean velocity in the inlet zone (1.53 m s^{-1} where $|e_r| = 0.013$), volumetric flow rate (0.027 m^3 s^{-1} from conservation of mass, where $|e_r| = 0.013$) and pressure in the differential manometer of 15 cm of Hg (difference in pressure between the inlet zone and the convergence zone, in cm of Hg, where $|e_r| = 0.100$):

$$|e_r| = \left| \frac{\text{observed value} - \text{simulated value}}{\text{observed value}} \right| \qquad (8)$$

After validating the model constructed with the CFD, eight additional scenarios were

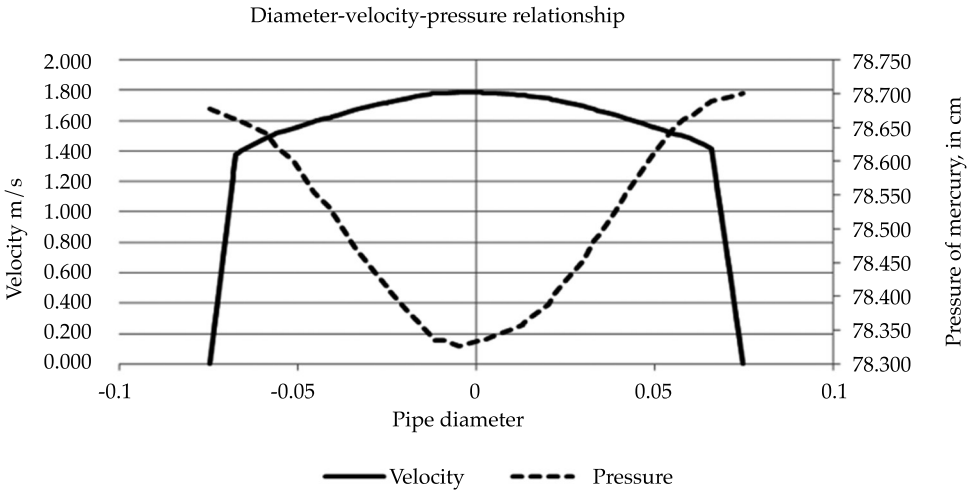

Figure 5. Velocity and pressure profiles (inlet zone).

Table 3. Results from the simulation of the experimental Venturi using *CFD*.

Inlet zone				Convergence zone				Outlet zone			
Mean pressure			Mean velocity	Pressure			Mean velocity	Mean pressure			Mean velocity
Pascal	cm de Hg	kg cm^{-2}	m s^{-1}	Pascal	cm de Hg	kg cm^{-2}	m s^{-1}	Pascal	cm de Hg	kg cm^{-2}	m s^{-1}
104 658	78.5	1.07	1.55	86 639	65	0.88	5.55	101 326	76	1.033	1.52

simulated with mean velocities between 0.028 and 2.264 m s^{-1}, corresponding to a variation in the volumetric flow rate from 0.005 to 0.040 m^3 s^{-1}. Table 4 shows the results from eight simulated scenarios (E2 through E9), where pressure is expressed in pascals, cm of Hg and kg cm^{-2}, and the mean velocities in the inlet, convergence and outlet zones are shown in m s^{-1}.

Based on the analysis of the results obtained by the simulations of the volumetric flow rate ranges of the operating Venutri (Q = [0.005 m^3 s^{-1}; Q = 0.040 m^3 s^{-1}]), and reported in Table 4, a regressive mathematical model was constructed of the volumetric flow rate (Q in m^3 s^{-1}) and head loss (Δh in cm of Hg) variables in the convergence zone of the Venturi device. This model is represented by a second-order equation and a determination coefficient of R^2 = 1 (Figure 6). This is fully congruent with the genesis of the local hydraulics in the convergence zone, given the fall in pressure resulting from the abrupt change in the flow velocity, in addition to local losses from friction also related to the flow velocity. This model reduces uncertainty by eliminating the need to select the discharge coefficient C_d when calculating the volumetric flow rate for any other initial velocity within the range modeled. That is, the problem is simplified to an equation with only one unknown. For example, using the graph of Figure 6 and considering the pipe diameter in the case study (D_1 = 0.15 m), if the read-

Table 4. Results from the *CFD* simulations for the eight scenarios proposed.

	Inlet zone				Convergence zone				Outlet zone			
	Pressure			Velocity	Pressure			Velocity	Pressure			Velocity
Version	Pascales	cm of Hg	kg cm^{-2}	mean m s^{-1}	Pascales	cm of Hg	kg cm^{-2}	mean m s^{-1}	Pascales	cm of Hg	kg cm^{-2}	mean m s^{-1}
E2	101 478	76.1	1.04	0.285	100 828	75.6	1.03	1.042	101 325	76.0	1.033	0.258
E3	101 829	76.4	1.04	0.577	99 319	74.5	1.01	2.082	101 323	76.0	1.033	0.569
E4	102 419	76.8	1.04	0.866	96 791	72.6	0.99	3.122	101 322	76.0	1.033	0.867
E5	103 223	77.4	1.05	1.140	93 237	69.9	0.95	4.161	101 327	76.0	1.033	1.126
E6	104 206	78.2	1.06	1.424	88 908	66.7	0.91	5.164	101 321	76.0	1.033	1.454
E7	105 397	79.1	1.08	1.725	82 770	62.1	0.84	6.202	101 326	76.0	1.033	1.690
E8	106 740	80.1	1.09	1.993	76 394	57.3	0.78	7.278	101 320	76.0	1.033	2.045
E9	108 301	81.2	1.10	2.268	69 015	51.8	0.70	8.316	101 319	76.0	1.033	2.234

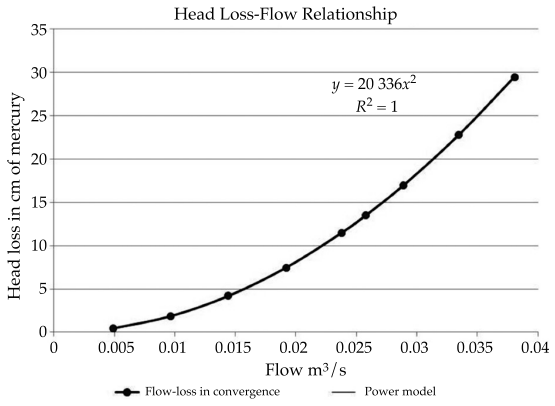

Figure 6. Determination of the losses in the convergence zone based on the value of the volumetric flow rate.

ing of the differential pressure manometer is $\Delta h = 0.15$ cm of Hg a volumetric flow rate of $Q = 0.027$ m^3 s^{-1} is obtained, which corresponds to a velocity of 1.53 m s^{-1}.

On the other hand, with the information provided by the CFD simulations, another mathematical model can be constructed to estimate total head loss in the Venutri meter for the range of volumetric flow rates studied. In effect, as in the previous case, the value of the fall in pressure between the initial and final zones of the device is taken into account by the relationship between this pressure differential and the volumetric flow rate at the inlet of the Venutri. The model presents pressure losses ((Δh in cm) of the water column *versus* the volumetric flow rate (Q in m^3 s^{-1}), as shown in Figure 7, which has a determination coefficient R^2 over 0.99. It is worth noting that this type of model cannot be constructed with conventional experimental laboratory studies alone.

Thus, for example, using the model from Figure 7, with a maximum volumetric flow rate of 0.040 m^3 s^{-1}, a total head loss along the length of the Venutri of 0.075 kg cm^{-2} was obtained. This total head loss corresponds to the distance between $\pm 4D_1$, from the convergence section to D_1, the inlet zone of the device.

Lastly, three other important results stand out which can only be obtained with the CFD simulation: a) the hydraulic head in the convergence of the operating Venturi should have a minimum pressure of 0.4 kg cm^{-2} for a maximum volumetric flow rate of 0.040 m^3 s^{-1} and thereby satisfy the conditions to prevent transient cavitation, as suggested by Webber (1971); b) because of the above conditions, the upper limit of the volumetric flow rate

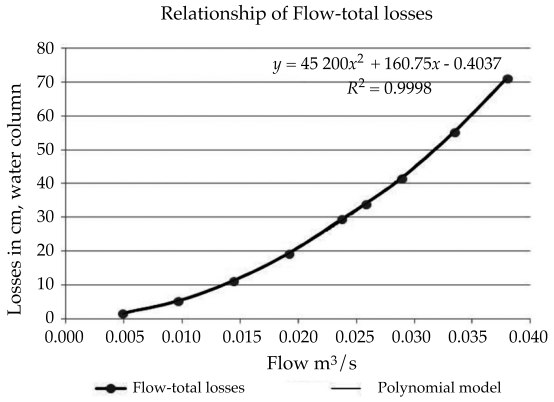

Figure 7. Determination of the total losses in the Venturi device between the initial and final sections.

for the dimensions and operating conditions is precisely 0.040 $m^3 s^{-1}$; and c) the total head loss over the length of the Venutri is 0.075 kg cm^{-2} for Q_{max} = 0.40 $m^3 s^{-1}$.

Conclusions

This work used computational fluid dynamics to model the functioning of a Venturi flow meter. The mathematical model was constructed and validated based on the experimental information obtained and reported by Sotelo-Ávila (1979). Very good agreement was obtained between experimental and simulated values for flow velocity, volumetric flow rate and decrease in pressure in the differential manometer. The CFD modeling was performed with the Fluent program using the finite volume method found in the ANSYS Workbench software, v. 14.5.

Based on the analysis herein, the following conclusions can be drawn:

1. Highly satisfactory agreement was found between the experimentally measured laboratory results and those obtained with the *CFD* numerical simulation.
2. The results obtained from the hydraulic scenarios modeled with the *CFD* contribute to a more in-depth understanding of the functioning of the Venturi and the determination of regressive mathematical models for the variability in its operating characteristics. The models obtained from the results of the *CFD* make it possible to determine the operating conditions for non-experimental situations without simulations, with a high level accuracy.
3. In particular, using the procedure proposed herein, it was possible to use a second-degree equation to model the ratio of the volumetric flow rate to the head loss in the convergence section of the Venturi and thereby eliminate uncertainty in the selection of the discharge coefficient (C_d). The relationship between volumetric flow rate and total head loss in the Venturi meter was also modeled, which is difficult to perform with traditional laboratory experiments.
4. *CFD* models can be used to design and define the optimal dimensions of a Venturi, taking into account different sizes, shapes, operating conditions and materials. The limit conditions that create a transient cavitation in the walls of the Venuturi can also be determined.

Lastly, it is important to mention that CFD modeling and laboratory experiments are complementary analytical methods in hydraulics and their combination is the best strategy to determine technical, practical, economic and reliable solutions, particularly for Venturi flow meters and their installation in irrigation systems.

References

Anderson, J. D. Jr. (1995). *Computational Fluid Dynamics. The Basics with Applications* (328 pp.). New York: McGraw-Hill.

ASME (1983). *Fluid Meters, their Theory and Application* (6th edition). In H. S. Bean (Ed.). New York: American Society of Mechanical Engineers, Research Committee on Fluid Meters.

Çengel, Y. A., & Cimbala, J. M. (2012). *Mecánica de fluidos-fundamentos y aplicaciones* (978 pp.) (2a edición). México, DF: McGraw Hill.

Chow, V. T. (1959). *Open Channel Hydraulics*. New York: McGraw-Hill.

Davies, J. A., & Stewart, M. (2002).*Predicting Globe Control Valve Performance*. Part I. *CFD*, Modeling. *ASME Journal of Fluids Engineering*, *124*(3), 772-777.

Flores-Velazquez, J., Mejia, E., Rojano, A., & Montero, J. (2011). Análisis del clima en un invernadero con ventilación mecánica, *Agrociencia*, *45*(5), 545-560.

Fluent (1998). *Fluent, v. 5.* Sheffield, UK: Fluent, Europe Ltf.

Gharahjeh, S., Aydin, I., & Altan-Sakarya, A. B. (2015). Weir Velocity Formulation for Sharp-Crested Rectangular Weirs. *Flow Measurement and Instrumentation*, *41*, 50-56.

IOS (1991). *Measurement of Flow by Means of Pressure Differential Devices*. Geneva: International Organization for Standardization ISO 5167-1.

Levy, E. (1957). *Mecánica de los fluidos* (266 pp.). México, DF: Instituto de ingeniería, UNAM.

Manzano, J., & Palau, G. (2005). *Hydraulic Modeling of Venturi injector by Means of CFD*. Tampa, USA: ASAE International Meeting.

Naghavi, B., Esmaili, K., Yazdi J., & Vahid, F. K. (2011). An Experimental and Numerical Study on Hydraulic Characteristics and Theoretical Equations of Circular Weirs. *Canadian Journal of Civil Engineering*, *38*(12), 1327-1334.

Palau, G., Arviza, J., & Frankel, S. (2004). *Tree-Dimensional Control Valve with Complex Geometry: CFD Modeling and Experimental Validation*. 34TH AIAA Fluid Dynamics Conference and Exhibit. IN AIAAA-2004- Portland, USA.

Ranald, V. G. (1978). *Mecánica de fluidos e Hidráulica* (2a edición). México, DF: McGraw-Hill.

Smetana J. (1957). *Hidráulika*. Praga: Ceskoslovenka Akademie, VED. Referencia de Sotelo-Ávila, G. (1995). *Hidráulica general* (277 pp.). México, DF: Limusa.

Sotelo-Ávila, G. (1979). *Hidráulica general* (277 pp.). México, DF: Limusa.

SARH (1973). *Proyecto de Zonas de Riego* (567 pp.). México, DF: Dirección de Proyectos de Irrigación, Departamento de Canales.

Temeepattanapongsa, S., Merkley, G. P., Barfuss, S. L., & Smith, B. (2014). Generic Unified Rating for Cutthroat Flumes. *Irrigation Science*, *32*(1), 29-40.

USDI (1979). *Water Measurement Manual* (3rd edition). Denver: US Department of Interior, Bureau of Reclamation, US Govern Printing Office.

Webber, N. B. (1971). *Fluid Mechanics for Civil Engineers* (330 pp.). London: Chapman & Hall.

White, F. (1994). *Fluid Mechanics* (736 pp.) (3rd edition). New York: McGraw Hill, Inc.

Wu, W., Rodi, W., & Wenka, T. (2000). 3D Numerical Modeling of Flow and Sediment Transport in Open Channels. *ASCE Journal of Hydraulic Engineering*, *126*(1), 4-15.

Zheng, G. (2000). Applications of CFD Tools to Design and Development of Pumps. *Turbomachinery*, *28*(11), 649-656.

Institutional Address of the Authors

Dr. Mauro Iñiguez Covarrubias
Dr. Jorge Flores Velazquez
Dr. Waldo Ojeda Bustamante
Dr. Roberto Mercado Escalante

Instituto Mexicano de Tecnología del Agua
Paseo Cuauhnáhuac 8532, Col. Progreso
62550 Jiutepec Morelos, México
Teléfono: +52 (777) 3 29 36 00
Fax: +52 (777) 319 4220
mic@tlaloc.imta.mx
jorge_flores@tlaloc.imta.mx
wojeda@tlaloc.imta.mx
rmercado@tlaloc.imta.mx

Dr. Carlos Díaz-Delgado

Universidad Autónoma del Estado de México
Centro Interamericano de Recursos del Agua
Facultad de Ingeniería
Carretera Toluca Atlacomulco km 14.5, Unidad San Cayetano
50200 Toluca, Estado de México, México.
Teléfono: +52 (722) 2965 550
cdiazd@uaemex.mx

Technical Note

Fitting of GPA, GLO and GEV Distributions with Trimmed *L*-moments (1,0)

• Daniel Francisco Campos-Aranda •
Profesor Jubilado de la Universidad Autónoma de San Luis Potosí, México
*Corresponding Author

Abstract

Campos-Aranda, D. F. (July-August, 2015). Technical Note. Fitting of GPA, GLO and GEV Distributions with Trimmed L-moments (1,0). *Water Technology and Sciences* (in Spanish), 6(4), 153-167.

Statistical moments have been used to characterize probability distributions and samples of observed data. This work briefly describes the theory of *L*-moments and trimmed *L*-moments (1,0), which can reduce the influence of the lowest value in a sample, in order to improve the fit and obtain more reliable extreme predictions. Recent equations found in the statistical literature that estimate the location, scale and shape of the probability distribution functions are cited, which are often used to analyze the frequencies of extreme hydrological data. These include the General Extreme Values (GEV), Generalized Logistic (GLO) and Generalized Pareto (GPA) equations. These three distributions were fitted with the methods of L-moments and trimmed *L*-moments (1,0) to 21 annual maximum flow registries from Hydrological Region No. 10 (Sinaloa). The quality of each fit was evaluated based on the standard error. The analysis of the results indicate that the GPA distribution provides the smallest fitting errors for 13 registries using the trimmed *L*-moments (1,0) and for the rest of the registries using *L*-moments. The conclusions suggest that the three probabilistic models studied can be applied with the trimmed *L*-moments (1,0) as an advanced version of the *L*-moments procedure which is universally used.

Keywords: *L*-moments, trimmed *L*-moments (1,0), probability distributions GEV, GLO and GPA, standard error of fit, Hydrological Region No. 10 (Sinaloa).

Resumen

Campos-Aranda, D. F. (julio-agosto, 2015). Nota técnica. Ajuste de las distribuciones GVE, LOG y PAG con momentos L depurados (1,0). Tecnología y Ciencias del Agua, *6(4), 153-167.*

Los momentos estadísticos han sido utilizados para caracterizar las distribuciones de probabilidad, así como las muestras de datos observados. En este trabajo se describe someramente la teoría de los momentos L y de los llamados momentos L depurados (1,0), que son capaces de reducir la influencia del valor más bajo de la muestra, para mejorar el ajuste y obtener predicciones extremas más confiables. Se citan las ecuaciones, recientemente expuestas en la literatura estadística, que permiten estimar los parámetros de ubicación (u), escala (a) y forma (k) de las tres funciones de distribución de probabilidades más utilizadas en los análisis de frecuencias de datos hidrológicos extremos, que son la General de Valores Extremos (GVE), la Logística Generalizada (LOG) y la Pareto Generalizada (PAG). Estas tres distribuciones se ajustaron con los métodos de momentos L y momentos L depurados (1,0), a los 21 registros de gasto máximo anual disponibles en la Región Hidrológica núm. 10 (Sinaloa). Se evaluó la calidad de cada ajuste a través del error estándar. El análisis de los resultados indica que la distribución PAG conduce a los menores errores de ajuste en trece registros con el método de los momentos L depurados (1,0) y en el resto con el de momentos L. Las conclusiones sugieren la aplicación sistemática de los tres modelos probabilísticos utilizados y del método de los momentos L depurados (1,0), como una versión avanzada del procedimiento de los momentos L, actualmente de uso universal.

***Palabras clave**: momentos L, momentos L depurados (1,0), distribuciones de probabilidad GVE, LOG y PAG, error estándar de ajuste, Región Hidrológica núm. 10 (Sinaloa).*

Received: 05/03/15
Accepted: 11/05/15

Introduction

Statistical moments have been traditionally used to characterize *probability distribution functions* (PDF) or observed data series. The more recent *L*-moments are linear combinations of the expected values of the order statistics (Asquith, 2011). They are comparable to conventional moments but have lower sampling variances and are more robust to the influence of dispersed or extreme values (outliers). Similar to statistical moments, first to fourth *L*- moments also characterize location, scale, skewness and kurtosis, respectively.

According to Karvanen (2006), the concept of *L*-moments was introduced in the late 1960s with various unconnected results about linear combinations of order statistics, culminating with works by Greenwood, Landwehr, Matalas and Wallis (1979). Hosking (1990) unified the *L*-moments theory and provided guides for its practical application which have been used in hydrology, meteorology, quality control and civil engineering. Karavan (2006) also cited recent theoretical advances, including: (1) Mudholkar and Hutson (1998) who replaced the expected values of the order statistics with functionals which provide quick estimators such as the median, the Gastwirth estimator and truncated mean. These analogs, called *LQ* moments, also exist and are simple to evaluate. (2) Elamir and Seheult (2003) introduced a natural extension of *L*-moments, called trimmed moments (*TL*), which means truncated or cut; (3) Elamir and Seheult (2004) also derived the exact structure of the sampling variance from *L*-moments.

Meanwhile, frequency analyses related to hydrology, floods, maximum rainfall and droughts primarily look for the values of these data that are associated with low exceedance probabilities. These magnitudes, called *predictions*, are obtained by fitting a PDF to the available sample data. The PDF most commonly used by these studies, and whose application has even been established as a rule, include General Extreme Values (GEV), Generalized Logistic (GLO) and Generalized Pareto (GPA) probabilistic models. Frequency analyses have adopted these PDF because of their heavy tail, which is the portion where the predictions are estimated (El Adlouni, Bobée, & Ouarda, 2008).

The objective of this work is to provide a detailed presentation of theoretical aspects related to *trimmed L-moments*, especially in regard to the elimination of the lowest value in a series or sample data and the fitting of GEV, GLO and GPA distributions. This is complemented with numerical comparisons of 21 annual flood records from Hydrological Region No. 10 (Sinaloa), where runoff is not affected by reservoirs. These records contained over 20 data corresponding to information updated as of the year 2011, provided by the National Water Commission (Conagua, Spanish acronym).

Summary of the Operating Theory

*Population Definition for **L**-moments*

Let X be a random variable and $X_{j:n}$ one of its order statistics, that is, a random variable distributed as the j^{nth} smallest element in a random sample of size n, taken from the distribution of X. Then, the *L*-moments of X are as follows(Hosking, 1990):

$$\lambda_1 = \mathrm{E}\left(X_{1:1}\right) \tag{1}$$

$$\lambda_2 = \frac{1}{2}\mathrm{E}\left(X_{2:2} - X_{1:2}\right) \tag{2}$$

$$\lambda_3 = \frac{1}{3}\mathrm{E}\left(X_{3:3} - 2X_{2:3} + X_{1:3}\right) \tag{3}$$

$$\lambda_4 = \frac{1}{4}\mathrm{E}\left(X_{4:4} - 3X_{3:4} + 3X_{2:4} - X_{1:4}\right) \tag{4}$$

whose general expression is:

$$\lambda_r = \frac{1}{r}\sum_{j=0}^{r-1}(-1)^j \binom{r-1}{j} \mathrm{E}\left(X_{r-j:r}\right) \qquad r = 1, 2, \ldots \tag{5}$$

In equation (5), the second parenthesis is a quotient of the factorials which define the number of possible combinations of m terms, taking q in each arrangement. Its general expression (Bhattarai, 2004; Asquith, 2011) is:

$$\binom{m}{q} = \frac{m!}{q!\,(m-q)!} \quad \text{for} \quad q \le m \qquad (6)$$

Conventionally, 0! = 1. Remembering that the Gamma function is $\Gamma(m+1) = m!$, which can be estimated with the Stirling formula (Davis, 1965), as described below. The expected values of the order statistics represented by equation (5) will be estimated with the expression (Hosking & Wallis, 1997; Kottegoda & Rosso, 2008; Asquith, 2011):

$$\mathrm{E}\left(X_{r:n}\right) = \frac{n!}{(r-1)!\,(n-r)!}\int_0^1 x(F)\cdot F^{r-1}\cdot(1-F)^{n-r}\,dF \qquad (7)$$

where $x(F)$ is the *quantile function* or inverse solution of the accumulated probability distribution function $F(x) = F$.

Population Corresponding to Trimmed L-*Moments and the Sample*

As was briefly indicated, *L*-moments are used in ways that are similar to conventional moments and are relatively robust to the effects of extreme values. In addition, the mean of the distribution always exists, although some higher order moments may not. Hosking (2007) indicated that these two advantages are not sufficient to manage certain data having many outliers and PDF with very heavy tails, since the first moment may not exist. *Trimmed* L-*moments* are generalizations that do not require the existence of the mean of the supporting PDF, and is generally defined as (Elamir & Seheult, 2003; Hosking, 2007):

$$\lambda_r^{(s,t)} = \frac{1}{r}\sum_{j=0}^{r-1}(-1)^j\binom{r-1}{j}\mathrm{E}\left(X_{r+s-j:r+s+t}\right) \quad r = 1, 2, \ldots \qquad (8)$$

where s and t are positive whole numbers. The trimmed term, or truncated or cut, is suitable given that the definition of $\lambda_r^{(s,t)}$ does not involve the expected values of the order statistics of s data or smaller values, or t values larger than the sample size $r + s + t$; that is, they are assigned a weight of zero. The trimmed *L*-moment quotients $\tau_r^{(s,t)} = \lambda_r^{(s,t)} / \lambda_2^{(s,t)}$ are dimensionless measurements of the shape of the distribution. Hosking (2007) indicated that one question to be decided is the appropriate degree of trimming and that the inspection of the data in the sample can help with this selection. Recently, Elamir (2010) found that the amount of trimming results in the estimators having different variances. Therefore, an optimal selection will be the minimum sum of absolute errors between the data and the estimates, by fitting the PDF with these trimmed *L*-moments.

Given an ordered sample $\left(x_{1} \le x_{2} \le \cdots \le x_{n}\right)$, the trimmed *L* moments $\lambda_r^{(s,t)}$ can be estimated in an unbiased manner with the following expression (Elamir & Seheult, 2003; Hosking, 2007):

$$l_r^{(s,t)} = \frac{1}{r}\sum_{i=s+1}^{n-t}\left[\frac{\sum_{j=0}^{r-1}(-1)^j\cdot\binom{r-1}{j}\cdot\binom{i-1}{r+s-j-1}\cdot\binom{n-i}{t+j}}{\binom{n}{r+s+t}}\right]\cdot x_i \qquad (9)$$

Populations Corresponding to Trimmed L-*Moments (1,0) and the Sample*

Ahmad, Shabri and Zakaria (2011b) reported that trimmed *L*-moments were introduced by Elamir and Seheult (2003) as an option to use with outliers. They are easy to calculate and more robust than *L*-moments to the presence of these atypical data, or outliers. They also indicate that most of the works that apply trimmed *L*-moments have focused on symmetrical cases and generally suppress the lowest and highest values in the concep-

tual sample ($s = t = 1$). For example, Abdul-Moniem and Selim (2009), and Bílková (2014) proposed the use of trimmed *L*-moments (1,0) in which only the lowest value in a sample is eliminated, in order to obtain a better fit of the PDF to higher outliers. Based on equation (8) and with $s = 1$ and $t = 0$, the following four first trimmed *L*-moments (1,0) are defined, according to Ahmad *et al.* (2011b):

$$\lambda_1^{(1,0)} = \mathrm{E}(X_{2:2}) \tag{10}$$

$$\lambda_2^{(1,0)} = \frac{1}{2}\mathrm{E}(X_{3:3} - X_{2:3}) \tag{11}$$

$$\lambda_3^{(1,0)} = \frac{1}{3}\mathrm{E}(X_{4:4} - 2X_{3:4} + X_{2:4}) \tag{12}$$

$$\lambda_4^{(1,0)} = \frac{1}{4}\mathrm{E}(X_{5:5} - 3X_{4:5} + 3X_{3:5} - X_{2:5}) \tag{13}$$

The the population quotients of trimmed *L*-skewness and *L*-kurtosis are, respectively:

$$\tau_3^{(1,0)} = \frac{\lambda_3^{(1,0)}}{\lambda_2^{(1,0)}} \tag{14}$$

$$\tau_4^{(1,0)} = \frac{\lambda_4^{(1,0)}}{\lambda_2^{(1,0)}} \tag{15}$$

The unbiased estimations of trimmed moments (1,0) are based on a sample (x_i) of progressively ordered data and obtained using a modification of equation (8):

$$l_r^{(1,0)} = \frac{1}{r}\sum_{i=2}^{n}\left[\frac{\sum_{j=0}^{r-1}(-1)^j\binom{r-1}{j}\cdot\binom{i-1}{r-j}\cdot\binom{n-i}{j}}{\binom{n}{r+1}}\right]\cdot x_i \tag{16}$$

Abdul-Moniem and Selim (2009) applied *L*-moments and symmetrical trimmed *L*-moments ($s = t = 1$) by fitting the Generalized Pareto. With known shape parameters (k), the location (u) and scale (a) parameters were estimated using synthetic samples of size 10(10)40, with 10,000 replications each, in which $u = 2$ and $a = 0.20(0.20)1.40$. They found that the mean quadratic error (MQE) between the estimated and real or assigned values decreased as n and the scale parameter increased, but this error was always less for the estimations performed with trimmed *L*-moments.

Ahmad *et al.* (2011b) also used the Generalized Pareto and with random simulation found that the trimmed *L*-moments (1,0) reduced the probable influence of the smallest datum in the sample when estimating events with high return periods. Results from the use of real data showed that trimmed *L*-moments (1,0) are better than *L*-moments in some cases, particularly to predict low- exceedance probability.

Ahmad, Shabri and Zakaria (2013) compared GEV, GLO and GPA fitted with *L*-moments and trimmed moments (1,0) and (1,1), based on 12 annual maximum flow records from northeast Malasia. They found that trimmed moments (1,0) provide better fits for most of the records processed.

Fitting the GEV, GLO and GPA with L-moments

According to Hosking and Wallis (1997) and their Table 5.1, when the shape parameter $k < 0$ these three probability distribution functions (PDF) have heavier tails than all the others typically used to perform frequency analyses with hydrological data. In addition, when $k > 0$ their boundary is higher and when $k = 0$ two-parameter distributions are defined (logistic and exponential Gumbel).

The use of *L*-moments to obtain the location, scale and shape parameters (u, a and k) corresponding to the GEV, GLO and GPA distribution can be consulted in Stedinger,

Vogel and Foufoula-Georgiou (1993), Hosking and Wallis (1997), and Rao and Hamed (2000), respectively. The mathematical formulas $F(x)$, inverse solutions or quantile functions $x(F)$ and the equations needed to estimate the three fit parameters for each of these PDF will be presented next.

General Extreme Values Distribution (GEV)

Interval of x: $u + a/k \leq x \infty$ when $k < 0$; $- \infty < x < \infty$ when $k = 0$ and $- \infty\ x \leq u + a/k$ when $k > 0$.

$$F(x) = e^{-e^{-y}} \tag{17}$$

where y is the reduced variable:

$$y = -\frac{1}{k}\ln\left[1 - k\left(\frac{x-u}{a}\right)\right] \quad \text{for } k \neq 0 \tag{18}$$

$$y = \frac{x-u}{a} \quad \text{for } k = 0 \tag{19}$$

$$x(F) = u + \frac{a}{k}\left[1 - \left(-\ln F\right)^{k}\right] \quad \text{for } k \neq 0 \tag{20}$$

$$x(F) = u - a \cdot \ln(-\ln F) \quad \text{for } k = 0 \tag{21}$$

$$c = \frac{2}{3 + t_3} - 0.63093 \tag{22}$$

$$k \cong 7.8590 \cdot c + 2.9554 \cdot c^2 \tag{23}$$

$$a = \frac{l_2 \cdot k}{\left(1 - 2^{-k}\right) \cdot \Gamma\left(1 + k\right)} \tag{24}$$

$$u = l_1 - \frac{a}{k}\left[1 - \Gamma\left(1 + k\right)\right] \tag{25}$$

The factorial Gamma function was estimated using the Stirling formula (Davis, 1965), which for large values of ε is quite accurate, with an error near zero, and is given by:

$$\Gamma\left(\varepsilon\right) \cong e^{-\varepsilon} \cdot \varepsilon^{\varepsilon - 1/2} \cdot \sqrt{2\pi} \cdot \left(1 + \frac{1}{12 \cdot \varepsilon} + \frac{1}{288 \cdot \varepsilon^2} - \frac{139}{51\,840 \cdot \varepsilon^3} - \frac{571}{2\,488\,320 \cdot \varepsilon^4} + \cdots\right) \tag{26}$$

Generalized Logistic Distribution

The interval of the GEV identified by the interval of x:

$$F(x) = \frac{1}{1 + e^{-y}} \tag{27}$$

where y is equal to equation (18):

$$x(F) = u + \frac{a}{k}\left\{1 - \left[\frac{\left(1-F\right)}{F}\right]^{k}\right\} \quad \text{for } k \neq 0 \tag{28}$$

$$x(F) = u - a \cdot \ln\left[\frac{\left(1-F\right)}{F}\right] \quad \text{for } k = 0 \tag{29}$$

$$k = -t_3 \tag{30}$$

$$a = \frac{l_2 \cdot \sin\left(\pi \cdot k\right)}{\pi \cdot k} \tag{31}$$

$$u = l_1 - a\left(\frac{1}{k} - \frac{\pi}{\sin\left(\pi \cdot k\right)}\right) \tag{32}$$

Pareto Generalized Distribution

Interval of : x: $u \leq x < \infty$ when $k \leq 0$; $u \leq x \leq u + a/k$ *when* $k > 0$

$$F(x) = 1 - e^{-y} \tag{33}$$

where y is equal to equation (18):

$$x(F) = u + \frac{a}{k}\left[1 - \left(1 - F\right)^{k}\right] \quad \text{for } k \neq 0 \tag{34}$$

$$x(F) = u - a \cdot \ln\left(1 - F\right) \quad \text{for } k = 0 \tag{35}$$

$$k = \frac{\left(1 - 3t_3\right)}{\left(1 + t_3\right)} \tag{36}$$

$$a = l_2\left(1 + k\right) \cdot \left(2 + k\right) \tag{37}$$

$$u = l_1 - l_2\left(2 + k\right) \tag{38}$$

Fitting of the GEV, GLO and the GPA distributions with trimmed L*-moments (1,0)*

Ahmad, Shabri and Zakaria (2011a) and Ahmad *et al.* (2013) obtained the expression to estimate the three fit parameters of these distribution based on trimmed *L*-moments (1,0), these are:

General Extreme Values Distribution

$$k = 0.4813 - 2.1364 \cdot t_3^{(1,0)} + 0.6994\ (t_3^{(1,0)})^2 - 0.1991 \cdot (t_3^{(1,0)})^3 \tag{39}$$

$$a = \frac{-2(6)^k \cdot l_2^{(1,0)} \cdot \left[1/\Gamma\left(k\right)\right]}{3\ \left(2^k - 3^k\right)} \tag{40}$$

$$u = l_1^{(1,0)} - \frac{a}{k} + \frac{a}{2^k \cdot \left[1/\Gamma\left(k\right)\right]} \tag{41}$$

Equation (39) was obtained based on the expression of t_3 in function of k as proposed by Ahmad *et al.* (2013), which is valid in the interval of k = -0.70 to 0.50. The reciprocal of the Gamma function was estimated with the following formula, from Euler's infinite product (Davis, 1965), which was evaluated for np = 50. With this, its five decimal places do not change:

$$1/\Gamma\left(z\right) = z \cdot e^{\gamma \cdot z} \prod_{np=1}^{\infty} \left[\left(1 + \frac{z}{np}\right) \cdot e^{-z/np}\right] \tag{42}$$

where γ = 0.5772156649, the Euler constant with the indicated approximate value. The function $1/\Gamma(z)$ is continuous and passes through zero at points z = 0, -1, -2, -3, ...

Generalized Logistic Distribution

$$k = \frac{4 - 27 \cdot t_3^{(1,0)}}{20} \tag{43}$$

$$a = \frac{4 \cdot k \cdot l_2^{(1,0)}}{6 \cdot \Gamma(2-k) \cdot \Gamma(1+k) - 3 \cdot \Gamma(3-k) \cdot \Gamma(1+k)} \tag{44}$$

$$u = l_1^{(1,0)} - \frac{a}{k} + \frac{a \cdot \Gamma(2-k) \cdot \Gamma(1+k)}{k} \tag{45}$$

Generalized Pareto Distribution

$$k = \frac{4 - 12 \cdot t_3^{(1,0)}}{4 + 3 \cdot t_3^{(1,0)}} \tag{46}$$

$$a = \frac{l_2^{(1,0)}\left(1 + k\right) \cdot \left(2 + k\right) \cdot \left(3 + k\right)}{3} \tag{47}$$

$$u = l_1^{(1,0)} - a\left[\frac{3 + k}{\left(1 + k\right) \cdot \left(2 + k\right)}\right] \tag{48}$$

Quantitative Indicator of Fit

Coles (2001) indicated that the reason to fit a PDF to data is to obtain conclusions about the population from which the available values are probably derived. Since the reliability of these conclusions depends on the accuracy of the fitted PDF, it is necessary to verify that the probabilistic model can reproduce the data used for the estimation (Flowers-Cano, Flowers, & Rivera-Trejo, 2014).

In the mid 1970s, the standard error of fit (SEF) was established as a quantitative measurement that estimates the statistical quality of the fit and also makes it possible to objectively compare different probability dis-

tributions that are tested or fitted to a sample, since the units of the data are already known. Its expression is (Kite, 1977):

$$EEA = \sqrt{\frac{\sum_{i=1}^{n}\left(x_i - \hat{x}_i\right)^2}{n - npa}} \qquad (49)$$

where n is the number of data in the sample; x_i are the data in order of lower to higher; $\hat{x}_i$ the values estimated with the quantile function or the inverse solution using the three fit parameters (u, a, k) which are tested for a non-exceedance probability $P(X < x)$, estimated with the Weibull formula (Benson, 1962):

$$P(X < x) = \frac{m}{n+1} \qquad (50)$$

in which m is the order number of the datum, where 1 is the smallest and n is the largest. Lastly, npa is the number of fit parameters, which is three for the GEV, GLO and PGA distributions.

Qualitative Indicators of Fit

Two diagnostic graphs have recently become popular— *Probabilities* and *Quantities* (Coles, 2001; Wilks, 2011). The probabilities graph represents the empirical probability estimated by equation (5) on the x-axis and the probability that defines the model for each available datum on the y-axis, in order of increasing magnitude $\left(x_{1} \le x_{2} \le \cdots \le x_{n}\right)$, which is estimated with equations (17), (27) and (33) for the GEV, GLO and PGA distributions, respectively. The quantities graph represents the value of the observed data $\left(x_{1} \le x_{2} \le \cdots \le x_{n}\right)$ on the x-axis and the value estimated with the inverse solution of the model on the y-axis—that is, equations (20), (28) and (34) for the GEV, GLO and PGA functions, respectively, for the empirical probability estimated with equation (50). In summary, the x and y coordinates of each graph are (Coles, 2001):

Probabilities

$$\left[\left(\frac{i}{n+1}, F(x_i)\right) : i = 1,\ 2, \cdots, n\right] \qquad (51)$$

Quantities

$$\left[\left(x_i, x\left(\frac{i}{n+1}\right)\right) : i = 1,\ 2, \cdots, n\right] \qquad (52)$$

Description of the Numerical Application

Hydrometric Records Processed

The numerical application described uses 21 annual maximum flow records from Hydrological Region No. 10 (Sinaloa). The runoff at these hydrometric stations was not affected by reservoirs and the records contained over 20 years of data from the BANDAS system (IMTA, 2002). The records from the Huites and Guamuchil hydrometric stations extended up to the year in which the reservoir was built, which affected runoff. The data from the San Francisco stations were taken from *Hydrological Bulletin 36* (SRH, 1975). This hydrometric information had been updated by the National Water Commission (Conagua) and 12 records were expanded with data up to the year 2011 (Santa Cruz, Jaina, Palo Dulce, Ixpalino, Chinipas, Tamazula, Acatitán, Choix, Badiraguato, Zopilote, Chico Ruiz and El Bledal stations). The first five columns of Table 1 show the overall characteristics of the records processed, in order of decreasing basin size. The shortest record contained 23 years and the largest 60 years, with a median of 33. Campos-Aranda (2014a) present a map with the locations of the 21 hydrometric stations processed and their respective drainage basins.

Statistical Tests Performed with the Records

To verify the statistical quality of the hydrometric records that were processed, one general test was applied as well as six specific tests, The latter included tests for persistence (Anderson and Sneyers), trends (Kendall and Spearman), too much or too little variability (Bartlett) and change in the mean (Cramer). The general test used was the Von Neumann test for randomness against unspecified deterministic components. All of these tests can be found in WMO (1971), and Machiwal and Jha (2008, 2012).

The Von Neumann test identified only two non-homogeneous records (Choix and Pericos), both of which had persistence according to the Anderson and Sneyers tests. Three records (Santa Cruz, Jaina and Acatitán) had descending trends and one (Badiraguato) had a slight increasing trend according to the Kendall and Spearman tests. Given that years were missing in the records that had a descending trend (primarily during the last periods from 1995 to 2011), they were considered susceptible for probabilistic processing since this deterministic component can be caused by the lack of continuity.

Trimmed L-*Moments (1,0)*

These moments were calculated based on equation (16), which are shown in columns 6, 7 and 8 in Table 1. The last column in this table presents the skewness quotient evaluated according to equation (14).

Table 1. General characteristics and trimmed *L*-moments (1,0) for the 21 annual maximum flow records from the hydrometric stations indicated, Hydrological Region No. 10 (Sinaloa).

No.	Hydrometric station	Basin area (km²)	Years of records (*n*)	$l_1 = l_1^{(0,0)}$	$l_1^{(1,0)}$	$l_2^{(1,0)}$	$l_3^{(1,0)}$	$t_3^{(1,0)}$
1	Huites	26 057	1942-1992 (51)	3328.333	4854.961	1706.992	802.426	0.4701
2	San Francisco	17 531	1941-1973 (33)	1724.636	2444.118	769.869	312.918	0.4065
3	Santa Cruz	8 919	1944-2011 (56)	972.500	1464.255	525.671	247.989	0.4718
4	Jaina	8 179	1942-2011 (60)	973.850	1441.582	519.757	259.900	0.5000
5	Palo Dulce	6 439	1958-1986 (26)	1083.423	1552.551	551.855	320.997	0.5817
6	Ixpalino	6 166	1953-2009 (46)	1191.891	1663.188	510.515	251.830	0.4933
7	La Huerta	6 149	1970-1999 (28)	945.107	1272.204	258.448	10.619	0.0411
8	Chinipas	5 098	1965-2008 (33)	981.030	1310.680	308.185	81.948	0.2659
9	Tamazula	2 241	1963-1999 (33)	593.909	772.023	181.468	78.403	0.4321
10	Naranjo	2 064	1939-1984 (45)	633.311	965.053	350.734	136.605	0.3895
11	Acatitán	1 884	1955-2008 (49)	797.878	1242.170	462.272	182.957	0.3958
12	Guamúchil	1 645	1940-1971 (32)	702.344	1003.141	319.356	141.162	0.4420
13	Choix	1 403	1956-2005 (41)	334.927	469.731	143.144	66.263	0.4629
14	Badiraguato	1 018	1960-1999 (40)	1033.350	1650.228	763.269	464.662	0.6088
15	El Quelite	835	1961-2001 (33)	479.091	697.343	216.313	71.132	0.3288
16	Zopilote	666	1939-2010 (60)	337.117	493.580	143.607	29.706	0.2069
17	Chico Ruiz	391	1977-2006 (23)	206.343	296.257	79.715	12.380	0.1553
18	El Bledal	371	1938-1994 (57)	288.895	411.405	126.451	53.259	0.4212
19	Pericos	270	1961-1992 (30)	250.800	336.685	81.431	22.299	0.2773
20	La Tina	254	1960-1983 (24)	104.958	165.297	67.297	36.277	0.5391
21	Bamícori	223	1951-1983 (33)	189.182	280.225	94.765	33.181	0.3501

Standard Error of Fit

Based on the *L*-moments and their quotients (Hosking & Wallis, 1997; Campos-Aranda, 2014a), the three fit parameters corresponding to the GEV, GLO and PGA distributions were obtained using equations (22) through (26), (30) to (32) and (36)to (38), respectively. After using their inverse solutions, equations (20), (28) and (34), estimations were performed of INSERTAR SIMBOLO or the predictions needed to apply equation (49), corresponding to the standard error of fit (SEF). The results are shown in Table 2 in the columns indicated by "moL."

In a similar manner but using the values of the trimmed *L*-moments (1,0) from Table 1, the three fit parameters were estimated for the GEV, GLO and PGA functions with equations (39) to (42), (43) to (45) and (46) to (48), respectively. Next, based on their inverse solutions, expressions (20), (28) and (34), the values of $\hat{x}_i$ were obtained to determine the standard errors of fit, which are shown in Table 2 in the columns marked as "moLD".

Diagnostic Graphs

Figures 1 and 2 show the probability graphs corresponding to the records from the San Francisco hydrometric station, with $n = 33$, for the GEV and PGA distributions. In general, the PGA shows a better fit with all the data from the sample, especially for low values for which the GEV had the largest spread.

Table 2. Standard errors of fit (m^3/s) obtained with the *L*-moments and trimmed *L*-moments (1,0), for the hydrometric stations shown, Hydrological Region No. 10 (Sinaloa).

No.	Hydrometric station	Standard errors of fit (*SEF*)						Relative error of the maxmium *SEF* (%)
		GEV		GLO		GPA		
		moL	moLD	moL	moLD	moL	moLD	
1	Huites	979	925	1061	976	834	(822)	29.1
2	San Francisco	377	351	419	385	302	(295)	42.0
3	Santa Cruz	388	389	402	398	393	(378)	6.3
4	Jaina	349	352	369	362	337	(335)	10.1
5	Palo Dulce	745	763	767	765	(716)	743	7.1
6	Ixpalino	346	354	366	364	(335)	337	9.3
7	La Huerta	96	134	124	211	(53)	54	298.1
8	Chinipas	101	102	118	123	90	[90]	36.7
9	Tamazula	144	145	148	148	146	(142)	4.2
10	Naranjo	156	148	173	164	127	(124)	39.5
11	Acatitán	189	191	210	207	176	(174)	20.7
12	Guamúchil	235	236	247	243	(225)	226	9.8
13	Choix	101	102	106	105	99	(98)	8.2
14	Badiraguato	838	836	888	829	808	(801)	10.9
15	El Quelite	87	86	98	98	74	[74]	32.4
16	Zopilote	51	56	63	79	28	(27)	192.6
17	Chico Ruiz	28	33	35	44	[17]	17	158.8
18	El Bledal	64	65	67	67	69	(64)	7.8
19	Pericos	29	28	33	34	(24)	25	41.7
20	La Tina	90	92	92	93	(87)	90	6.9
21	Bamícori	52	49	57	54	43	(41)	39.0

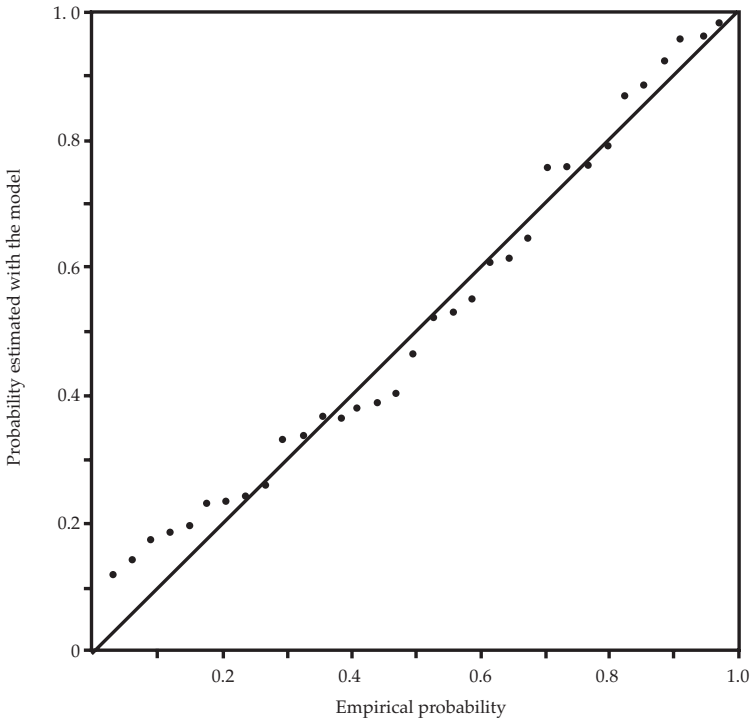

Figure 1. Probability graph for the yearly floods records from the San Francisco hydrometric stations, by fitting the GEV distribution with a *SEF* = 351 m^3/s.

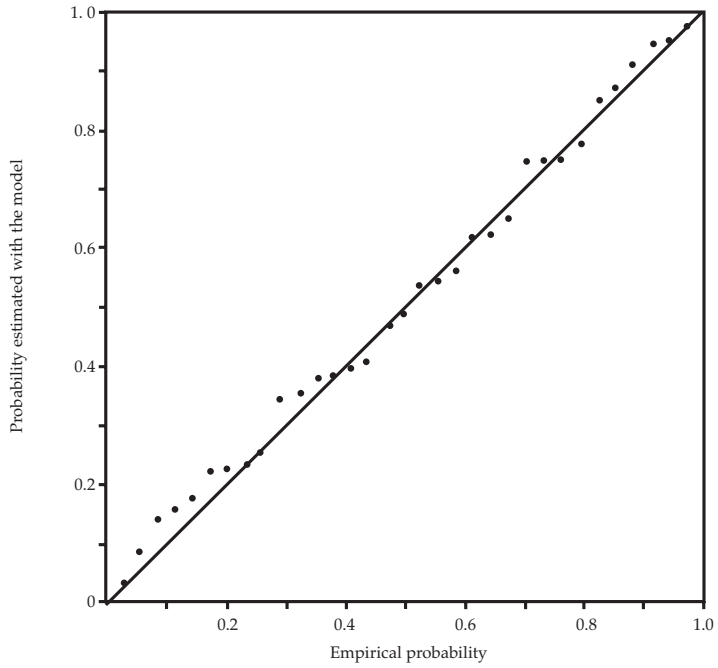

Figure 2. Probability graph for the yearly floods records from the San Francisco hydrometric stations, by fitting the GPA distribution with a *SEF* = 295 m^3/s.

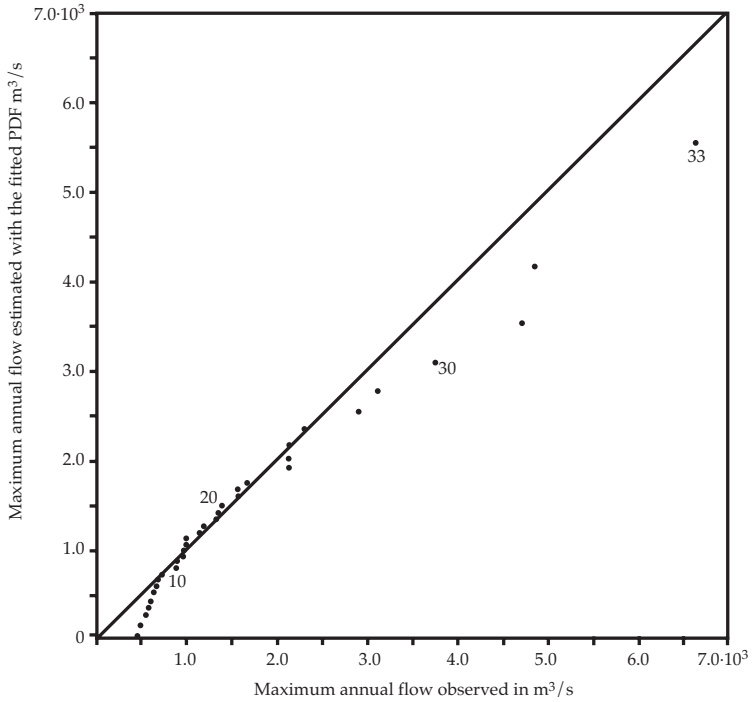

Figure 3. Probability graph for the yearly floods records from the San Francisco hydrometric stations, by fitting the GLO distribution with a *SEF* = 385 m³/s.

The graphs of quantities for GLO and PGA distributions are shown in Figures 3 and 4, for the same records from the San Francisco station. An excellent fit was found with the PGA function for low values and neither functions could reproduce high values in the records, beginning with datum 28.

Analysis of the Results and Design Predictions

The numbers in parenthesis in Table 2 represent the lowest standard error of fit values. The PGA distribution resulted in the lowest values for all the records and therefore its predictions are presented in Table 3. Campos-Aranda (2014b) describe several simple methods for the fit of the PGA function.

Three records (Chinipas, El Quelite and Chico Ruiz stations) resulted in equal SEF values and for these cases the highest predictions by the *L*-moments and the trimmed *L*-moments (1,0) methods were adopted, which are indicated in brackets in Table 2. It is worth mentioning that in the first two records cited, the fit of the PGA distribution with trimmed *L*-moments (1,0) resulted in the highest predictions for high return periods.

It is also worth noting that fitting the PGA function with trimmed *L*-moments (1,0) resulted in a lower SEF for over half (14) of the 21 records processed. This shows that the method gives more weight to larger data values through a better fit of the PDF.

With trimmed *L*-moments (1,0) appreciably lower SEF were obtained from the fit of the GEV distribution for some of the records (Huites, San Francisco, Naranjo, Badiraguato

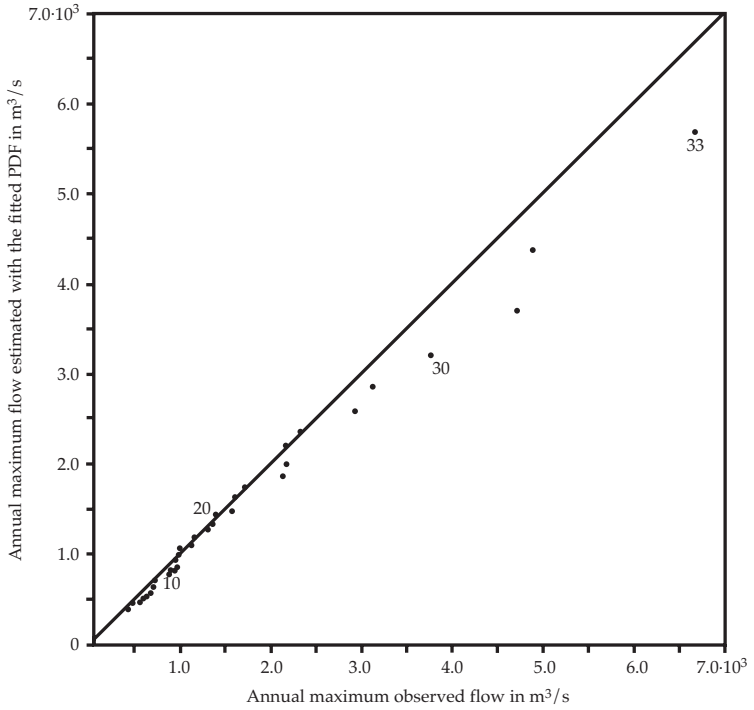

Figure 4. Graph of quantities for annual flood records from the San Francisco station, by fitting the PGA distribution with a *SEF* = 295 m³/s.

and Bamícori). With the GLO function, this also occurred with the same records in addition to those from Jaina and Guamuchil.

When individually comparing the predictions shown in Table 3 with those adopted by Campos-Aranda (2014a), corresponding to the GEV, GLO and Log-Pearson type 3 distributions, a high similarity can be seen in all the hydrometric stations up to a return period of 100 years. Nevertheless, with some of the records, the PGA function resulted in the lowest predictions for high return periods (> 100 years). The last column of Table 2 shows the maximum relative error of the SEF, calculated with the following expression:

$$RE = \frac{SEF_M - SEF_m}{SEF_m} 100 \qquad (53)$$

where SEF_M and SEF_m are the standard errors of the maximum and minimum fits corresponding to the six values calculated. The RE from the La Huerta, Zopilote y Chico Ruiz stations stand out, whose records lacked outliers. This is because the from parameter (k), estimated with the *L*-moments from the PGA distribution, was positive for all three stations. The GEV function also resulted positive for La Huerta while for the other two stations it was near zero. For these three records, the fit of the GEV and GLO distributions with the trimmed *L*-moments (1,0) resulted in SEF that were higher than those obtained with the *L*-moments method, which indicates that it is not useful to eliminate the lowest datum.

Conclusions

The numerical results from this work indicate that the Generalized Pareto distribution is a useful probabilistic model to test with flood frequency analyses and other extreme hy-

Table 3. Predictions (m^3/s) obtained with the Generalized Pareto distribution for the 21 yearly flood records from the hydrometric stations shown, Hydrological Region No. 10 (Sinaloa).

No.	Hydrometric station	Fitting method	Return periods, in years						
			5	10	25	50	100	500	1 000
1	Huites	moLD	4 480	6 760	10 612	14 326	18 909	34 121	43 336
2	San Francisco	moLD	2 433	3 500	5 116	6 515	8 086	12 525	14 840
3	Santa Cruz	moLD	1 346	2 047	3 235	4 383	5 804	10 538	13 417
4	Jaina	moLD	1 278	1 951	3 146	4 355	5 910	11 464	15 058
5	Palo Dulce	moL	1 301	1 973	3 251	4 635	6 526	14 025	19 350
6	Ixpalino	moL	1 608	2 307	3 421	4 433	5 622	9 236	11 256
7	La Huerta	moL	1 521	1 764	1 935	2 002	2 041	2 079	2 085
8	Chinipas	moLD	1 442	1 853	2 328	2 642	2 921	3 455	3 645
9	Tamazula	moLD	754	1 003	1 398	1 754	2 171	3 428	4 125
10	Naranjo	moLD	979	1 467	2 184	2 786	3 445	5 226	6 115
11	Acatitán	moLD	1 251	1 894	2 848	3 659	4 555	7 017	8 267
12	Guamúchil	moL	996	1 438	2 111	2 696	3 357	5 237	6 225
13	Choix	moLD	442	634	955	1 261	1 635	2 853	3 580
14	Badiraguato	moLD	1 154	1 966	3 668	5 691	8 689	22 446	33 516
15	El Quelite	moLD	748	1 047	1 440	1 734	2 026	2 696	2 981
16	Zopilote	moLD	579	759	943	1 049	1 133	1 269	1 309
17	Chico Ruiz	moL	348	446	540	593	633	694	710
18	El Bledal	moLD	404	578	849	1 089	1 366	2 177	2 616
19	Pericos	moL	374	480	599	676	742	865	906
20	La Tina	moL	150	239	392	539	722	1 335	1 709
21	Bamícori	moLD	296	428	608	749	893	1 245	1 403

drological data, since it results in the lowest standard errors of fit (*SEF*).

In 10 of the 21 records processed with the numerical application described, the SEF obtained with GEV and GLO distributions were within 10% of the relative error (equation (53)), as seen in the last column in Table 2. Therefore it should be continued to be applied as a norm or rule.

The SEF results shown in Table 2 indicate that in over half of the 21 records processed, the trimmed *L*-moments (1,0) is a good option to reduce errors and obtain the best fits with each of the three probability functions applied (GEV, GLO and PGA). Therefore, its systematic use is suggested as an advanced version of *L*-moments, which already is universally used in hydrological frequency analyses.

Acknowledgements

Thank you to the engineers at Conagua, José Luis Juárez Rubio with the Local San Luis Potosí Department and Alejandro García Ruiz from GASIR, for providing the author with the updated hydrometric information related to the annual floods from 19 gauging stations in Hydrological Region 10 (Sinaloa).

References

Abdul-Moniem, I. B., & Selim, Y. M. (2009). TL-Moments and L-Moments Estimation for the Generalized Pareto Distribution. *Applied Mathematical Sciences*, *3*(1), 43-52.

Ahmad, U. N., Shabri, A., & Zakaria, Z. A. (2011a). Flood Frequency Analysis of Annual Maximum Stream Flows Using L-Moments and TL-Moments Approach. *Applied Mathematical Sciences*, *5*(5), 243-253.

Ahmad, U. N., Shabri, A., & Zakaria, Z. A. (2011b). Trimmed L-Moments (1,0) for the Generalized Pareto Distribution. *Hydrological Sciences Journal*, *56*(6), 1053-1060.

Ahmad, U. N., Shabri, A., & Zakaria, Z. A. (2013). An Analysis of Annual Maximum Stream Flows in Terengganu, Malaysia using TL-Moments Approach. *Theoretical and Applied Climatology*, *111*(3-4), 649-663.

Asquith, W. H. (2011). *Distributional Analysis with L-moment Statistics using the R Environment for Statistical Computing*. Chapter 3: Order Statistics (pp. 47-59) and Chapter 6: L-Moments (pp. 87-122). Texas, USA: Author Edition (ISBN-13: 978-1463508418).

Benson, M. A. (1962). Plotting Positions and Economics of Engineering Planning. *Journal of Hydraulics Division*, *88*(6), 57-71.

Bhattarai, K. P. (2004). Partial L-Moments for the Analysis of Censored Flood Samples. *Hydrological Sciences Journal*, *49*(5), 855-868.

Bílková, D. (2014). Trimmed L-Moments: Analogy of Classical L-Moments. *American Journal of Mathematics and Statistics*, *4*(2), 80-106.

Campos-Aranda, D. F. (2014a). Análisis regional de frecuencia de crecientes en la Región Hidrológica núm. 10 (Sinaloa), México. 2: contraste de predicciones locales y regionales. *Agrociencia*, *48*(3), 255-270.

Campos-Aranda, D. F. (octubre-diciembre, 2014b). Predicción de crecientes usando la distribución Pareto Generalizada ajustada con tres métodos simples. *Revista digital Tláloc*, *65*.

Coles, S. (2001). Theme 2.6.7: Model Diagnostics (pp. 36-44). In *An Introduction to Statistical Modeling of Extreme Values*. London: Springer-Verlag.

Davis, P. J. (1965). Gamma Function and Related Functions. Chapter 6 (pp. 253-296). In M. Abramowitz & I. A. Stegun (Eds.). *Handbook of Mathematical Functions*. New York: Dover Publications.

El Adlouni, S., Bobée, B., & Ouarda, T. B. M. J. (2008). On the Tails of Extreme Event Distributions in hydrology. *Journal of Hydrology*, *355*(1-4), 16-33.

Elamir, E. A. H. (2010). Optimal Choices for Trimming in Trimmed L-Moment Method. *Applied Mathematical Sciences*, *4*(58), 2881-2890.

Elamir, E. A. H., & Seheult, A. H. (2003). Trimmed L-Moments. *Computational Statistics & Data Analysis*, *43*(3), 299-314.

Elamir, E. A. H., & Seheult, A. H. (2004). Exact Variance Structure of Sample L-Moments. *Journal of Statistical Planning and Inference*, *124*(2), 337-359.

Flowers-Cano, R. S., Flowers, R. F., & Rivera-Trejo, F. (2014). Evaluación de criterios de selección de modelos probabilísticos: validación con series de valores máximos simulados. *Tecnología y Ciencias del Agua*, *5*(5), 189-197.

Greenwood, J. A., Landwehr, J. M., Matalas, N. C., & Wallis, J. R. (1979). Probability Weighted Moments: Definition and Relation to Parameters of Several Distributions Expressible in Inverse Form. *Water Resources Research*, *15*(5), 1049-1054.

Hosking, J. R. M. (1990). L-moments: Analysis and Estimation of Distributions Using Linear Combinations of Order Statistics. *Journal of the Royal Statistical Society, B*, *52*(1), 105-124.

Hosking, J. R. M. (2007). Some Theory and Practical Uses of Trimmed *L*-Moments. *Journal of Statistical Planning and Inference*, *137*(9), 3024-3039.

Hosking, J. R. M., & Wallis, J. R. (1997). Chapter 2: L-Moments (pp. 14-43); Chapter 5: Choice Of A Frequency Distribution (pp. 73-86); Appendix: L-Moments For Some Specific Distributions (pp. 191-209). In *Regional Frequency Analysis. An Approach Based on L-moments*. Cambridge, England: Cambridge University Press.

IMTA (2002). *Banco Nacional de Datos de Aguas Superficiales (BANDAS)*. 8 CD. Jiutepec, México: Comisión Nacional del Agua, Secretaría de Medio Ambiente y Recursos Naturales, Instituto Mexicano de Tecnología del Agua.

Karvanen, J. (2006). Estimation of Quantile Mixtures Via L-Moments and Trimmed L-Moments. *Computational Statistics & Data Analysis*, *51*(2), 947-959.

Kite, G. W. (1977). Chapter 12: Comparison of Frequency Distributions (pp. 156-168). In *Frequency and Risk Analyses in Hydrology*. Colorado, USA: Water Resources Publications.

Kottegoda, N. T., & Rosso, R. (2008). Chapter 3: Random Variables and their Properties (pp. 83-164). In *Applied Statistics for Civil and Environmental Engineers*. Chichester, United Kingdom: Blackwell Publishing.

Machiwal, D., & Jha, M. K. (2008). Comparative Evaluation of Statistical Tests for Time Series Analysis: Application to Hydrological Time Series. *Hydrological Sciences Journal*, *53*(2), 353-366.

Machiwal, D., & Jha, M. K. (2012). Chapter 4: Methods for Time Series Analysis (pp. 51-84). In *Hydrologic Time Series Analysis: Theory and Practice*. Dordrecht, The Netherlands: Springer.

Mudholkar, G. S., & Hutson, A. D. (1998). LQ-Moments: Analogs of L-Moments. *Journal of Statistical Planning and Inference*, *71*(1-9), 191-208.

Rao, A. R., & Hamed, K. H. (2000). Chapter 9: The Logistic Distribution (pp. 291-321). In *Flood Frequency Analysis*. Boca Raton, USA: CRC Press.

SRH (1975). *Boletín Hidrológico núm. 36. Región Hidrológica núm. 10 (Sinaloa)*. Tomos I y VI. México, DF: Secretaría de Recursos Hidráulicos, Dirección de Hidrología.

Stedinger, J. R., Vogel, R. M., & Foufoula-Georgiou, E. (1993). Chapter 18: Frequency Analysis of Extreme Events (pp. 18.1-18.66). In D. R. Maidment (Ed.). *Handbook of Hydrology*. New York: McGraw-Hill.

Wilks, D. S. (2011). Theme 4.5: Qualitative Assessments of the Goodness Fit (pp. 112-116). In *Statistical Methods in the Atmospheric Sciences* (3rd edition). San Diego, USA: Academic Press (Elsevier).

WMO (1971). Annexed III: Standard Tests of Significance to Be Recommended in Routine Analysis of Climatic Fluctuations (pp. 58-71). Technical Note No. 79. In *Climatic Change*. Geneva: World Meteorological Organization.

Author's Address

Dr. Daniel Francisco Campos Aranda

Profesor Jubilado de la Universidad Autónoma de San Luis Potosí
Genaro Codina 240, Colonia Jardines del Estadio
78280 San Luis Potosí, San Luis Potosí, México
campos_aranda@hotmail.com

El Pescador Stream, Municipality of Pueblo Nuevo, Durango, Mexico.

Photo: Gerardo Esquivel Arriaga.

Discussion

Technical notes and technical articles are open to discussion according to the following guidelines:

- The discussion will be written in the third person.
- The writer of the discussion shall use the term "commentator" when referring to oneself and the term "author" when referring to the one responsible for the technical note or article.
- The discussion shall be sent within 12 months of the last day of the quarter in which the a technical article or note was published.
- The length of the discussion may be extended by written request from the commentator.
- The discussion is to be presented according to the Guide for Collaborators published in this journal (omitting data referring to the length and abstract). In addition, the bibliographical citation of the technical notes or articles to which the discussion refers shall be included.
- The maximum length of the discussion is 4 journal pages (approximately 10 cuartillas, including figures and tables).
- The figures and tables presented by the commentator shall be progressively marked with Roman numbers and when citing those generated by the author the original numeration should be respected.
- The editors will suppress data that does not pertain to the subject of the discussion.
- The discussion will be rejected if it contains topics addressed by other sources, promotes personal interests, is carelessly prepared, raises controversy involving already established facts, is purely speculative or falls outside the purpose of the journal.
- The discussion will be published along with commentaries from the author or authors to which it refers.
- The discussion will be directed by the editor in chief.

The upper portion of the basin is shown from Bacanton Alto, where differences in forest cover between Guatemala (left) and Mexico (right) can be seen, which reflect good water catchment in the basin below.

Photo: Neptalí Ramírez Marcial.

Guide for Collaborators

The journal ***Water Technology and Sciences*** invites specialists to collaborate with original, unpublished technical articles or notes **related to water, resulting from investigations and provide original contributions**, based on the disciplines of hydrology, hydraulics, water management, water and energy, water quality, and physical, biological and chemical sciences as well as political and social sciences, among other disciplines, according to the guidelines stated below.

PREPARATION OF THE ARTICLE

FORMAT

Font: Palatino throughout the entire document (body of text, tables and figures).

Font Size: Use 8, 9, 10 and 20 points, according to the following table:

8 points (Palatino)	9 points (Palatino)
• Tables. • Figures. • Acknowledgements.	• Name of authors. • Institution of authors. • Abstract. • *Abstract* and *keywords*. • Institutional address of the authors.
10 points (Palatino)	**20 points capital letters (Palatino)**
• Body of the text. • Title of the work in Spanish.	• Title of the work in English.

Line Spacing: double-spaced.

Page Numbers: all pages shall be numbered.

Length

Technical article: **30 pages** (numbered), including figures and tables.

Technical note: **10 pages** (numbered), including figures and tables.

CONTENS

Title

The article shall present significant contributions to scientific and technological knowledge pertaining to the specialty. It shall be based on finished works or those that have completed a development cycle. It shall show results from a series of experiences over 1 year or more of investigations and be supported by an adequate bibliographical review. **The basic structure of the text shall contain an introduction, the development and the conclusions**. The classic layout is preferable: abstract, introduction, methodology, results, discussion, conclusion and references.

Title

The title, **written in Spanish and English**, shall be informative and not exceed 12 words.

Abstract

The abstract, **written in Spanish and English**, shall be concise and provide a broad overview of the investigation (objective, method, results and conclusions) without exceeding 250 words.

Key Words

Eight words or key phrases (maximum) shall be provided **in Spanish and English** that facilitate the identification of the information.

Footnotes

Not admitted. The information is to be incorporated into the text.

Acknowledgements

To be included after the text and before the references.

Tables

- One page for each table.
- A list of all the tables cited shall be presented after the references.

Figures

- One page for each figure.
- All the names of the figures shall be included after the tables.
- They should be high-resolution (300 dpi).

Note: When the article is approved by the publication, the author shall send each figure in JPG format with high-resolution (300 dpi).

References

- The entire bibliography must be referenced in the main body of the text.
- In the case of addressing scientific and technological topics that are common domain, works that denote the knowledge of the authors about the state-of-art shall be cited.
- Avoid self-citations to the extent possible
- APA format shall be used as a basis.

Some examples of references in APA format are:

Complete Books

Last name, A. A. (Year). Title of work. city published: Publisher.
Last name, A. A. (Year). Title of work. Consulted at http://www.xxxxx
Last name, A. A. (Year). Title of work. doi:xxxxx
Last name, A. A. (Ed.). (year).City published: Publisher.

Book Chapters

Last Name, A. A., & Last Name, B. B. (Year).. Title of chapter or entry. In A. Last Name, B. Last Name & C. Last Name (Eds.), Title of book (pp. xxx-xxx). Place: Publisher.
Last Name, A. A., & Last Name, B. B. (Year).. Title of chapter or entry. In A. Last Name, B. Last Name & C. Last Name (Eds.), Title of book (pp. xxx-xxx). Consulted at http://www.xxxxxxx

Newspaper Article or Note Consulted Online

Last Name, A. A., & Last Name, B. B. (Year). Title of article. Title of publication, issue (number), pp. Consulted at http://www.xxxxxxx

That is: Last Name, A. A., & Last Name, B. B. (Year). Title of article. Title of publication, 1(2), 5-17, pp. Consulted at http://www.xxxxxxx

Printed Newspaper Article or Note

Last Name, A. A., & Last Name, B. B. (Year). Article Title. Title of publication, 8(1), 73-82.

Newspaper Article Publication with DOI

Last Name, A. A., & Last Name, B. B. (Year). Article Title. Title of publication, 8(1), 73-82, doi:xxxxxx

Conferences or Symposiums

Collaborator, A. A., Collaborator, B. B., Collaborator, C. C., & Collaborator, D. D. (Month, year). Title of collaboration. In E. E. President (Presidency), Title of symposium. Symposium held at the conference by Name of Organization, Place.

Language

Spanish or English

Separation of numbers and use of decimal points

In *Tecnología and Ciencias del Agua*, the separation between thousands is denoted with a blank space. A decimal point is used to separate whole numbers from fractions. In this regard, refer to Diccionario panhispánico de dudas, edited by the Real Academia Espyearla and the Asociación de Academias de la Lengua Espyearla, in 2005, with respect to numeric expressions: "**the Anglo-Saxon use of the period is accepted, normal in some Hispano-American countries…: $\pi = 3.1416$.".**

Delivery of Article

Send the article in *Word* with the name of the authors and institutional address to **revista.tyca@gmail.com**, with copy to Elizabeth Peña Montiel, elipena@tlaloc.imta.mx.

General Information

The review process will begin once the material is received, during which time the manuscript could be rejected. If the text is suitable for review, having fulfilled the Editorial Policy and the Editorial Committee having determined so, it will proceed to the review stage.

Depending on the review process, the text may be accepted without changes, with minor changes, with extensive changes or rejected.

Once a work is published, the main author has the right to two journals and ten offprints free of charge.

In there are any questions, please write to Helena Rivas López, hrivas@tlaloc.imta.mx or Elizabeth Peña Montiel, elipena@tlaloc.imta.mx

Citations within the body of the text

Type of citation	First appearance in text	Subsequent appearances	Format in parenthesis, first citation in text	Format in parenthesis, subsequent citing in text
Work by one author	Last name (Year)	Last name (Year)	(Last name, year)	(Last name, year)
Work by two authors	Last name and Last name (Year)	Last name and Last name (Year)	(Last name & Last name, Year)	(Last name & Last name, Year)
Work by three authors	Last name, Last name and Last name (Year)	Last name *et al*. (Year)	(Last name, Last name, & Last name, year)	(Last name of first author *et al*., year)
Work by four authors	Last name, Last name, Last name and Last name (Year)	Last name *et al*. (Year)	(Last name, Last name, Last name, & Last name, year)	(Last name of first author *et al*., year)
Work by five authors	Last name, Last name, Last name, Last name and Last name (Year)	Last name *et al*. (Year)	(Last name, Last name, Last name, Last name, & Last name, year)	(Last name of first author *et al*., 2008)
Work by six or more authors	Last name of first author *et al*. (Year)	Last name of first author *et al*. (Year)	(Last name of first author *et al*., Year)	(Last name of first author *et al*., year)
Groups (easily identified with abbreviations) such as authors	Complete name of institution (Acronym, year)	Acronym (Year)	(Complete name of institution [acronym], year)	(Institution, year)
Groups (without abbreviations) such as authors	Complete name of institution (year)	Complete name of institution (year)	(Complete name of institution, year)	

Editorial Policy

Mission

Disseminate scientific and technical knowledge and advances related to water through the publication of previously unpublished articles and technical notes that provide original contributions.

Our Principles

- Impartiality
- Objectivity
- Honesty

Our Values

- Knowledge
- Experience
- Thematic expertise

Contents

Interdisciplinary, composed of previously unpublished articles and technical notes related to water, that result from research and provide original scientific and technological contributions or innovations, developed based on the fields of knowledge of diverse disciplines.

Topics Covered

Interdisciplinary, related to water, with priority topics in the following knowledge areas:

- Water and energy
- Water quality
- Physical, biological and chemical sciences
- Hydro-agricultural sciences
- Political and social sciences
- Scientific and technological development and innovation
- Water management
- Hydrology
- Hydraulics

Type of Contributions

Technical article: scientific document that addresses and communicates, for the first time, results from a successful investigation or innovation, whose contributions provide and increase current knowledge about the topic of water.

Technical note: text that addresses advances in the field of hydraulic engineering and professional practices in the field of water, while not necessarily making an original contribution in every case it must be a previously unpublished work.

Some of the articles submitted to the review process can result in being published as notes and vice versa. This will occur through a proposal and process of mutual agreement between the authors and the editor responsible for the topic. The article and the note have nearly the same structure (abstract, introduction, methodology, results, discussion, conclusion, references).

Review Process

The journal is governed by a rigorous review process which establishes that each article be analyzed separately by three reviewers who recommend its acceptance, acceptance with minor changes, acceptance with extensive changes, rejection or acceptance as a technical note with the required changes.

At least one of three reviewers will be sought from a foreign institution.

The reviewers may not belong to the same institution as the authors proposing the article for publication.

When the decisions are opposing or inconsistent, the involvement of other reviewers or the members of the Editorial Committee may be requested.

On occasion, the approval of an article will be decided by two reviewers in addition to the opinion of the editor of the corresponding topic or, the editor in chief.

A rejected article will not be accepted for a new review process.

The review process will be performed in such a way that neither the authors nor the reviewers know the names of the other party.

The review process is performed by high-level specialists and experts who are national and internationally renowned in their professional fields and have the ability to reliably evaluate, in a timely manner, the quality as well as the originality of contributions, in addition to the degree of scientific and technological innovation in the topic under which it is submitted for possible publication.

This participation is considered a professional contribution and will be performed as a courtesy.

The reviews have a "Guide for the Reviewer" provided by the journal's Editorial Department.

Final Ruling

The ruling resulting from the review process is not subject to appeal.

Authors

Works are published from authors of any nationality who present their contributions in Spanish; nevertheless, we all accept works in Spanish or English.

Responsibility of the Authors

Submitting a proposal for the publication of an article commits the author not to simultaneously submit it for consideration by other publications. In the event an article has been submitted to another media for eventual publication, the author agrees to do so with the knowledge of the Editorial Department, which will suspend the review process and inform the Editorial Committee of the decision by the authors.

Collaborators whose articles have been accepted will formally cede the copyright to ***Tecnología y Ciencias del Agua***.

The authors are responsible for the contents of the articles.

The author is responsible for the quality of the Spanish used. If the writing is deficient the work will be rejected. ***Water Technology and Sciences*** will only be responsible for the editorial management.

The author commits to making the changes indicated by the editor of the topic in the time frame establish by the editor. In the event these indications are not met, the article will be removed from the review process and be classified as rejected.

The author shall be attentive to resolving the questions and proposals presented by the editors and the editorial coordinator.

Each author shall approve the final printed proofs of their texts.

It is suggested that authors consult the "Guide for Collaborators."

Readers

Academics, investigators, specialists and professionals interested in the analysis, investigation and search for knowledge and solutions to problems related to water.

Reception of Articles

The reception of articles and notes is ongoing.

Time period

Bimonthly, appearing in the second month of the period.

Subscription and Distribution

The journal is distributed through paid and courtesy subscriptions.

Open Access

Water Technology and Sciences, previously ***Hydraulic Engineering in Mexico***, provides a digital version of all the material published since 1985.

Special editions and issues

Water Technology and Sciences will publish special numbers independently or in collaboration with other journals, professional associations or editorial houses with renowned prestige and related to water resources.

In addition, it will publish articles by invitation, acknowledging the professional advances of prominent investigators.

In both cases, the quality of the technical continents and scientific contributions will be reviewed.

Water Technology and Sciences is registered in the following national and international indices and abstracts:

• Thomson Reuters Science Citation Index® (ISI) • Expanded Thomson Reuters Research Alert® (ISI) • Índice de revistas mexicanas de investigación científica y tecnológica del Consejo Nacional de Ciencia y Tecnología (Conacyt) (2013-2018) • Sistema de Información Científica Redalyc (Red de Revistas Científicas de América Latina y El Caribe, España y Portugal), Universidad Autónoma del Estado de México • EBSCO (Fuente Académica Premier NISC; Geosystems, como Marine, Oceanographic and Freshwater Resources) • ProQuest (Cambridge Scientific Abstracts) • Elsevier (Fluid Abstracts: Process Engineering; Fluid Abstracts: Civil Engineering) • CAB Abstracts, CAB International • Latindex (Sistema Regional de Información en Línea para Revistas Científicas de América Latina, el Caribe, España y Portugal), Universidad Nacional Autónoma de México • Periódica (Índice de Revistas Latinoamericanas en Ciencias), Universidad Nacional Autónoma de México • Catálogo Hela (Hemeroteca Latinoamericana), Universidad Nacional Autónoma de México • Actualidad Iberoamericana, CIT-III, Instituto Iberoamericano de Información en Ciencia y Tecnología.

Other Sources

The journal can also be found archived in Google scholar.